UNIVERSITAT DE BARCELONA

Study of the effects of PPAR-β/δ activators in the treatment of MASH

Meijian Zhang

ADVERTIMENT. La consulta d'aquesta tesi queda condicionada a l'acceptació de les següents condicions d'ús: La difusió d'aquesta tesi per mitjà del servei TDX (**www.tdx.cat**) i a través del Dipòsit Digital de la UB (**diposit.ub.edu**) ha estat autoritzada pels titulars dels drets de propietat intel·lectual únicament per a usos privats emmarcats en activitats d'investigació i docència. No s'autoritza la seva reproducció amb finalitats de lucre ni la seva difusió i posada a disposició des d'un lloc aliè al servei TDX ni al Dipòsit Digital de la UB. No s'autoritza la presentació del seu contingut en una finestra o marc aliè a TDX o al Dipòsit Digital de la UB (framing). Aquesta reserva de drets afecta tant al resum de presentació de la tesi com als seus continguts. En la utilització o cita de parts de la tesi és obligat indicar el nom de la persona autora.

ADVERTENCIA. La consulta de esta tesis queda condicionada a la aceptación de las siguientes condiciones de uso: La difusión de esta tesis por medio del servicio TDR (**www.tdx.cat**) y a través del Repositorio Digital de la UB (**diposit.ub.edu**) ha sido autorizada por los titulares de los derechos de propiedad intelectual únicamente para usos privados enmarcados en actividades de investigación y docencia. No se autoriza su reproducción con finalidades de lucro ni su difusión y puesta a disposición desde un sitio ajeno al servicio TDR o al Repositorio Digital de la UB. No se autoriza la presentación de su contenido en una ventana o marco ajeno a TDR o al Repositorio Digital de la UB (framing). Esta reserva de derechos afecta tanto al resumen de presentación de la tesis como a sus contenidos. En la utilización o cita de partes de la tesis es obligado indicar el nombre de la persona autora.

WARNING. On having consulted this thesis you're accepting the following use conditions: Spreading this thesis by the TDX (**www.tdx.cat**) service and by the UB Digital Repository (**diposit.ub.edu**) has been authorized by the titular of the intellectual property rights only for private uses placed in investigation and teaching activities. Reproduction with lucrative aims is not authorized nor its spreading and availability from a site foreign to the TDX service or to the UB Digital Repository. Introducing its content in a window or frame foreign to the TDX service or to the UB Digital Repository is not authorized (framing). Those rights affect to the presentation summary of the thesis as well as to its contents. In the using or citation of parts of the thesis it's obliged to indicate the name of the author.

UNIVERSITAT DE BARCELONA

University of Barcelona

Faculty of Pharmacy and Food Sciences

Department of Pharmacology, Toxicology and Therapeutic Chemistry

PhD Program in Biomedicine

Study of the effects of PPAR-β/δ activators in the treatment of MASH

Meijian Zhang

2024

University of Barcelona

Faculty of Pharmacy and Food Sciences

Department of Pharmacology, Toxicology and Therapeutic Chemistry

PhD Program in Biomedicine

Study of the effects of PPAR-β/δ activators in the treatment of MASH

Dissertation presented by Meijian Zhang to qualify for the doctorate degree from the University of Barcelona

Director

Dr. Manuel Vázquez-Carrera &

Dr. Emma Barroso Fernández

PhD Student

Meijian Zhang

Meijian Zhang

2024

The present doctoral thesis has generated two original scientific papers, one of them published (attached in the annex section) and the other one is under review:

[1] **Zhang, M**., Barroso, E., Ruart, M., Peña, L., Peyman, M., Aguilar-Recarte, D., ... & Vázquez-Carrera, M. (2023). **Elafibranor upregulates the EMT-inducer S100A4 via PPARβ/δ.** *Biomedicine & Pharmacotherapy*, 167, 115623.

[2] **Zhang, M**., Barroso, E., Peña. L., Rada. P., Valverde. Á., Wahli. W., Palomer. X., & Vázquez-Carrera, M. **PPARβ/δ activation attenuates hepatic fibrosis by inhibiting the SMAD3 pathway via modulation of the negative crosstalk between AMPK and ERK1/2 in hepatic stellate cells.** Under review.

In addition, during my PhD I conducted a study not related to the content of my thesis, which is included in the annex section.

[1] **Zhang, M.**, Bagán, A., Martínez, D., Barroso, E., Palomer, X., Vázquez, S., ... & Vázquez-Carrera, M. (2023). **Design and Synthesis of AMPK Activators and GDF15 Inducers**. *Molecules*, 28(14), 5468.

INDEX

Abbreviations

16:0/18:1-PC	1-palmitoyl-2-oleoyl-sn-glycero-3-phosphocholine
9cRA	9-cis retinoic acid
ABC	ATP-binding cassette
ACC	Acetyl-CoA carboxylase
ADMA	Asymmetric dimethylarginine
ADRP	Adipose differentiation related protein
AF-1	Activation function 1
AKT	V-Akt murine thymoma viral oncogene homolog
ALT	Alanine aminotransferase
AMPK	AMP-activated protein kinase
APC	Adenomatous polyposis coli
APP	Acute-phase protein
APRT	Adenine phosphoribosyltransferase
ASB2	Ankyrin repeat and suppressor of cytokine signaling box containing protein 2
ASK1	Apoptosis signal-regulating kinase 1
AST	Aspartate aminotransferase
α-SMA	Alpha-smooth muscle actin
ATF6	Activating transcription factor 6
AUC	Area under the cure
BCRP	Breast cancer resistance protein
BI-1	Bax inhibitor-1
BiP	Binding immunoglobulin protein
BMI	Body mass index
BMP	Bone morphogenetic protein
BSA	Bovine serum albumin
BSEP	Bile salt export pump

C/EBP	CCATT/enhancer binding protein
CaMKKβ	Calmodulin-dependent protein kinase β
cAMP	Cyclic adenosine monophosphate
CBM	Carbohydrate-binding module
CBP	cAMP-response-element-binding-protein-binding protein
CBS	Cystathionine-β-synthase
CCL2	Chemokine (C-C motif) ligand 2
CCl_4	Carbon tetrachloride
Cdc42	Cell division control protein 42
CD-HFD	Choline-deficient high-fat diet
cDNA	Complementary DNA
CHOP	C/EBP homologous protein
CLR	C-type lectin receptor
CoA	Coenzyme-A
COL1A1	Collagen type I alpha 1
CPT-1	Carnitine palmitoyltransferase-1
CRN	Clinical Research Network
CVC	Cenicriviroc
CVD	Cardiovascular disease
CXCL1	C-X-C motif chemokine ligand 1
CYP	Cytochrome P450
DAMP	Damage-associated molecular pattern
DBD	DNA-binding domain
DDAH1	Dimethylarginine dimethylaminohydrolase-1
DGAT	Diacylglycerol acyltransferase
DMEM	Dulbecco's modified eagle's medium
DNA	Deoxyribonucleic acid
DNL	*De novo* lipogenesis
dNTP	Deoxynucleotide

ECM	Extracellular matrix
EDTA	Ethylenediaminetetraacetic acid
eIF2α	Eukaryotic translation initiation factor 2α
EMT	Epithelial-mesenchymal transition
EndMT	Endothelial-mesenchymal transition
eNOS	Endothelial nitric oxide synthase
ER	Endoplasmic reticulum
ERK	Extracellular signal-regulated kinase
FABP	Fatty acid-binding protein
FABPpm	Fatty acid binding protein-plasma membrane
FAT/CD36	Fatty acid translocate/CD36
FATP	Fatty acid transporter protein
FBS	Fetal bovine serum
FDA	U.S. Food and Drug Administration
FFA	Free fatty acid
FGF21	Fibroblast growth factor 21
Fra-2	Fos-related antigen 2
FSP1	Fibroblast-specific protein 1
FXR	Farnesoid X receptor
G-6-P	Glucose 6-phosphate
GADD34	Growth-arrest and DNA damage-inducible protein 34
Gal-3	Galectin-3
GAPDH	Glyceraldehyde 3-phosphate dehydrogenase
GDF	Growth and differentiation factor
GDP	Guanosine diphosphate
GIP	Glucose-dependent insulinotropic polypeptide
GLP-1	Glucagon-like peptide-1
GLUT	Glucose transporter protein
Grb2	Growth factor receptor-bound protein 2

GS	Gly-Ser–rich
GSK-3β	Glycogen synthase kinase-3β
GTP	Guanosine triphosphate
GTT	Glucose tolerance test
H&E	Hematoxylin and eosin
H_2O_2	Hydrogen peroxide
HBV	Hepatitis B virus
HCC	Hepatocellular carcinoma
HCV	Hepatitis C virus
HFCF	High fat, cholesterol, and fructose
HMGCR	3-hydroxy-3-methyl-glutaryl-CoA reductase
HSC	Hepatic stellate cell
HVPG	Hepatic venous pressure gradient
IL-1	Interleukin-1
iNOS	Inducible nitric oxide synthase
IR	Insulin resistance
IRE1	Inositol-requiring enzyme 1
I-SMAD	Inhibitory SMAD
ITT	Insulin tolerance test
JNK	C-Jun N-terminal kinase
K-18	Keratin-18
KD	Ketogenic diet
LAP	N-terminal precursor remnant
LBD	Ligand-binding domain
LCFAs	Long-chain fatty acids
LFC	Liver fat content
LKB1	Tumor suppressor liver kinase B1
LLC	Large latent complex
LTBP	Large TGF-β binding protein

LXR-α	Liver X receptor-α
MAP3K	MAP kinase kinase kinase
MAPK	Mitogen-activated protein kinase
MASH	Metabolic dysfunction-associated steatohepatitis
MASLD	Metabolic dysfunction-associated steatotic liver disease
MCD	Methionine-choline-deficient
MDR1	Multidrug resistance protein 1
MEK	MAPK-ERK kinase
MET	Mesenchymal- epithelial transition
MFB	Myofibroblast
ML	Machine learning
MMPs	Matrix metalloproteinases
MRE	Magnetic resonance elastography
MRI	Magnetic resonance imaging
MRI-PDFF	Magnetic resonance imaging proton density fat fraction
MRP2	Multidrug resistance protein 2
mTOR	Mammalian target of rapamycin
MTP	Microsomal transfer protein
MUFA	Monounsaturated FA
NAC	N-acetylcysteine
NAFLD	Nonalcoholic fatty liver disease
NAS	NAFLD activity score
NASH	Nonalcoholic steatohepatitis
NEFA	Non-esterified fatty acids
NF-κB	Nuclear factor
NLRs	Nod-like receptors
NMIIA	Non-muscle myosin IIA
NTCP	Sodium taurocholate co-transporting polypeptide
OCA	Obeticholic acid

OCT	Optimal cutting temperature
ORO	Oil red O
OvNa	Sodium orthovanadate
P/CAF	p300/CBP associated factor
PAGE	Polyacrylamide gel electrophoresis
PAI-1	Plasminogen activator inhibitor-1
PAK	p21-activated kinase
PERK	PKR-like ER kinase
PF	Portal fibroblast
PGC-1α	PPAR-γ co-activator-1α
PI3K	Phosphatidylinositol-3-kinase
PKA	Protein kinase A
PKR	RNA-dependent protein kinase
PMSF	Phenylmethylsulphonyl fluoride
PPAR	Peroxisome proliferator-activated receptor
PPRE	Peroxisome proliferator response element
Pro-C3	Procollagen III
PRR	Pathogen recognition receptor
PTM	Post-translational modification
PVDF	Polyvinylidene difluoride
RIDD	Regulated IRE1-dependent RNA decay
RNA	Ribonucleic acid
ROCK	Rho-associated protein kinase
ROS	Reactive oxygen species
R-SMADs	Receptor-regulated SMAD family
RXR	Retinoid X receptor
S100A4	S100 calcium-binding protein A4
SCD1	Stearoyl-CoA desaturase 1
SDS-PAGE	Sodium-dodecyl-sulphate polyacrylamide gel electrophoresis

SEC	Sinusoidal endothelial cell
SER	Smooth endoplasmic reticulum
SFA	Saturated FA
ShcA	Src homology and collagen A
siRNA	Small interference RNA
SLC	Small latent complex
SMAD	Suppressor of mothers against decapentaplegic
Smurf1	SMAD ubiquitination regulatory factor 1
Sos	Son of sevenless
SREBP-1c	Sterol regulatory element-binding protein-1c
ST2	Tumorigenicity 2 receptor
T2DM	Type 2 diabetes mellitus
TBS	Tris-buffered saline solution
TCF4	T cell factor 4
TG	Triglycerides
TGF-β	Transforming growth factor β
THR	Thyroid hormone receptor
TIMPs	Tissue inhibitors of metalloproteinases
TLR	Toll-like receptor
TM	Tunicamycin
TNF-α	Tumor necrosis factor-α
TRAF2	Tumor necrosis factor receptor-associated factor 2
TZD	Thiazolidinediones
UPR	Unfolded protein response
VLDL	Very low-density lipoproteins
VLDLr	VLDL receptor
WT	Wild-type
XBP1	X-box binding protein 1

Summary

Metabolic dysfunction-associated steatotic liver disease (MASLD), formerly known as nonalcoholic fatty liver disease (NAFLD), is the most common chronic liver disease around the world, affecting more than 30% of the global population. MASLD ranges from isolated lipid accumulation or steatosis to its active inflammatory form, metabolic dysfunction-associated steatohepatitis (MASH). MASH is a serious progressive liver disease in which liver inflammation may lead to liver fibrosis and liver dysfunction over time. MASH is often associated with other health problems [e.g. hypertension and type 2 diabetes mellitus (T2DM)] and is a leading cause of liver-related mortality. The increasing burden of MASH on global health systems has created an urgent need to develop effective and safe treatments. In this regard, peroxisome proliferator-activated receptor (PPAR)-β/δ agonists have been proven to be effective in attenuating the progression of MASLD by ameliorating insulin resistance (IR), reducing lipogenesis, and alleviating inflammation and endoplasmic reticulum (ER) stress. However, the role of PPAR-β/δ in hepatic fibrosis remains controversial. In the present thesis, we show that two PPAR-β/δ agonists, elafibranor and GW501516, prevented glucose intolerance and IR and reduced collagen accumulation in the liver of MASH mice. Surprisingly, elafibranor, a dual PPAR-α/-β/δ agonist, increased the levels of the EMT-promoting protein S100A4 via PPAR-β/δ activation, as confirmed in liver cells. Additionally, it decreased the levels of ASB2, a protein promoting S100A4 degradation. Conversely, GW501516, a specific PPAR-β/δ ligand, inhibited TGF-β1-induced HSC activation by reducing the suppressor of mothers against

decapentaplegic (SMAD)3, as well as the levels of the SMAD3 co-activator p300 via AMP-activated protein kinase (AMPK) activation and the subsequent inhibition of extracellular signal-regulated kinase-1/2 (ERK1/2). Overall, these findings reveal novel mechanisms underlying the therapeutic effects of PPAR-β/δ agonists in liver diseases.

I. Introduction

1. Metabolic dysfunction-associated steatotic liver disease (MASLD): definition, incidence, and new nomenclature

Nonalcoholic fatty liver disease (NAFLD) is the most common global pandemic, with the highest prevalence in the Middle East (32%) and South America (31%), 24% in North America, and the lowest prevalence in Africa (14%) (Younossi, Koenig et al. 2016). Moreover, in recent years global prevalence has increased from 25% in 2016 to 32% in 2022 (Riazi, Azhari et al. 2022). This increase has important health implications since NAFLD is an important cause of liver-related morbidity and mortality (Chan, Chuah et al. 2023). NAFLD is diagnosed when steatosis, or fat accumulation, is present in more than 5% of liver cells without significant alcohol consumption (Sheka, Adeyi et al. 2020), and its occurrence is commonly associated with type 2 diabetes mellitus (T2DM), insulin resistance (IR), dyslipidemia, and obesity. NAFLD ranges from isolated steatosis (NAFL), characterized by the presence of hepatic steatosis without significant necroinflammation in histology, to nonalcoholic steatohepatitis (NASH) in an ongoing process. NASH is the advanced form of NAFLD with hepatocytes ballooning and lobular inflammation (Figure 1), with or without progression to fibrosis (Singh, Allen et al. 2015) that may increase the risk of more serious conditions such as cirrhosis, hepatocellular carcinoma (HCC, 0.5%-2.6% in NASH cirrhosis) (Huang, El-Serag et al. 2021) and cardiovascular disease (CVD). The diagnosis of NASH is based on histological features and its prevalence is 1.5%-6.5% (7%-30% in NAFLD patients) (Younossi, Koenig et al. 2016). NASH has become the leading indication for liver transplantation in many countries with a growing rate, whereas the waiting list for

patients with hepatitis C virus (HCV)-related cirrhosis has decreased significantly after the advent of direct-acting antivirals (Ferrarese, Battistella et al. 2022). The pathogenesis of NASH has not yet been fully elucidated, and recent advances in knowledge may soon lead to the development of more effective treatments.

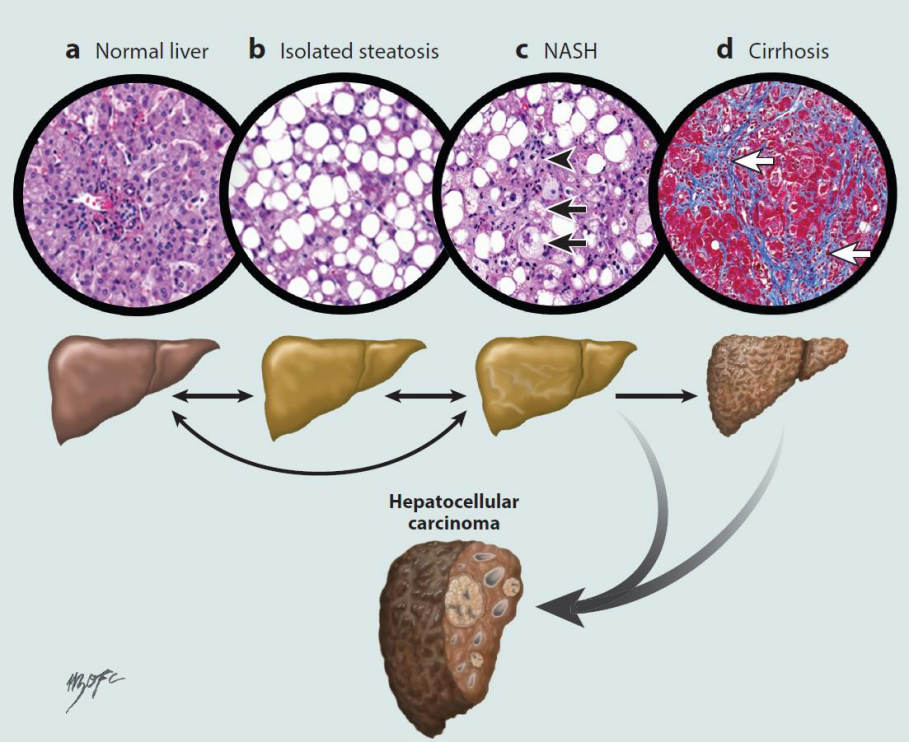

Figure 1. The spectrum of nonalcoholic fatty liver disease (NAFLD). NAFLD encompasses a spectrum of diseases, including steatosis in which there is noninflammatory isolated fat accretion in hepatocytes. Nonalcoholic steatohepatitis (NASH), a more aggressive form of the disease, is characterized by steatosis, inflammatory changes (*arrowhead*), and hepatocyte cell ballooning (*black arrows*) associated with varying degrees of liver fibrosis. Cirrhosis is characterized by the presence of collagen bands surrounding liver nodules (*white arrows*). Hepatocellular carcinoma can arise from both precirrhotic NASH and cirrhosis (Arab, Arrese et al. 2018).

The terms NAFLD, NAFL, and NASH are widely used, but it has long been believed that the term "non-alcoholic" does not accurately describe the disease's etiology, and some also feel that the term "fatty" is shameful. Recently, a vast majority of research members from 56 countries believed that the terms NAFLD and NASH were too limited and unanimously agreed to rename them as metabolic dysfunction-associated steatotic liver disease (MASLD) and metabolic dysfunction-associated steatohepatitis (MASH) (Rinella, Lazarus et al. 2023). In addition, a new category called metabolic dysfunction-associated alcohol-related liver disease (MetALD) is used to describe MASLD patients who consume excessive alcohol weekly (140 g/week for females and 210 g/week for males). It is worth noting that the new terms emphasize nomenclature and definition, rather than determining what constitutes liver fat deposition or assessing disease severity, which is beneficial for raising disease awareness, reducing stigma, and accelerating the development of drugs and biomarkers.

2. Metabolic functions of the liver

Liver, the largest metabolic organ of the human body (approximately 2% to 3% of the average body weight), is located beneath the rib cage in the right upper abdomen, and its structure is essential for performing over 500 vital functions (Adams 2003), including albumin production, bile production, filtering blood, and processing glucose. The liver consists of four lobes: the large right lobe and left lobe, and the smaller caudate lobe and quadrate lobe (Figure 2). The biggest difference between rat liver and

human liver is that it lacks a gallbladder. The liver is a storehouse of large amounts of blood, mainly derived from the hepatic portal vein (around 75%) and hepatic artery, thereby promoting material exchange between blood and hepatocytes (Shneider 2008).

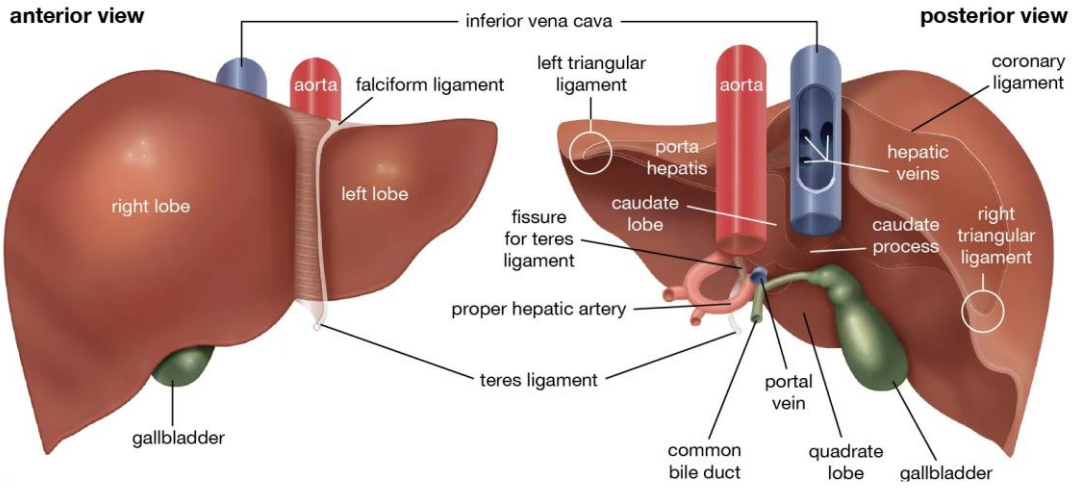

Figure 2. The Structure of the human liver. Britannica, The Editors of Encyclopedia. "Liver". Encyclopedia Britannica, https://www.britannica.com/science/liver. Accessed 19 November 2023.

The hepatocyte plate constitutes the hepatic lobule, the most basic structural unit of the liver. Hepatocytes are arranged in flat plates separated by sinusoids, which are lined with fenestrated endothelial cells (Figure 3). The extravascular gap between liver sinusoids and hepatocytes is called the perisinusoidal space or diss space (Ramadori and Ramadori 2010). Bile canaliculi are small channels between adjacent hepatocytes that carry bile into the intrahepatic bile ducts. The liver tissue is mainly composed of parenchymal cells (approximately 70%-80% of the liver volume) and non-parenchymal cells (6.5% of the liver volume) (Kmieć 2001). Hepatocytes represent the primary

parenchymal cells pivotal for the execution of essential physiological functions within the liver, including blood filtration, the regulation of insulin and glucose, protein metabolism, and lipophagy. Additionally, the liver comprises other significant cell types (Figure 3), including biliary epithelium, Kupffer cells (remove pathogens in the circulation and release cytokines to inhibit many kinds of inflammation), sinusoidal endothelial cells (SECs, an important medium for the exchange of substances between the blood and hepatocytes), and hepatic stellate cells (HSCs, participate in the process of fibrogenesis and regulation of sinusoidal blood flow) (Dutta, Mishra et al. 2021).

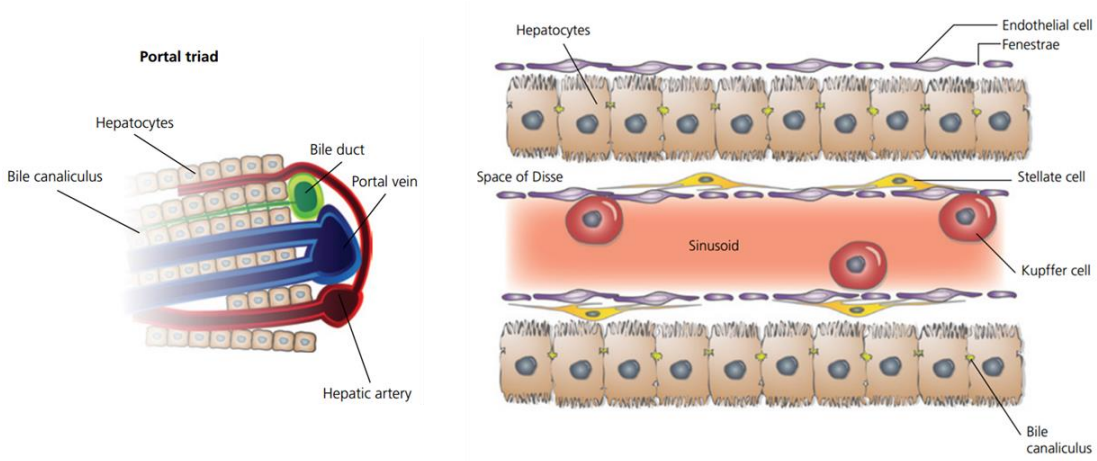

Figure 3. Liver portal trial (left) and hepatic lobule structure (right). Hepatocytes are organized in plates interspersed by liver blood sinusoids, which are encased by fenestrated endothelial cells. The interstitial area between the liver sinusoids and hepatocytes is termed the perisinusoidal space or space of Disse (Dufour and Mertens 2015).

2.1. Protein and biliary secretion

Hepatocytes contain many secretory organelles and mitochondria, which are

central in the metabolism of proteins while synthesizing the vast majority of circulating proteins for the organism. In general, hepatocytes secrete proteins similar to most cells. Proteins are initially synthesized by ribosomes, and nascent polypeptides enter the endoplasmic reticulum (ER) groove via transport through Sec61/SecY channels. Finally, proteins are transported from the Golgi to the basolateral plasma membrane via separate vesicular carriers and in the process known as exocytosis (Saucan and Palade 1994, Rapoport, Li et al. 2017). Hepatocytes secrete many serum proteins into circulation including carrier proteins, immune-related proteins, and coagulation factors (Table 1). At the same time, hepatocytes play a regulatory role in amino acid metabolic homeostasis (Paulusma, Lamers et al. 2022), and hepatocyte amino acid catabolism into keto acids, ammonia, and glutamine directly affects the concentration of amino acids in portal blood. Aspartate aminotransferase (AST) and alanine aminotransferase (ALT) are two of the central enzymes of amino acid metabolism, which are released from the hepatocytes when the liver undergoes damage such as inflammation, necrosis, and toxicity (Kasarala and Tillmann 2016).

Protein	Function
Albumin	Carrier protein and main protein maintaining normal oncotic pressure
Transferrin	Iron binding/transport
Ceruloplasmin	Central regulator of copper homeostasis

Haptoglobin	Protects kidneys from hemoglobin damage
Lipoproteins	Involve in metabolism/oxygen transport/inflammation
Acute-phase proteins (APPs)	Group of approximately 30 different biochemically and functionally unrelated immune-related plasma proteins involved in systemic inflammatory response
Clotting factors	Coagulation and fibrinolysis

Table 1. Selected secreted and membrane-localized proteins of the hepatocyte.

Bile, a unique and important aqueous solute produced by the liver, serves two primary functions: firstly, the excretion of hepatocyte's metabolites and secondly, the facilitation of intestinal absorption of lipids and fat-soluble vitamins. Following the synthesis of bile, it undergoes transport across the parietal membrane into bile canaliculi formed between adjacent hepatocytes. Facilitated by an osmotic gradient, bile traverses ductules and ultimately reaches the bile ducts, undergoing additional modifications by bile duct cells and ductal epithelial cells during the transportation. Subsequently, bile enters the gallbladder and is released into the intestine in response to a stimulatory signal (Banales, Huebert et al. 2019). An amount of 750 to 1000 ml of bile is produced daily from the liver (Pitt and Nakeeb 2017), which consists of two-thirds of canalicular bile secreted by apical membrane of hepatocytes and one-third of ductular bile that is

secreted by bile ducts. Bile consists of approximately 95% water and dissolves a variety of organic solutes, such as bile salts, cholesterol, bilirubin, and phospholipids (Schiff, Maddrey et al. 2017). The hepatic uptake mechanism on the basolateral membrane of hepatocytes plays a decisive role in the entry of organic solutes into the liver (Boyer 2013). Sodium taurocholate co-transporting polypeptide (NTCP) is primarily involved in the uptake of bound bile salts from sinusoidal blood. In contrast, unbound bile salts are taken up by the liver at the basolateral sinusoidal membrane of hepatocytes via a sodium-independent mechanism on the SLCO superfamily of carriers. Hepatocyte apical ATP-binding cassette (ABC) superfamily transporter proteins excrete cytotoxic and xenobiotic substances into the bile in response to ATP-dependent depletion, and disruption of the multidrug resistance 1 (*MDR1*) or *ABCB1* gene leads to elevated levels of the drug in many tissues in mice (Schinkel, Smit et al. 1994). Furthermore, various other ABC transporter proteins, such as bile salt export pump (BSEP)/ABCB11, multidrug resistance protein 2 (MRP2)/ABCC2, and human breast cancer resistance protein (BCRP)/ABCG2, facilitate the transport of diverse bile constituents, encompassing an array of drugs, bilirubin diglucuronide, and sulfate conjugates, into the bile ducts.

2.2. Detoxification

The human organism may be exposed to a variety of exogenous chemical substances in food, water, pharmaceutical agents, and environmental contaminants

every day, many of which are highly lipophilic and extremely toxic. The liver is the primary organ protecting body from toxification by converting lipophiles into water-soluble metabolites that can be excreted in the urine (Apte and Krishnamurthy 2011). This protective capacity of hepatocytes stems primarily from biotransformation, which can be divided into phase I and phase II reactions. Phase I, including oxidation, reduction and hydrolysis, centers on the cytochrome P450 (CYP) system, which identifies more than 100 genes that encode CYP. Only about a dozen enzymes (belonging to the CYP1, 2, and 3 families) are responsible for the biotransformation of most exogenous substances, with CYP 3A4, 2C9, 2C8, 2E1, and 1A2 being the most highly expressed forms in the liver (Zanger and Schwab 2013), and its reducing equivalents are transferred from NADPH via CYP reductase co-localized with smooth endoplasmic reticulum (SER). The phase II reaction is mainly a conjugation or synthesis reaction of the phase I product i.e. the addition of water-soluble side groups to make it suitable for renal or intestinal excretion (Grant 1991).

The human organism synthesizes approximately 300 mg of bilirubin daily, primarily derived from the heme molecule of senescent erythrocytes. A sinusoidal membrane transport protein facilitates the uptake of bilirubin from the blood into hepatocytes. Subsequently, bilirubin is predominantly excreted in the form of bilirubin glucuronide through the bile canalicular membrane into the bile (Kamisako, Kobayashi et al. 2000), thereby averting intracellular toxicity. Hepatocytes primarily metabolize alcohol by converting it to acetaldehyde using the enzyme ethanol dehydrogenase and

then further converting acetaldehyde to acetic acid with the enzyme acetaldehyde dehydrogenase in the mitochondria. This metabolism heavily relies on NAD^+, and depletion of this cofactor would alter the redox state of ethanol-exposed hepatocytes. In chronic alcohol metabolism, the microsomal P450 enzyme system becomes more involved in the metabolic process (Lieber 2005).

2.3. Role of the liver in the modulation of glucose and insulin

In healthy individuals, during the postprandial period the liver takes up glucose to minimize the fluctuation of glycemia via glucose transporter proteins (GLUTs). The transport of glucose by GLUTs may not require consumptive capacity, and GLUT2 is generally recognized as the major hepatic GLUT in humans. In the hepatocyte, free glucose is phosphorylated by hexokinase isoenzymes to produce glucose 6-phosphate (G-6-P) further modified to G-1-P, and finally stored as glycogen (100-200 g) to form a fuel reserve that can be used during fasting (Adeva-Andany, Pérez-Felpete et al. 2016).

Insulin serves as a critical regulator of hepatic glucose uptake (HGU), under hyperinsulinemic/hyperglycemic conditions. Direct hepatic insulin action was able to fully stimulate HGU, whereas an indirect effect was not required (Kraft, Coate et al. 2021). Insulin is transcribed and expressed in the β-cells of the pancreas, and 50% - 80% of the insulin reaching the liver via the portal vein is cleared by the hepatocytes before reaching the muscle and adipocytes, where it promotes the translocation of GLUT4 and

facilitates glucose uptake (Tokarz, MacDonald et al. 2018). Under low blood glucose levels, glucagon secreted by pancreatic α-cells induces cyclic adenosine monophosphate (cAMP)-mediated activation of α-phosphatase, which stimulates hepatic glycogenolysis and gluconeogenesis to restore glucose homeostasis (Habegger, Heppner et al. 2010).

2.4. Lipid metabolism

The liver is an important site for lipid uptake, storage, breakdown, and release. The hepatocytes acquire lipids in the form of free fatty acids (FFA), which emanate either from adipocytes following the lipolysis of stored triglycerides (TG) or from dietary fat bound to albumin and lipoproteins. Long-chain fatty acids (LCFAs) enter the hepatocytes through passive diffusion and protein-mediated FA translocation across the plasma membrane. Fatty acid binding protein-plasma membrane (FABPpm), fatty acid translocase/CD36 (FAT/CD36), fatty acid transport protein (FATP), and caveolin-1 have critical functions in facilitating this process. The LCFAs bind to FABP, leading to the formation of LCFA-coenzyme-A (CoA) with an active acyl-CoA, which is subsequently utilized in the esterification of phospholipids, TG, cholesteryl esters, and other specific lipids for storage and metabolism (He, Chen et al. 2023).

Intracellular FAs, upon entry, undergo either oxidation within the mitochondria or esterification of TG in the ER through a pathway mediated by diacylglycerol

acyltransferase (DGAT). The three potential sources of FAs entering the hepatic TG storage pool are plasma non-esterified fatty acids (NEFA), *de novo* lipogenesis (DNL), and residual lipoproteins, whereas the main export products are mainly very-low-density lipoproteins (VLDL) and ketone bodies (Gibbons 1990). Insulin stimulates the synthesis of FFA from hepatic DNL by activating glucokinase, thereby enhancing glucose metabolism. Subsequently, this process involves the activation of the transcription factor sterol regulatory element-binding protein-1c (SREBP-1c), which belongs to a transcription factors family involved in the regulation of genes based on cellular cholesterol availability (Musso, Gambino et al. 2009). The acetyl-CoA carboxylation to malonyl-CoA is stimulated by insulin via activating acetyl-CoA carboxylase (ACC). A high level of malonyl-CoA reflects active DNL, wherein FFAs are preserved from oxidation and directed toward esterification for TG synthesis, and lower malonyl-CoA enhances carnitine palmitoyltransferase-1 (CPT-1) activity, thereby facilitating the transport of FAs to the mitochondria for β-oxidation (Tessari, Coracina et al. 2009).

There appears to be a link between TG lipolytic activity and VLDL secretion rate, stabilized by apo-B lipoproteins (Gibbons, Islam et al. 2000). At the same time, the expression of apo-B is impacted by TG and FFA levels, as well as microsomal transfer protein (MTP). Insulin inhibits apo-B synthesis, whereas it stimulates lipogenesis through SREBP-1 activation (Figure 4), so the balance between FFA and insulin action plays a critical role in whether TG binds to apo-B VLDL particles and is secreted or

retained in the liver (Tessari, Coracina et al. 2009).

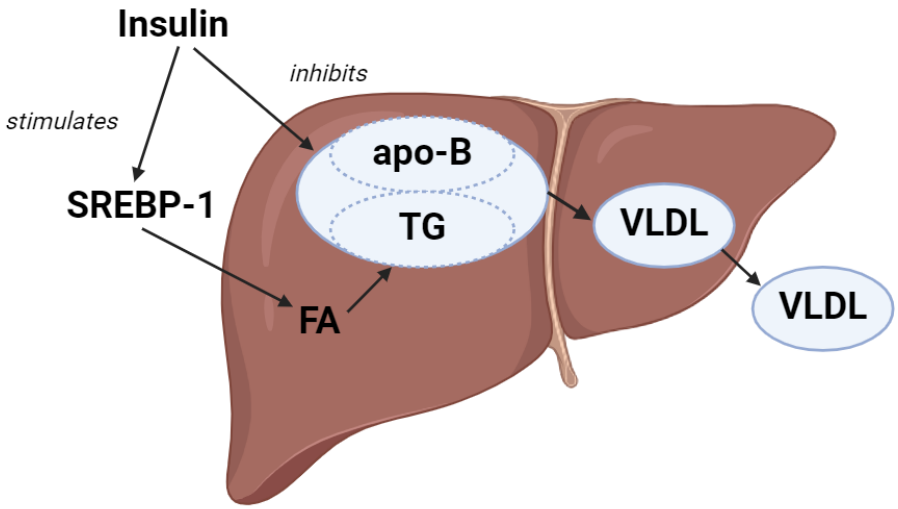

Figure 4. Role of insulin in the regulation of VLDL-apo-B synthesis and secretion in the liver. Insulin inhibits apo-B synthesis and stimulates lipogenesis through SREBP-1 activation. VLDL synthesis and secretion may be indirectly affected by insulin (Tessari, Coracina et al. 2009).

A highly conserved master regulator of energy metabolism and/or IR is AMP-dependent protein kinase (AMPK). Activation of AMPK inhibits the synthesis of FA and sterol, resulting in activating ATP-producing catabolic pathways, while switching off ATP-consuming processes (Viollet, Foretz et al. 2006). AMPK phosphorylates multiple proteins in the liver, such as ACC1 and ACC2, to control cellular lipid metabolism. AMPK inhibits malonyl-CoA produced by ACC1 to reduce FA synthesis and promotes FA oxidation in mitochondria by alleviating the inhibition of carnitine palmitoyltransferase 1 (CPT1) by malonyl-CoA produced by ACC2 (Viollet, Foretz et

al. 2006). AMPK also phosphorylates and inhibits 3-hydroxy-3-methyl-glutaryl-coenzyne A reductase (HMGCR) (Liu, Jing et al. 2015), a key enzyme in FA and cholesterol synthesis.

3. The pathogenesis of MASLD

3.1. The “multiple-hit” hypothesis in MASLD

The rationale for the intricate nature of MASH pathogenesis has transitioned from the conventional "two-hit" hypothesis to the "multiple-hit" hypothesis (Figure 5). This revised perspective incorporates factors such as gut-derived bacterial toxins, adipokine imbalance, mitochondrial dysfunction, oxidative damage, dysregulated apoptosis, activation of pro-inflammatory mediators and pro-fibrogenic factors, and activation of HSCs and Kupffer cells (Jung and Choi 2014).

IR and imbalanced lipid metabolism are considered as “first hit” due to the increase of DNL, reduction of FFAs oxidation, and hepatic VLDL secretion resulting in steatosis and hypertriglyceridemia. Overload of FFAs influx from adipose tissue to the liver affects the offset between DNL and TGs, and VLDL secretion (Green and Hodson 2014, Oseini and Sanyal 2017), and causes an increase in hepatocyte lipotoxicity accompanied by mitochondrial dysfunction (Mota, Banini et al. 2016), ultimately leading to liver cell injury. The increased production of reactive oxygen species (ROS) caused by tumor necrosis factor-α (TNF-α) and ceramides or the excess

free cholesterol results in apoptosis and ER stress. This imbalance changes within ER stress and leads to the activation of unfolded protein response (UPR)-mediated transmembrane protein to restore ER function.

In MASH, pro-inflammatory cytokines, including interleukin (IL)-1, IL-6, and TNF-α, play a vital role. The initiation of pathogen recognition receptors (PRRs), including toll-like receptors (TLRs), nod-like receptors (NLRs), and C-type lectin receptors (CLRs), leads to the activation of pro-inflammatory factor cascades. Consequently, this process recruits diverse immune cell populations such as macrophages and T cells, culminating in the induction of IR and the progression of fatty liver disease (Meli, Mattace Raso et al. 2014). Kupffer cells can contribute to the pathogenesis of the liver disease, with the stimulation of the lipopolysaccharide (LPS)-TLR4 pathway producing a variety of cytokines, such as TNF-α, IL-1β, IL-6, IL-12, and IL-18 (Seki, Tsutsui et al. 2001). IL-1β and TNF-α, similar to transforming growth (TGF)-β, can activate HSCs in a quiescent state into myofibroblasts, leading to liver fibrosis (De Minicis and Svegliati-Baroni 2011).

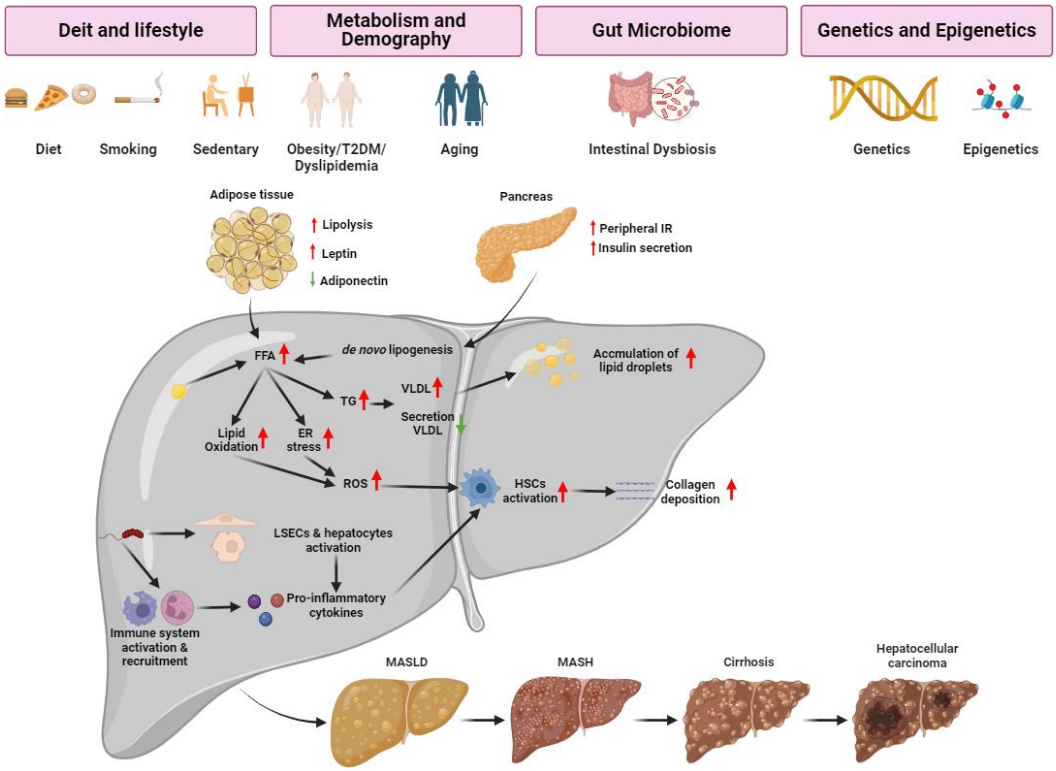

Figure 5. Major risk factors and pathophysiology of MASLD. Genetically predisposed people are susceptible to MASLD under unfavorable environmental conditions such as smoking, or a poor diet rich in fat/fructose. Obesity, multiple sclerosis, T2DM, dyslipidemia and age all increase the risk of developing fatty liver. Lipotoxicity due to elevated lipid levels in the liver induces ROS production due to increased lipid oxidation and endoplasmic reticulum stress. ROS and pro-inflammatory cytokine production drive HSC activation and collagen deposition, which induces hepatic fibrosis and the progression of liver disease from simple steatosis to steatohepatitis, cirrhosis, and hepatocellular carcinoma (Juanola, Martínez-López et al. 2021).

3.2. Metabolic risk factors and gut microbiome composition

Different studies have shown a strong relationship between MASLD and obesity, with body mass index (BMI) and waist circumference positively correlating with disease progression. The prevalence of MASLD in the obese population was 75.3%,

whereas that of MASH was 33.7% (Quek, Chan et al. 2023). Despite this, there exists a proportion of MASLD patients with relatively normal BMI, with 8%-19% of subjects found to have MASLD in Asia (BMI <25 kg/m^2) (Fan, Kim et al. 2017). Excessive fat accumulation in the liver is more common in obese patients due to the involvement of different mechanisms, mainly oxidative stress and mitochondrial dysfunction (Angulo 2006). Adipokines are polypeptides produced by adipose tissue, such as adiponectin and leptin. However, as adipose tissue expands, adipokine alterations occur, including an increase in leptin levels and a decrease in adiponectin levels, contributing to the progression of MASH and even cirrhosis.

Although the pathogenesis of T2DM and MASLD is complex and not fully understood, the prevalence of MASLD and MASH in the patients with T2DM is 55%-70% and 30%-40%, respectively (Younossi, Golabi et al. 2019). IR is an integral feature of the metabolic syndrome and contributes to the development of T2DM. Systemic IR induces lipolysis, leading to elevated levels of circulating FFA, which results in an accumulation in the liver and contributes to the development and exacerbation of hepatic IR (Ziolkowska, Binienda et al. 2021). Indeed, insulin-resistant patients with or without T2DM have similar dyslipidemia, caused primarily by excessive hepatic production of VLDL (Adiels, Olofsson et al. 2008). This dyslipidemia is mainly characterized by a high plasma TG concentration, a decrease in anti-atherosclerotic HDL cholesterol and an increase in small dense LDL-cholesterol particles, leading to a high risk of suffering from CVD (Mooradian 2009). Accordingly, CVD exhibits a

robust association with MASLD, representing a significant contributor to both its morbidity and mortality (Henson, Simon et al. 2020).

The gut microbiota exerts influence over hepatic carbohydrate and lipid metabolism, concurrently contributing to inflammatory responses and the progression of hepatic fibrosis, affecting MASLD and its progression to MASH (Boursier and Diehl 2015). It has been demonstrated a correlation between the severity of MASLD and the alterations in gut microbiota composition, indicative of gut dysbiosis and metabolic functional changes. Notably, patients with MASH and fibrosis stage $F \geq 2$ (Table 2) exhibited a noteworthy rise in the *Bacteroides* abundance and a decrease in *Prevotella* abundance (Boursier, Mueller et al. 2016). The gut microbiome of patients with MASLD is dominated by members of the *Firmicutes* and *Bacteroidetes*, followed by *Proteobacteria* and *Actinobacteria*. However, the abundance of the *Proteobacteria phylum* increases significantly with the development of advanced fibrosis, whereas the abundance of *Firmicutes phylum* decreases (Loomba, Seguritan et al. 2017). Another study showed significant enrichment of *Enterococcus sp* and oral species, such as *Streptococcus oralis* and *Streptococcus parasanguinis* in cirrhotic patients compared to healthy subjects (Solé, Guilly et al. 2021). All in all, an in-depth comprehension of the reciprocal interactions between the gut microbiota and the liver holds the potential for the development of efficacious microbiota-based therapeutic interventions.

Stage	Severity of fibrosis	Description
F0	No fibrosis	None
F1	Mild fibrosis	A small amount of scar tissue around some of the portal area.
F2	Moderate fibrosis	Scar tissue begins extending between the portal area and occasional nodules.
F3	Severe fibrosis	Presence of lots of scar tissue across most of the portal area, marked bridging, and occasional nodules.
F4	Cirrhosis	Permanent scarring and damage of the liver with liver dysfunction.

Table 2. The scoring systems and fibrosis stages.

The causes of MASH are complex and, in addition to metabolism and gut microbiology as described above, are associated with interactions between environmental factors, demographics, genetics and epigenetics (Figure 5) (Juanola, Martínez-López et al. 2021).

3.3. Hepatic liver inflammation

Hepatocytes are a pivotal trigger of liver inflammation and fibrosis via intercellular communication (Wree, Holtmann et al. 2019), and their injury and inflammation lead to the development of chronic liver disease. The severity of hepatocyte injury may be influenced by organelle damage such as mitochondria, lysosomes, and ER. Increasing evidence suggests that hepatocytes constitutively

generate and release various factors that are pivotal in immunomodulation and fibrogenesis (Seki and Schwabe 2015). Damage-associated molecular patterns (DAMPs), liberated from apoptotic or necrotic cells, are thought to trigger sterile inflammation in immune cells subsequent to tissue injury (Luedde, Kaplowitz et al. 2014). Hepatocyte lipotoxicity causes cellular stress leading to cell death, which activates DAMPs to restore homeostasis (Ibrahim, Hirsova et al. 2018).

3.3.1. The molecular link between ER stress and liver inflammation

The ER is an important organelle in eukaryotic cells for the synthesis and secretion of membrane proteins, the synthesis and transport of lipid, and calcium homeostasis. ER stress arises from an excessive buildup of unfolded and misfolded proteins within the ER, or from the depletion of calcium stores.

During ER stress, the UPR is activated by the activation of transmembrane sensors [i.e., inositol-requiring enzyme 1α (IRE1α), double-stranded RNA-dependent protein kinase (PKR)-like ER kinase (PERK), and activating transcription factor 6 (ATF6)], initiating the downstream UPR signaling cascades to restore ER homeostasis and to promote cell survival (Malhotra and Kaufman 2007). These three ER stress sensors are activated by dissociation of the ER protein chaperone binding immunoglobulin protein (BiP) and/or direct association with unfolded/misfolded proteins (Figure 6): 1) the kinase IRE1α induces transcriptionally active X-box binding protein 1 (XBP1) through

an atypical splicing mechanism as well as a regulated IRE1-dependent RNA decay (RIDD)-dependent preemptive mechanism. In addition, it also recruits tumor necrosis factor receptor-associated factor 2 (TRAF2) and apoptosis signal-regulating kinase 1 (ASK1) to mediate the activation of c-Jun N-terminal kinase (JNK) and nuclear factor (NF-κB) pathways. 2) Phosphorylation of eukaryotic translation initiation factor 2α (p-eIF2α) by active PERK selectively increases ATF4 that promotes adaptation to ER stress through activation of UPR target genes encoding proteins required for antioxidant response and amino acid metabolism, and inhibits global translation and decrease protein influx into the ER thereby alleviated ER stress. 3) ATF6 dissociates from BiP to produce ATF6N and transcriptionally regulates the expression of target genes associated with ER stress, including XBP1, CCAAT-enhancer-binding protein (C/EBP) homologous protein (CHOP), and BiP (Karagöz, Acosta-Alvear et al. 2019, Liu and Green 2019)

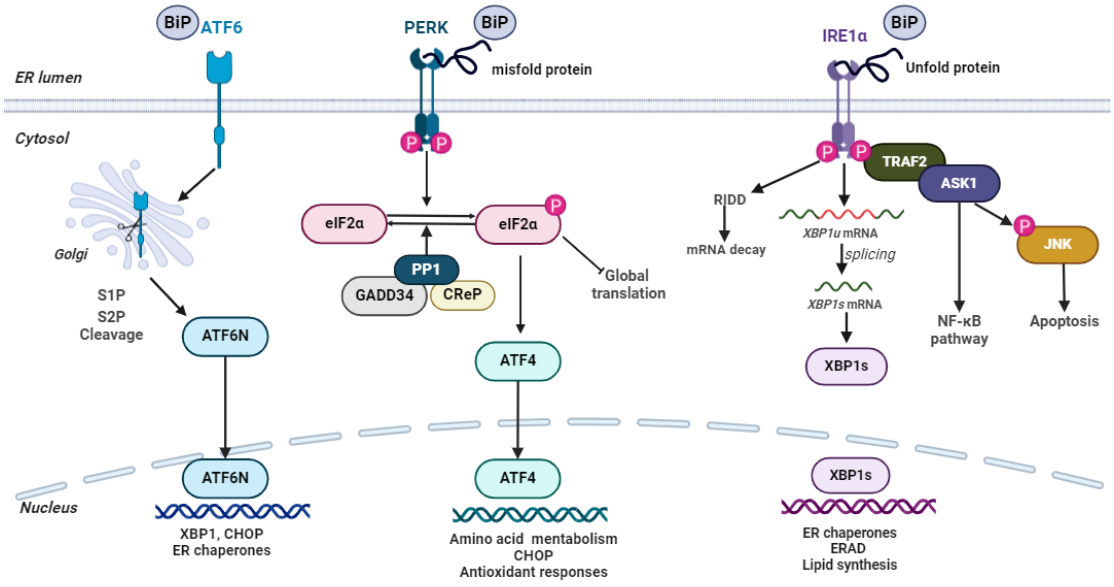

Figure 6. The UPR pathways in ER stress. During ER stress, three ER stress sensors are activated through dissociation of the ER protein chaperone BiP and/or direct binding to unfolded/unfolded poorly folded proteins (Liu and Green 2019).

ER stress stimulates several processes that contribute to the development of MASLD/MASH. Thus, hepatocytes with chronic ER stress activate inflammatory and apoptotic pathways (Mollica, Lionetti et al. 2011). Moreover, chronic ER stress has been reported to play a critical role in MASLD progression by promoting lipid accumulation (Baiceanu, Mesdom et al. 2016), IR (Jurczak, Lee et al. 2012) and regulating hepatic autophagic flux (González-Rodríguez, Mayoral et al. 2014). In fact, ER homeostasis is closely related to lipid metabolism, since the ER is the location for TG synthesis and VLDL assembly before reaching the Golgi apparatus. Likewise, the induction of ER stress stimulates hepatic steatosis by increasing VLDL receptor (VLDLR) expression (Jo, Choe et al. 2013), activating SREBPs (Kammoun, Chabanon et al. 2009), and decreasing FA oxidation. Likewise, hepatocyte-specific deletion of IRE1α decreases lipid partitioning into the ER lumen and reduces VLDL secretion, contributing to hepatic steatosis and hypolipidemia (Wang, Chen et al. 2012). Finally, it has been shown that ER stress markers in adipose tissue decrease significantly in subjects who lose weight after bariatric surgery (Gregor, Yang et al. 2009), suggesting that ER stress develops with obesity.

In line with a role of ER in the development of hepatic steatosis, mice with

hyperactive IRE1α RNase activity induced by deletion of the negative IRE1α regulator bax inhibitor-1 (BI-1) are more susceptible to hepatic steatosis caused by the pharmacological ER stress activator tunicamycin (TM) or a high-fat diet (HFD), as well as hepatocellular injury augmented by inflammasome signaling, hepatocellular death, fibrosis, and dysregulated lipid homeostasis (Lebeaupin, Vallée et al. 2018). In addition, BI-1 overexpression downregulates the *C/EBPα* gene to prevent IR associated with obesity (Bailly-Maitre, Belgardt et al. 2010).

The PERK/p-eIF2α/ATF4 pathway also regulates lipid homeostasis, since the deletion of eIF2α in mice inhibited the expression of C/EBPα protein, and enhanced c-Jun and adipose differentiation related protein (ADRP) expression, and hepatic steatosis (Rutkowski, Wu et al. 2008). Likewise, p-eIF2α-mediated UPR signaling was compromised in growth-arrest and DNA damage-inducible protein 34 (GADD34) in transgenic mice, which resulted in downregulation of peroxisome proliferator-activated receptor (PPAR)-γ, C/EBPα and C/EBPβ, lower liver glycogen levels and hepatosteatosis (Oyadomari, Harding et al. 2008). In a study, patients with isolated steatosis and MASH displayed increased eIF2α phosphorylation and enhanced levels of ATF4, but with no significant changes in other UPR markers (Malhi and Kaufman 2011).

ATF6 is also involved in the regulation of lipid metabolism by enhancing the

transcriptional activity of PPAR-α, thereby activating its downstream targets to promote mitochondrial FA oxidation. Moreover, hepatic overexpression of the active form of ATF6 promotes hepatic FA oxidation and prevents hepatic steatosis in diet-induced insulin-resistant mice, yet the opposite is true for the inactivated form of ATF6 (Chen, Zhang et al. 2016). Lack of ATF6α cells initially promotes recovery from acute stress, but is ineffective at recovering from exposure to persistent chronic stress (Wu, Rutkowski et al. 2007). Likewise, ER stress leads to hepatic lipid accumulation and inhibition of FA oxidation in ATF6α knockout mice (DeZwaan-McCabe, Sheldon et al. 2017). In addition, ATF6 regulates lipid and glucose homeostasis by repressing SREBP-2-regulated transcription (Zeng, Lu et al. 2004).

Moreover, hepatitis B virus (HBV) and HCV cause chronic infections, and ER stress occurs during viral infection, which initiates autophagy to enhance HBV viral replication (Wang, Wei et al. 2022). Likewise, HCV envelope protein expression regulates PERK-dependent CHOP expression and XBP1 splicing (Chan and Egan 2005).

In conclusion, ER stress and UPR activation are important in the pathogenesis of many chronic liver diseases, and further studies may provide the opportunity to identify novel therapeutic targets for their treatment.

3.3.2. Hepatic cytokines involved in liver inflammation

Cytokines are important players in systemic inflammation-associated diseases, and pro-inflammatory factors exert significant influence over various features in liver disease. Hepatocytes have the capacity to generate a diverse array of cytokines aimed at regulating processes involved in liver injury, repair, and inflammatory responses within the context of hepatic injury.

The pleiotropic cytokine IL-6 activates a variety of cells (e.g., immune cells, hepatocytes, hematopoietic stem cells, and osteoblasts), resulting in a wide range of biological activities in inflammation, hematopoiesis, tumorigenesis, and immunomodulation (Kishimoto 2010). In alcoholic liver disease, IL-6 is thought to have a protective role because it prevents ethanol-induced oxidative stress and mitochondrial dysfunction in hepatocytes by inducing metallothionein expression (El-Assal, Hong et al. 2004). Moreover, multiple studies have shown that IL-6 trans-signaling plays a protective role in chronic liver damage (Giraldez, Carneros et al. 2021). In fact, IL-6 levels were reported to be significantly increased in patients with MASLD compared to normal subjects and were positively correlated with the severity of MASLD (Das and Balakrishnan 2011). Notably, IL-6 improves liver regeneration and repair, but it can also sensitize the liver to injury, stimulate hepatocyte apoptosis, and induce IR (Yamaguchi, Itoh et al. 2010). Another investigation illustrated that moderate blockade of enhanced IL-6/STAT3 signaling may be beneficial in MASH. However, a

profound defect in IL-6/STAT3 activation may lead to the progression of MASH (Yamaguchi, Itoh et al. 2011).

IL-1α/β contributes to the pathogenesis of both steatosis and steatohepatitis. The *Il-1* gene was significantly expressed in diet-induced steatosis and steatohepatitis mouse models. In fact, the transition from steatosis to steatohepatitis and liver fibrosis were significantly reduced in the absence of IL-1α or IL-1β (Kamari, Shaish et al. 2011). Furthermore, IL-1β production was inhibited in TLR9-deficient mice, which exhibited less steatohepatitis and liver fibrosis, as well as IL-1R knockout mice (Miura, Kodama et al. 2010). IL-1β-deficient mice exhibited mild adipose proinflammation and a significant reduction in adipose tissue macrophage lipid content (Nov, Shapiro et al. 2013).

IL-10 is considered an anti-inflammatory factor, and its secretion during high-fat feeding prevents hepatic steatosis but does not improve insulin sensitivity (den Boer, Voshol et al. 2006). In humans, *Esposito* and co-workers showed an inverse correlation between IL-10 levels and metabolic syndrome in obese women, suggesting a potential IL-10-mediated benefit in metabolic syndrome patients also affected by MASLD (Esposito, Pontillo et al. 2003). An overabundance of lipid accumulation in hepatocytes induces the secretion of IL-11 protein, and autocrine IL-11 activity leads to hepatocyte death and underlies the transition from MASLD to MASH (Dong, Viswanathan et al.

2021). IL-32 plays a key role in the pathogenesis of MASLD, mediating IR and regulating cholesterol homeostasis, and its expression is significantly elevated in the liver of MASLD patients (Dali-Youcef, Vix et al. 2019). IL-33 is an "alarmin" released from hepatocytes during cell death, and the alarm function is mediated by the release of large amounts of the active form of IL-33, which affects the recruitment and activation of suppression of tumorigenicity 2 (ST2) receptor positive target immune cells in the liver (Arshad, Piquet-Pellorce et al. 2012).

TNF-α is an inflammatory factor synthesized by macrophages/monocytes or other cells/tissues in response to acute inflammation, exerting its activity across multiple cell types. In the liver, TNF-α is secreted directly by hepatocytes and Kupffer cells and indirectly by abdominal fat, resulting in hepatocyte apoptosis (Montecucco and Mach 2008). A growing number of studies showed that TNF-α plays a pivotal role and is elevated in MASH. In fact, the degree of liver fibrosis in MASH patients showed a positive correlation with TNF-α expression (Lesmana, Hasan et al. 2009). Another investigation similarly evidenced elevated *TNF-α* gene expression in both the liver and adipose tissue of MASH patients with significant fibrosis compared to patients with mild or no fibrosis (Crespo, Cayn et al. 2001). The relationship between TNF-α and IR in obesity was first described by *Hotamisligil et al.* (Hotamisligil, Shargill et al. 1993). This study demonstrated that adipose tissue triggers inflammation and IR through TNF-α expression. Furthermore, supporting the essential role of TNF-α in IR, increased TNF-α expression was observed in adipose tissue of different animal models of obesity

and diabetes (Hotamisligil, Shargill et al. 1993). TNF-α or TNFR deficiency led to significantly improved insulin sensitivity in diet-induced and genetic (*ob/ob*) animal models of obesity (Uysal, Wiesbrock et al. 1997). Likewise, the efficacy of anti-TNF-α antibody was demonstrated against necrosis, inflammation, and fibrosis in an experimental model of methionine-choline-deficient (MCD) diet-induced MASH (Koca, Bahcecioglu et al. 2008). Despite the positive effects of TNF-α inhibition in animal models of MASH, the association of TNF-α with IR and MASH remains controversial. Several studies found no direct correlation between IR and TNF-α, casting doubts about its true biological activity (Lucero, Zago et al. 2011). The detrimental impacts of TNF-α in the liver might be modulated by additional soluble mediators, including adiponectin, leptin, and IL-6.

Apart from the above, hepatocytes can also generate several chemokines to recruit immune cells in response to liver injury, such as chemokine (C-C motif) ligand 2 (CCL2) (also known as monocyte chemoattractant protein 1, MCP-1) and C-X-C motif chemokine ligand 1 (CXCL1). CCL2 is mainly derived from damaged hepatocytes and activated Kupffer cells, while HSCs and hepatic SECs also secrete CCL2 (Saiman and Friedman 2012). The increase of CCL2 expression in the liver facilitates the recruitment of myeloid cells, which in the presence of dietary fat induces hepatosteatosis (Obstfeld, Sugaru et al. 2010). Hepatocytes produce CXCL1 in response to necrotic cell challenge via Kupffer cell sense DAMPs and release TNF-α to activate the NF-κB pathway, which ultimately leads to dead cell clearance (Su, Li et al. 2018).

3.4. Hepatic stellate cells (HSCs) in liver fibrosis

Different hepatotoxic substances and mechanisms may induce parenchymal cell injury, leading to fibrogenesis. Fibrosis is usually benign during wound healing and maintains tissue integrity, but persistent and progressive fibrosis can be pathogenic, which ultimately leads to the main cause of mortality in MASH patients (Heyens, Busschots et al. 2021). Several cell types are involved in the progression to MASH, but the most notable are hepatic myofibroblasts (MFBs), initially derived from HSCs, portal fibroblasts (PFs), and mesothelial cells. Notably, HSCs activation and fibrosis are closely related to many signaling pathways such as TGF-β, hedgehog, inflammasome (NLRP3)-caspase 1, and Wnt/β-catenin. In addition to the above, it was simultaneously proposed that hepatic epithelial cells, and perhaps even endothelial cells, might be an extra source of hepatic MFBs through the process of epithelial-mesenchymal transition (EMT) or endothelial-mesenchymal transition (EndMT) (Figure 7) (Dewidar, Meyer et al. 2019).

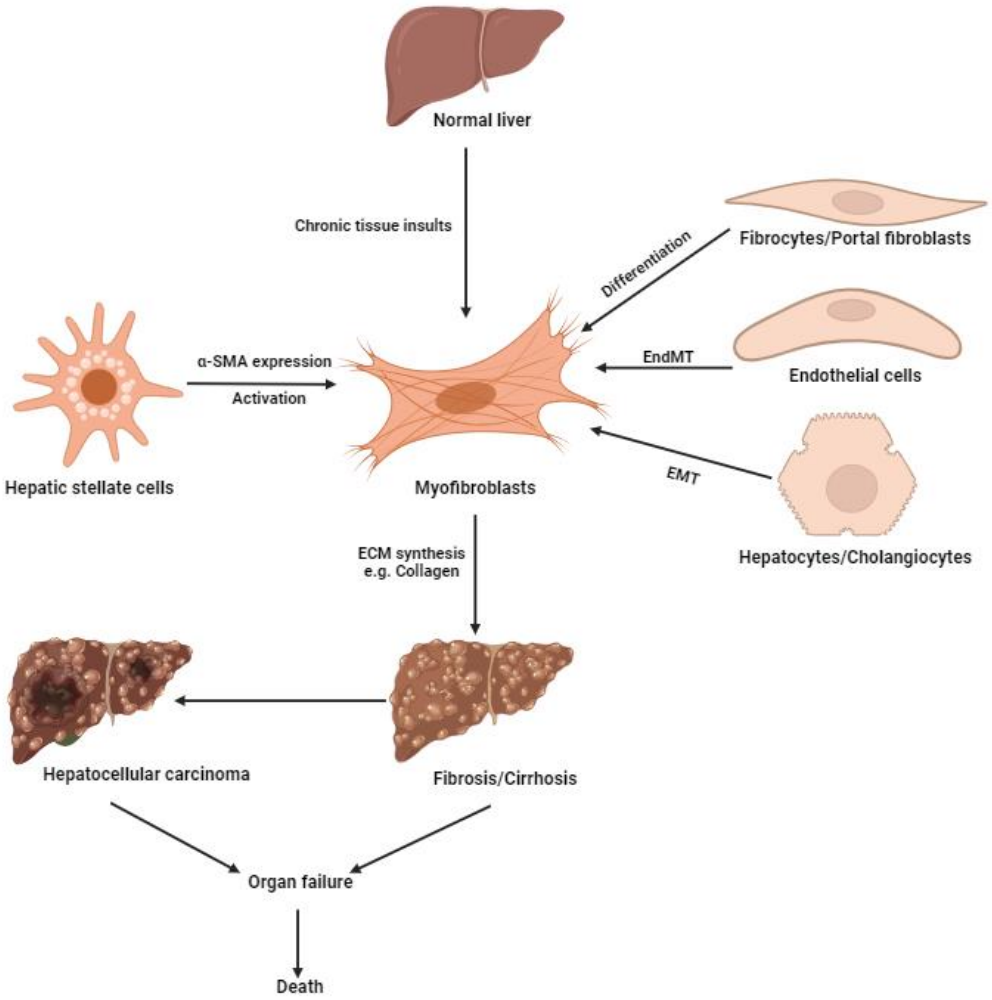

Figure 7. Activation of hepatic stellate cells (HSCs) and origin of myofibroblasts (MFBs) in chronic liver diseases. During activation, HSCs lose intracellular lipid droplets, develop a fibroblast-like shape, and express large amounts of α-smooth muscle actin (α-SMA) and extracellular matrix proteins (ECM). Also, endothelial cells and epithelial cells, i.e., hepatocytes and cholangiocytes, might contribute to liver MFBs pool through an epithelial-mesenchymal transition (EMT) and endothelial-mesenchymal transition (EndMT), respectively (Dewidar, Meyer et al. 2019).

In general, HSCs are in a quiescent non-proliferative state, with a star-shaped appearance that exhibits the ability to store containing vitamin A as retinyl palmitate (Tsuchida and Friedman 2017). HSCs activation involves a complex cascade of events,

which includes fibrotic mediators or cell-cell interactions that promote HSC activation and transformation into MFBs by triggering different signaling cascades. The novel method of single-cell RNA sequencing has been employed to delineate the activation profiles of HSCs/MFBs, revealing inherent heterogeneity among these cell populations (Krenkel, Hundertmark et al. 2019).

The differentiation of HSCs into MFBs is the most significant type in liver fibrosis, accompanied by losing retinoid content, the excessive expression and accumulation of the contractile protein α-smooth-muscle actin (α-SMA) and extracellular matrix (ECM) components, which includes the secretion of fibrillar collagens (collagen I and III) (Figure 7) (Tsukamoto, Zhu et al. 2011). Generally, short-term tissue repair can reverse MFBs to differentiated cells. For example, following HSC activation, matrix metalloproteinases (MMPs) such as MMP-9 significantly increase and bind to collagen III, leading to the breakdown of ECM products (Veidal, Vassiliadis et al. 2010). However, MMPs are inhibited by tissue inhibitors of metalloproteinase (TIMPs), and abundant expression of TIMP1 causes MMP/TIMP imbalance in CCl_4-induced mice, thereby promoting ECM synthesis and fibrosis (Yoshiji, Kuriyama et al. 2000). Likewise, profibrogenic molecules such as leptin stimulate the expression of TIMP1 and collagen I and represses the production of MMP1 in HSCs.

3.4.1. The transforming growth factor β (TGF-β) pathway in liver fibrosis

3.4.1.1. TGF-β family

TGF-β members, consisting of 33 genes in mammals, encompass TGF-βs, growth and differentiation factors (GDFs), nodal proteins, activins, and bone morphogenetic proteins (BMPs) (Table 3) (Heldin and Moustakas 2016). In contrast to the numerous TGF-β ligands, there are fewer receptors (TβRI and TβRII) and downstream intracellular effectors [suppressor of mothers against decapentaplegic (SMAD) proteins] to mediate the transduction of intracellular signaling. There are seven type I receptors and five type II receptors in mammalian, and type I receptors induce receptor-regulated SMAD family (R-SMADs) by phosphorylating two C-terminal serine residues. TGF-β induces SMAD2 and SMAD3 phosphorylation to play a central role in pathological processes, whereas BMP phosphorylates SMAD1, SMAD5 and SMAD8 (Morikawa, Derynck et al. 2016). SMAD4, also known as co-SMAD, is not directly phosphorylated or binds to the receptor complex, but it interacts with phosphorylated R-SMAD and they translocate to the nucleus as heterotrimers.

Subfamily	Members of the family	Biological function	Receptor
Activin/ Inhibin	Activin A/B, Inhibin C/E/A, Nodal, Lefty1, Lefty 2	Involved in mesoderm induction, inflammation, or immunity, required for body pattern determination and cell stemness.	Alk4, Alk7, Cripto, ActR-II/IIb

TGF-β	TGF-β1, TGF-β2 and TGFβ3	Proliferation and differentiation regulators in multiple cell types. Dual role function in cancer progression.	Alk1/Alk5, TβR-II
BMPs and GDFs	BMP-2/4, BMP-5/6/7/8, BMP-9/10, GDF-5/6/7, GDF-8/11, GDF-1/3, GDF-10/BMP/3	BMPs can induce bone growth with different potency depending on the cell type. Involved in heart development, skeletogenesis, neurogenesis, or muscle growth control.	Alk1/2/3/4/5/6, Cripto, BMPR-II, ActR-II, ActR-IIB
Distant members	Anti-muellerian hormone (AMH), GDNFs (GDNF, Artemin, Persephin, Neurturin), GDF15	GDNFs act as neurotrophic factors that promote neuron survival and control dopamine uptake. GDF15 is an anti-inflammatory cytokine with no affinity to other family receptors, becoming the most distant member.	Alk3/6, GFRa, GFRAL, AMHR-IIret

Table 3. TGF-β subfamily members.

TGF-βs are synthesized in the ribosomes and fold in the ER to form latent precursor proteins that are proteolytically processed by furin-like proteases, resulting in the formation of an N-terminal precursor remnant (LAP) and a C-terminal polypeptide (mature TGF-β) (Figure 8) (Tzavlaki and Moustakas 2020). After cleavage,

the LAP remains non-covalently bound to the mature TGF-β to form a complex named the small latent complex (SLC) and keeps TGF-βs latent (Ten Dijke and Arthur 2007). Subsequently, the SLC is covalently bound to the large TGF-β binding protein (LTBP), thereby forming the large latent complex (LLC) (Robertson and Rifkin 2016). Finally, the complex can be cleaved by various proteases to release active TGF-β. All TGF-β isoforms undergo this process to be secreted as latent complexes, whereas some BMPs and activins are not released as latent complexes (Derynck and Budi 2019). There are three TGF-β isoforms: TGF-β1, -β2, and -β3. TGF-β1 expression and activation exacerbate fibroblast proliferation and ECM protein deposition. Similar to TGF-β1, TGF-β2 shows robust fibrotic activity, while TGF-β3 seems to exhibit antifibrotic activity in certain tissues (Walton, Johnson et al. 2017).

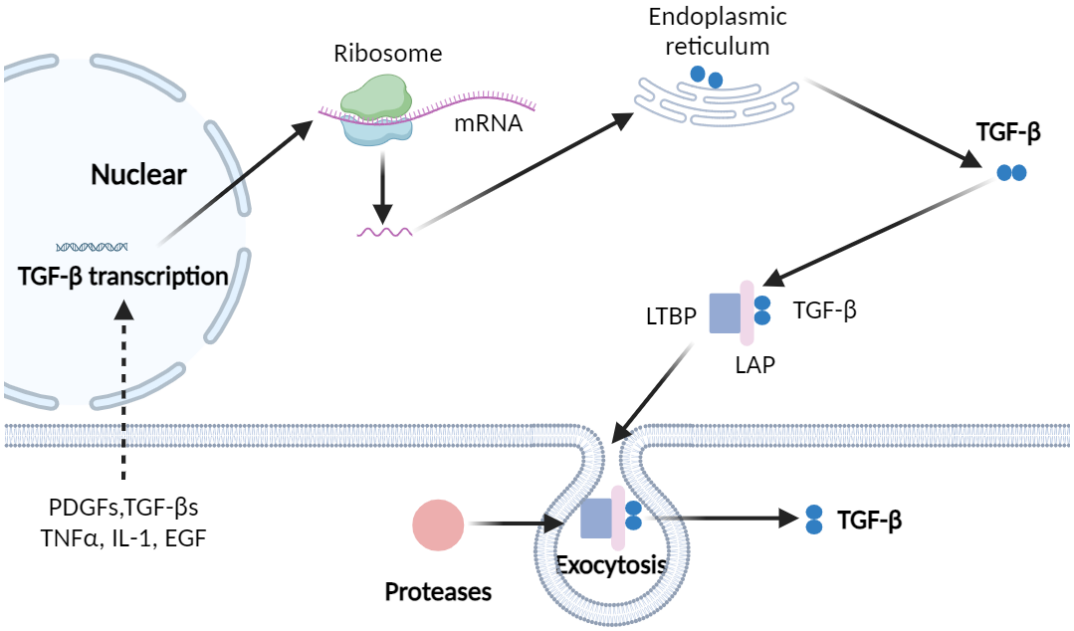

Figure 8. Biosynthesis and extracellular deposition of TGF-β. Ribosomes attached to the endoplasmic reticulum (ER) translate TGF-β mRNA into TGF-β protein. This is followed by a

series of biochemical events leading to the formation of a large latent complex (LLC), which can eventually be cleaved by a variety of proteases, releasing the active TGF-β.

3.4.1.2. TGF-β pathway

TGF-β binds to TβR-II, forming a receptor complex, and subsequently recruits and phosphorylates TβR-I in the Gly-Ser-rich (GS) domain, resulting in a tetrameric receptor complex (Meng, Nikolic-Paterson et al. 2016). The activation of kinase domains within the receptor complex potentiates phosphorylation cascades acting on SMADs (i.e., SMAD2 and SMAD3) transcription factors (Figure 9). After being activated by phosphorylation, pSMAD2 and pSMAD3 interact with SMAD4 (also known as deleted in pancreatic carcinoma locus 4, DPC4) to form heterocomplexes that translocate into the nucleus. There, they bind to the SMAD binding element (SBE) and activate transcription of multiple genomic levels (Chung, Chan et al. 2021), including α-SMA, collagens, fibronectin, and plasminogen activator inhibitor-1 (PAI-1). In the absence of SMAD4, R-SMADs can induce the activation of a few TGF-β target genes. SMAD3 shows a weak DNA-binding affinity whereas SMAD2 does not directly bind to DNA (Morikawa, Koinuma et al. 2013); consequently, these heterocomplexes typically interact with extra transcriptional co-activators to stabilize the transactivation complexes.

The p300/cAMP-response-element-binding-protein-binding protein (CBP)-

associated factor (P/CAF) augmented the transcriptional responses induced by TGF-β/SMAD3, a process further bolstered by co-activators histone acetyltransferase p300 and SMAD4. Furthermore, P/CAF might thus engage in the activation of SMAD-mediated transcriptional responses either autonomously or in collaboration with p300/CBP (Itoh, Ericsson et al. 2000). Likewise, p300/CBP modulates transcription by enhancing SMAD3 transactivation in response to TGF-β receptor activation in a SMAD4/DPC4-dependent manner, which acts as a transcriptional co-activator (Feng, Zhang et al. 1998). SMAD2-mediated transcription involves the recruitment of p300 and presents changed substrate specificity, particularly in acetylated nucleosome histone H3 (Ross, Cheung et al. 2006).

SMAD7, an inhibitory SMAD (I-SMAD), is a nuclear protein secreted from the nucleus to the cytoplasm and is a predominant negative regulator of the TGF-β signaling pathway. For example, SMAD7 not only inhibits phosphorylation of SMAD2/SMAD3 by TGF-β-receptor polymers, but also induces degradation of TGF-β-TβRI and SMAD2/SMAD3, thus disrupting the heterodimerization of SMAD2/SMAD3 with SMAD4 (Hu, He et al. 2021). Furthermore, SMAD7 combines with SBE-containing DNA sequences, thereby influencing the assembly of functional SMAD-DNA complex triggered by TGF-β signaling (Li 2015). Hence, regulating the stability or degradation of SMAD7 influences TGF-β signaling activity. For instance, p300 induces acetylation at the N-terminus of SMAD7 to prevent subsequent ubiquitination, which in turn protects against degradation of the TGF-β pathway

(Grönroos, Hellman et al. 2002).

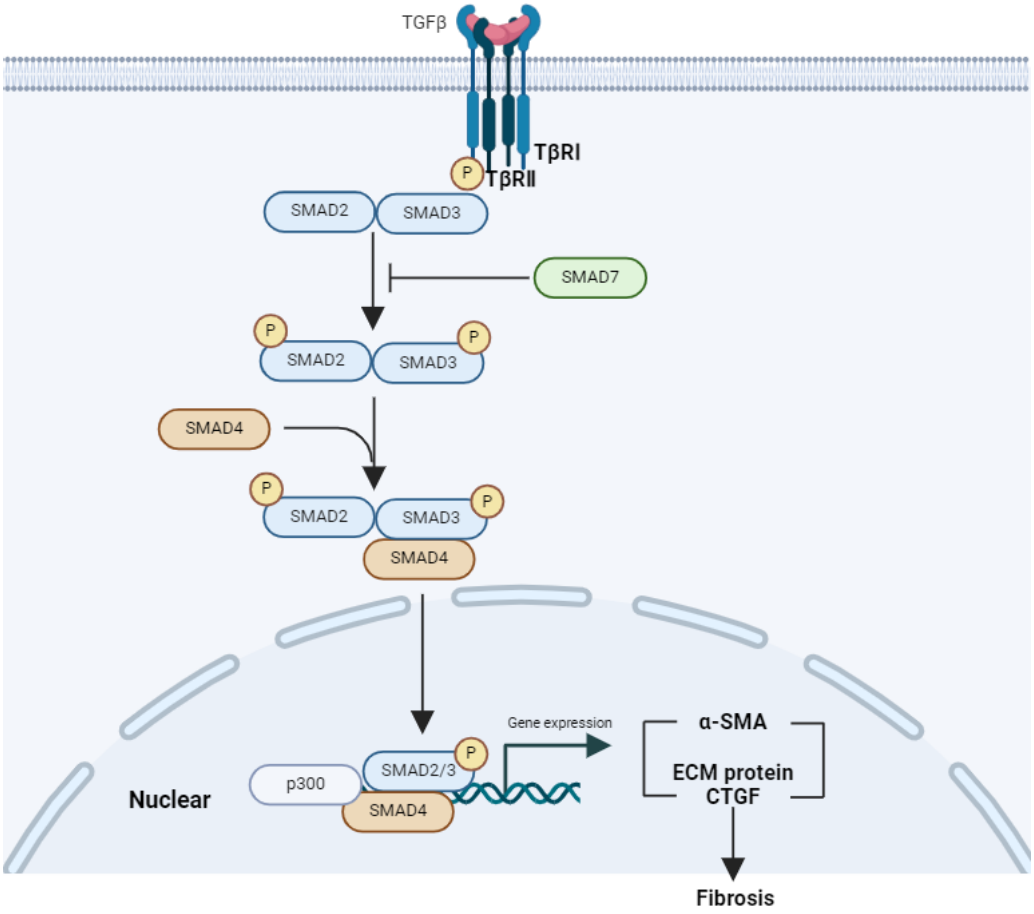

Figure 9. Canonical pathway of TGF-β signaling. In a canonical signaling cascade, activated TGF-β-TβRI leads to phosphorylation of SMAD2/3, which then binds to SMAD4 and translocates to the nucleus to induce gene transcription. In a negative feedback loop, SMAD7 inhibits TGF-β signaling by providing competition of TβRI, blocking phosphorylation and activation of SMAD2.

Besides, emerging evidence supports that there are non-canonical signaling pathways (Figure 10) activated by TGF-β including mitogen-activated protein kinase (MAPK)/extracellular signal-regulated kinase (ERK), mammalian target of rapamycin

(mTOR)/phosphatidylinositol-3-kinase (PI3K)/V-Akt murine thymoma viral oncogene homolog (AKT), and Rho-like guanosine triphosphate (GTP)ase pathways. The TGF-β non-canonical pathway offers an extensive platform for intracellular crosstalk. For instance, R-SMAD signaling to the nucleus may undergo interactions with other pathways, as demonstrated by the capacity of SMAD2/SMAD3 to activate ERK and protein kinase A (PKA).

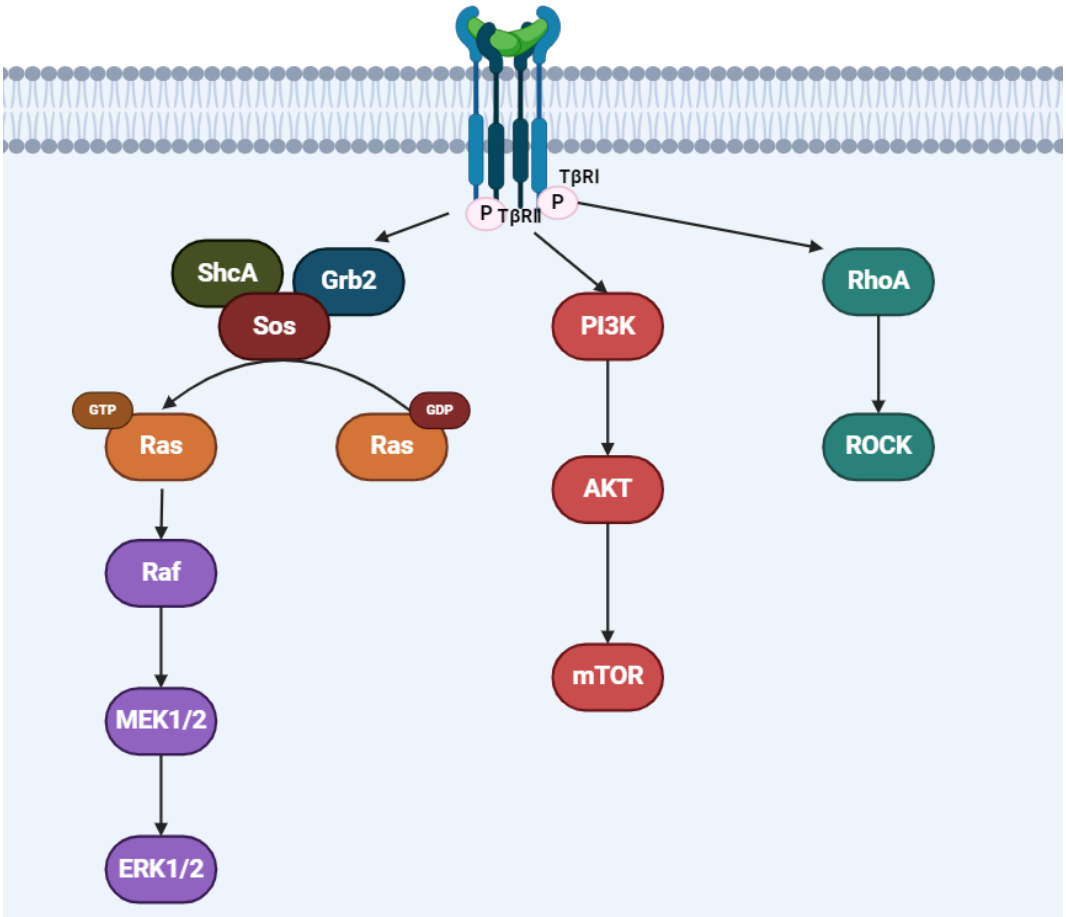

Figure 10. Non-canonical pathway of TGF-β signaling. Phosphorylation of TGF-β type I and type II receptors also activates downstream non-canonical pathways, including Rho, PI3K/Akt, and Grb2/SOS signaling, in a SMAD-independent manner (Chung, Chan et al. 2021).

After activation and phosphorylation of TβRI/TβRII by TGFβ, induced src homology and collagen A (ShcA) tyrosine phosphorylation promotes ShcA/growth factor receptor-bound protein 2 (Grb2)/son of sevenless (Sos) complex formation and promotes the exchange of guanosine diphosphate (GDP) to GTP for inducing GTPase Ras activation (Lee, Pardoux et al. 2007). The formation of a small GTPase Ras causes the recruitment of Raf, a MAP kinase kinase kinase (MAP3K), leading to the activation of ERK1/2 via MEK1/2, which in turn triggers the genetic regulation (Figure 11). For instance, the stimulation significantly increased transcriptional factors such as Fos-related antigen 2 (Fra-2) expression and induced DNA binding of Fra-2 in a phosphorylated ERK-dependent manner (Reich, Maurer et al. 2010).

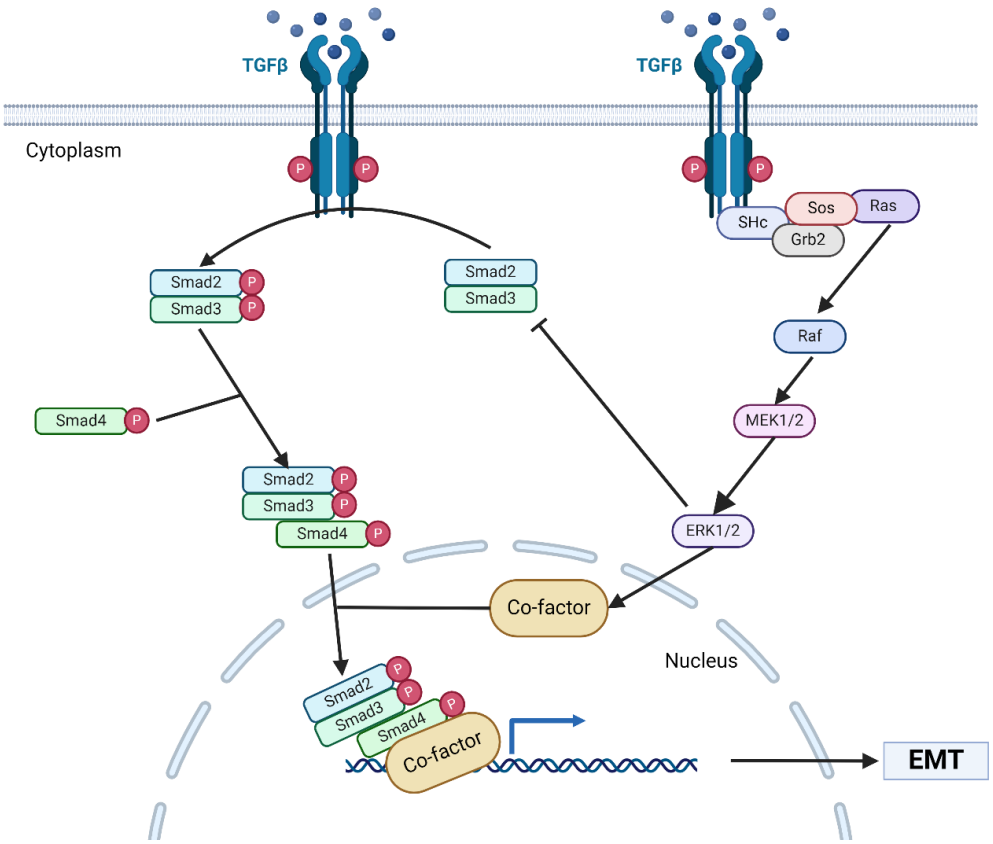

Figure 11. The ERK non-SMAD pathway. Phosphorylation of tyrosine residues in TβRI/TβRII leads to the recruitment of Grb2/Sos, which activates ERK through Ras, Raf, and its downstream MAPK cascade, and then ERK controls EMT through its downstream transcription factors that work together with SMADs to regulate target gene transcription (Zhang 2009).

Mounting evidence has revealed that PI3K/AKT plays an important role in TGF-β signaling. PI3K can be activated by TGF-β via induction of physical association between TβRI receptor and p85 (Yi, Shin et al. 2005), which induces activation of AKT. Subsequently, the activation PI3K/AKT pathway then regulates the transcription reactions via mTOR/S6K, which in turn interacts indirectly with SMAD-mediated transcriptional processes in the EMT process (Zhang 2009). In addition, AKT has the ability to antagonize TGF-β-induced apoptosis and growth arrest by suppressing the activation of FoxO transcription factor.

The Rho-like GTPases, including RhoA, Rac and cell division control protein 42 (Cdc42) contribute to the regulation of dynamical cytoskeletal organization, cell movement, and genetic expression via a variety of effectors such as Rho-associated protein kinases (ROCKs) (Jaffe and Hall 2005). Similar to the ERK/MAPK pathway, RhoA and ROCK can be regulated by TGF-β stimulation through either SMAD-independent or SMAD-dependent manner to induce stress fiber formation in the EMT progress (Zhang 2017). Par6 is a scaffolding protein that binds to TβRI at tight junctions

and modulates cell polarity in polarized epithelial cells. Interestingly, TβRII possesses the capability to directly induce the phosphorylation of Par6 (Figure 12), consequently facilitating the recruitment of the E3 ubiquitin ligase SMAD ubiquitination regulatory factor 1 (Smurf1), which targets RhoA for proteasomal degradation (Ozdamar, Bose et al. 2005). Additionally, TGF-β also recruits Cdc42 or Rac within the TGF-β receptor complex, thereby activating p21-activated kinase (PAK) signaling (Wilkes, Murphy et al. 2003), which is implicated in tight junction dissociation and cell migration during the EMT process.

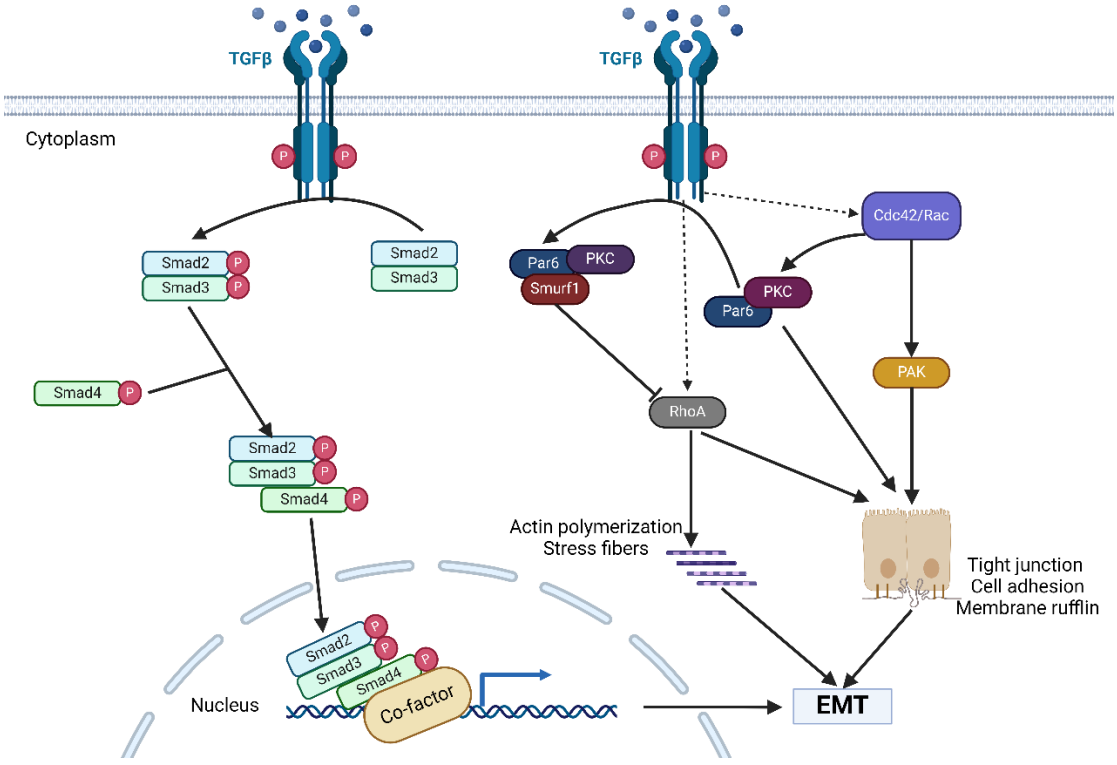

Figure 12. TGF-β-induced regulation of the Rho family of small GTPases. RhoA can be activated by TGF-β via either SAMD-dependent or independent routes to induce actin stress fiber formation during EMT (Zhang 2009).

3.4.1.3. The TGF-β/SMAD pathway in liver fibrosis

TGF-β1 plays a central role in fibrogenesis and is thought to be a mediator of fibrosis in numerous liver diseases, especially in chronic liver injury. The *Tgfb1* gene is significantly overexpressed in patients with MetALD and cirrhosis (Chen, Li et al. 2002). Moreover, TGF-β1 levels were markedly elevated in patients with MASLD and positively correlated with this condition (Das and Balakrishnan 2011). Animal models of MASH exhibit HSC activation and collagen deposition accompanied by elevated *Tgfb1* gene expression (Stärkel, Sempoux et al. 2003). The increased expression and activation of TGF-β1 released by necrotic hepatocytes leads to trans-differentiation of adjacent quiescent HSCs into MFBs, thereby producing ECM (Liu, Hu et al. 2006).

Notably, TGF-β1 promotes fibrogenesis by 1) inhibiting MMP expression and promoting the repression of ECM degradation by TIMP, 2) activating SMAD-dependent/non-SMAD-dependent mechanisms to induce ECM production, 3) promoting EMT-induced MFBs formation (detailed description in the next section).

In addition to the ECM, activated HSC increases MMP-2 and -9 expression, which act as regulators of ECM accumulation, as well as increased TIMP expression. Generally, the synthesis and accumulation of ECM are tightly regulated by MMP-mediated turnover of ECM proteins, and the activity of MMP is in turn monitored by TIMP, with this coordination being essential for organ homeostasis (Tsukada, Parsons

et al. 2006). However, when the liver is challenged by pro-fibrotic injury, the MMP/TIMP ratio is unbalanced. In particular, MMP-2, which is significantly expressed in activated HSC, induces HSC migration and proliferation through TGF-β1-mediated signaling pathways, further promoting the fibrotic process (Yang, Zeisberg et al. 2003). Interestingly, activated HSC is a primary source of TIMP-1 and -2, and it has been reported that TIMP-1 expression inhibits apoptosis of activated HSC *in vitro* (Murphy, Issa et al. 2002), thereby abrogating the degradation of ECM by MMP.

It has been shown that SMAD3 and SMAD4 are crucial inducers within the context of hepatic fibrosis, while SMAD2 and SMAD7 confer antifibrotic protection (Xu, Liu et al. 2016). Many fibrogenic genes (collagen) and markers (α-SMA and E-cadherin) are dependent on SMAD3, which binds directly to the DNA sequences that regulates these target genes (Latella, Vetuschi et al. 2009). In addition, TGF-β inhibits ECM degradation by phosphorylating SMAD3 to induce TIMP-1, and overexpression of SMAD3 inhibits MMP-1 activity in fibroblasts (Xu, Liu et al. 2016). Interestingly, the knockdown of SMAD2 in LX-2 cells increased SMAD3 phosphorylation, nuclear translocation, and type I collagen promoter binding, thereby enhancing SMAD3-dependent liver fibrosis (Zhang, Liu et al. 2015). According to the above-mentioned, TGF-β exerts its biological effects through activation of the downstream mediators SMAD2/SMAD3, while being negatively regulated by the inhibitory SMAD7 (Lan and Chung 2011). SMAD7 expression was significantly reduced in fibrotic livers during TGF-β1-induced HSC activation and in MFB-like cells across the course of chronic

liver injury (Bian, Huang et al. 2014). Moreover, disruption of the *Smad-7* gene enhances CCl_4-dependent hepatic injury and fiber formation in mice (Hamzavi, Ehnert et al. 2008).

Leptin, a circulating adipogenic hormone with pro-fibrogenic effects, is essential for the induction of TGF-β1 activity in the setting of chronic liver injury (Leclercq, Farrell et al. 2002). Leptin upregulates microRNA21, which targets and inhibits SMAD7 to promote SMAD2/3-SMAD4 co-localization in the nucleus (Arab, Arrese et al. 2018). Likewise, leptin activates HSC by mediating the downregulation of *Ppar-γ* gene expression, an antifibrotic nuclear receptor that reverses HSC activation and sustains HSC quiescence (Zhou, Jia et al. 2009). During the progression of MASH by feeding mice with a MCD diet, HSC was progressively activated, along with the decrease in hepatic PPAR-γ expression and activation of the TGF-β/SMAD signaling pathway in the liver (Ni, Li et al. 2021). This study also demonstrated that PPAR-γ agonists reduce the expression of TGF-β1 and p-SMAD2/3 while increasing SMAD7 expression. Treatment of activated HSCs with forced expression of PPAR-γ reversed MFBs to differentiated cells and restored lipid and vitamin A stores (Hazra, Xiong et al. 2004).

In addition, PPAR-γ is involved in the crosstalk between TGF-β1 and other signaling pathways. For example, TGF-β1 significantly down-regulated PPAR-γ

expression and activity in cultured HSCs through the β-catenin/Wnt pathway and promoted β-catenin protein expression and stability via the ERK1/2-glycogen synthase kinase-3β (GSK-3β) axis (Qian, Niu et al. 2012). Along this line, activated HSC displays enhanced signaling of canonical Wnt (Wnt3a and Wnt10b) (Cheng, She et al. 2008), which effectively inhibits adipocyte differentiation by suppressing the adipogenic transcription factors C/EBP-α and PPAR-γ (Ross, Hemati et al. 2000).

3.4.2. The epithelial to mesenchymal transition (EMT) process and fibrosis

It is well known that EMT is a process by which polarized epithelial cells are transformed into mesenchymal cells and acquire migratory capacity. When EMT dominates mesenchymal-to-epithelial transition (MET), liver repair occurs primarily through fibrosis, whereas when MET exceeds EMT, normal epithelial proliferation and fibrosis are reduced (Chen, Fan et al. 2020). Thereby, EMT is a potential target for antifibrotic strategies, since epithelial cells can acquire fibroblastic phenotype and contribute to fibrogenesis (Yu, Li et al. 2018). EMT is classified into three types: type I EMT is mainly associated with the development of cellular bioembryos, type II EMT is involved in organ fibrosis, damage repair and tissue regeneration, and type III EMT is closely related to tumor invasion and metastasis (Kalluri and Weinberg 2009).

Furthermore, a portion of EMT refers to an intermediate phenotype of cellular transformation, with a progressive loss of epithelial markers (E-cadherin, ZO-1) and

progressive mesenchymal markers such as vimentin and S100 calcium-binding protein A4 (S100A4, also known as fibroblast-specific protein 1; FSP1) (Figure 13) (Kalluri and Weinberg 2009).

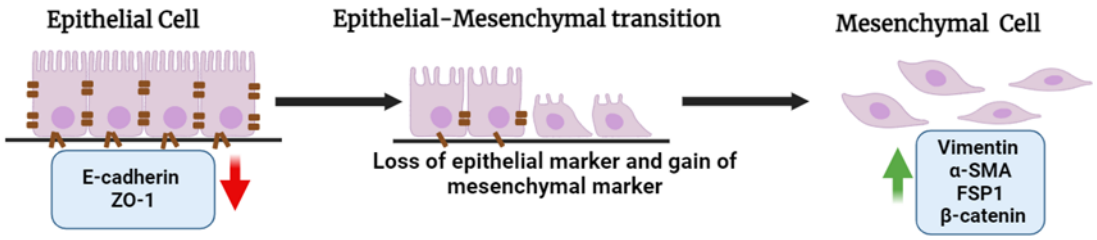

Figure 13. Schematic cellular processes during EMT. The EMT process requires intercellular contacts, apical-basal polarity, and loss of adhesion molecules (e.g., E-cadherin). Expression of mesenchymal markers is increased in transformed epithelial cells.

A previous study showed that 45% of S100A4-positive fibroblasts originated from hepatocytes EMT in CCl_4-induced liver fibrosis (Zeisberg, Yang et al. 2007). Indeed, S100A4 is considered an inducer of the EMT program (Li, Wang et al. 2020). Interestingly, S100A4-knockout mice fed a MCD diet show attenuated liver fibrosis and inflammation, as well as an inhibition of hepatocyte apoptosis (Helfman, Kim et al. 2005). S100A4 also seems to play a role in liver tumorigeneses, since S100A4-deficient mice develop significantly fewer and smaller liver tumor nodules, while showing decreases in liver fibrosis and the expression of stem cell markers in the HCC tissues (Kalluri and Weinberg 2009). In fact, increased S100A4 protein levels correlate with poor prognosis in several cancers, with S100A4 promoting the development of

metastasis in mouse models of cancer (Helfman, Kim et al. 2005). The effects of S100A4 have been associated with the formation of oligomers of this protein, which is stimulated by oxidation (Garrett, Varney et al. 2006). Moreover, S100A4 does not possess enzymatic activity, but instead interacts with target proteins and regulates their activity. Intracellular targets of S100A4 include p53 and non-muscle myosin IIA (NMIIA) (Santamaria-Kisiel, Rintala-Dempsey et al. 2006). Overall, these findings point to S100A4 as a regulator of both fibrogenesis and tumorigeneses in the liver.

Studies have shown that critical intracellular EMT signaling pathways involve the TGF-β/non-SMAD signaling pathway, as well as the Notch and hedgehog pathways. Importantly, TGF-β is a key regulator of fibrogenesis and EMT, and TGF-β can directly activate neighboring hepatocytes via SMAD signaling to induce EMT, leading to ECM accumulation and fibrosis (Xue, Wu et al. 2013). In addition, several EMT-related signaling pathways facilitate the expression of transcription factors, such as Snail1, Snail2 (Slug), and ZEB1, with Snail proteins being the most common, which repress the expression of E-cadherin and other epithelial markers, and upregulate mesenchymal markers (Cano, Pérez-Moreno et al. 2000). TGF-β induces Snail and activates the SMAD2/3 pathway, mediating phenotypic changes and plasticity toward EMT (Kaimori, Potter et al. 2007).

In conclusion, multiple cells of the liver are converted to MFBs by EMT and are

coordinately regulated by various signaling pathways. Hepatic fibrogenesis is a complex process, and the activation and EMT of HSCs into MFBs are usually considered to be the most critical processes.

3.5. AMP-activated protein kinase (AMPK) pathway in hepatic metabolism

AMPK, a highly evolutionarily conservative serine/threonine kinase across all eukaryotes, has attracted intense interest because of its vital role in the modulation of energy homeostasis and acts as a signaling hub to balance nutrient supply and energy demand in the cell. AMPK protects cells from ATP depletion and inhibition of ATP synthesis. In general, AMPK is sensitive to the relative change in AMP:ATP and ADP:ATP ratios and restores energy homeostasis by inhibiting non-essential anabolic ATP-consuming processes, while promoting ATP-generating catabolic pathway (Garcia and Shaw 2017). Moreover, AMPK modulates cellular energy metabolism via the phosphorylation of central enzymes in carbohydrates, lipids, and proteins for short-term impact, and phosphorylation of transcription factors for longer-term regulatory effects (Cantó and Auwerx 2010).

Considering these properties, AMPK has attracted widespread attention as a therapeutic target for pathological conditions characterized by metabolic diseases, especially diabetes, but also obesity, inflammation, and cancer. It is now recognized that pharmacological activation of AMPK improves glucose homeostasis, lipids, and

blood pressure in insulin-resistant rodents.

3.5.1. Structure and regulation of AMPK

AMPK exists as a heterotrimeric enzyme consisting of a catalytic subunit α, a scaffolding β subunit, and a regulatory γ subunit. In mammals, the α subunit is encoded by two isoforms (α1 and α2), and the β and γ subunit are encoded by two (β1 and β2) and three isoforms (γ1, γ2, and γ3), respectively (Ross, MacKintosh et al. 2016).

The α subunit undergoes phosphorylation at Thr172 site by an upstream kinase, which is a process essential for its kinase activity, as well as the C-terminal region is required for binding to the β subunit (Figure 14). The C-terminal region of the β subunit forms a heterotrimeric complex by interacting with the α and γ subunits and contains a central carbohydrate-binding module (CBM), which is essential for the heterotrimeric complex formation. The γ subunit isoform encompasses a variable N-terminal region and features four consecutive repeats in its C-terminal region known as the cystathionine-β-synthase (CBS) motif. This motif serves as a binding site for the regulatory nucleotides AMP, ADP, and ATP (Yan, Zhou et al. 2018).

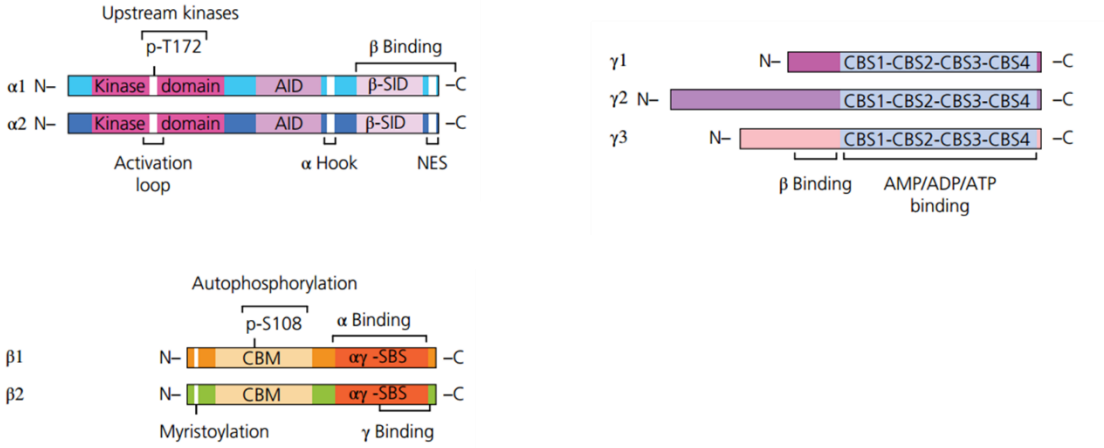

Figure 14. The Structure of AMPK. Schematic representation of AMPK subunit isoforms showing regions implicated in the regulation of AMPK activity. α subunits: AID, autoinhibitory domain; β-SID, β-subunit interacting domain; β subunits: CBM, carbohydrate-binding module; αγ-SBS, αγ-subunit binding sequence; γ subunits: CBS1, CBS2, CBS3, CBS4, cystathione β-synthase repeats; NES, nuclear export signal (Dufour and Clavien).

All of these subunits are encoded by separate genes and variable splice variants, resulting in a diverse collection of αβγ heterotrimer combinations. However, not all combinations are present in all tissues. It has been demonstrated that each heterotrimeric combination exhibits a different activation profile and phosphorylation profile in human skeletal muscle in response to physical exercise (Jensen, Wojtaszewski et al. 2009). In hepatocytes, immunodetection and chemical proteomics analyses revealed that only a limited number of AMPK heterotrimeric assemblies were present and that there were significant differences in abundance. In human hepatocytes, α1β2γ1 was identified as the predominant AMPK heterotrimeric complex, whereas in dog and rodent hepatocytes, α1β1γ1 and α1/α2β1γ1 complexes were predominantly expressed, respectively (Figure 15) (Stephenne, Foretz et al. 2011, Wu, Puppala et al. 2013).

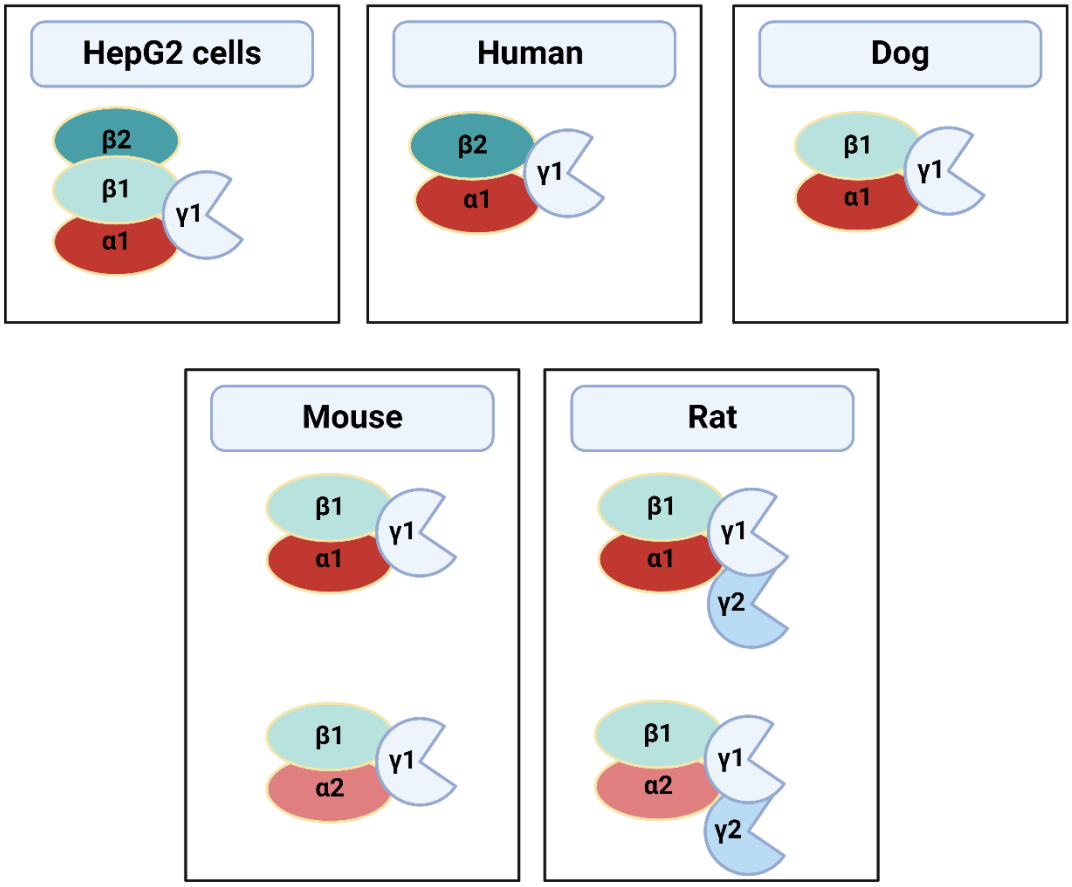

Figure 15. Expression of AMPK subunit isoforms in hepatocytes from different species. A cartoon of predominant AMPK heterotrimers in HepG2 cells and hepatocytes of human, dog, rat, and mouse (Dufour and Clavien).

The reversible phosphorylation of the Thr172 site in the activation loop of the structural domain of the α-subunit kinase, and the stimulated metastable binding of AMP to the CBS motif within the γ subunit, are two essential steps in the activation mechanism of AMPK (Viollet and Foretz 2015). In the normal energy state, ATP competitively binds to the γ subunit, which allows the phosphatase to enter Thr172. Under metabolic stress, the AMP:ATP and ADP:ATP ratios are elevated, resulting in the replacement of ATP by AMP and ADP at the two exchange sites on the γ subunit.

When AMP and ADP bind to γ-regulatory subunit causes AMPK to be metastable, which prevents Thr172 residue from entering phosphatase protein 2A (PP2A), thereby inhibiting dephosphorylation and inactivation of the enzyme (Figure 16). AMP, but not ADP, leads to further conformational activation of phosphorylated AMPK. In addition, this alteration in conformation also enables the upstream kinase with AMPK kinase (AMPKK) activity to phosphorylate the α subunit, thereby increasing the overall activation of AMPK. This phosphorylation process is primarily mediated by a complex involving two upstream kinases the tumor suppressor liver kinase B1 (LKB1) or Ca^{2+}/calmodulin-dependent protein kinase β (CaMKKβ) (Oakhill, Steel et al. 2011, Xiao, Sanders et al. 2011).

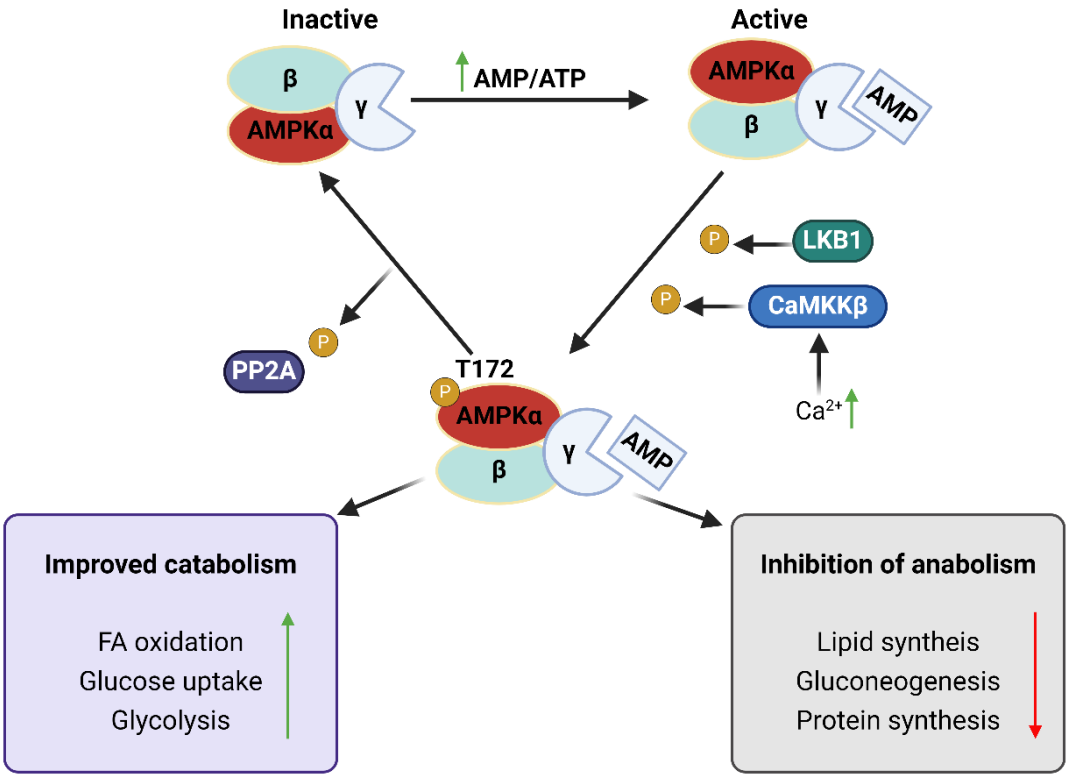

Figure 16. Allosteric and functional activation of AMPK. AMPK remains in an inactive state

when the AMP/ATP ratio is low. AMP binding to the γ subunit allosterically activates AMPK by inducing a conformational change in the enzyme, allowing LKB1 to phosphorylate AMPK and become functionally active. An increase in intracellular Ca^{2+} may also induce AMPK phosphorylation by CaMKKβ. Active AMPK positively regulates catabolic pathways that produce ATP and inhibit anabolic pathways that consume ATP (Aguilar Recarte 2021).

3.5.2. AMPK activation in the liver

AMPK activation attenuates MASLD primarily through three pathways: inhibiting hepatic lipogenesis, increasing hepatic FA oxidation, and enhancing mitochondrial functional integrity in adipose tissue (Smith, Marcinko et al. 2016). For instance, AMPK activation suppresses FA and cholesterol synthesis by downregulating the expression of adipogenic genes, such as *Srebp-1c*, *Acc*, and *Hmgcr* (Fang, Pan et al. 2022). Moreover, AMPK signaling pathway-related proteins not only effectively balance dietary influences and energy consumption, but also facilitate mitochondrial FA oxidation and mitochondrial biogenesis, which further enhance FA and glucose metabolism and ultimately inhibit the progression of fatty liver (Dahlhoff, Worsch et al. 2014). Recently, liver-specific *Ampk* gene activation has been established by genetic engineering techniques to decrease hepatic steatosis and inhibit the expression of inflammatory and fibrotic genes (Garcia, Hellberg et al. 2019). Consistent with this protective role of this kinase, liver-specific AMPK knockdown mediated caspase-6 activation, leads to exacerbated liver injury in the mouse MASH model (Zhao, Sun et al. 2020). These findings further support the role of AMPK as a potential preventive and therapeutic target for MASLD.

To test the potential of AMPK as a therapeutic target, reliable pharmacological tools are needed to specifically activate AMPK and decipher its cellular function. Unlike other pharmacological AMPK activators, A-769662 directly activates natural AMPK in cell-free assays, suggesting that it is a variant activator. Notably, there was no effect on cellular ATP levels and mitochondrial oxidative phosphorylation in A-769662-treated hepatocytes (Guigas, Sakamoto et al. 2009). In addition, A-769662 had the highest concentrations in the liver and relatively low concentrations in extrahepatic tissues (Cool, Zinker et al. 2006). Metformin is a first-line therapeutic agent for T2DM and most studies have attributed the hypoglycemic effect of metformin to inhibition of mitochondrial respiratory chain complex I activity. Pharmacological concentrations of metformin directly activate AMPK, whereas supra-pharmacological metformin concentrations (~5 mM) suppress glucose production by inhibiting mitochondrial respiratory chain complex I, thereby enhancing AMP and subsequently activating AMPK (Figure 17) (He and Wondisford 2015). However, a recent study has demonstrated that metformin reduces glycerol-derived hepatic gluconeogenesis by inhibiting complex IV activity (LaMoia, Butrico et al. 2022).

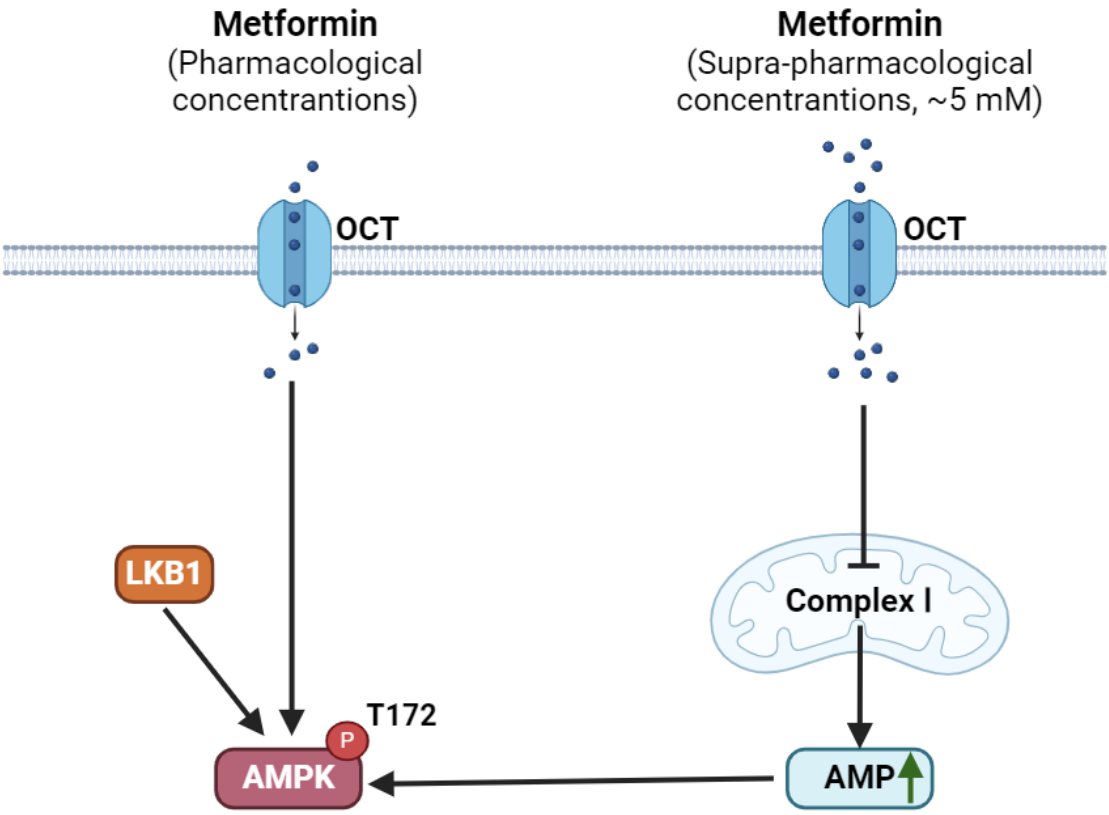

Figure 17. Metformin directly or indirectly causes AMPK activation mechanisms. At low metformin concentrations, AMPK is directly activated in the liver by promoting Thr172 phosphorylation of AMPKα, whereas at high metformin concentrations AMPK is activated indirectly by inhibition of mitochondrial respiratory chain complex I.

Besides, ERK1/2 has been reported to be involved in a negative crosstalk with AMPK in myotubes (Salvadó, Barroso et al. 2014). In fact, ER stress-mediated reduction of AMPK was restored when ERK function was blocked by its selective inhibitor U0126 (Hwang, Jeong et al. 2013). The negative regulatory mechanism between AMPK and ERK is a key therapeutic target for ER stress-induced IR.

3.6. Peroxisome proliferator-activated receptors (PPARs)

PPARs are a superfamily of nuclear hormone receptors that act as transcription factors in response to the binding of ligands. This family consists of three subtypes, namely PPAR-α, PPAR-β (also known as PPAR-δ), and PPAR-γ. Of these, PPAR-α was first identified in rodent hepatocytes, while PPAR-β/δ and PPAR-γ were subsequently discovered and characterized. PPAR-α is particularly abundant in the liver but is also found in muscle, bone, and heart (Figure 18), and is mainly associated with FA metabolism (Figure 19). PPAR-γ is expressed in white and brown adipose tissue, colon and spleen and plays a key role in the regulation of adipogenesis, energy homeostasis and lipid biosynthesis, as well as in lipoprotein metabolism and insulin sensitivity. PPAR-β/δ is expressed in most tissues of the body, but it is particularly abundant in the liver, intestine, kidney, and abdominal adipose tissue, all of which are involved in lipid metabolism (Grygiel-Górniak 2014).

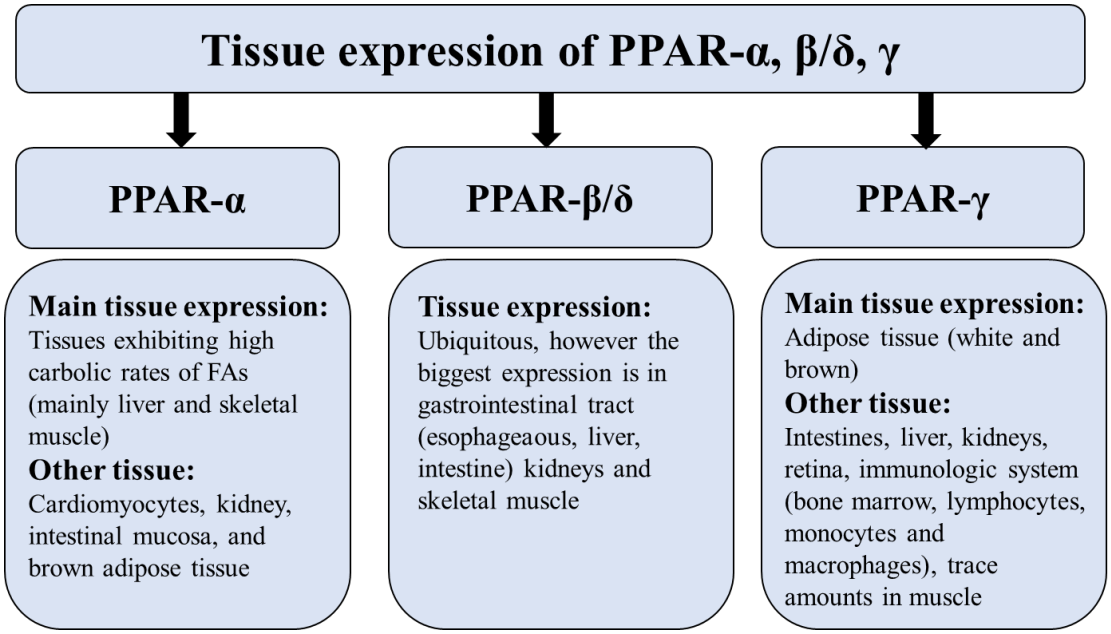

Figure 18. The expression of PPARs in specific tissues (Grygiel-Górniak 2014)**.**

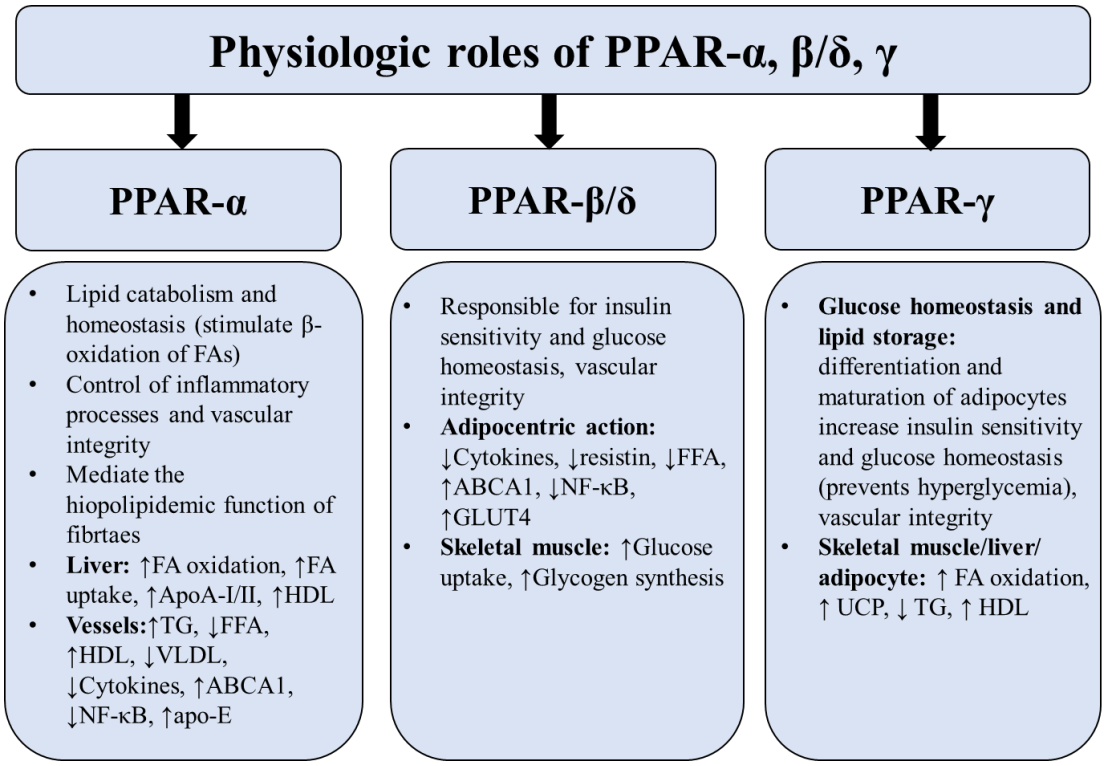

Figure 19. The role of PPARs (↑ - increase, ↓ - decrease)**.**

3.6.1. Structure of PPARs

As nuclear receptors, the structural domains of each subtype of PPAR are very similar. PPARs have four typical domain organizations: A/B, C, D, and E/F, which are the amino-terminal domain (A/B domain) containing ligand-independent activation function 1 (AF1), the central zinc-finger DNA-binding domain (DBD, C domain), the carboxyl-terminal ligand-binding domain (LBD, E/F domain) containing a ligand-dependent activation function (AF2), and a minor hinge region (D) connecting the DBD to the LBD (Figure 20a) (Poulsen, Siersbæk et al. 2012).

The DBD and the LBD are the most conserved regions among the three PPARs. PPARs form specialized heterodimers with retinoid X receptors (RXR) and bind to specific DNA sites consisting of direct repeats of hexametric sequences separated by a single base pair, located in the promoter/enhancer regions of target genes (Figure 20b) (Wang 2010). In the target gene, the peroxisome proliferator response element (PPRE) is a specialized DNA region that interacts with PPAR. The heterodimerization between PPAR and RXR is ligand-independent and dependent on the heterodimerization interface in the LBD and DBD of the two receptors. PPAR is activated by FAs and FA derivatives, and its activity is regulated by post-translational modifications (PTMs) in the AF1, whereas RXR is activated by 9-cis retinoic acid (9cRA) and certain FAs (Figure 20b) (Poulsen, Siersbæk et al. 2012).

The unusually large ligand-binding pocket of PPAR compared to other nuclear receptors, allows PPAR to accommodate a wide range of endogenous lipids, including FAs, eicosanoids, oxidized and nitrated FAs, and derivatives of linoleic acid (Bensinger and Tontonoz 2008).

The AF2 helix is important for co-activator binding and transcriptional activation and is located at the C-terminal end of the LBD. In addition, although more than four-fifths of the ligand-binding cavity residues are conserved across all PPAR isoforms, the remaining one-fifth yields ligand specificity between isoforms. For example, in PPAR-β/δ, the cavity adjacent to the AF2 helix and Arm I is significantly narrower, which prevents PPAR-β/δ from accommodating the large headed thiazolidinediones (TZD) and L-tyrosine agonists.

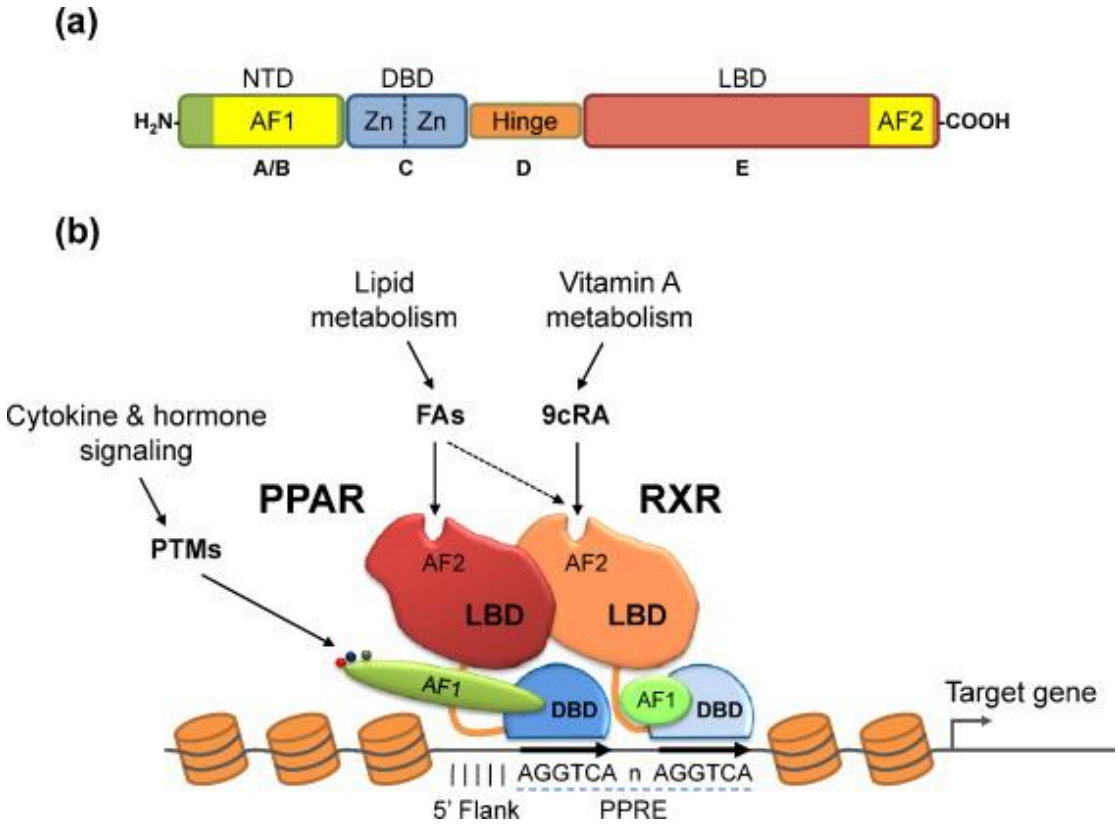

Figure 20. The structure of PPARs and their mode of action. (a) Domain structure of nuclear receptors. The N-terminal domain (NTD, A/B domain) contains the ligand-independent activation function (AF1). The highly conserved DNA-binding domain (DBD, C domain) contains two zinc fingers. The hinge region (D domain) is highly flexible. The ligand binding domain (LBD, E domain) contains the ligand-dependent activation function (AF2). (b) Simplified model of the PPAR: RXR transcriptional complex. PPAR:RXR binds the peroxisome proliferator response element (PPRE) in a head-to-tail fashion (Poulsen, Siersbæk et al. 2012)

3.6.2. PPAR activation in the liver

PPAR regulates many of the processes impaired in MASLD (Figure 21), such as lipid and glucose metabolism and inflammation.

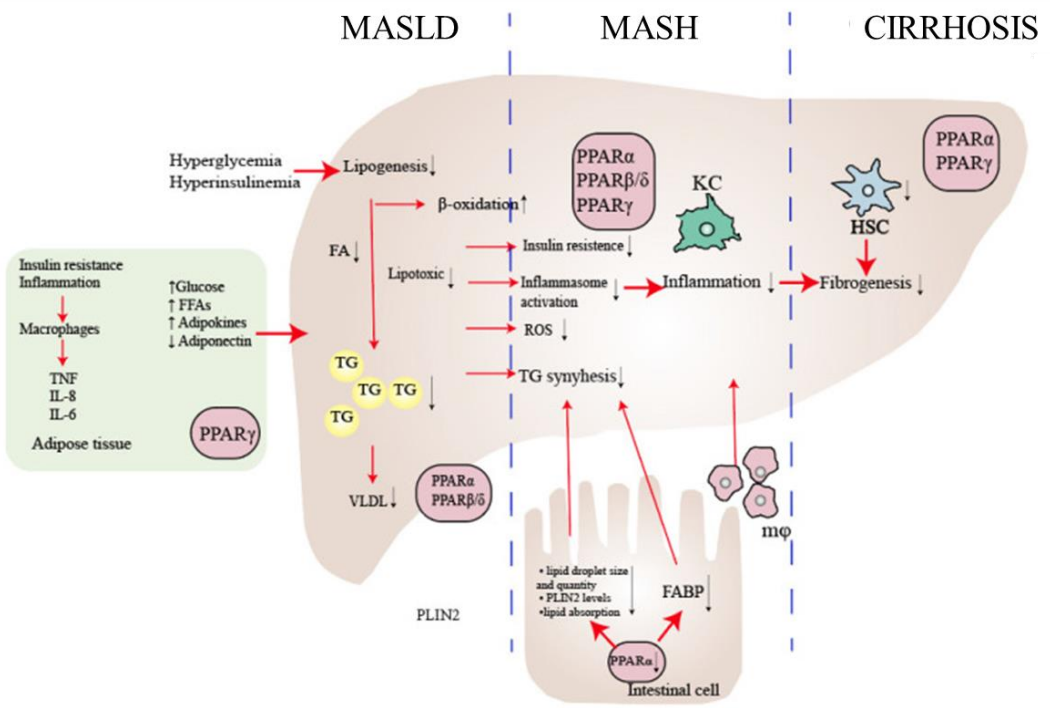

Figure 21. The role of PPARs in MASLD. PPAR-α plays a crucial role in enhancing lipid metabolism by regulating lipid flow, controlling FA transport, and promoting β-oxidation. PPAR-β/δ suppresses the inflammatory phenotype of macrophages and contributes to the selective activation of the desired phenotype. PPAR-γ, which primarily regulates insulin sensitivity within adipose tissue, is a key regulator of HSCs (Yang, Danzeng et al. 2024).

PPAR-α assumes a pivotal role in augmenting lipid metabolism through the regulation of lipid flux, modulation of FA transport, and the facilitation of FA β-oxidation. In addition, PPAR-α is a major regulator of the hepatic response to fasting, and consistent with this, PPAR-α-deficient mice exhibited elevated FFA levels and hypoketonemia after fasting (Kersten, Seydoux et al. 1999). In this case, *Ppar-α* gene expression is induced during fasting in wild-type (WT) mice in response to increased

hepatic FA oxidation (Leone, Weinheimer et al. 1999). During fasting, PPAR-α is also important for the induction of fibroblast growth factor 21 (FGF21), which is required for the normal activation of FA oxidation, TG clearance, and ketogenesis due to the ketogenic diet (KD) (Badman, Pissios et al. 2007). In glucose metabolism, PPAR-α regulates the expression of genes involved in the hepatic gluconeogenesis pathway, the process by which the liver produces glucose from non-carbohydrate sources (Kersten 2014). It was shown that PPAR-α expression was negatively correlated with MASH histologic severity, but increased with improvement in histologic status with weight management (Francque, Verrijken et al. 2015). Another study showed that 8 weeks of aerobic exercise in MASLD reduced the progression of steatosis and inflammation via the AMPK-PPAR-α signaling pathway (Diniz, de Lima Junior et al. 2021). However, hepatocyte PPAR-α deficiency disrupts FA homeostasis, stimulates hepatic steatosis in aging (Montagner, Polizzi et al. 2016), and promotes MASLD and liver inflammation in HFD-fed mice (Régnier, Polizzi et al. 2020). In addition, PPAR-α acts as a modulator of systemic inflammation and related vascular responses, as it negatively regulates TNF-α, IL-1, and IL-6 cytokines (Mansouri, Baugé et al. 2008).

PPAR-γ primarily governs insulin sensitivity within adipose tissue and acts as a key regulator of HSC differentiation. Through the inhibition of HSC activation, PPAR-γ assumes a pivotal role in mitigating fibrogenesis. In fact, aP2-Cre mice with specific deletion of PPAR-γ in HSCs showed exacerbated liver damage and fibrogenic response to CCl_4 (Morán-Salvador, Titos et al. 2013). It seems that there is a positive correlation

between PPAR-γ and fibrosis in activated HSCs. However, it has been shown that hepatocyte PPAR-γ promotes steatosis in mice on a high-fat diet. Likewise, hepatocyte-specific PPAR-γ deletion protects mice from diet-induced MASH and enhances the benefits of TZD on MASH (Lee, Pusec et al. 2021). PPAR-γ expression is generally low in lean livers whereas *Ppar-γ* gene is increased in the livers of obese MASLD patients with steatosis and steatohepatitis (Pettinelli and Videla 2011).

PPAR-β/δ has multiple metabolic effects and physiological roles, and activation of PPAR-β/δ may inhibit and ameliorate metabolic disorders associated with obesity. For instance, PPAR-β/δ regulates hepatic metabolic programs through transcriptional mechanisms, and increases monounsaturated FA (MUFA) production and decreases saturated FA (SFA) production (Liu, Hatano et al. 2011). MASLD is characterized by the accumulation of hepatic TGs, which are synthesized from FAs, the main sources of which are NEFAs and DNL. The decrease in serum NEFAs caused by PPAR-β/δ activation is also a consequence of increased FA oxidation in tissues such as the liver and skeletal muscle (Barroso, Rodríguez-Calvo et al. 2011). Interestingly, activation of PPAR-β/δ increased hepatic levels of 1-palmitoyl-2-oleoyl-sn-glycero-3-phosphocholine (16:0/18:1-PC), an endogenous ligand for PPAR-α (Barroso, Rodríguez-Calvo et al. 2011). In turn, this 16:0/18:1-PC is regulated by circadian hepatic PPAR-β/δ activity, which reduces postprandial lipid levels, while increasing muscle use of FAs through activation of PPAR-α (Liu, Brown et al. 2013). Furthermore, PPAR-β/δ regulates hepatic levels of PPAR-γ co-activator (PGC)-1α, a major regulator

of mitochondrial biogenesis, which regulates FA oxidation (Barroso, Rodríguez-Calvo et al. 2011). SREBP-1c is a critical transcription factor involved in the regulation of genes in the DNL pathway, and PPAR-β/δ-deficient mice exhibit increased SREBP-1c activity leading to steatosis compared to WT mice (Goudarzi, Koga et al. 2013). Thus, overexpression or activation of PPAR-β/δ ameliorates hepatic steatosis by inhibiting the role of SREBP-1c in DNL pathway. Moreover, it has been reported that PPAR-β/δ inhibits hepatic steatosis and prevents MASLD progression by regulating VLDLR (Zarei, Barroso et al. 2018). However, the expression and the activity of this transcription factor are reduced in the liver of patients with MASLD, compared to healthy subjects. The progression of MASH involves the development of inflammation and hepatocyte damage. The adipocyte-derived cytokine IL-4 induces PPAR-β/δ expression, which promotes alternative activation of Kupffer cells (macrophages residing in the liver) toward an anti-inflammatory M2 phenotype (Vázquez-Carrera 2016). A recent study found that PPAR-β/δ activation ameliorated histologic features of steatohepatitis in mice, as well as reduced macrophage activation (Lefere, Puengel et al. 2020). Consistent with this, macrophages lacking PPAR-β/δ show significantly impaired alternative activation, leading to adipocyte dysfunction, IR, and hepatosteatosis (Kang, Reilly et al. 2008). In addition, PPAR-β/δ has been reported to exhibit inhibitory effects in hepatocyte proliferation and HCC (Vacca, D'Amore et al. 2014).

Collectively, these findings suggest that activation of PPARs provides a valuable

strategy for preventing the progression of MASLD and MASH.

The above evidence supports the positive effects of PPAR-β/δ in the treatment of obesity, inflammation, and steatosis. However, there has been controversy regarding the role of PPAR-β/δ in various diseases, and the use of PPAR-β/δ-targeted drugs require caution. For instance, studies have shown that the activation of PPAR-β/δ attenuates chemically induced colon carcinogenesis (Harman, Nicol et al. 2004, Marin, Peraza et al. 2006). In contrast, other studies support the aberrant expression of PPAR-β/δ in colorectal cancer through adenomatous polyposis coli (APC)/β-catenin/T cell factor 4 (TCF4) target genes (He, Chan et al. 1999, Gupta, Tan et al. 2000, Takayama, Yamamoto et al. 2006). Likewise, ultraviolet (UV)-induced PPAR-β/δ activity, which upregulates Src expression and the EGFR/ERK1/2 signaling pathway, leads to skin cancer in mice (Montagner, Delgado et al. 2014). Furthermore, the PPAR-β/δ agonist GW501516 was not only involved in CCl_4-induced mice hepatic fibrosis but also stimulated HSC proliferation through the p38-JNK pathways (Kostadinova, Montagner et al. 2012). However, in another study, PPAR-β/δ agonists exhibited antifibrotic effects in mice with liver injury (Iwaisako, Haimerl et al. 2012). These findings further illustrate the complexity of PPAR-β/δ mechanisms in cancer.

4. Current and future therapies in MASLD

MASH has become the leading cause of liver-related mortality and a growing

burden on healthcare systems worldwide. Despite a wealth of emerging evidence providing explanations for the pathogenesis of MASH disease, effective therapies are currently limited. Of note, the U.S. Food and Drug Administration (FDA) recently approved the activator of thyroid hormone receptor (THR) resmetirom (Rezdiffra®) as the first treatment for adults with non-cirrhotic MASH who suffer from intermediate to advanced hepatic scarring (fibrosis), along with diet and exercise.

4.1. Lifestyle intervention

Although the FDA has recently approved the first treatment for MASH, lifestyle modifications remain the safest and most effective treatment, but they are not effective for advanced fibrosis or cirrhosis. Controlling body weight and metabolic dysregulation can be achieved by increasing physical activity and altering dietary habits (controlling calorie intake) (Figure 22). The challenge lies in implementing these measures in the long term.

<table>
<tr><td>Weight Reduction</td><td colspan="2">Overweight/obesity MASLD
• 5-10% weight reduction achieved by any heathy deit that the patient can adhere to in the long-term</td><td>Non-obesity MASLD
• 3-5% reduction of weight even within the normal BMI range (especially if recent weight gain ocurred or abdominal obesity is present)</td></tr>
<tr><td>Lifestyle advice for all patients with MASLD</td><td>Recommended foods
 
• n-3 FAs found in fish, and walnuts
• Olive oil
• Fruits, vegetables, polyphenols
•Home-cooked meals
•Mediterranean dietary pattern</td><td>Non-recommended foods or minimize consumption
 
• Added sugar (e.g. by reducing sweets, processed foods ang beverages)
• Saturated fat and cholesterol
•Ultra-processed foods and drinks, red and processed meat</td><td>Recommended activity
 
• Aerobi exercise ≥ 3 days/ week (≥ 150 min/week moderate intensity)
• Resistance exercise ≥ 2 days/weeks
• Reduce sedentary behaviour</td></tr>
</table>

Figure 22. Lifestyle recommendations for patients with MASLD. BMI, body mass index; MASLD, metabolic dysfunction-associated steatotic liver disease; MASH, metabolic dysfunction-associated steatohepatitis (Dufour, Anstee et al. 2022).

Physical exercise: The population with transitional obesity, metabolic syndrome, and T2DM often engage in sedentary behaviors, and as sedentary time increases, it can lead to an increased susceptibility to MASLD. It is recommended that MASLD patients engage in more physical exercise, which may reduce the likelihood of IR and impaired glucose tolerance. Exercise can reduce the risk of diabetes, hypertension, and metabolic syndrome, thus reducing the likelihood of MASH occurrence. Although moderate weight loss of about 3%-5% may reduce hepatic steatosis, in MASH patients, a weight loss of up to 10% or more is needed to reduce inflammation and fibrosis regression, which is challenging (Vilar-Gomez, Martinez-Perez et al. 2015).

Dietary habits: Excessive calorie intake may lead to obesity, while calorie control can effectively utilize body fuel and reduce oxidative damage to cells. Carbohydrate intake is associated with MASLD. A low-carbohydrate diet can reduce blood glucose load, improve IR and pancreatic β-cell insulin secretion, increase HDL, and lower serum TGs and glucose (Ludwig and Ebbeling 2018). There has been a sharp increase in the consumption of processed foods, which are a major source of added sugars and saturated fats, as well as being energy-dense with low nutritional value. Therefore, changing dietary habits is an important starting point. The best evidence of the benefits of this change comes from the Mediterranean diet, characterized by an abundant intake of olive oil, vegetables, fruits, nuts, legumes, whole grains, and seafood, and a low intake of red meat and processed meat, especially with reduced carbohydrate intake (40% of calories *vs*. 50%-60% in a typical low-fat diet), particularly sugars (Dufour, Anstee et al. 2022).

4.2. Pharmacological therapies

Besides the first specific drug recently approved by the FDA for the treatment of MASH, many compounds have been developed for this condition (Figure 23), which include (1) PPAR agonists (elafibranor, saroglitazar), farnesoid X receptor (FXR) agonists (obeticholic acid; OCA, tropifexor, LJN-452), glucagon-like peptide (GLP)-1 receptor agonists (tirzepatide, semaglutide), (2) agents with antioxidant and antiapoptotic activity, such as apoptosis signaling kinase 1 (ASK1) inhibitor, (3)

lipotoxicity-based targets such as inhibitors of DNL (aramchol, ACC inhibitor), (4) several hepatic antifibrotic agents, such as cysteine–cysteine motif chemokine receptor-2/5 antagonists (cenicriviroc; CVC) and galectin 3 (Gal-3) antagonists (Raza, Rajak et al. 2021).

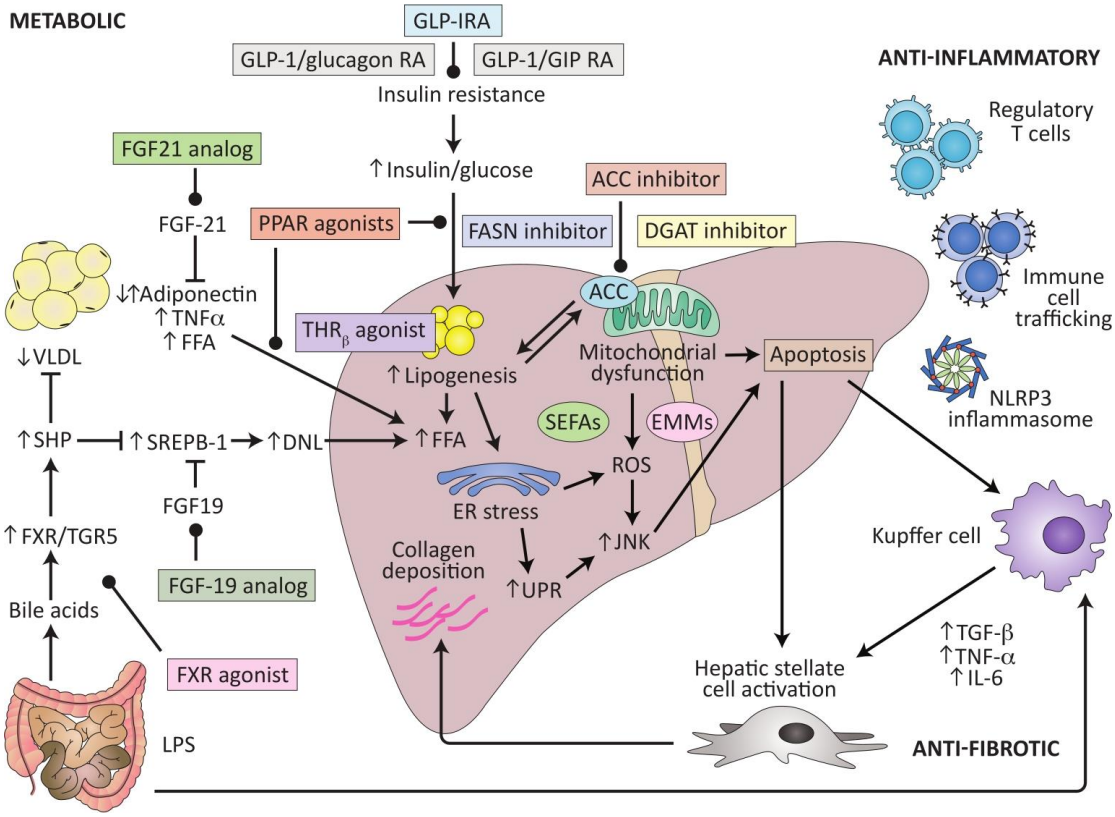

Figure 23. Potential therapeutic targets for MASLD/MASH. ACC, Acetyl-CoA Carboxylase; ASK, Apoptosis signal-regulating kinase; DNL, *de novo* lipogenesis; ER, endoplasmic reticulum; FGF, fibroblast growth factor; FFA, free fatty acids; FXR, Farnesoid X receptor; IL, interleukin; LPS, lipopolysaccharide; ROS, reactive oxygen species; SHP, small heterodimer partner; SREBP, Sterol regulatory element binding proteins; TGF, Transforming growth factor; TNF, tumor necrosis factor; UPR, unfolded protein response; VLDL, very low-density lipoprotein (Staufer and Stauber 2023).

Several different drugs including OCA, resmetirom, aramchol, tirzepatide, selonsertib, and CVC are currently undergoing evaluation in a global phase III clinical trial for the treatment of MASH (Table 4), among a range of other medications in development. Interestingly, even though saroglitazar is still in phase II trial, this drug has been approved for the treatment of non-cirrhotic MASH in India. Notably, resmetirom had been approved by the FDA, but the phase III clinical trial is still ongoing, which will evaluate the clinical efficacy of resmetirom after 54 months of treatment.

The trial design and endpoints for assessing the effectiveness of drugs in treating MASLD must adhere to predetermined criteria before receiving approval from regulatory authorities. Due to the current lack of effective treatments for MASH, the FDA and EMA have conditionally approved phase III trials for MASH drug development, demonstrating histological endpoints of fibrosis improvement [≥ stage of fibrosis in MASH Clinical Research Network (CRN) fibrosis score)] without worsening MASH and/or MASH resolution [NAFLD activity score (NAS) of 0-1 for inflammation, 0 for ballooning] but without worsening fibrosis (Loomba, Ratziu et al. 2022). The search for effective drugs targeting suitable therapy target remains the most urgent.

Drug	Mechanism of action	Phase in clinic trial	ClinicalTrials.gov number
Elafibranor	PPAR-α/-β/δ agonist	III	NCT01694849 NCT02704403
Saroglitazar	PPAR-α/-γ agonists	II	NCT03061721
Obeticholic acid	FXR agonist	III	NCT02548351
Tropifexor	FXR agonist	IIb	NCT02855164
Resmetirom	THR-β agonist	III	NCT03900429 NCT04197479
Selonsertib	ASK1 inhibitor	III	NCT03053050 NCT03053063
Aramchol	SCD1 inhibitor	III	NCT04104321
Tirzepatide	GLP-1-GIP co-agonist	III	NCT03861039
Cotadutide	GLP-1-glucagon agonist	II	NCT04515849
Cenicriviroc	CCR2/CCR5 inhibitor	III	NCT03028740
GR-MD-02	Galectin-3 inhibitor	II	NCT02462967 NCT02421094 NCT04365868

Table 4. List of clinical trials for the anti-MASH drugs.

4.2.1. PPAR agonists

As depicted previously, PPAR ligands play a key role in the transcriptional regulation of glucose and lipid metabolism, exerting a dominant role in MASLD and MASH (Figure 24). The activation of only one PPAR subtype renders limited efficacy, while the broad activation with pan-PPAR agonist may have a more effective and curative therapeutic potential for MASH through multiple pathological mechanisms.

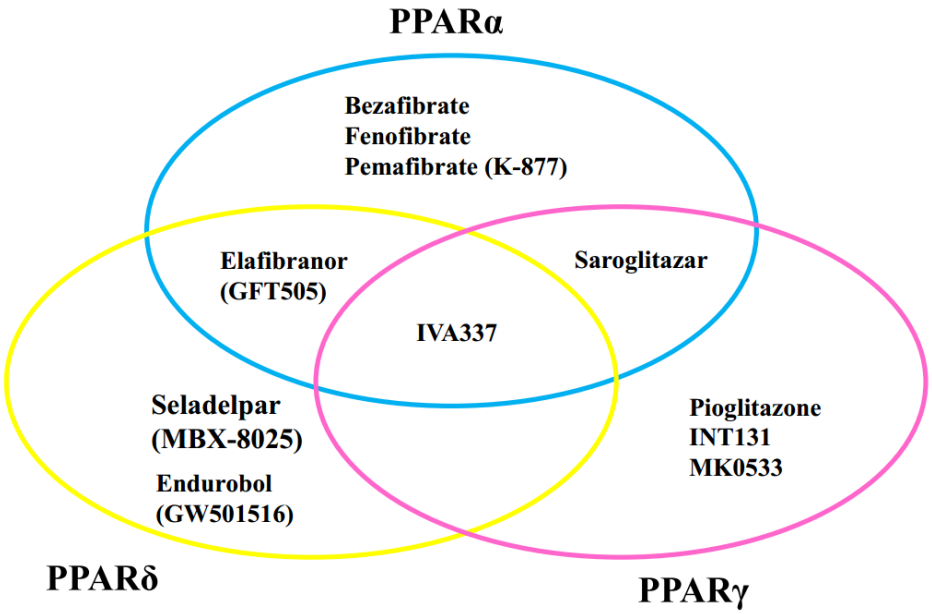

Figure 24. PPAR agonists for MASLD/MASH (Sumida and Yoneda 2018).

4.2.1.1. Elafibranor

Elafibranor [also known as GTF-505 or 2-(2,6-dimethyl-4-(3-(4-(methylthio) phenyl)-3-oxo-1-propenyl) phenoxyl)-2-methylpropanoic acid, Genfit, France] is a dual PPAR-α/-β/δ agonist, known to improve lipid metabolism, insulin sensitivity and

glucose homeostasis, and it also reduces inflammation in MASLD and MASH. In PPAR-α knockout mice, elafibranor prevents liver steatosis and inflammation, suggesting that these actions are mediated by PPAR-β/δ activation (Staels, Rubenstrunk et al. 2013).

A multicenter, randomized, double-blind, placebo-controlled phase IIb trial (NCT01694849, Europe and USA) was conducted to evaluate the efficacy and safety of elafibranor at doses of 80 mg and 120 mg once daily in reversing MASH and preventing fibrosis progression (Ratziu, Harrison et al. 2016). The study enrolled 276 patients (18-75 years of age) with non-cirrhotic MASH allocated into three groups: 92 patients in the placebo group, 93 patients in the elafibranor 80 mg group, and 91 patients in the elafibranor 120 mg group. Each patient underwent a screening period (4 to 16 weeks) prior to the 52-week double-blind treatment phase and 3 months of follow-up, with a total study duration of 80 weeks. Compared to the placebo group, a higher proportion of patients in the 120 mg elafibranor group showed resolution of MASH without worsening fibrosis (19% *vs.* 12%; odds ratio=2.31). In a post-hoc analysis of patients with NAS ≥4 (n=234), elafibranor 120 mg resolved MASH in higher proportions of patients than placebo (20% *vs.* 11%; odds ratio=3.16). Compared with the placebo group, the elafibranor 120 mg group showed significant reductions in liver enzymes, lipids, glucose profile, and systemic inflammatory markers. Elafibranor was well tolerated, and did not cause weight gain or cardiac events, but led to a mild, reversible increase in serum creatinine (4.31 ± 1.19 μmol/l).

The RESOLVE-IT phase III trial of elafibranor treatment compared to placebo for MASH and fibrosis patients started in 2016, recruiting a total of 1,070 patients in the intention to treat (ITT) population. Patients were randomly allocated in a 2:1 ratio to receive either elafibranor 120 mg (n=717) or placebo (n=353) once daily, with liver biopsies performed at week 72 to assess histological endpoints (MASH resolution, fibrosis non-worsening, or at least one stage improvement in fibrosis). Elafibranor did not demonstrate a statistically significant impact on the primary endpoint of MASH resolution and did not worsen fibrosis. The rate of resolution in patients treated with elafibranor 120 mg was 19.2%, while the rate in the placebo group was 14.7%. For the fibrosis key secondary endpoint, 24.5% of patients in the elafibranor 120 mg treatment group achieved at least one stage improvement in fibrosis, compared to 22.4% in the placebo group. The trial was prematurely terminated and will no longer continue (https://www.fiercebiotech.com/biotech/genfit-cans-phase-3-nashtrial-after-failing-interim-analysis).

4.2.1.2. Saroglitazar

Saroglitazar is a dual PPAR-α/-γ agonist that can improve insulin sensitivity as well as lipid and glucose parameters. In animal models, saroglitazar improved MASH histology, with a significant decrease in the liver index and correction of ALT, AST, leptin, and adiponectin levels (Akbari, Behdarvand et al. 2021). In a randomized, double-blind clinical trial, EVIDENCES IV phase II RCT (NCT03061721), a total of

106 patients with MASLD/MASH were randomly assigned to receive placebo or saroglitazar at 1 mg, 2 mg, or 4 mg for 16 weeks. The primary efficacy endpoint was the percentage change in ALT levels relative to baseline at week 16, assessed through magnetic resonance imaging (MRI) proton density fat fraction for liver fat content (LFC). The least-squares mean percent change from baseline in ALT for saroglitazar at 1 mg, 2 mg, and 4 mg were -25.5% (SE=5.8), -27.7% (SE=5.9), and -45.8% (SE=5.7) respectively, while the placebo group showed a change of 3.4% (SE=5.6). Compared to placebo, saroglitazar at 4 mg significantly improved LFC, adiponectin, IR, and atherogenic dyslipidemia in participants with MASLD/MASH, and also improved the composition and size of lipoprotein particles while reducing the levels of atherogenic lipid species (Gawrieh, Noureddin et al. 2021).

4.2.1.3. GW501516

In animal models, the PPAR-β/δ agonist GW501516 (CAS ID 317318-70-0) treatment protected mice from obesity induced by an HFD. Rat L6 myotubes treated with GW501516 showed increased FA oxidation by regulating genes involved in FA transport, β-oxidation, and mitochondrial respiration (Tanaka, Yamamoto et al. 2003). Furthermore, administration of GW501516 to mice fed an HFD improved diet-induced obesity and IR. Similar reports suggested that GW501516 significantly improves blood lipid abnormalities and IR in monosodium L-glutamate metabolic syndrome mice (Chen, Wang et al. 2008). In mice fed with a MCD diet, the administration of

GW501516 (10 mg/kg/day) once a day for 5 weeks inhibited the elevation of hepatic TG and thioacetamide-reactive substances, as well as the histopathological increase in hepatic lipid droplets, liver inflammation, and activated HSC count, while decreasing levels associated with inflammatory cytokines or chemokines (Nagasawa, Inada et al. 2006). In an early limited trial, 6 healthy subjects were given the PPAR-β/δ agonist GW501516 (10 mg) and a placebo for a period of 2 weeks. In addition to improving lipid profiles, GW501516 treatment also resulted in a 20% reduction in LFC ($P < 0.05$) and a 30% decrease in urinary prostaglandin ($P = 0.01$) (Risérus, Sprecher et al. 2008). The validity of the results was compromised by the limited number of patients, short duration, and broad exclusion criteria in this study, reducing its generalizability. A total of 268 patients with HDL cholesterol (1.16 mmol/L) were given GW501516 (2.5, 5.0, or 10.0 mg) or a placebo for 12 weeks. GW501516 (10 mg) increased HDL cholesterol by 16.9% and apo-A-I by 6.6%, and decreased LDL cholesterol by -7.3%, TGs by -16.9%, apo-B by -14.9%, and FFAs by -19.4% (Olson, Pearce et al. 2012). Although GW501516 appeared very promising in initial clinical trials, it was withdrawn due to safety concerns and it is currently used in research studies to evaluate the effects of PPAR-β/δ activation in cellular and animal models.

4.2.2. Other Pharmacological Therapies

4.2.2.1. Compounds targeting metabolic regulation

4.2.2.1.1. Farnesoid X receptor (FXR) agonists

FXR, a bile acid (BA)-activated nuclear receptor, regulates the metabolism of BA and lipids as well as serves as a key regulator in hepatic steatosis, inflammation, and fibrosis. Activating the FXR-SREBP-1 signaling pathway can reduce HFD-induced lipid accumulation in the liver, thereby maintaining metabolic homeostasis (Liu, Zhang et al. 2020). Moreover, FXR activation prevents the development of lipid-mediated tubule-interstitial fibrosis through β-catenin signaling in HFD-fed mice (Sun, Yuan et al. 2024). Regulation of endothelial nitric oxide synthase (eNOS) in hepatocytes may be an important target in the development and progression of MASLD to MASH. The FXR agonist could potentially elevate eNOS levels by influencing serum asymmetric dimethylarginine (ADMA) levels through direct regulation of hepatic dimethylarginine dimethylaminohydrolase-1 (*Ddah1*) gene expression (Hu, Chouinard et al. 2006). A dual agonist of FXR and liver X receptor-α (LXR-α), withaferin A, has been reported to suppress hepatic inflammation and liver fibrosis in a MASLD model mice and *in vitro*, it also attenuated lipid accumulation by inhibiting NF-κB and TGF-β pathways (Shiragannavar, Sannappa Gowda et al. 2023).

OCA is a potent FXR agonist and synthetic BA derivative that inhibits the progression of MASH by preventing disruption of the intestinal epithelial and intestinal

vascular barriers (Mouries, Brescia et al. 2019). The FLINT trial (a multicenter, randomized, double-blind, placebo-controlled study, NCT01265498) included 283 patients with biopsy evidence of MASH receiving a daily dose of 25 mg OCA (n=141) or placebo (n=140) for 72 weeks. The results of this study showed a significant improvement in histologic status in the OCA group (45% *vs*. 21% of the control group; P=0.0002), as well as an improvement in fibrosis scores (35% *vs*. 19% of the control group; P=0.004). However, OCA has not yet been approved by FDA for the treatment of MASH, as itching has been observed in treated patients (23%), as well as an increase in patients' total cholesterol and LDL cholesterol, raising concerns about the drug's tolerability (Siddiqui, Van Natta et al. 2020). Notably, the phase III trial (NCT02548351, 2,480 patients) evaluating the safety and efficacy of OCA in MASH subjects was completed in September 2023, and the FDA has now indicated that the review is complete and determined that it cannot be approved.

4.2.2.1.2. Thyroid hormone receptor (THR) β agonists

Thyroid hormone (TH) regulates many processes of hepatic TG and cholesterol metabolism to lower serum cholesterol and intrahepatic lipid content, and it acts as a ligand for two receptors, THR-α and THR-β (Sinha, Bruinstroop et al. 2019). THRβ is mainly expressed in the liver and plays a crucial role in lowering TGs and cholesterol, improving insulin sensitivity, promoting liver regeneration, and reducing apoptosis. Patients with MASLD or MASH have a higher incidence of clinical and subclinical

hypothyroidism than the general population, which may be related to reduced hepatic TH levels. Therefore, treatment of MASLD or MASH with liver-specific thyroid-stimulating drugs is an attractive option because of its additional metabolic benefits.

Resmetirom (MGL-3196) is an orally active liver-directed and selective THR-β agonist (> 28-fold of THR-α) that has demonstrated an excellent safety profile in a rat cardiac model (Kelly, Pietranico-Cole et al. 2014). A phase IIb clinical trial (NCT02912260) evaluated its effect in 125 patients with MASH (fibrosis stage 1-3) and > 10% hepatic fat received resmetirom (n=84) or placebo (n=41) once a day for 12 or 36 weeks. Based on magnetic resonance imaging proton density fat fraction (MRI-PDFF), resmetirom-treated patients (n=78) showed a relative reduction of hepatic fat compared with placebo (n=38) at week 12 (-32.9% resmetirom *vs.* -10.4% placebo), which is closed to week 36 [-37.3% resmetirom (n=74) *vs.* -8.5% placebo (n=34)]. The MASH resolution in the resmetirom group was increased by 27% (n=73) compared to the placebo group (6%, n=31) via liver biopsy, and an increase of up to 39% in the 46 patients with MRI-PDFF response in the resmetirom group (p=0.0013). In addition, resmetirom showed a significant reduction in atherogenic lipids and lipoproteins, such as LDL cholesterol (-22.3%), apo-B (-27.6%), TGs (-30.8%), and lipoprotein (a) (-37.9%).

Additionally, a 52-week phase III trial involving 1,143 patients to evaluate the

safety and biomarkers of resmetirom in MASLD (MAESTRO-MASLD-1, NCT04197479) was completed in 2023. Resmetirom was safe and well tolerated, the treatment-emergent adverse events (TEAEs) occurred in 86.1% (100 mg resmetirom), 88.4% (80 mg resmetirom) and 81.8% (placebo) of patients. The higher incidence of TEAEs in the patients treated with resmetirom than in the placebo group included diarrhea and nausea at the initiation of treatment (Harrison, Taub et al. 2023).

Meanwhile, another double-blind, randomized phase III trial (MAESTRO-MASH, NCT03900429) enrolling 1,759 patients is ongoing and is scheduled to conclude in 2028. This trial aims to determine whether 80 or 100 mg of resmetirom may resolve MASH and/or reduce fibrosis on liver biopsy and prevent progression to cirrhosis and/or advanced liver disease compared to placebo. Based on the partial results of this trial, MAESTRO-MASH achieved both primary endpoints. MASH resolution without worsening fibrosis was achieved in 25.9% of subjects who received 80 mg resmetirom and 29.9% of subjects who received 100 mg resmetirom, compared to 9.7% of those who received a placebo. Fibrosis improvement by at least one stage without worsening of the NAS was achieved in 24.2% of subjects in the 80 mg resmetirom group and 25.9% of those in the 100 mg resmetirom, as compared with 14.2% of those in the placebo group (Harrison, Bedossa et al. 2024). Currently, resmetirom has been approved by FDA as the first treatment for patients with liver fibrosis due to fatty liver disease, but MAESTRO-MASH is ongoing, which will assess clinical benefit after 54 months of resmetirom treatment.

4.2.2.1.3. Glucagon-like peptide (GLP)-1 receptor agonists

GLP-1, an intestinal hormone secreted by ileum cells in response to food intake, has multiple effects including lowering glucose by stimulating insulin secretion and inhibiting glucagon secretion from islet cells, delaying gastric emptying, appetite suppression, enhancing peripheral insulin sensitivity, and hepatic lipogenesis suppression. These metabolic functions of GLP-1 suggested that the potential role of GLP-1 agonists is relevant to the treatment of MASLD and MASH.

Tirzepatide (LY3298176) is a novel and dual agonist of glucose-dependent insulinotropic polypeptide (GIP) and GLP-1 receptors, and its therapeutic efficacy on MASH and fibrosis in patients with T2DM had been reported previously in a clinical trial (NCT03131687). This study showed that tirzepatide significantly reduced MASH-related biomarkers [ALT, AST, keratin-18 (K-18), procollagen III (Pro-C3)] and increased adiponectin in patients receiving higher doses (Hartman, Sanyal et al. 2020). However, tirzepatide is associated with some of the most common gastrointestinal side effects, including vomiting, nausea, decreased appetite, diarrhea, and abdominal distension, which were dose-dependent and considered mild to moderate in severity (Coskun, Sloop et al. 2018). Semaglutide, another GLP-1 receptor agonist, was evaluated for efficacy and safety in a 72-week phase II trial (NCT02970942) involving 320 patients with biopsy-confirmed MASH. The 59% of patients in the 0.4 mg semaglutide showed MASH resolution without worsening of fibrosis compared to the

placebo group (17%) (Newsome, Buchholtz et al. 2021). However, it was unable to achieve the secondary outcome of improved fibrosis without worsening of MASH, even though semaglutide treatment resulted in a significantly higher proportion of patients with MASH resolution than placebo. In addition, semaglutide treatment was also associated with common gastrointestinal side effects.

4.2.2.1.4. Fibroblast growth factor (FGF) analogues

Within the FGF peptide family, FGF19 (FGF15) and FGF21 have emerged as attractive new targets for MASLD and MASH drug development due to their immunomodulatory effects, improved hepatic steatosis, and metabolic regulation (Ocker 2020). Nevertheless, the upregulation of FGF1 and FGF2 expression is observed in the context of chronic liver disease, fibrogenesis, and HCC. These growth factors play a pivotal role in mediating fibrosis by activating HSC, establishing a linkage between the regulation of the ECM and the processes of carcinogenesis in the context of MASLD and MASH.

FGF19 is a hormone that regulates BA balance, glycogen synthesis and energy homeostasis. FGF19 provides cytoprotection against ER stress by activating the FGFR4-GSK3β-Nrf2 signaling cascade (Teng, Zhao et al. 2017). NGM282 is a recombinant non-tumorigenic variant of FGF19 that selectively targets binding to FGFR4/β-Klotho and inhibits CYP7A1 but does not activate STAT3 signaling (Zhou,

Wang et al. 2014). In a placebo-controlled phase II study, 82 patients were randomly assigned to receive a placebo (n=27), 3 mg of NGM282 (n=27) or 6 mg of NGM282 (n=28), which significantly reduced LFC in patients with MASH (Harrison, Rinella et al. 2018). In a new trial, patients treated with NGM282 1 mg or 3 mg had ≥ 2-point of improvement in NAS without worsening of fibrosis (50% and 63%, respectively), and ≤ 1-stage of improvement in liver fibrosis without worsening of steatohepatitis (25% and 42%, respectively) (Harrison, Rossi et al. 2020).

Growing evidence indicated that cellular expression of klotho β (KLB) allows FGF21 to bind to FGFR1, 2, and 3, but not to FGFR4 (Wu, Ge et al. 2010). FGF21 is acknowledged as a prominent regulator of glucose and lipid homeostasis. In murine models of genetic (*ob/ob*) and diet-induced obesity (DIO), the administration of FGF21 induces a swift reduction in blood glucose levels, resulting in immediate enhancements in glucose tolerance and insulin sensitivity (Xu, Stanislaus et al. 2009). FGF21 is subject to regulation by PPAR-α, contributing to the amelioration of associated lipid metabolism (Badman, Pissios et al. 2007). Moreover, FGF21 exerts mitigating effects on hepatic steatosis and peroxidative damage in MASH through the modulation of FA activation and oxidation pathways within the liver (Fisher, Chui et al. 2014). BMS-986036 (Pegbelfermin) is a recombinant polyethylene glycolated analog of human FGF21 and has been shown to significantly increase lipocalin levels and decrease serum Pro-C3 in T2DM patients predisposed to fatty liver (Charles, Neuschwander-Tetri et al. 2019). In a placebo-controlled phase II trial in patients with confirmed MASH, fibrosis,

and obesity (NCT02413372), 184 patients were given injections of BMS-986036 in a daily (10 mg/d) or a weekly (20 mg/week) frequency for 16 weeks (Sanyal, Charles et al. 2019). There was a significant decrease in hepatic fat fraction in the BMS-986036 treatment (-6.8% and -5.2%, respectively) compared with placebo (-1.3%) and improvement in serum ALT. In addition, a significant proportion of patients demonstrated improvements in serum Pro-C3 (30% and 19%) and liver stiffness (36.4% and 33.3%), as well as adiponectin (> 15%).

4.2.2.2. Compounds targeting oxidative stress and apoptosis

4.2.2.2.1. Vitamin E

Vitamin E is a fat-soluble compound present in a variety of compounds and the phospholipid bilayer of the cell membrane, which belongs to tocopherol and tocotrienol. Vitamin E, as a powerful biological antioxidant, has a protective effect on against mitochondrial damage and inhibits the intrinsic apoptotic pathway, thereby reducing liver injury (Soden, Devereaux et al. 2007).

In a successful PIVENS trial (NCT00063622), 247 adults with MASH and non-diabetes received vitamin E at a dose of 800 IU daily (n=84), pioglitazone at a dose of 30 mg daily (n=80), or placebo (n=83) for 96 weeks. This study showed vitamin E was associated with a significantly higher rate of improvement in MASH resolution (43%

vs. 19%, p=0.001) compared with placebo, and improved hepatic steatosis (P=0.005) and lobular inflammation (P=0.02), but without improvement in fibrosis scores (P=0.24) (Sanyal, Chalasani et al. 2010). Although vitamin E has not been specifically studied in diabetic MASH patients, the results of this PIVENS trial suggest that indirect evidence of vitamin E's superiority to placebo also supports the efficacy of vitamin E in diabetic patients. It is important to note that unknown long-term adverse events that may occur with vitamin E therapy must be considered when deciding whether to use this vitamin (Miller, Pastor-Barriuso et al. 2005).

4.2.2.2.2. Apoptosis signal-regulating kinase 1 (ASK1) inhibitor

ASK1, a member of the MAP3K family, is activated by TNF-α, ER stress and LPS, which causes oxidative stress-related apoptosis and hepatic inflammation, leading to liver fibrogenesis through the activation of MAPK and p38/JNK (Yoon, Fang et al. 2020). The inhibition of ASK1-mediated activation of the P38/JNK cascade abrogates the exacerbating effects of inflammation and hepatic lipid accumulation (Xiang, Wang et al. 2016).

Selonsertib (GS-4997) is a selective ASK1 inhibitor that may play a role in hepatic steatosis and fibrosis, which has been evaluated in patients with MASH or liver fibrosis (F2/F3). In this open-label phase II trial, patients received 6 or 18 mg of selonsertib orally once daily (± simtuzumab) for 24-week, and the effect of treatment was assessed

by liver biopsies and MRI-PDFF. The proportion of patients with ≥ 1-stage reduction in fibrosis in the 18 mg and 6 mg selonsertib groups was 43% and 30%, respectively (Loomba, Lawitz et al. 2018). A phase III trial was conducted in patients with MASH and bridging fibrosis (F3, STELLAR-3) or compensated cirrhosis (F4, STELLAR-4) to receive selonsertib 18 mg/6 mg, or placebo once daily for 48 weeks. Even in STELLAR-3, improvement in fibrosis was observed in 10% (P=0.49 *vs.* placebo), 12% (P=0.93 *vs.* placebo), and 13% of patients in the selonsertib 18 mg, selonsertib 6 mg, and placebo groups, respectively, without worsening of MASH. As improvements appeared to be limited, STELLAR 4 did not meet its primary endpoint, therefore the STELLAR program was also canceled (Harrison, Wong et al. 2020).

4.2.2.3. Lipotoxicity-based targets

4.2.2.3.1. Stearoyl-CoA desaturase 1 (SCD-1) inhibitor

SCD1 catalyzes the rate-limiting step in the synthesis of MUFAs such as oleic acid, a major component of tissue lipids. SCD1 expression plays an important role in lipid metabolism, and alterations in SCD1 expression differentially affect cellular functions (Liu, Strable et al. 2011). High expression of SCD1 is associated with metabolic diseases such as obesity and IR, and obese individuals with MASH have higher SCD1 activity (Walle, Takkunen et al. 2016). In contrast, the inhibition or deficiency of SCD1 activity reduces hepatic steatosis, prevents inflammation in white adipose tissue and improves insulin signaling (Liu, Miyazaki et al. 2010). Despite the beneficial metabolic

effects provided by SCD1 deficiency, abnormal skin function is observed in SCD1-deficient mice (MacDonald, van Eck et al. 2009).

Aramchol, a partial SCD1 inhibitor, is a cholic-arachidic acid conjugate that impacts fat synthesis and was evaluated in a multicenter, Phase IIb, randomized, double-blind, placebo-controlled trial (NCT02279524, ARREST). In the ARREST clinical trial, 247 patients with MASH were randomly divided into aramchol 400 mg (n=101), 600 mg (n=98) and placebo arms (n=48), respectively. Although aramchol 600 mg reduced the levels of liver fat (-3.1%), it did not meet the prespecified significance level (p=0.05). The rate of MASH resolution without worsening fibrosis was 16.7% (*vs.* 5% in the placebo group) and the proportion of those with ≥ 1-stage of fibrosis improvement without worsening MASH was 29.5% (*vs.* 17% in the placebo group) (Ratziu, de Guevara et al. 2021). A phase III trial to evaluate the efficacy and safety of aramchol in subjects with MASH (ARMOR) is ongoing.

4.2.2.3.2. Acetyl-CoA carboxylase (ACC) inhibitors

Individuals diagnosed with MASH exhibit a notable augmentation in DNL, fostering the accumulation of TG within hepatocytes and instigating persistent steatosis, thereby contributing to lipotoxicity, inflammation, and fibrosis. ACC stands out as the pivotal enzymatic determinant governing DNL, with ACC1/ACC2 serving as critical regulators orchestrating FA synthesis and metabolism, respectively (Wu and Huang

2020). Consequently, an inhibitor could serve as a therapeutic avenue for mitigating MASH by curtailing DNL and augmenting mitochondrial FA β-oxidation.

Currently, ACC inhibitors, namely GS-0976 (Firsocostat) and PF-05221304, are undergoing phase IIa clinical trials. In an open-label clinical trial of GS-0976, 10 patients with MASH received 20 mg once daily for 12-week. There was a 22% reduction in median hepatic DNL in patients with MASH, and the reduction of LFC measured by MRI-PDFF was -15.7% *vs.* -9.1% at baseline, while liver stiffness, measured by magnetic resonance elastography (MRE), was 3.4 kPa *vs.* 3.1 kPa at baseline (Lawitz, Coste et al. 2018). A similar phase II trial enrolled 126 patients with hepatic steatosis (liver stiffness ≥ 2.5kPa or F1-F3 fibrosis) who received GS-0976 at 20 mg or 5 mg, or placebo daily for 12 weeks. GS-0976 20 mg administration reduced hepatic steatosis, fibrosis markers, and liver biochemical levels (Loomba, Kayali et al. 2018). Based on safety and efficacy data, the ATLAS phase II trial (NCT03449446) evaluated the safety and tolerability of GS-0976, selonsertib, and cilofexor by administering them alone or in combination. The cilofexor/firsocostat combination met the primary endpoint (21%; P=0.17) and was well tolerated, with significant reductions in the machine learning (ML) MASH CRN fibrosis score (P=0.040) and ≥ 2-point NAS (Loomba, Noureddin et al. 2021).

Two parallel phase IIa studies investigated the effects of liver-targeted ACC1/2

inhibitors in adult patients with MASLD, including NCT03248882, which examined the effects of monotherapy with the novel ACC1/2 inhibitor PF-05221304 (2, 10, 25, and 50 mg) *vs.* placebo for 16 weeks, and NCT03776175, which examined the effects of the combination of PF-05221304 (15 mg) with the diacylglycerol acyltransferase 2 (DGAT2) inhibitor PF-06865571 (300 mg) *vs.* placebo after 6 weeks of treatment (Calle, Amin et al. 2021). PF-05221304 monotherapy at doses ≥ 10 mg resulted in dose-dependent reductions in liver fat of 50%-65%, and 49.9%, 55.9% and 64.8% at 10, 25 and 50 mg, respectively. Adverse effects may occur with monotherapy, including elevated serum TG levels with increasing doses. However, it is possible to mitigate these limitations by co-administering with PF-05221304 and PF-06865571.

4.2.2.4. Compounds targeting inflammation and fibrogenesis

4.2.2.4.1. CCR2/CCR5 inhibitor

Cenicriviroc (CVC) is a dual CCR2/CCR5 chemokine receptor antagonist, located on HSCs and Kupffer cells, causing inhibition of monocyte/macrophage recruitment and the disruption of signals that activate HSCs, effectively addressing both inflammation and fibrogenesis in animal models (Lefebvre, Moyle et al. 2016). According to phase IIb trial (CENTAUR; NCT02217475), CVC treatment significantly achieved the key secondary endpoint, with improvement in fibrosis and no worsening of steatohepatitis reaching 20% (*vs.* 10% of placebo) after 1 year (Friedman, Ratziu et al. 2018). Based on these findings, a phase III trial (AURORA, NCT03028740) was

conducted involving 1,778 adult patients (part 1: n=1293; part 2: n=485) with histological evidence of MASH with stage F2/F3 fibrosis that received CVC 150 mg or placebo daily (Anstee, Neuschwander-Tetri et al. 2024). This study did not demonstrate the efficacy of CVC treatment in mitigating liver fibrosis. Both the CVC and placebo groups exhibited comparable proportions in achieving the primary endpoint (22.3% *vs.* 25.5%) and complete resolution of steatohepatitis and no worsening of fibrosis (23.0% *vs.* 27.2%).

4.2.2.4.2. Galectin-3 (Gal-3) inhibitor

Gal-3 is a β-galactoside-binding mammalian lectin with potent pro-fibrotic effects that modulates fibroblast and macrophage activity in chronically inflamed organs (Slack, Mills et al. 2021). Thus, inhibition of Gal-3 may slow common fibrotic pathways. GR-DM-02 (belapectin) is a novel complex carbohydrate galectin inhibitor, that significantly reduces hepatic fibrosis and reverses cirrhosis *in vivo* (Traber, Chou et al. 2013). Two phase II clinic trials have evaluated GR-DM-02 in MASH patients with fibrosis/cirrhosis (NCT02462967 and NCT02421094). A phase II clinical trial involved the enrollment of 30 patients diagnosed with MASH exhibiting advanced fibrosis and the assessment of fibrotic changes was conducted through MRI. Ultimately, this investigation did not achieve the predefined primary endpoint. In a subsequent phase II trial, GR-DM-02 exhibited no statistically significant impact on liver fibrosis or NAS. However, the administration of 2 mg/kg of GR-DM-02 demonstrated a

reduction in hepatic venous pressure gradient (HVPG) and the development of varicose veins in a subgroup analysis (Chalasani, Abdelmalek et al. 2020).

II. Objectives

MASLD, which is the most common global pandemic usually associated with T2DM and obesity, ranges from hepatic steatosis to a more severe condition known as MASH. MASH is characterized by hepatocyte ballooning and liver inflammation, with or without fibrosis. Despite a wealth of emerging evidence providing explanations for the pathogenesis of MASH disease, effective therapies are currently limited.

The role of PPAR-β/δ in liver fibrosis remains controversial, with studies presenting conflicting evidence regarding its role in the progression or alleviation of fibrotic processes. While some research suggests that activation of PPAR-β/δ may mitigate liver fibrosis by regulating inflammatory responses and promoting lipid metabolism, other studies propose that its activation could exacerbate fibrosis by enhancing HSC activation and collagen deposition.

Considering this, the overall goal of this PhD thesis is to reveal the effects of a PPAR-α/-β/δ agonist on the development of MASH and to clarify the controversy over the role of PPAR-β/δ in the pathogenesis of liver fibrosis. For this purpose, the thesis has set the following objectives:

Objective 1: To examine the effects of the PPAR-α/-β/δ agonist elafibranor in mice fed a CD-HFD.

Objective 2: To assess the effects of a PPAR-β/δ ligand on the pathogenesis of liver fibrosis and the activation of HSC in response to the pro-fibrotic stimulus TGF-β.

III. Materials and methods

1. Animal studies

Male C57BL/6 mice (10-12-week-old) (Envigo, Barcelona, Spain) and *Ppard*-null (*Ppard*$^{-/-}$) mice (8-9-week-old) with their WT littermates (*Ppard*$^{+/+}$) with the same genetic background (C57BL/6 × 129/SV) were housed and maintained under a constant temperature (22 ± 2 ℃), humidity (55%) and lighting (12-h light-dark cycles). The mice had free access to a standard diet and a continuous supply of fresh water. After acclimatization (1 week), the mice were randomly divided into experimental groups of n=6 per group.

All the experiments were performed in accordance with European Community Council directive 86/609/EEC. The experimental procedures and the number of animals were determined according to the expected effects and were approved by the Institutional Animal Care and Use Committee of the University of Barcelona. The research of animals complied with the ARRIVE Guidelines. All animals received a humane treatment, always trying to minimize the suffering in the experiments.

1.1. PPAR-α/-β/δ agonist (elafibranor) administration to C57BL/6 mice

Male C57BL/6 mice (10-12-week-old) were randomly distributed into three different experimental groups (n=6): the control group fed a daily standard chow and the treated group received a choline-deficient high-fat diet (CD-HFD; 44.9 kcal% fat, 35.1 kcal% carbohydrates, and 20.0 kcal% protein, without added chlorine; D050402,

Research diets, New Brunswick, NJ, USA) for 12 weeks. The standard group and one of the treated groups received one daily administration of vehicle [0.5% (w/v) carboxymethylcellulose medium viscosity] by oral (*per os*, P.O.) gavage and the remaining treated group received one daily P.O. gavage dose of 10 mg/kg/day of PPAR-α/-β/δ agonist elafibranor (Table 5) dissolved in the vehicle during the last 4 weeks. The final administered volume of vehicle and elafibranor was 1 ml/kg. After the treatment, mice were sacrificed by cervical dislocation under isoflurane (IsoFlo, Esteve) anesthesia, liver samples were frozen in liquid nitrogen and then stored at - 80°C and blood was collected in blood collection tubes to obtain the serum.

1.2. PPAR-β/δ agonist (GW501516) administration to C57BL/6 mice

Ten to twelve-week-old male C57BL/6 mice were randomly distributed into three different experimental groups (n=6), the control group was fed a daily standard chow and the treated group received a choline-deficient high-fat diet (CD-HFD; D050402, Research diets) for 12 weeks. The standard group and one of the treated groups received one daily administration of vehicle [0.5% (w/v) carboxymethylcellulose medium viscosity] by P.O. gavage, while the remaining treated group received one daily P.O. gavage dose of 5 mg/kg/day of the PPAR-β/δ agonist GW501516 (Table 5) dissolved in the vehicle during the last 4 weeks. The final administered volume of the vehicle and GW501516 was 1 ml/kg. At the end of treatment, mice were sacrificed by cervical dislocation under isoflurane (IsoFlo, Esteve) anesthesia, liver samples were frozen in

liquid nitrogen and then stored at - 80°C and blood was collected in blood collection tubes to obtain the serum.

1.3. Wild-type (WT) and *Ppard* $^{-/-}$ mice

Ppard $^{-/-}$ mice (8-9-week-old) with their WT littermates (*Ppard* $^{+/+}$) received a daily control diet. Mice were sacrificed by cervical dislocation under isoflurane anesthesia, liver samples were frozen in liquid nitrogen and then stored at - 80°C.

Product	Manufacturer	Reference	Conditions
Elafibranor	AXON Medchem	Axon 2727	10 mg/kg/day
GW501516	Sigma-Aldrich	SML1491	5 mg/kg/day

Table 5. Drugs used in *in vivo* studies.

2. Glucose tolerance test (GTT) and insulin tolerance test (ITT)

Four hours before the end of the treatment, a glucose tolerance test (GTT) and insulin tolerance test (ITT) were performed on mice. The body weight of mice was checked regularly during the treatment. Mice received 2 g/kg body weight of glucose or 0.75 IU/kg body weight of insulin, respectively, through an intraperitoneal injection. Blood was collected from the tail vein at 0, 15, 30, 60 and 120 min and a small drop of

blood was placed along the edge of glucose meter (Accu-Chek). The Area under the Curve (AUC) was obtained through calculating the area generated by the glucose disappearance curve *vs.* time.

3. Liver histology

For histological staining studies, fresh liver sections were collected in 4% paraformaldehyde in PBS or embedded in a cryomold optimal cutting temperature (OCT, Tissue-Tek) compound. 4-µm sections obtained from fixed paraffin-embedded samples were washed with xylene and ethanol at different concentrations and were stained with hematoxylin and eosin (H&E) to assess liver histology, as well as Sirius Red to assess fibrosis. Oil Red O (ORO) staining (Sigma-Aldrich) to assess lipid content was performed in cryopreserved 10-µm liver sections. Trichrome staining was used to assess fibrosis and stain collagen blue.

Fifteen images at a magnification of 20 × were captured to quantify the red-stained collagen or lipid droplets, with the red-stained area evaluated per total area using the IHC profiler plugin of the Image J software.

4. Analysis of 1-palmitoyl-2-oleoyl-sn-glycero-3-phosphocholine (16:0/18:1-PC)

Total lipids from liver homogenates were extracted according to Bligh and Dyer (Bligh and Dyer 1959), evaporated, and redissolved in methanol-water (9:1). Total lipid separation, identification, and quantification were carried out by liquid chromatography/mass spectrometry using a Hitachi LaChrom Elite L-2130 binary pump and a Hitachi autosampler L-2200 (Merck, Darmstadt, Germany) coupled to a Bruker esquire 6000 ion-trap mass spectrometer (Balgoma, Astudillo et al. 2010). The effluent was split, entering at 0.2 ml/min into the electrospray interface of the mass spectrometer. The nebulizer was set to 30 ψ, the dry gas to 8 l/min, and the dry temperature to 350ºC. A Supelcosil LC-18 column of 5 μm particle size, measuring 250 × 2.1 mm and with a particle size of 5 μm (Sigma-Aldrich) was used, protected by a Supelguard LC-18 guard cartridge column measuring 20- × 2.1 -mm guard cartridge column (Sigma-Aldrich). The mobile phase was used a gradient of solvent A [methanol/water/hexane/ammonium hydroxide, 87.5:10.5:1.5:0.5 (vol/vol/vol/vol)], solvent B [methanol/hexane/ammonium hydroxide, 87.5:12:0.5 (vol/vol/vol)], and solvent C [methanol/water, 9:1 (vol/vol)]. The gradient started at 100% A, decreased linearly to 50% A (50% B) in 17.5 min and to 0% A (100% B) in 12.5 min, before being maintained at 100% B for 5 min, changed to 100% C in 3 min, maintained at 100% C for 9 min, and then changed to 100% B in 3 min. The flow rate was 0.5 ml/min and the injection volume was 80 μl. Data acquisition was carried out in the full scan and positive mode, detecting PC species as $[M^{+}H]^{+}$ ions with the capillary current set at - 4000 V.

The 16:0/18:1-PC species were characterized by tandem mass spectrometry in the multiple reaction monitoring and negative mode, with a post-column addition of acetic acid for $[M^{+}CH_3CO_2]$-adduct formation (100 µl/h). 1,2-Dinonadecanoyl-sn-glycero-3-phosphocoline (*m*/*z*=818.6) was used as the internal standard and in a calibration curve for quantification.

5. Cell culture

The different cell lines were utilized in a series of studies (reagents are in Table 6). After the different treatments, cells were washed 1-2 times with PBS 1× (Sigma) and the excess liquid was absorbed. Then, protein lysis solution was added to the culture plate, and cells were collected from wells using a cell scratcher and centrifuged at 10,000 g for 20 min at 4°C to collect the supernatant. For RNA extraction, cells were collected by direct homogenization using TRItidy (PanReac AppliChem, Spain) reagent to isolate RNA.

Product	Manufacturer	References	Condition
A769662	Tocris Bioscience	3336	60 µM
AMPKα1/2 siRNA	Santa Cruz	sc-45312	70 nM
ASB2 CRISPR/Cas9 activation plasmid	Santa Cruz	sc-425766-ACT	1.5 µg/well

Control CRISPR/Cas9 activation plasmid	Santa Cruz	sc-437275	1.5 µg/well
Control siRNA	Santa Cruz	sc-37007	100 nM
DMEM	Gibco	10569010	-
DMSO	Sigma-Aldrich	5895690100	-
FBS	Gibco	10100147	-
GSK0660	Sigma-Aldrich	G5797	60 µM
H_2O_2	Sigma-Aldrich	H1009	0.5 mM
L-glutamine	Gibco	11510626	-
Lipofectamine 2000	Invitrogen	11668019	6 µL/ml
N-acetylcysteine	Sigma-Aldrich	A7250	2 mM
Opti-MEM	Gibco	31985070	-
PBS 1×	Thermo Scientific	J61196-AP	-
penicillin/streptomycin	Gibco	15140122	-
S100A4 siRNA	Thermo Fisher Scientific	10167104	100 nM
TGF-β1	R & D systems	240-B-010	10 ng/ml
Trypsin 1×	Sigma-Aldrich	R001100	-

U0126	Sigma-Aldrich	662005	10 μM and 20 μM

Table 6. The list of reagents used for cell culture.

5.1. BRL-3A cell line

The hepatocyte cell line BRL-3A (P9-13, RRID: CVCL_0606), a fibroblast-like cell isolated from the liver of rat, was purchased from the European Collection of Authenticated Cell Cultures (ECACC, Salisbury, United Kingdom). BRL-3A were cultured in high glucose Dulbecco's Modified Eagle Medium (DMEM, Thermo-Fisher Scientific) containing 10% fetal bovine serum (FBS, Gibco) and 1% penicillin/streptomycin (Thermo-Fisher Scientific) under standard culture conditions (37℃, 5% CO_2). Cells were passaged using trypsin/EDTA (Sigma) solution when it reached 70-80% confluence and replated at approximately 1:4 dilution or stored in complete medium containing 10% DMSO at - 80℃. Different treatments were performed when the cell reached 90%-100% confluency and incubated in serum-free DMEM in the absence or presence of the drug.

Elafibranor: BRL-3A cells were plated in 6-wells plated at 1.5×10^5 cells/well with serum-free DMEM, after 8-12 h, changed to DMEM in the presence of the PPAR-α/-β/δ agonist elafibranor (30 μM or 60 μM) or DMSO. At the end of treatment, cells were collected for protein or RNA extraction.

GW501516: GW501516 was resuspended in DMSO to produce a stock solution of 20 mM and BRL3A was treated at a final concentration of 10 μM for 24 h.

GSK0660: The PPAR-β/δ antagonist GSK0660 (60 μM) was added into the culture medium 2 hours before exposing the cells to elafibranor (30 μM) for 24 hours.

U0126: The MEK inhibitor U0126 at concentrations of 10 μM or 20 μM was used in BRL-3A cells exposed to elafibranor for 24 h.

Hydrogen Peroxide (H_2O_2) and N-acetylcysteine (NAC): BRL-3A cells were exposed to 0.5 mM H_2O_2 for 90 min, and then the medium was changed to completed medium. Cells exposed to 60 μM elafibranor alone or co-incubated with the antioxidant NAC (2 mM).

siRNA transfection: The siRNA transfection allows to knockdown of target genes to reduce their expression. Cells were seeded in 6-well plates with antibiotic-free normal growth medium containing FBS. After cells reached 50%-70% confluency, one hour before transfection cells were incubated in free medium to avoid interferences with the siRNAs. BRL-3A cells were transiently transfected with 100 nM siRNA against S100A4 or control siRNA in Opti-MEM medium (Gibco) using Lipofectamine 2000

(Invitrogen, Carlsbad, CA, USA) (13.2 µl per 2.2-ml/well) in a final volume of 500 µl per well according to the manufacturer's instructions. The siRNA transfection reagent mixture was incubated at room temperature for 30-45 min, then added to each well containing 1 ml of incubation Opti-MEM medium. After 6 hours from the first step of the transfection, the medium was aspirated and replaced with complete normal growth medium. Finally, 24 hours later the different treatments were performed.

CRISPR/dCas 9 transfection: To overexpress ASB2 in the BRL-3A cells, the CRISPR/dCas9 activation system was used. The ASB2 CRISPR/dCas9 activation plasmid consisted of a pool of three plasmids designed to overexpress the *Asb2* gene and the control CRISPR/dCas9 activation plasmid was used as a negative control. Cells were counted using complete media without antibiotics to seed 1.0×10^5 cells per well in 6-well culture plates 24 h before transfection. Cells were used at 50%-60% confluence to avoid the negative impact of high confluence. Diluted ASB2 CRISPR/dCas9 activation system (1.5 µg) or Lipofectamine 2000 in Opti-MEN and incubated for 5 min, then the transfection complexes were incubated at room temperature for 25-30 min and added to the cell plates. Cells were incubated under standard culture conditions in a humidified incubator for 48 h and then the different treatments were conducted.

5.2. Primary mouse hepatocytes

Primary mouse hepatocytes were isolated from non-fasting male C57BL/6 mice (10-12-week-old) by perfusion with collagenase as described elsewhere (Benveniste, Danoff et al. 1988). The liver was exposed through an abdominal incision and cannulated through the inferior vena cava via the right atrium. An initial perfusion with calcium- and magnesium-free buffer was performed to disrupt the bridge particles that form the tight junctions between cells, followed by a second perfusion with calcium-rich buffer containing collagenase to further digest the cellular junctions.

At the end of the perfusion period, the liver was removed from the body cavity, the hepatocytes were separated, filtered through two layers of gauze, and washed twice with DMEM. The viable cells were grown in 24-well tissue-culture plates containing complete medium and incubated at 37°C in a humidified of 5% CO_2 - 95% air atmosphere. The primary mouse hepatocytes were exposed to 30 μM elafibranor or 10 μM GW501516 for 24 h.

5.3. LX-2 cell line

The LX-2 human HSC line (was kindly donated by Dr. Jiménez from Biomedical Diagnostic Center, Spain) was cultured in high glucose DMEM supplement with 2% FBS, 1% L-glutamine, and 1% penicillin/streptomycin. Cells were passaged every 3-4 days and cells below 10 passages were cryopreserved in liquid nitrogen. LX-2 cells

were starved for 8-12 hours before different treatments.

TGF-β1: TGF-β1 with bovine serum albumin (BSA) as a carrier protein was reconstituted at 10 μg/ml in sterile 4 mM HCl. LX-2 cells were exposed to 10 ng/ml TGF-β1 after GW501516 (10 μM) incubation or DMSO (in control cells) for 24 h.

A769662: A769662 activates AMPK by inhibiting AMPK dephosphorylation on Thr172 and was added into serum-free medium at a concentration of 60 μM in the absence or presence of TGF-β1.

U0126: The MEK inhibitor U0126 at concentrations of 10 μM was co-incubated with TGF-β1 in LX-2 cells.

siRNA transfection: LX-2 cells were transiently transfected with 70 nM siRNA against AMPKα1/2, or control siRNA in Opti-MEM medium using Lipofectamine 2000 in a final volume of 500 μl per well according to the manufacturer's instructions. The siRNA transfection reagent mixture was incubated at room temperature for 30-45 min, then added to each well containing 1 ml of incubation Opti-MEM medium. After 6 hours from the first step of the transfection, the medium was aspirated and replaced with complete normal growth medium. After 24 hours, LX-2 cells were exposed to

TGFβ1 in the presence or absence of GW501516.

Cell migration: LX-2 cells were seeded in 12-well culture plates and treated with TGF-β1 or TGF-β1 combined with GW501516. After the treatment, a sterile tip was used to obtain the scratched band of the cells and the migration distances were measured at 0 and 24 h under the microscope. At least triplicate pictures were obtained in each group and then Image J was used for area calculation. The following formula was used to calculate the relative migration distance and then normalized based on the control group.

$$Relative\ migration\ distance\ =\ [(D0 - D24)/D0] \times 100\%$$

5.4. HSCs

Primary HSCs were isolated from the livers of male (8-9 weeks old) *Ppard*$^{-/-}$ mice (n=6) and their WT littermates (*Ppard*$^{+/+}$) perfused in situ with collagenase: HSCs were purified by arabinogalactan density centrifugation and the purity of HSCs was assessed by an ultraviolet excited fluorescence microscope and exceeded 94%.

6. Quantitative polymerase chain reaction (qPCR)

Total RNA extraction

For total RNA extraction, 1 ml of PBS was used to wash cell plates or liver pellet

one time and TRItidy reagent (Table 7) was added to isolate intact total RNA. Chloroform can effectively separate RNA from DNA and protein into the aqueous phase and then added isopropanol precipitates RNA from the aqueous phase through -OH hydrophilic interaction. The precipitated pellet was washed once with 75% ethanol to remove all remaining proteins and inorganic salts, then dried and redissolved. Quantification of RNA was conducted using a NanoDrop 1000 (Thermo-Fisher Scientific) and then proceeded with subsequent experimental steps.

Plate	TRItidy (ml)	Chloroform (ml)	Isopropanol (ml)	75% ethanol (ml)
P12	0.5	0.1	0.25	0.5
P6	1	0.2	0.5	1

Table 7. Reagents used for RNA extraction.

Reverse transcription and RT-qPCR

Isolated RNA was reversed transcribed to obtain 1 µg of complementary DNA (cDNA) using Random Hexamers (Thermo Scientific), 10 mM deoxynucleotide (dNTP) mix (Table 8) and the reverse transcriptase enzyme derived from the Moloney murine leukemia virus (M-MLV, Thermo-Fisher). The experiment was run in a thermocycler (BioRad) and consisted of a program with different steps and the temperature: 65 °C for 5 min, 4 °C for 5 min, 37 °C for 2 min, 25 °C for 2 10 min, 37 °C for 50 min, and

70 ℃ for 15 min.

Reagents	Dose
dNTP (10 mM)	0.5 mM
Random Hexamers (50 µM)	0.3 µM
Buffer 5×	1×
DTT (100 mM)	10 mM
RNaseOUT™ (40 U/µl)	1 U/µl
M-MLV RT (200 U/µl)	10 U/µl

Table 8. Reagents used for reverse transcription.

The relative levels of specific mRNA (cell or tissues) were assessed by real-time PCR in a Mini 48-well T100™ (Bio-Rad) or a 98-well StepOnePlus™ (Applied Biosystems) thermal cycling block, using the SYBR Green Master Mix (Applied Biosystems), as previously described. Briefly, samples had a final volume of 20 ml, with 20 ng of total cDNA, 0.9 mM of the primer mix, and 10 ml of 2× SYBR Green Master Mix (For StepOnePlus™, will pre-added 4 µl ROS per 1 ml SYBR Green). The thermal cycler protocol for real-time PCR included a first step of denaturation at 95℃ for 10 min followed by 40 repeated cycles of 95 ℃ for 15 s, 60℃ for 30 s, and 72 ℃

for 30 s for denaturation, primer annealing, and amplification respectively. Primer sequences were designed using the Primer-BLAST tool (NCBI), based on the full mRNA sequences to find the optimal primers for amplification, and evaluated with the Oligo-Analyzer Tool (Integrated DNA Technologies) to ensure an optimal melting temperature™ and avoid the formation of homo/heterodimers or non-specific structures that can interfere with the interpretation of the results. The primer sequences were designed specifically to span the junction between the exons. The primer sequences used are provided in Table 9. Values were normalized to the glyceraldehyde 3-phosphate dehydrogenase (GAPDH) or adenine phosphoribosyltransferase (APRT) expression levels, and measurements were performed in triplicate. All changes in expression were normalized to the control group.

Gene	**Primer sequences**	
	Forward (5'-3')	Reverse (5'-3')
m *Aprt*	CAGCGGCAAGATCGACTACA	AGCTAGGGAAGGGCCAAACA
m *Arg1*	CATTGGCTTGCGAGACGTAGAC	GCTGAAGGTCTCTTCCATCACC
m *Asb2*	CTTGACATGGAGCCCATATA	GGGGTCCATAGCCGCCATC
m *Ccl2*	GCTACAAGAGGATCACCAGCAG	GTCTGGACCCATTCCTTCTTGG
m *Col1a1*	ACGCCATCAAGGTCTACTGC	ACTCGAACGGGAATCCATCG

m *Col3a1*	GACCAAAAGGTGATGCTGGACAG	CAAGACCTCGTGCTCCAGTTAG
m *Ctgf*	GCAGCGGTGAGTCCTTCC	AATGTGTCTTCCAGTCGGTAGG
m *Ep300*	GTGATGACCCTTCCCAACCTCA	CTCGTGGTGAAGGACACAGATC
m *Fgf21*	CAGGGAGGATGGAACAGTGGTA	TGACACCCAGGATTTGAATGAC
m *Gapdh*	AGACGGCCGCATCTTCTT	TTCACACCGACCTTCACCAT
m *Il-6*	ACACATGTTCTCTGGGAAATCGT	AAGTGCATCATCGTTGTTCATACA
m *Nos2*	GGTGAAGGGACTGAGCTGTT	ACGTTCTCCGTTCTCTTGCAG
m *Ppard*	GCCACAACGCACCCTTTG	CCACACCAGGCCCTTCTCT
m *S100a4*	AGCACTTCCTCTCTCTTGGTC	TCATCTGTCCTTTTCCCCAGG
m *Serpine1*	TCAGCCCTTGCTTGCCTCAT	GCATAGCCAGCACCGAGGA
m *Tgfb*	GCTGCGCTTGCAGAGATTAA	GTAACGCCAGGAATTGTTGCTA
m *Tnfa*	ATGGCCCAGACCCTCACA	TTGCTACGACTGGGCTACA
r *Aprt*	CAGCGGCAAGATCGACTACA	AGCTAGGGAAGGGCCAAACA
r *Gapdh*	AAGTTCAACGGCACAGTCAAGG	CATACTCAGCACCAGCATCACC
r *S100a4*	CTCTCTCTTGGTCTGGTCTCAA	TCACCCTCGTTGCCTGAGTA

Table 9. Primer sequences designed for qPCR. r: rat genes, m: mouse genes.

7. Immunoblotting

Total protein extraction

To extract total proteins from tissue (which needed to be ground in advance) or cells, lysis buffer was added to the pellets containing RIPA: Cocktail inhibitor: Sodium orthovanadate (OvNa): Phenylmethylsulfonyl fluoride (PMSF) =100: 1: 1: 1 (v/v/v/v) (Table 10), and incubated for 20 min (cell samples) or 2 hours (tissue samples) on a rotator under a condition of 30 rpm at 4 ℃. Next, the lysate was centrifuged at 10,000 *g* at 4 ℃ for 20 min and the supernatant fraction was collected.

Reagent	Dose
Cell lysis buffer, RIPA 1X	1 ml
Sodium orthovanadate (100 mM)	1 mM
Cocktail inhibitor (100 mM)	1 mM
PMSF (200 mM)	2 mM

Table 10. Cells lysis buffer system.

Quantification of protein

The Bradford (Bio-Rad) method was used to quantify protein and BSA was the standard (range of 2.5-20 µg/ml). The protein-pigment conjugate has a maximum light

absorption at a wavelength of 595 nm and the light absorption value is proportional to the protein content. Samples (10-50 µg per well) were heated at 95°C for 5 minutes in a heat block to obtain loading sample.

SDA-PAGE

Sodium-dodecyl-sulfate polyacrylamide gel electrophoresis (SDS-PAGE) (8%-15%) was used to separate the total protein based on the molecular weight. Samples and molecular weight markers were loaded in wells of the gel and the electrophoresis was at 120 Volts until the sample buffer reached the bottom of the gel (90-120 min). Methanol was used to activate the polyvinylidene difluoride (PVDF) membrane (Bio-Rad) in advance and then the SDS-PAGE gel transfer was conducted (200 mA, 105 min). After transference, the PVDF membrane was blocked with a commercially available blocking agent (WestVision™ Block and Diluent, Vector Lab) on a shaker for 1 hour at room temperature, and then the membrane was incubated with the primary antibody (diluted 1:500-1:2000 in the blocking solution, see Table 11) at 4°C overnight. The membrane was washed 3 times for 5 min with Tris-buffered saline (TBS) solution containing 0.1% Tween® 20 detergent (Sigma) (TBS-T) and then was incubated with secondary antibody (1:2500-1:5000 dilution in TBS-T) working solution for 1 hour at room temperature. The membrane was washed with TBS-T 3 times for 5 min to remove an excessive amount of secondary antibody, and then protein was detected by chemiluminescence using an ECL reagents kit (Millipore). Signal acquisition was

obtained with the Bio-Rad ChemiDoc or Amersham Imager 680 instrument and quantification of the immunoblot signal was performed with Bio-Rad Image Lab software. The quantification of protein was normalized to the levels of housekeeping protein (GAPDH, α-Tubulin or β-actin) to avoid unwanted sources of variation.

Primary antibody	Manufacturers	References	Condition
(p)P44/42 MAPK	Cell signaling	9194s	1:1000
AMPK	Cell Signaling	#2532	1:1000
COL1A1	Cell signaling	91144s	1:1000
E-Cadherin	Santa Cruz	sc-8426	1:500
Filamin A	Santa Cruz	sc-376241	1:1000
GAPDH (G-9)	Santa Cruz	sc-365062	1:2000
p300	Santa Cruz	sc-585	1:1000
P44/42 MAPK	Cell signaling	9101s	1:1000
p-AMPK	Cell Signaling	#9271	1:1000
p-SMAD3	Santa Cruz	sc-517575	1:1000
S100A4/FSP1	EMD Millipore	07-2274	1:800
SMAD3	Santa Cruz	sc-101154	1:1000

Vimentin	Santa Cruz	sc-6260	1:1000
α-SMA	Invitrogen	14-9760-82	1:1000
α-Tubulin	Sigma	T6074	1:2000
β-actin	Sigma	A5441	1:2000

Table 11. The list of primary antibodies used for western blot.

8. Statistical analysis and illustrations

All the results were at least triplicate and were expressed as the mean ± standard error of the mean (SEM). Significant differences were assessed by either Student's T-test or one-way ANOVA, according to the number of groups compared, using the GraphPad Prism program (version 9.0.2) (GraphPad Software Inc, Sandiego, CA, USA). When significant variations were found by ANOVA, Tukey's post-hoc test for multiple comparisons was performed only if F achieved a *p-value* <0.05. Differences were considered significant at p <0.05 (*), p <0.01 (**) and p <0.005(***).

Part of the illustrations in the introduction come from the bibliography, while the rest were created with the online design tool BioRender (BioRender.com) and have been made public under a licensing agreement.

IV. Results

Objective 1. Elafibranor upregulates the EMT-inducer S100A4 via PPAR-β/δ

1.1. The dual PPAR-α/-β/δ agonist elafibranor improves MASLD, but upregulates hepatic S100A4 levels in mice fed a CD-HFD

In order to accomplish the first objective, first, we evaluated the effects of elafibranor on body weight and glucose metabolism. Elafibranor treatment did not reduce the body weight gain caused by the CD-HFD, but it did ameliorate the glucose intolerance and peripheral IR caused by the CD-HFD (Figure 25A-C). Although PPAR-β/δ activation has been reported to increase the hepatic levels of the PPAR-α endogenous ligand 16:0/18:1-PC (Chakravarthy, Lodhi et al. 2009), it is unknown whether elafibranor affects the amount of this ligand that may potentiate the beneficial actions of the drug. The CD-HFD did not affect the hepatic levels of 16:0/18:1-PC (Figure 25D). However, elafibranor markedly increased the levels of this PPAR-α ligand in the liver. This effect of elafibranor has been reported previously for the PPAR-β/δ activator GW501516 (Barroso, Rodriguez-Calvo et al. 2011). Therefore, the fact that 16:0/18:1-PC levels were reduced in the livers of *Ppard*$^{-/-}$ mice compared with WT mice (Figure 25E) suggests that the effect of elafibranor on 16:0/18:1-PC levels is mediated by PPAR-β/δ. These findings indicate that elafibranor, besides its direct effect on PPAR-α, may also indirectly activate this nuclear receptor by increasing the amount of 16:0/18:1-PC. Since FGF21 is a target in the treatment of MASH and given that PPAR-α activation increases its levels (Zarei, Aguilar-Recarte et al. 2021), we determined the hepatic mRNA levels of *Fgf21*. The CD-HFD had no significant increase in *Fgf21* mRNA levels, whereas treatment with elafibranor significantly increased *Fgf21* expression (Figure 25F).

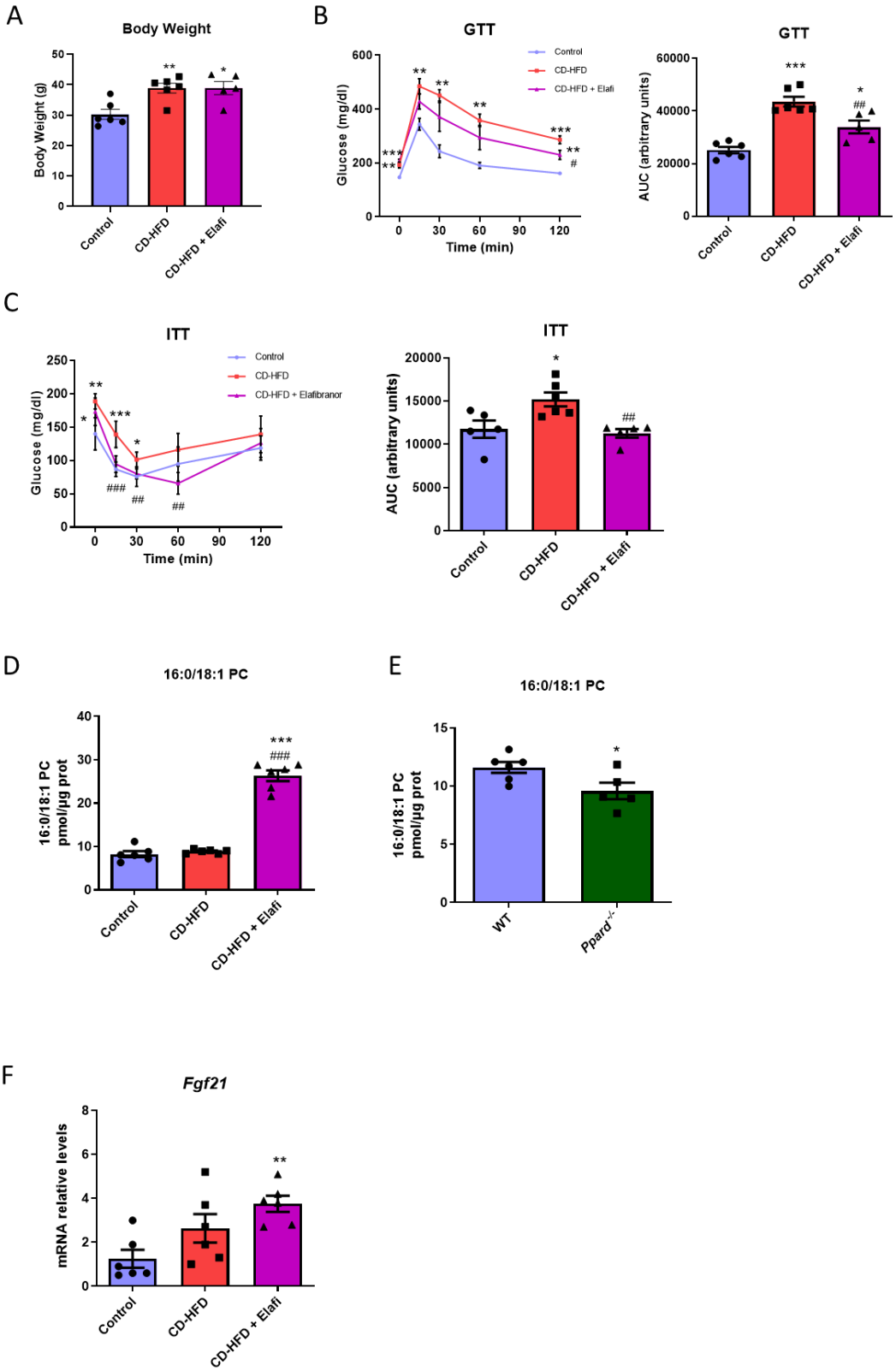

Figure 25. Elafibranor improves insulin sensitivity in mice fed a CD-HFD. (**A**) Final body weight in mice (n=6 animals) fed a standard diet (control) or a choline-deficient high-fat diet (CD-HFD) for 12 weeks and treated with vehicle or 10 mg/kg/day of elafibranor during the last

4 weeks. (**B**) Glucose tolerance test (GTT) and area under the curve (AUC) (n=6 animals). (**C**) Insulin tolerance test (ITT) and AUC (n=6 animals). (**D**) Hepatic levels of the PPAR-α endogenous ligand 1-palmitoyl-2-oleoyl-sn-glycero-3-phosphocholine (16:0/18:1-PC). (**E**) 16:0/18:1-PC hepatic levels in wild-type (WT) and *Ppard*$^{-/-}$ mice (n=5 animals). (**F**) *Fgf21* mRNA levels in mice (n=6 animals) fed a standard diet (control) or a CD-HFD and treated with vehicle or 10 mg/kg/day of elafibranor during the last 4 weeks. Data are presented as the mean ± SEM. $^{*}p < 0.05$, $^{**}p < 0.01$, and $^{***}p < 0.001$ *vs.* control or WT. $^{\#\#}p < 0.01$ and $^{\#\#\#}p < 0.001$ *vs.* CD-HFD-fed mice. *P-values* were determined by one-way ANOVA with Tukey's post hoc test (**A, B, C, D, and F**) or two-tailed unpaired Student's t-test (**E**).

H&E and ORO staining showed that the CD-HFD caused significant hepatic lipid accumulation that was reduced by elafibranor (Figure 26A, B). The CD-HFD led to a non-significant increase in the accumulation of collagen in the liver, as demonstrated by the Sirius Red staining, suggesting that a longer exposure to the CD-HFD is required to induce clear fibrosis. Remarkably, elafibranor decreased collagen accumulation (Figure 26C). Consistent with findings of the Sirius Red staining, the CD-HFD did not significantly increase the protein levels of the fibrosis markers α-SMA and collagen type I alpha 1 (COL1A1), but treatment with elafibranor caused a significant reduction (Figure 26D, E).

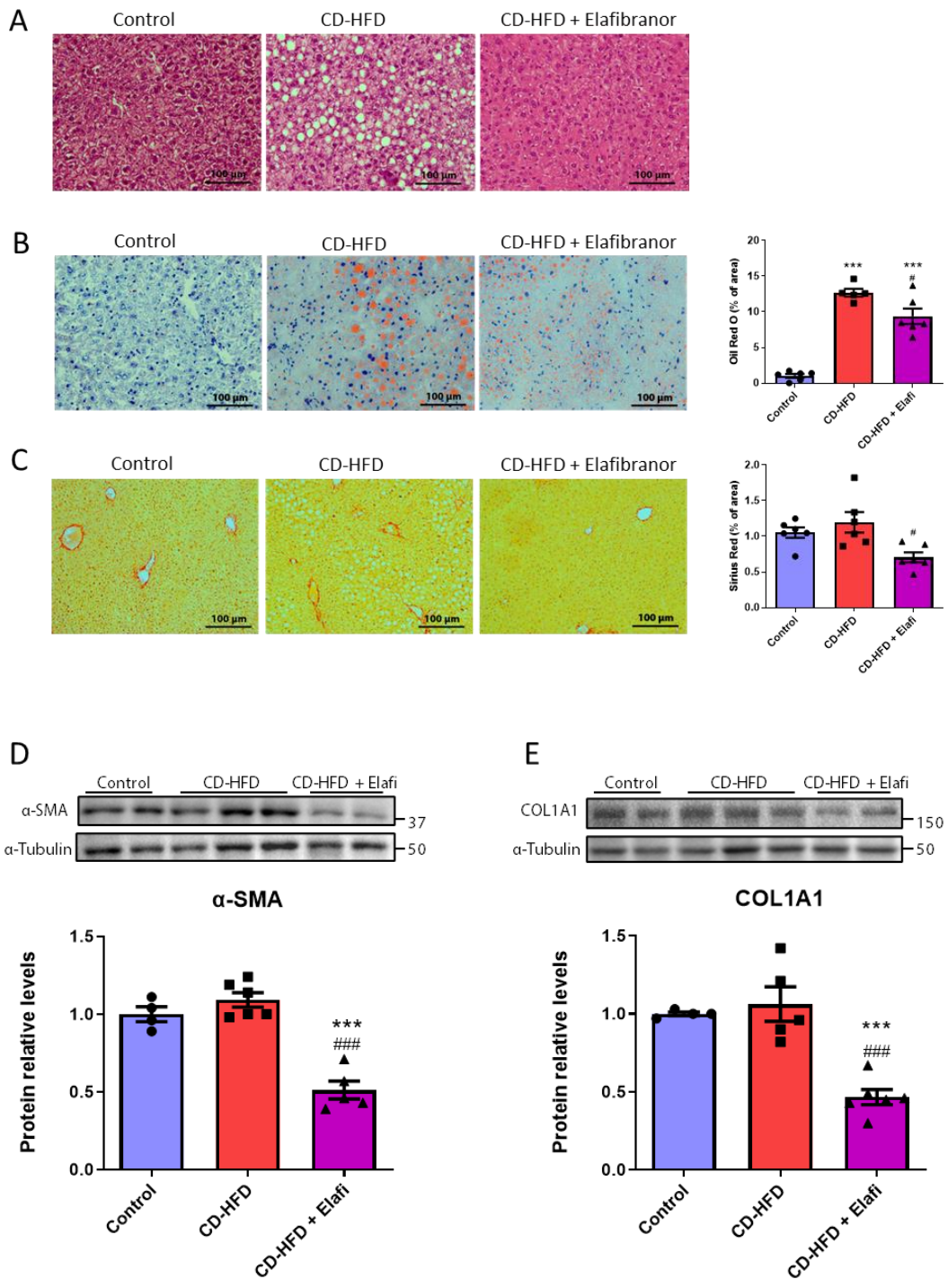

Figure 26. Elafibranor decreases markers of fibrosis in mice fed a CD-HFD. (**A**) Hematoxylin and eosin (H&E), (**B**) Oil Red O (ORO) and (**C**) Sirius Red staining of liver sections and quantification of ORO and Sirius Red staining of samples from mice (n=6 animals) fed a standard diet (control) or a CD-HFD for 12 weeks and treated with vehicle or 10 mg/kg/day of elafibranor during the last 4 weeks. Scale bar: 100 µm. Liver cell lysate extracts were assayed via western blot analysis with antibodies against α-SMA (**D**) and COL1A1 (**E**)

(n=6 animals). Data are presented as the mean ± SEM. $^{*}p < 0.05$ *vs.* control. $^{\#}p < 0.05$, $^{\#\#}p < 0.01$, and $^{\#\#\#}p < 0.001$ *vs.* CD-HFD-fed mice. *P-values* were determined by one-way ANOVA with Tukey's post hoc test.

When we examined the effects of elafibranor on S100A4 expression, we observed that the CD-HFD in mice treated with vehicle and in those administered elafibranor did not significantly affect the mRNA levels of this gene (Figure 27A). The S100A4 protein can be detected either as a monomer or a dimer, the latter being S-glutathionylated, with apparent molecular weights of 11.5-kDa and approximately 21-29-kDa, respectively (Tanaka, Yamamoto et al. 2003, Malashkevich, Dulyaninova et al. 2010). No changes were observed in the hepatic protein levels of S100A4 in mice fed the CD-HFD. By contrast, mice fed the CD-HFD and treated with elafibranor displayed a robust increase in the protein with a molecular weight of ~ 23-kDa (Figure 27B). The effect of elafibranor on S100A4 was likely to be the result of PPAR-β/δ activation, since the mice treated with the selective agonist for this receptor, GW501516, also showed increased hepatic protein levels of S100A4 (Figure 27C). Moreover, the band corresponding to S100A4 was reduced in the livers of *Ppard*$^{-/-}$ mice compared to their WT littermates, indicating that this protein is regulated by this nuclear receptor (Figure 27D). Since an increase in the mesenchymal marker S100A4 might indicate that elafibranor activates the EMT program, we analyzed the other markers of this program such as the epithelial marker E-cadherin and the mesenchymal marker vimentin. In agreement with the increase in S100A4 levels and the subsequent induction of the EMT

program, elafibranor reduced the protein levels of E-cadherin and increased those of vimentin (Figure 27E, F). These findings suggest that PPAR-β/δ activation by elafibranor increases the hepatic protein levels of S100A4 and activates the EMT program in the liver.

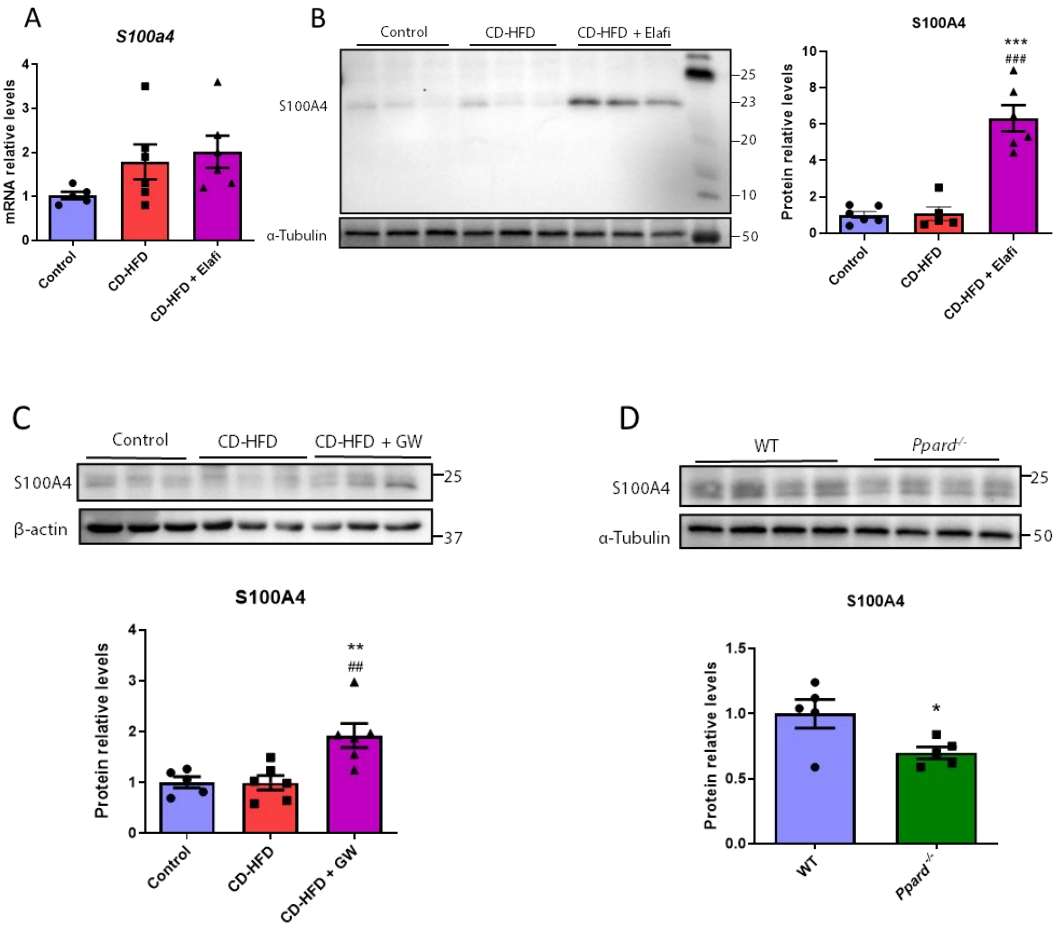

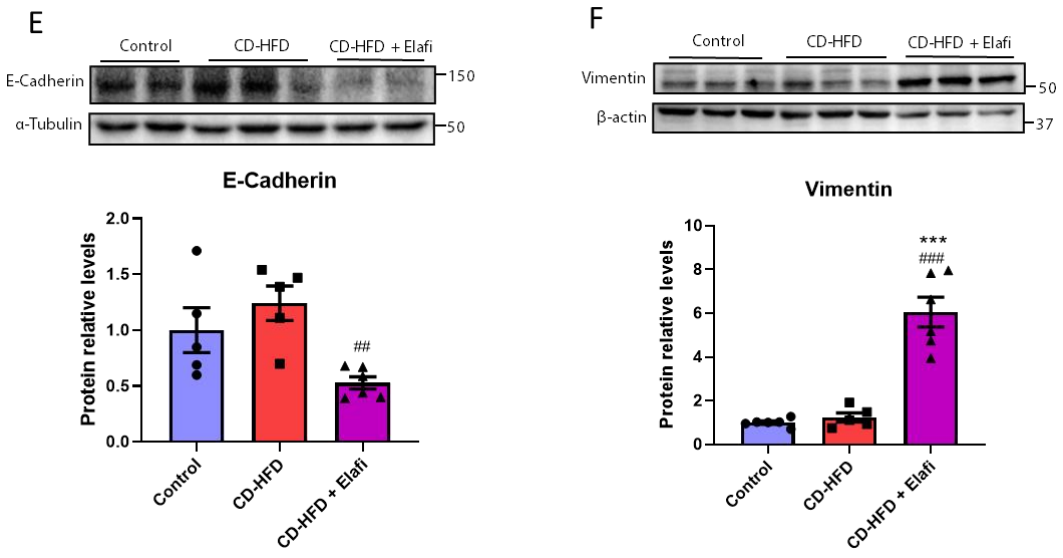

Figure 27. Elafibranor upregulates S100A4 protein levels in the liver. (**A**) mRNA levels of *S100a4* in the livers of mice (n=6 animals) fed a standard diet (control) or a CD-HFD for 12 weeks and treated with vehicle or 10 mg/kg/day of elafibranor during the last 4 weeks. (**B**) Liver cell lysate extracts were assayed via western blot analysis with antibodies against S100A4 (n=6 animals). (**C**) S100A4 protein levels in the livers of mice (n=6 animals) fed a standard diet (control) or a CD-HFD for 12 weeks and treated with vehicle or 5 mg/kg/day of GW501516 during the last 4 weeks. (**D**) S100A4 protein levels in the livers of WT and *Ppard*$^{-/-}$ mice (n=5 animals). E-cadherin (**E**) and vimentin (**F**) protein levels in the livers of mice (n=6 animals) fed a standard diet (control) or a CD-HFD for 12 weeks and treated with vehicle or 10 mg/kg/day of elafibranor during the last 4 weeks. Data are presented as the mean ± SEM. $^{*}p < 0.05$ and $^{***}p < 0.001$ *vs.* control. $^{\#\#}p < 0.01$ and $^{\#\#\#}p < 0.001$ *vs.* CD-HFD fed mice. *P-values* were determined by one-way ANOVA with Tukey's post-hoc test.

1.2. Elafibranor increases S100A4 protein levels in BRL-3A rat liver cells and in a mouse primary culture of hepatocytes

Treatment of the rat liver cell line BRL-3A with either GW501516 (a selective agonist of PPAR-β/δ at concentrations of up to 10 μM (House, Pozzuto et al. 2011)) or

elafibranor (at a concentration of 30 or 60 µM) did not increase *S100a4* mRNA levels compared to control cells (Figure 28A). By contrast, elafibranor at both concentrations increased S100A4 protein levels, whereas GW501516 had no effect (Figure 28B). The S100A4 protein upregulated by elafibranor in the rat BRL-3A cells showed a higher molecular weight than that detected in mice, suggesting interspecies differences in the S-glutathionylation of this protein (Bowers, Manevich et al. 2012). S100A4 knockdown by siRNA transfection in the BRL-3A cells caused a reduction in the protein levels of S100A4, confirming that the protein band detected was S100A4 (Supplementary Figure 1A). Elafibranor at 60 µM reduced E-cadherin protein levels (Figure 28C) and increased vimentin protein levels (Figure 27D), while GW501516 only increased vimentin levels without affecting E-cadherin levels (Figure 28C, D). The increase in S100A4 protein levels caused by elafibranor was prevented by the PPAR-β/δ antagonist GSK0660 (Figure 28E), confirming the involvement of PPAR-β/δ in the changes caused by its activation. The effects of elafibranor were confirmed in a mouse primary culture of hepatocytes, where elafibranor increased S100A4 protein levels (Figure 28F). In these primary hepatocytes, GW501516 increased S100A4 protein levels, in contrast to that observed in the BRL-3A cells, suggesting that the primary hepatocytes respond better than the rat BRL-3A cells (Figure 28G). Overall, these findings indicate that elafibranor increases the protein levels of S100A4 in hepatocytes via PPAR-β/δ.

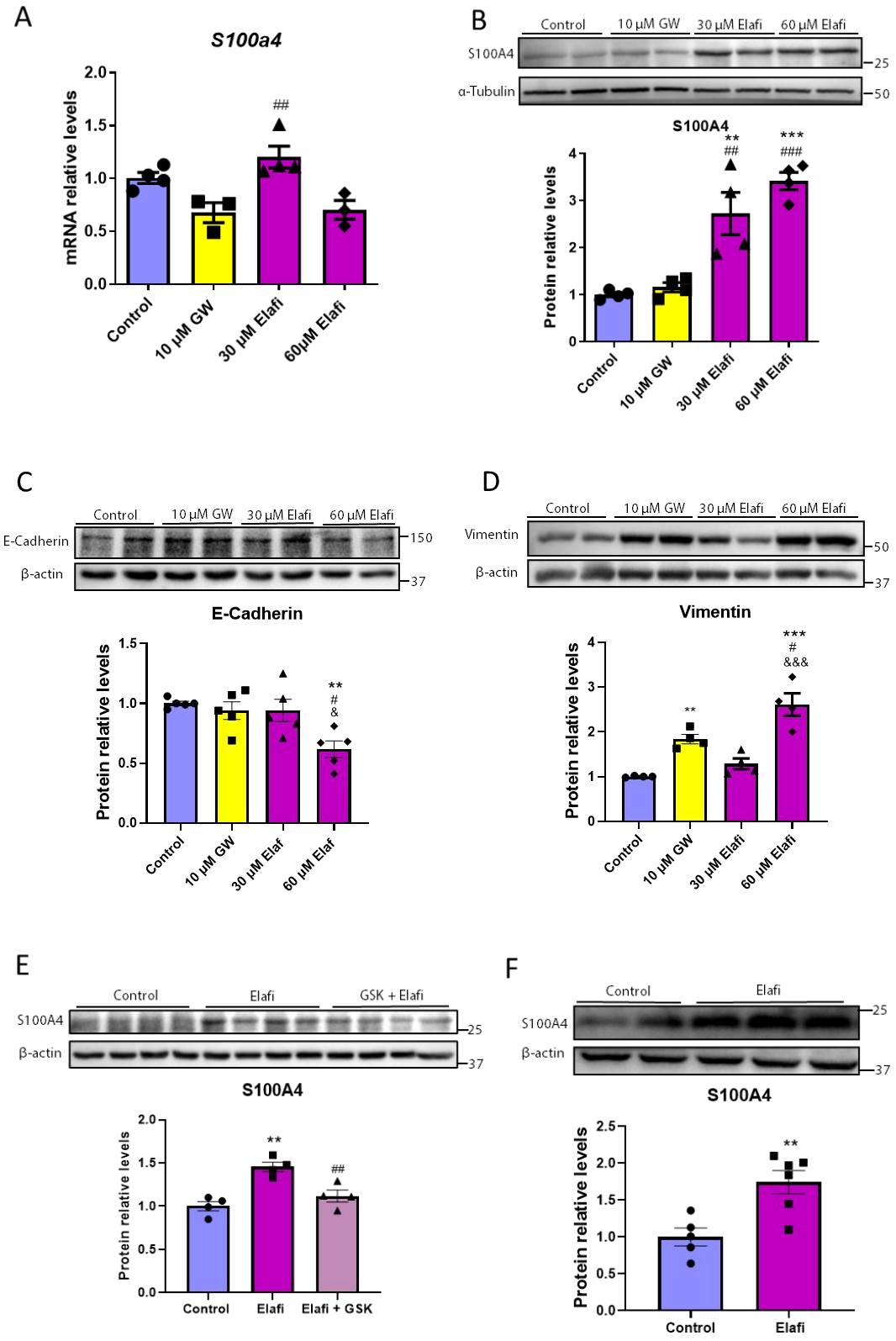
A
S100a4
mRNA relative levels
2.0
1.5
1.0
0.5
0.0
##
Control
10 µM GW
30 µM Elafi
60µM Elafi
B
Control
10 µM GW
30 µM Elafi
60 µM Elafi
S100A4
α-Tubulin
25
50
S100A4
Protein relative levels
**
##
***
###
Control
10 µM GW
30 µM Elafi
60 µM Elafi
C
Control
10 µM GW
30 µM Elafi
60 µM Elafi
E-Cadherin
β-actin
150
37
E-Cadherin
Protein relative levels
**
#
&
Control
10 µM GW
30 µM Elaf
60 µM Elaf
D
Control
10 µM GW
30 µM Elafi
60 µM Elafi
Vimentin
β-actin
50
37
Vimentin
Protein relative levels
**
***
#
&&&
Control
10 µM GW
30 µM Elafi
60 µM Elafi
E
Control
Elafi
GSK + Elafi
S100A4
β-actin
25
37
S100A4
Protein relative levels
**
##
Control
Elafi
Elafi + GSK
F
Control
Elafi
S100A4
β-actin
25
37
S100A4
Protein relative levels
**
Control
Elafi

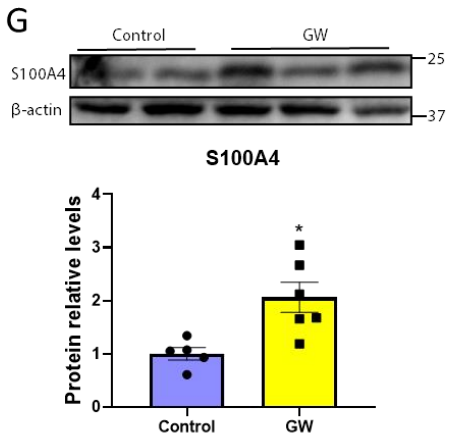

Figure 28. Elafibranor increases S100A4 protein levels in hepatocytes. *S100A4* mRNA levels (**A**) and S100A4 protein levels (**B**) in the rat liver cell line BRL-3A exposed to 10 μM GW501516 or elafibranor (30 or 60 μM) for 24 h. E-cadherin (**C**) and vimentin (**D**) protein levels in the BRL-3A cells exposed to elafibranor (30 or 60 μM) for 24 h. S100A4 protein levels (**E**) in the BRL-3A cells exposed to 30 μM elafibranor in the presence or absence of 60 μM of the PPAR-β/δ antagonist GSK0660 for 24 h. S100A4 protein levels in the mouse primary culture of hepatocytes exposed to 30 μM elafibranor (**F**) or 10 μM GW501516 (**G**) for 24 h. Data are presented as the mean ± SEM. $^{**}p < 0.01$ and $^{***}p < 0.001$ *vs.* control. $^{\#}p < 0.05$, $^{\#\#}p < 0.01$, and $^{\#\#\#}p < 0.001$ *vs.* GW501516-treated cells. $^{\&\&\&}p < 0.001$ *vs.* elafibranor-treated cells. *P-values* were determined by one-way ANOVA with Tukey's post-hoc test (**A-E**) or two-tailed unpaired Student's t-test (**F, G**).

1.3. Elafibranor increases S100A4 by reducing the protein levels of the ubiquitin E3 ligase ASB2

Next, we examined whether there was a potential post-transcriptional mechanism by which elafibranor increased S100A4 protein levels. Since ROS modifies S100A4 activity and dimerization (Tsuchiya, Yamaguchi et al. 2014), we explored the involvement of ROS in the effects of elafibranor. Under our conditions, the incubation

of BRL-3A cells with H_2O_2 or the co-incubation of elafibranor-exposed cells with the antioxidant N-acetylcysteine did not affect S100A4 protein levels, indicating that ROS were not involved (Supplementary Figure 1B).

Interestingly, it has been reported that the inhibition of the activities of ERK1/2 reduces the activity of several E3 ubiquitin ligases (Zakaria, Lamsoul et al. 2013). Since we have previously reported that PPAR-β/δ activation inhibits ERK1/2 activity (Rodriguez-Calvo, Serrano et al. 2008), we evaluated whether the inhibition of this kinase mediated the effects of elafibranor on S100A4. Consistent with the previous findings reported for PPAR-β/δ activation (Rodriguez-Calvo, Serrano et al. 2008, Braumann, Thottakara et al. 2018), elafibranor reduced phosphorylated ERK1/2 levels in the livers of mice fed the CD-HFD (Figure 29A). However, the ERK1/2 inhibitor U0126, which reduced phosphorylated ERK1/2 levels even more than elafibranor (Figure 29B), did not increase the protein levels of S100A4 in the BRL-3A cells (Figure 29C), thereby indicating that ERK1/2 inhibition was not the mechanism responsible for the elafibranor-induced increase in S100A4 levels.

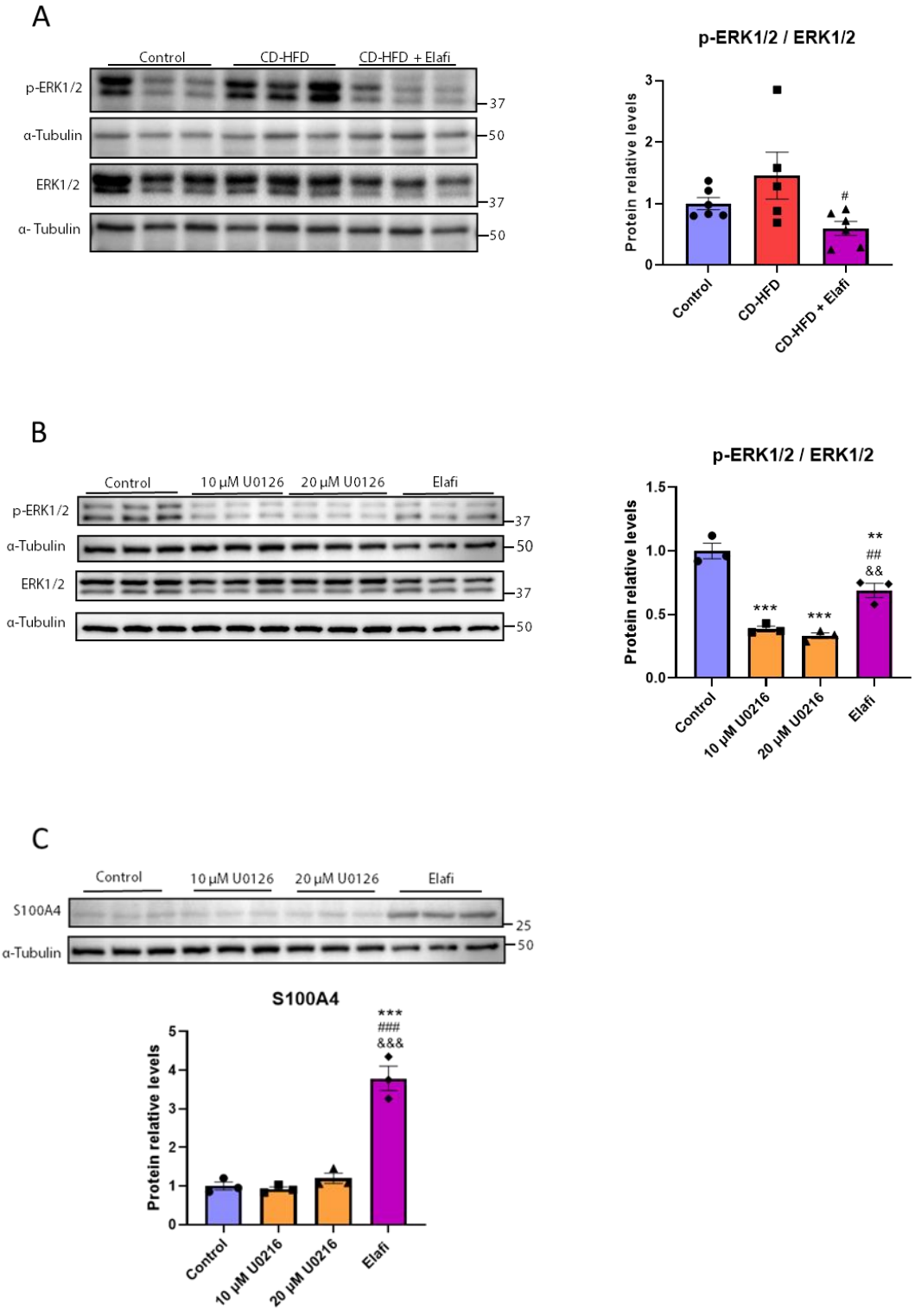

Figure 29. ERK1/2 inhibition is not likely to be involved in the increase in S100A4 protein levels caused by elafibranor. (**A**) Total and phosphorylated ERK1/2 levels in the livers of mice (n=6 animals) fed a standard diet (control) or a CD-HFD for 12 weeks and treated with vehicle or 10 mg/kg/day of elafibranor during the last 4 weeks. Total and phosphorylated

ERK1/2 levels (**B**) and S100A4 protein levels (**C**) in the BRL-3A cells exposed to 60 μM elafibranor or the ERK1/2 inhibitor U0126 (10 or 20 μM). Data are presented as the mean ± SEM. $^{*}p < 0.05$, $^{**}p < 0.01$, and $^{***}p < 0.001$ *vs.* control cells. $^{\#}p < 0.05$, $^{\#\#}p < 0.01$, and $^{\#\#\#}p < 0.001$ *vs.* CD-HFD or control cells. $^{\&\&}p < 0.01$ and $^{\&\&\&}p < 0.001$ *vs.* U0126-treated cells. *P-values* were determined by one-way ANOVA with Tukey's post-hoc test.

ASB2β is the specificity subunit of a multimeric E3 ubiquitin ligase (Bello, Lamsoul et al. 2009) that has been reported to induce the degradation of S100A4 (Braumann, Thottakara et al. 2018). We therefore speculated that the increased S100A4 protein levels induced by elafibranor were due to the reduced expression of ASB2β. In the protein lysates of both mouse livers and BRL-3A cells, a 70-kDa band corresponding to ASB2β was detected with an antibody raised against a peptide common to both the ASB2α and ASB2β isoforms (Figure 30A, B). The amount of this protein was reduced in the livers of the CD-HFD-fed mice treated with elafibranor (Figure 30A). Likewise, elafibranor reduced the amount of this protein in the BRL-3A cells (Figure 30B), and a similar behavior was observed in the mouse primary culture of hepatocytes (Figure 30C). Since ASB2α but not ASB2β induces the proteasomal degradation of filamin A (Heuze, Lamsoul et al. 2008, Bello, Lamsoul et al. 2009), we examined the levels of filamin A in the BRL-3A cells. Indeed, we observed that elafibranor did not affect filamin A levels (Figure 30D), suggesting that this isoform of ASB2 was not affected by elafibranor. Thus, ASB2β isoform was affected by elafibranor treatment. These findings suggested that elafibranor increases S100A4 protein levels by reducing its ASB2β-mediated degradation. To confirm this, we used

CRISPR/dCas9 activation plasmids designed to specifically upregulate the *Asb2* gene. Overexpression of *Asb2* (Supplementary Figure 1C, D) in the BRL-3A cells treated with vehicle reduced the basal protein levels of S100A4, confirming that this E3 ubiquitin ligase degrades S100A4 (Figure 30E). Interestingly, the increase in S100A4 levels caused by elafibranor was prevented by *Asb2* overexpression, indicating that ASB2 is involved in the effects of elafibranor on S100A4 levels.

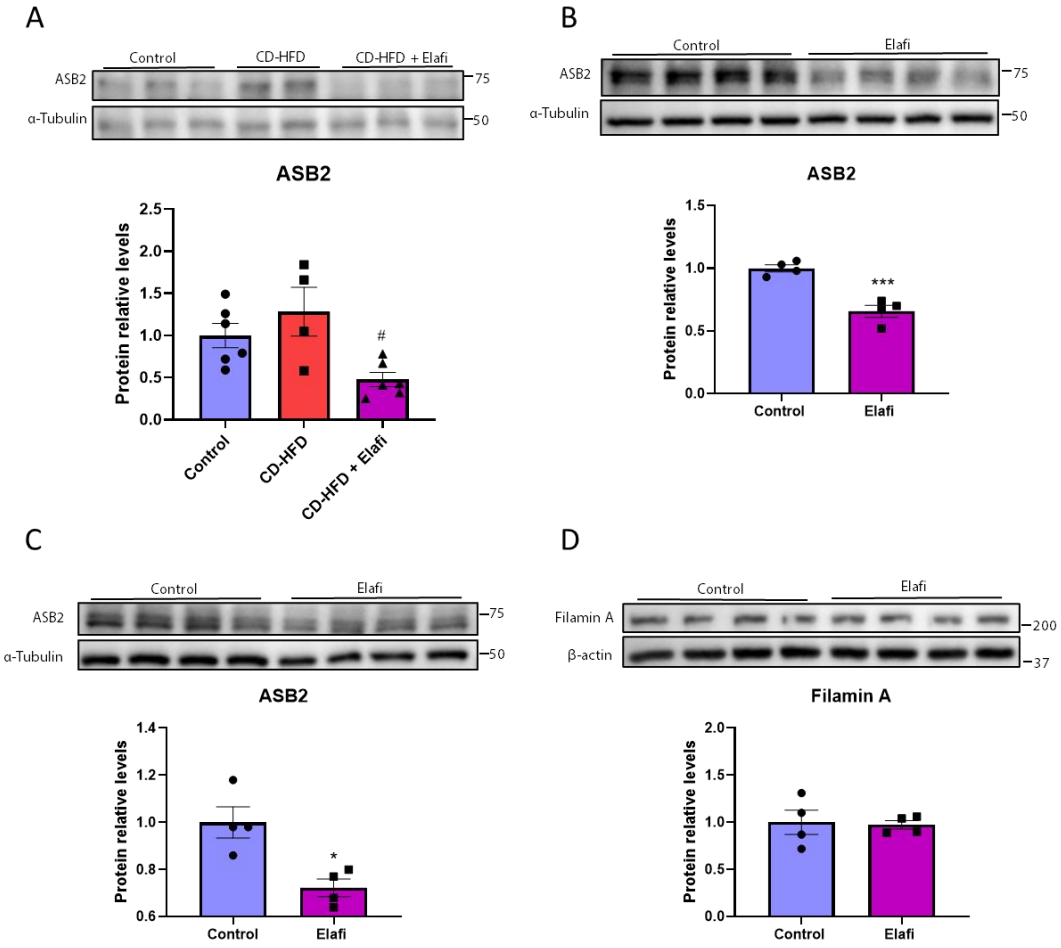

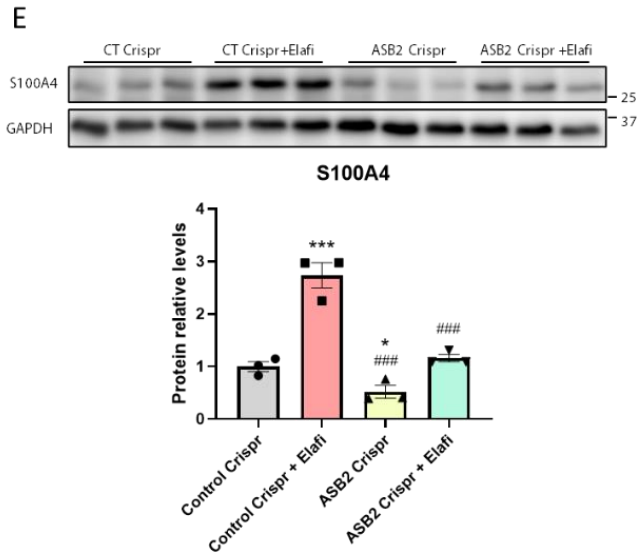

Figure 30. *Asb2* overexpression prevents the upregulation of S100A4 by elafibranor. (**A**) ASB2 protein levels in the livers of mice (n=6 animals) fed a standard diet (control) or a CD-HFD for 12 weeks and treated with vehicle or 10 mg/kg/day of elafibranor during the last 4 weeks. ASB2 protein levels in the BRL-3A cells exposed to 60 µM elafibranor for 24 h (**B**) or in the mouse primary culture of hepatocytes exposed to 30 µM elafibranor for 24 h (**C**). Filamin A protein levels (**D**) in the BRL-3A cells exposed to 60 µM elafibranor for 24 h. S100A4 protein levels (**E**) in the BRL-3A cells transfected with the ASB2 CRISPR/dCas9 activation plasmids or control CRISPR/dCas9 activation plasmids and treated with either vehicle or 60 µM elafibranor for 24 h. Data are presented as the mean ± SEM. $^{*}p < 0.05$ and $^{***}p < 0.001$ *vs.* control. $^{\#}p < 0.05$ and $^{\#\#}p < 0.01$ *vs.* CD-HFD-fed mice or CT CRISPR and elafibranor. *p-values* were determined by one-way ANOVA with Tukey's post-hoc test (**A, E**) or two-tailed unpaired Student's t-test **(B, C, D)**.

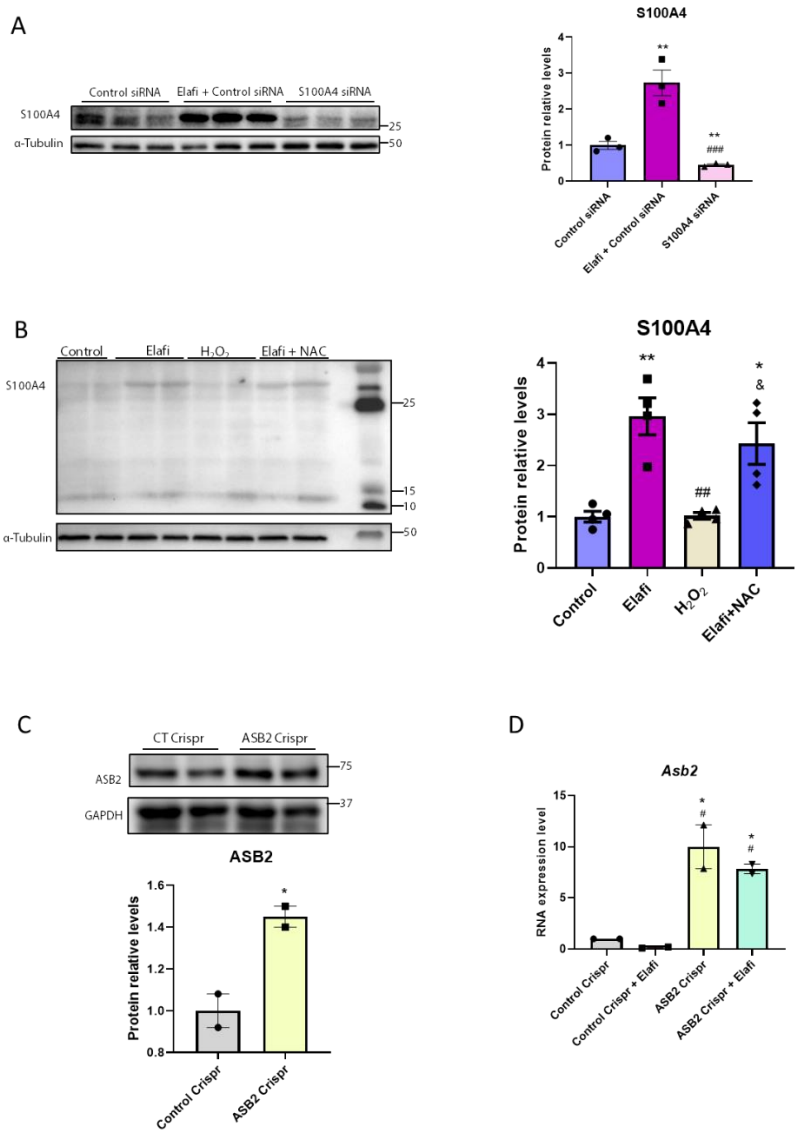

Supplementary Figure 1. (**A**) S100A4 protein levels in BRL-3 cells transfected with Control siRNA and S100A4 siRNA for 6 hours, after 24 hours the BRL-3A cells exposed to 60 μM elafibranor for 24 h. (**B**) S100A4 protein levels in BRL-3A cells incubated with H_2O_2 and co-incubation of elafibranor-exposed cells with the antioxidant N-acetylcysteine. ASB2 protein levels (**C**) and *Asb2* mRNA levels (**D**) in the BRL-3A cells transfected with the ASB2 CRISPR/dCas9 activation plasmids or control CRISPR/dCas9 activation plasmids and treated with either vehicle or 60 μM elafibranor for 24 h. Data are presented as the mean ± SEM. $^{*}p < 0.05$ and $^{**}p < 0.01$ *vs.* control. $^{\#}p < 0.05$, $^{\#\#}p < 0.01$ and $^{\#\#\#}p < 0.01$ *vs.* CD-HFD-fed mice or CT CRISPR and elafibranor. *p-values* determined by one-way ANOVA with Tukey's post-hoc test (**C**) or two-tailed unpaired Student's t-test (**A**, **B**, **D**).

Objective 2. PPAR-β/δ activation attenuates hepatic fibrosis by inhibiting the SMAD3 pathway via modulation of the negative crosstalk between AMPK and ERK1/2 in HSCs

2.1. PPAR-β/δ activation improves hepatic fibrosis in mice fed a CD-HFD diet

To achieve the second objective, we first assessed whether the PPAR-β/δ agonist GW501516 improved the metabolic alterations caused by the CD-HFD in mice. GW5101516 did not reduce the increase in body weight caused by the CD-HFD (Figure 31A), but completely prevented glucose intolerance and peripheral IR caused by this diet (Figure 31B, C). H&E and ORO staining of liver sections showed that the CD-HFD caused a significant hepatic lipid accumulation, which was reduced by the GW501516 treatment (Figure 31D, E). In addition, feeding the CD-HFD resulted in a significant increase in the accumulation of collagen in the liver, as demonstrated by the Sirius Red staining, whereas Trichrome staining caused a non-significant increase (Figure 31F, G). In both cases, GW501516 reduced collagen accumulation to values similar to those present in control mice.

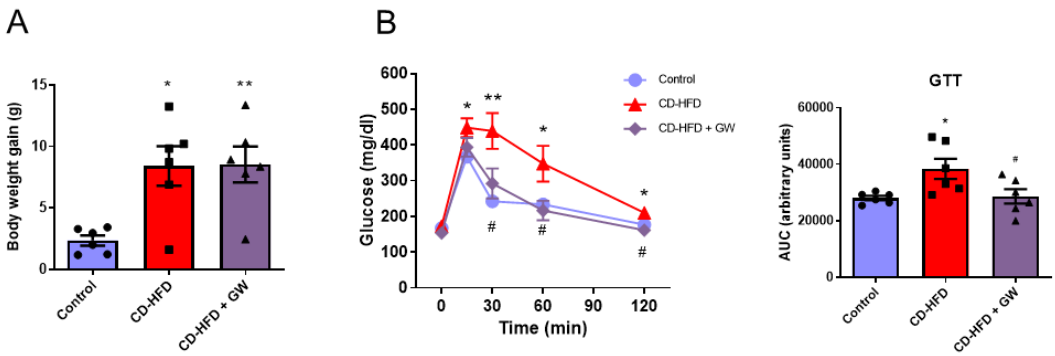

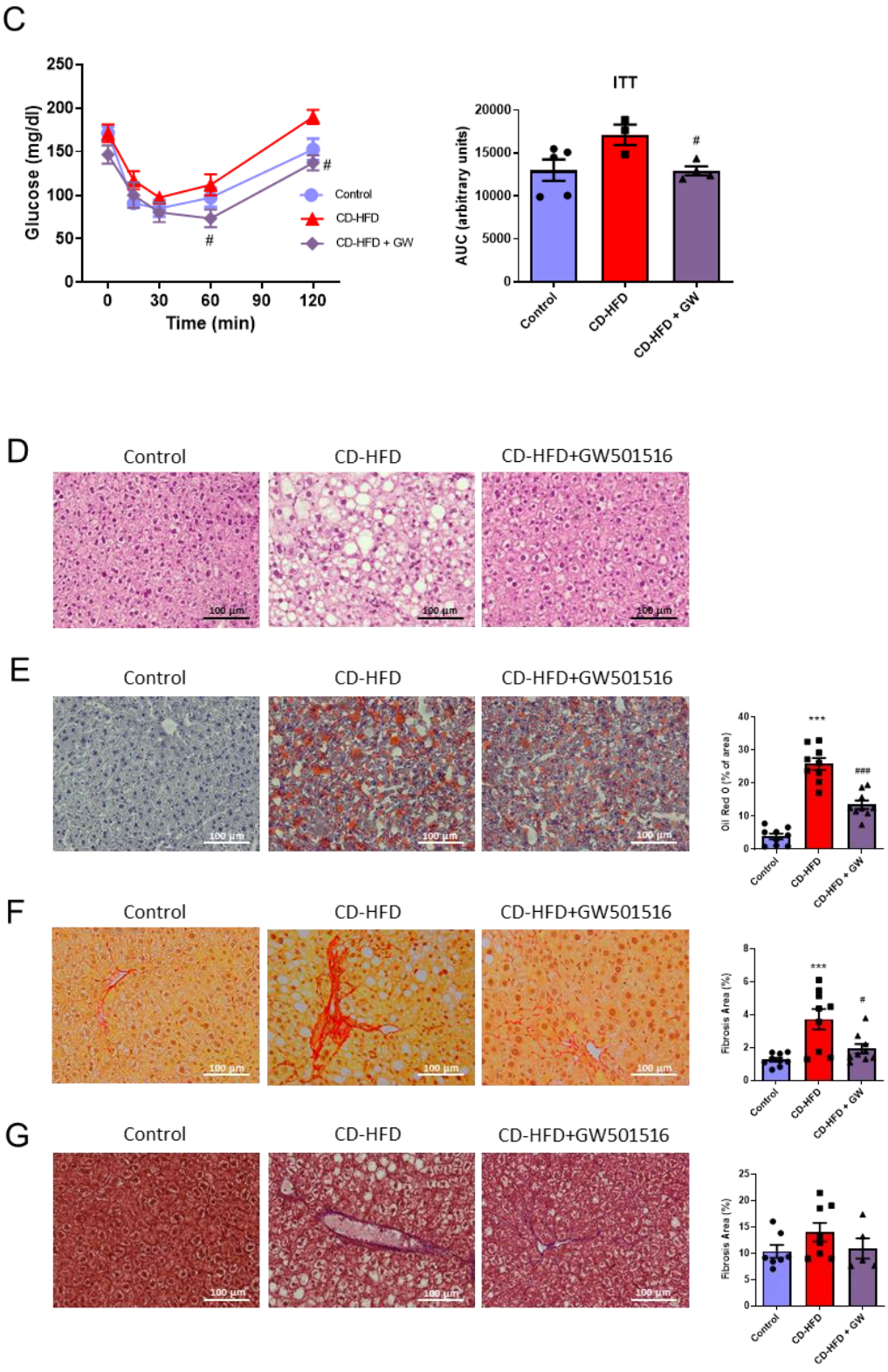

Figure 31. PPAR-β/δ activation improves hepatic fibrosis in mice fed a CD-HFD. (**A**) Body weight gain in control mice, mice fed the CD-HFD for 12 weeks, and mice fed the CD-HFD for 12 weeks and treated with the PPAR-β/δ agonist GW501516 for the last 4 weeks. n=6 per group. (**B**) GTT and area under the curve (AUC). n=6 per group. (**C**) ITT and AUC. n=6 per

group. Representative images of liver sections and quantification of H&E (**D**), ORO (**E**), Sirius red (**F**) and Masson's trichrome (**G**) staining in control mice, mice fed the CD-HFD for 12 weeks, and mice fed the CD-HFD for 12 weeks and treated with the PPAR-β/δ agonist GW501516 for the last 4 weeks. Scale bar: 100 μm. n=9 per group. Data are presented as the mean ± SEM. Significant differences were established by ANOVA. $^{***}p < 0.001$, $^{**}p < 0.01$ and $^{*}p < 0.05$ *vs.* control. $^{###}p < 0.001$, $^{##}p < 0.01$, $^{#}p < 0.05$ *vs.* mice fed the CD-HFD.

Consistent with the histology findings, the CH-HFD increased the expression levels of *Col1a1* and *Col3a1* and GW501516 attenuated this increase, although in the case of the latter differences were not significant (Figure 32A). Moreover, the increase in the expression of the inflammatory genes *Il6*, *Ccl2* (also known as *Mcp1*) and *Tnfa* caused by the CD-HFD was abrogated by the treatment with the PPAR-β/δ agonist (Figure 32B). Treatment with GW501516 reduced the hepatic expression of *Tgfb* as well as that of the SMAD3-target gene *Ctgf*, whereas the expression of *Serpine1*, which codes PAI-1, was not affected (Figure 32C). Interestingly, it has been reported that PPAR-β/δ regulates macrophage polarization toward the anti-inflammatory M2 phenotype (Kang, Reilly et al. 2008). In agreement with this, GW501516 completely abolished the increase in the expression of the M1 marker *Nos2* caused by the CD-HFD, while preventing the reduction in the M2 marker *Arg1* (Figure 32D). Collectively, these findings show that PPAR-β/δ activation improves the metabolic alterations caused by feeding the CD-HFD and prevents liver fibrosis.

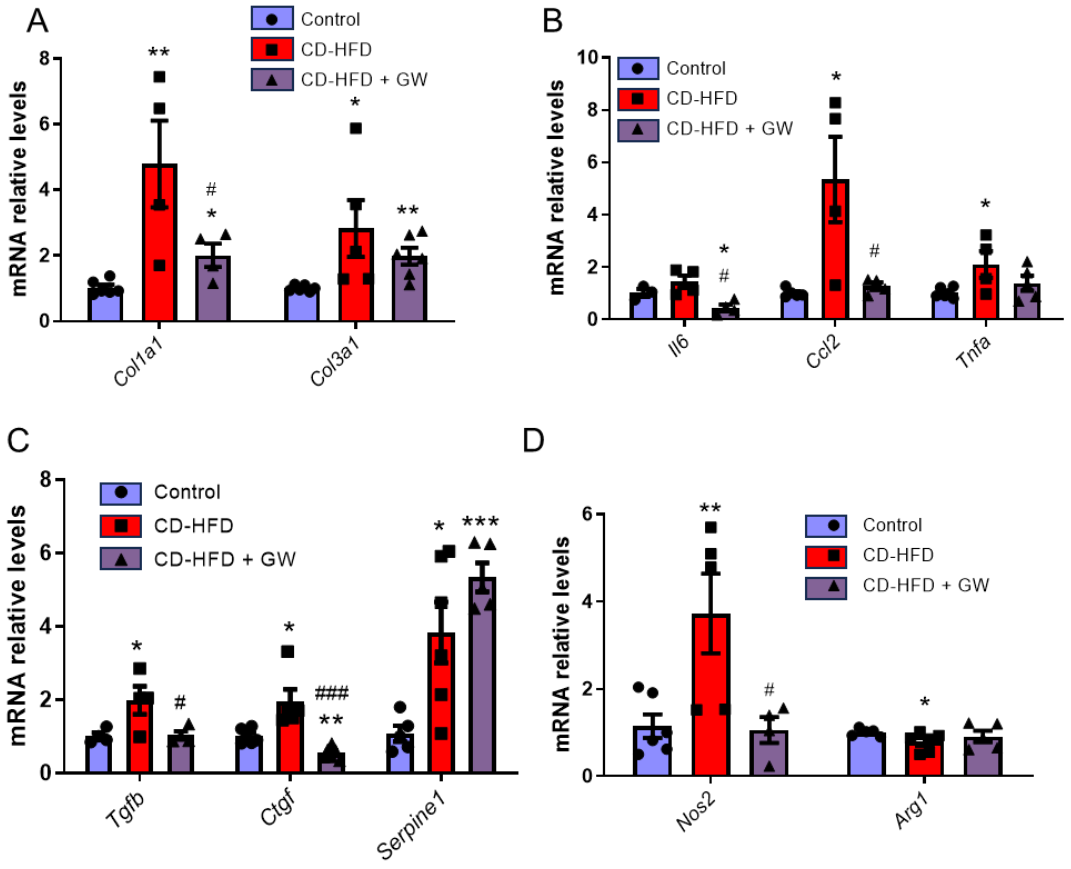

Figure 32. PPAR-β/δ activation regulates hepatic mRNA levels of markers of fibrosis, inflammation and macrophage polarization in mice fed a CD-HFD. (**A**) mRNA levels of fibrotic markers *Col1a1* and *Col3a1* in the livers of control mice, mice fed the CD-HFD for 12 weeks, and mice fed the CD-HFD for 12 weeks and treated with the PPAR-β/δ agonist GW501516 for the last 4 weeks. (**B**) mRNA levels of inflammatory markers *Il6*, *Ccl2* and *Tnfa*. (**D**) mRNA levels of *Tgfb* and the SMAD3-target genes *Ctgf* and *Serpine1*. (E) mRNA levels of the macrophage polarization markers *Nos2* and *Arg1*. n=4-6 per group. Data are presented as the mean ± SEM. Significant differences were established by ANOVA. $^{***}p < 0.001$, $^{**}p < 0.01$ and $^{*}p < 0.05$ *vs.* control. $^{###}p < 0.001$, $^{##}p < 0.01$, $^{#}p < 0.05$ *vs.* mice fed the CD-HFD.

2.2. Primary HSCs isolated from *Ppard*$^{-/-}$ mice show increased mRNA levels of *Col1a1*

Since HSCs are the central effector in hepatic fibrosis, we next focused on the role of PPAR-β/δ in these cells. In primary HSCs isolated from WT and *Ppard*$^{-/-}$ mice (Figure 33A), we observed that deficiency of this nuclear receptor increased the expression levels of *Col1a1* (Figure 33B), whereas no changes were observed in the expression of *Tgfb* and *Col3a1*(Figure 33C, D). These findings suggest that, at least in part, *Ppard* deficiency impacts the regulation of a marker of liver fibrosis and HSC activation.

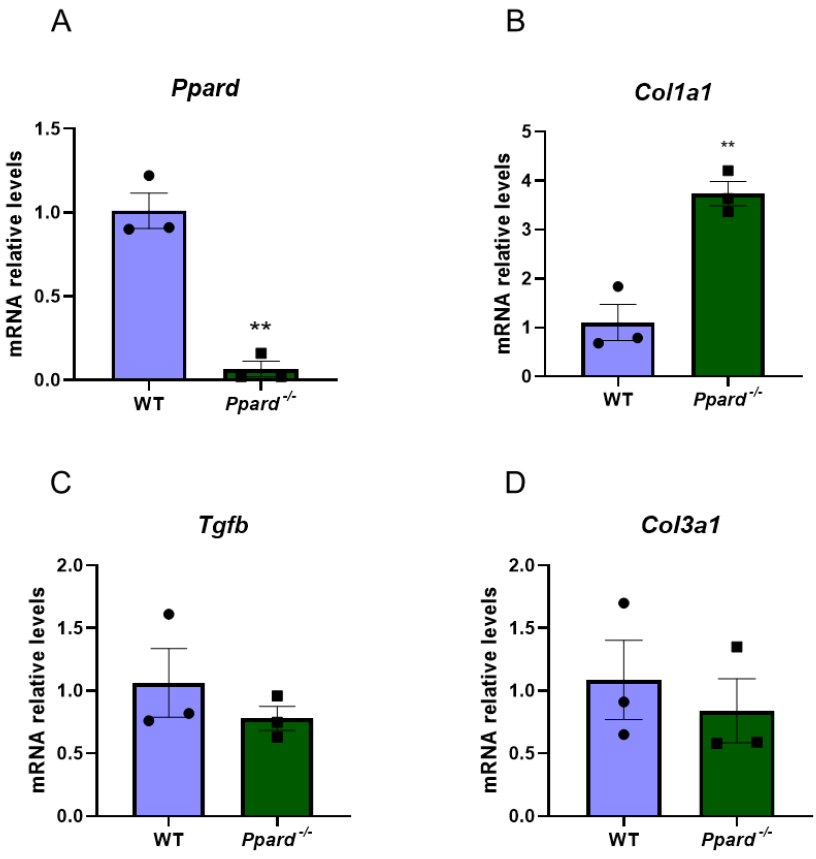

Figure 33. Primary HSC isolated from *Ppard*$^{-/-}$ mice show increased mRNA levels of *Col1a1*. mRNA levels of (**A**) *Ppard,* (**B**) *Col1a1,* (**C**) *Tgfb* and (**D**) *Col3a1* in primary HSC isolated from WT and *Ppard*$^{-/-}$ mice. n=3 per group. Data are presented as the mean ± SEM. Significant differences were established by the Student's t-test. $^{*}p < 0.05$, $^{**}p < 0.01$ and $^{***}p < 0.001$ *vs.* WT.

2.3. PPAR-β/δ activation abrogates TGF-β1-mediated cell migration and SMAD3 activation in LX-2 cells

To evaluate whether antifibrogenic effects observed in the liver of mice fed a CD-HFD could occur through an independent action on HSCs, direct effects of GW501516 were assessed in the LX-2 human HSC line, which provides a valuable tool in the study of liver fibrosis (Xu, Hui et al. 2005). Since the increase in HSC migrating activity is indicative of cell activation, we examined the effects of GW501516 on cell migration in response to TGF-β1 by conducting wound-healing analysis in which cells were serum starved for 16 hours and plates scratched to form cell-free paths. The remaining cells were then incubated in medium for 24 hours, in the presence or the absence of TGF-β1 with or without GW501516. In response to TGF-β1, cells migrated faster and GW501516 elicited a robust inhibition of TGF-β1-triggered closure of scratch (Figure 34A). Consistent with this, GW501516 completely abolished the increase in the protein levels of COL1A1 and α-SMA, two reliable markers of HSC activation and liver fibrosis (Figure 34B). Next, we determine the activation of SMAD3. This transcription factor is activated by phosphorylation via type I TGF-β receptors, but also by intracellular kinases such as ERK1/2 (Dong, Chowdhury et al. 2021). Once

phosphorylated, SMAD3 interacts with SMAD4 and translocates to the nucleus, where it binds to the co-activator p300 to activate transcription (Dong, Chowdhury et al. 2021). As expected, TGF-β1 increased SMAD3 phosphorylation, but this was not observed when LX-2 cells were co-incubated with GW501516 (Figure 34C). Similarly, GW501516 abolished the increase in p300 caused by TGF-β1 (Figure 34D). Consistent with this, the livers of *Ppard*$^{-/-}$ mice exhibited increased p300 protein levels compared to WT mice (Figure 34E) and primary HSC isolated from *Ppard*$^{-/-}$ mice displayed enhanced *Ep300* mRNA levels (Figure 34F). Overall, these results show that PPAR-β/δ activation abolishes TGF-β1 signaling in HSCs and prevents HSC activation, SMAD3 activation by phosphorylation and the increase in p300.

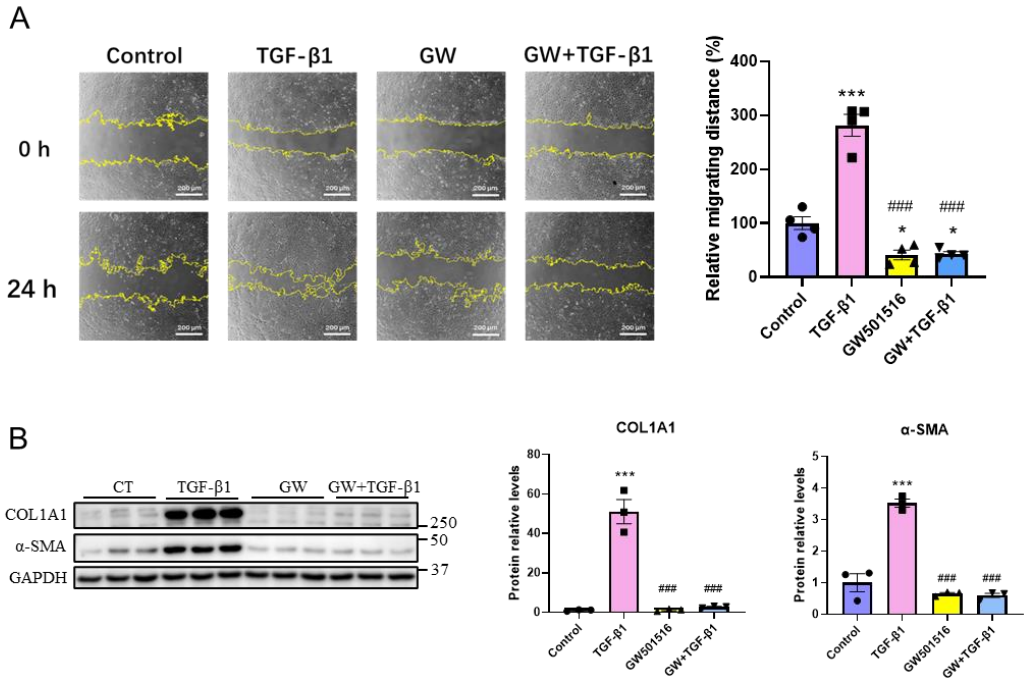

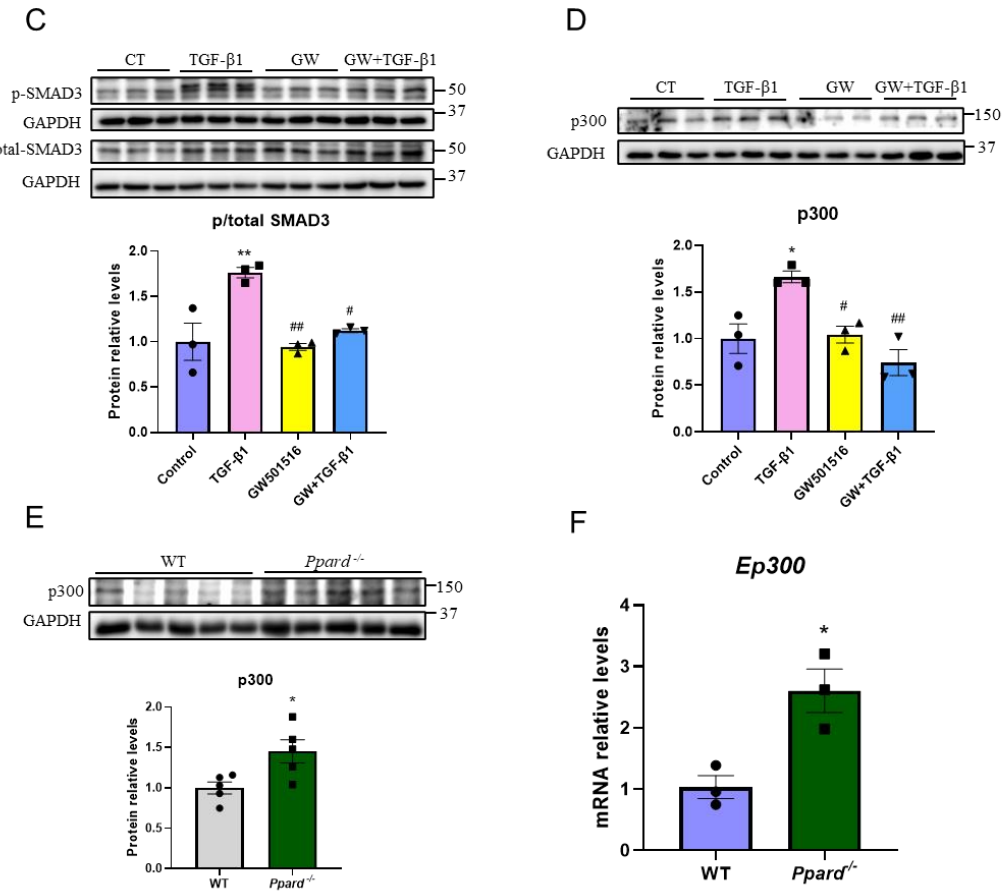

Figure 34. PPAR-β/δ activation abrogates TGF-β1-mediated cell migration and SMAD3 activation in LX-2 cells. (**A**) The wound healing assay was used to detect the ability of PPAR-β/δ activation to attenuate TGF-β1-induced migration. The bars on the right represent relative migration distance in percentage. Immunoblot analysis of (**B**) COL1A1 and α-SMA, (**C**) total and phosphorylated SMAD3 and (**D**) p300 in LX-2 cells exposed to 10 ng/ml TGF-β1 in the presence or absence of 10 µM GW501516 for 24 h. n=3 per group. Data are presented as the mean ± SEM. Significant differences were established by ANOVA. $^{***}p < 0.001$, $^{**}p < 0.01$ and $^{*}p < 0.05$ *vs.* control. $^{###}p < 0.001$, $^{##}p < 0.01$, $^{#}p < 0.05$ *vs.* TGF-β1-incubated cells. (**E**) Immunoblot analysis of p300 in the liver of WT and *Ppard*$^{-/-}$ mice. n=5 per group. (**F**) mRNA levels of E*p300* in primary HSC isolated from WT and *Ppard*$^{-/-}$ mice. n=3 per group. Data are presented as the mean ± SEM. Significant differences were established by the Student's t-test. $^{*}p < 0.05$ *vs.* WT.

2.4. PPAR-β/δ activation prevents the reduction in phosphorylated AMPK and the increase in phosphorylated ERK1/2 caused by TGF-β1 in LX-2 cells

Of note, PPAR-β/δ ligands activate AMPK (Vazquez-Carrera 2016, Zarei, Aguilar-Recarte et al. 2021) and activation of this kinase has been reported to reduce hepatic fibrosis in animal models and to suppress the expression of fibrogenic genes in HSCs (Lim, Oh et al. 2012, Zhao, Sun et al. 2020, Dong, Chowdhury et al. 2021). In addition, TGF-β1 also activates ERK1/2, which directly phosphorylates SMAD3 (Zhang 2017). Likewise, the presence of the inhibitory crosstalk between AMPK and ERK1/2 reported in myotubes (Hwang, Jeong et al. 2013, Salvado, Barroso et al. 2014), but not in HSCs, might regulate SMAD3 activity and fibrosis. Considering this, we examined the levels of AMPK and ERK1/2 in LX-2 cells exposed to TGF-β1. Treatment with this cytokine reduced phosphorylated AMPK levels in HSCs (Figure 35A). Interestingly, co-incubation of the cells with GW501516 increased AMPK phosphorylation (Figure 35B) and prevented the increase in phosphorylated ERK1/2 caused by TGF-β1 (Figure 35C).

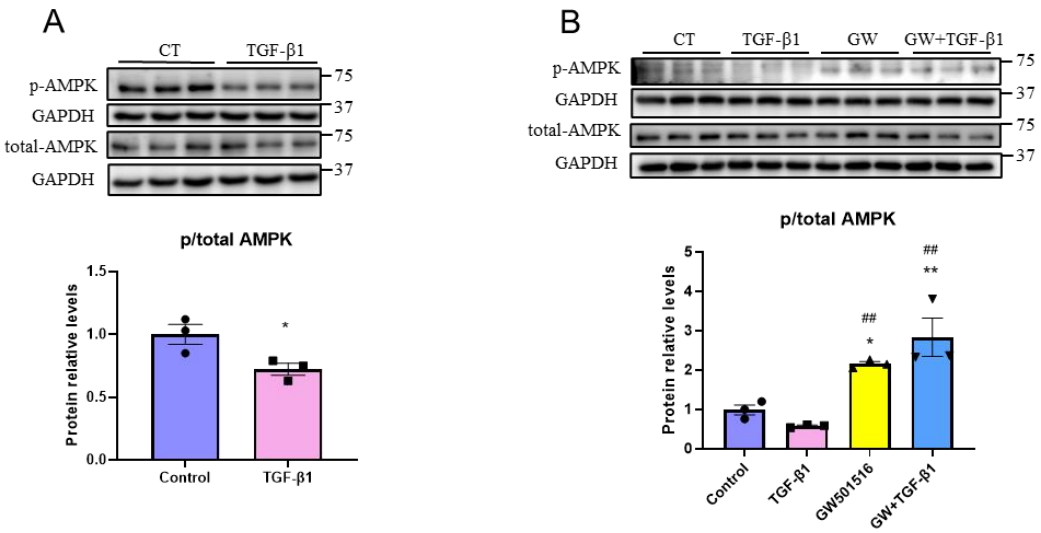

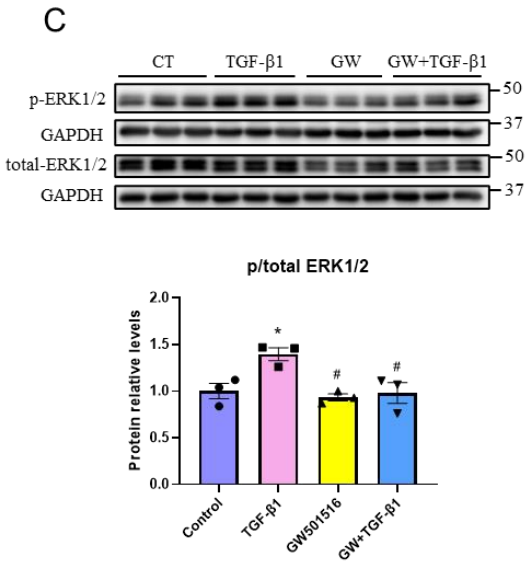

Figure 35. PPAR-β/δ activation prevents the reduction in phosphorylated AMPK and the increase in phosphorylated ERK1/2 caused by TGF-β1 in LX-2 cells. (**A**) Immunoblot analysis of total and phosphorylated AMPK in LX-2 cells exposed to 10 ng/ml TGF-β1 for 24 h. n=3 per group. Data are presented as the mean ± SEM. Significant differences were established by the Student's t-test. $^{*}p < 0.05$ *vs.* WT. Immunoblot analysis of (**B**) total and phosphorylated AMPK and (**C**) total and phosphorylated ERK1/2 in LX-2 cells exposed to 10 ng/ml TGF-β1 in the presence or absence of 10 μM GW501516 for 24 h. n=3 per group. Data are presented as the mean ± SEM. Significant differences were established by ANOVA. $^{**}p < 0.01$ and $^{*}p < 0.05$ *vs.* control. $^{\#\#}p < 0.01$, $^{\#}p < 0.05$ *vs.* TGF-β1-incubated cells.

To deepen into the effects of AMPK activation on HSC in our conditions, we used the specific AMPK activator A769662. Activation of AMPK with this compound prevented the reduction in phosphorylated AMPK caused by TGF-β1 in LX-2 (Figure 36A) and this was accompanied by the complete abolishment of the upregulation of COL1A1 (Figure 36B) and α-SMA (Figure 36C). Moreover, the A769662 treatment caused a significant reduction in the phosphorylation of SMAD3 (Figure 36D) and in

the increase in p300 observed in cells exposed to TGF-β1 (Figure 36E).

It is worth noting that in agreement with the presence of the inhibitory crosstalk between AMPK and ERK1/2, the AMPK activator A769662 reduced the levels of phosphorylated ERK1/2 (Figure 36F).

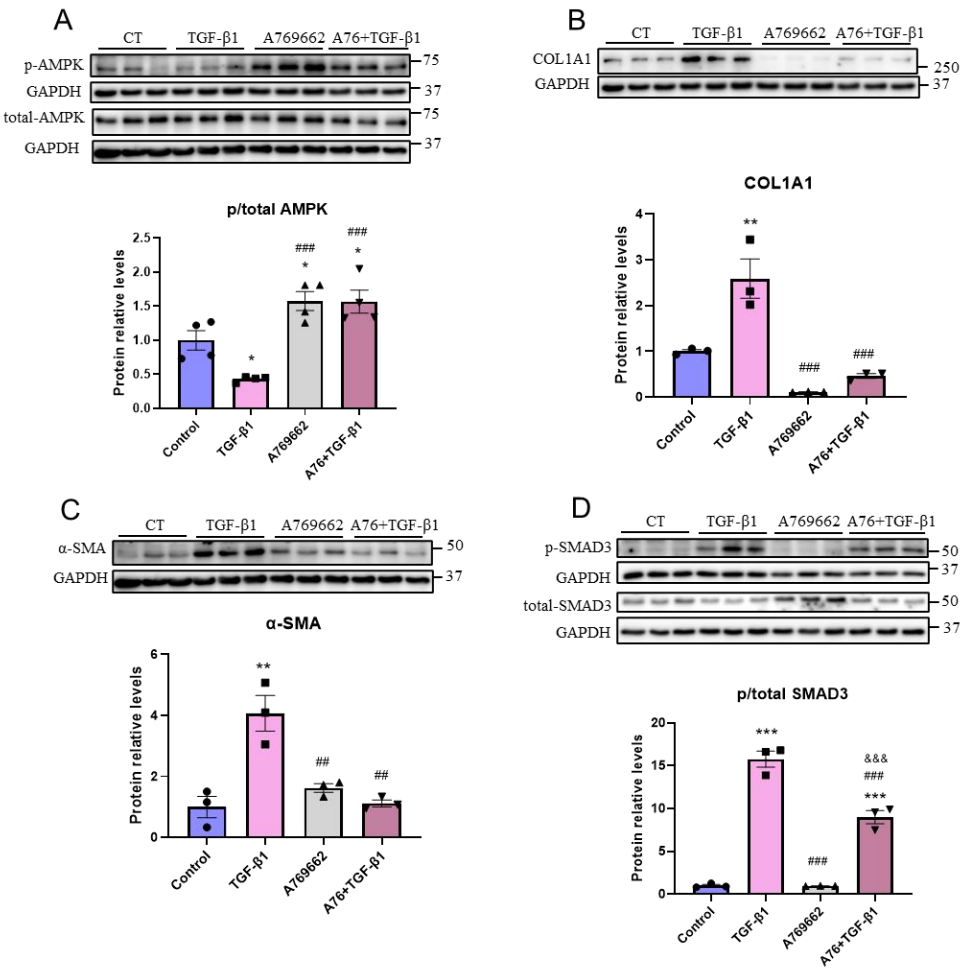

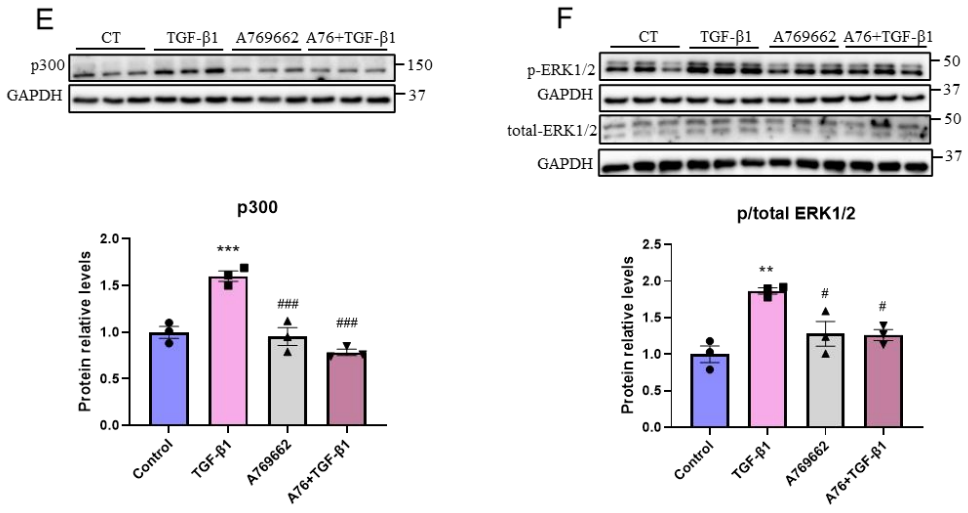

Figure 36. AMPK activation prevents the increase in fibrosis markers, the phosphorylation of ERK1/2, and the increase in p300 caused by TGF-β1 in LX-2 cells. Immunoblot analysis of (**A**) total and phosphorylated AMPK, (**B**) COL1A1, (**C**) α-SMA and (**D**) total and phosphorylated SMAD3, (**E**) p300 and (**F**) total and phosphorylated ERK1/2 in LX-2 cells exposed to 10 ng/ml TGF-β1 in the presence or absence of 60 μM A769662 for 24 h. n=3 or 4 per group. Data are presented as the mean ± SEM. Significant differences were established by ANOVA. $^{***}p < 0.001$, $^{**}p < 0.01$ and $^{*}p < 0.05$ *vs.* control. $^{###}p < 0.001$, $^{##}p < 0.01$, $^{#}p < 0.05$ *vs.* TGF-β1-incubated cells.

Next, we assessed whether ERK1/2 inhibition by the specific inhibitor U0126 influenced the parameters studied in LX-2 cells. Thus, the reduction in phosphorylated ERK1/2 caused by treatment with U0126 (Figure 37A) was accompanied by an increase in phosphorylated AMPK (Figure 37B), supporting the presence of the negative crosstalk between these two kinases in LX-2 cells. Treatment with the ERK1/2 inhibitor also mitigated the increase in COL1A1 (Figure 37C) and α-SMA (Figure 37D) caused by the exposure to TGF-β1. Similar to what we observed with A769662, the U0126 inhibitor also attenuated the increase in phosphorylated SMAD3 (Figure 37E) and p300

(Figure 37F) caused by TGF-β1.

Collectively, these findings suggest that the activation of AMPK prevents the increase in SMAD3 phosphorylation and p300 levels in HSC by reducing ERK1/2 activation. Therefore, these findings point to ERK1/2 inhibition as a new target responsible for the antifibrotic effect of PPAR-β/δ and AMPK activation.

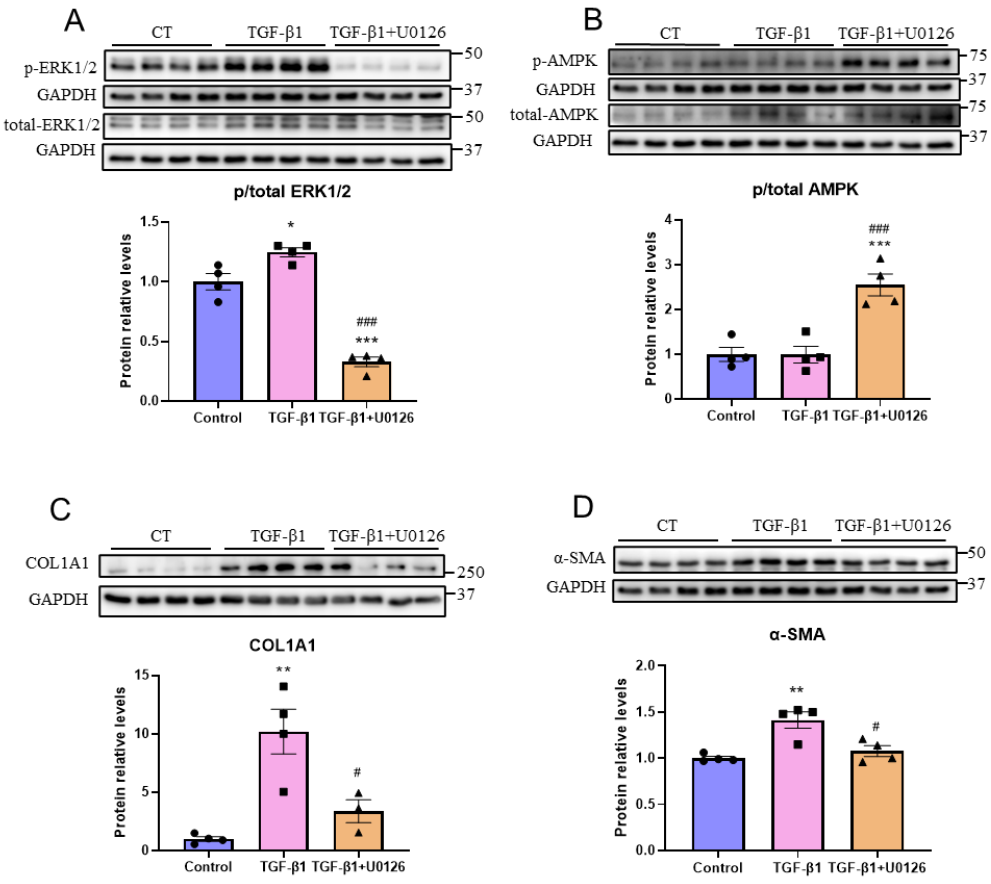

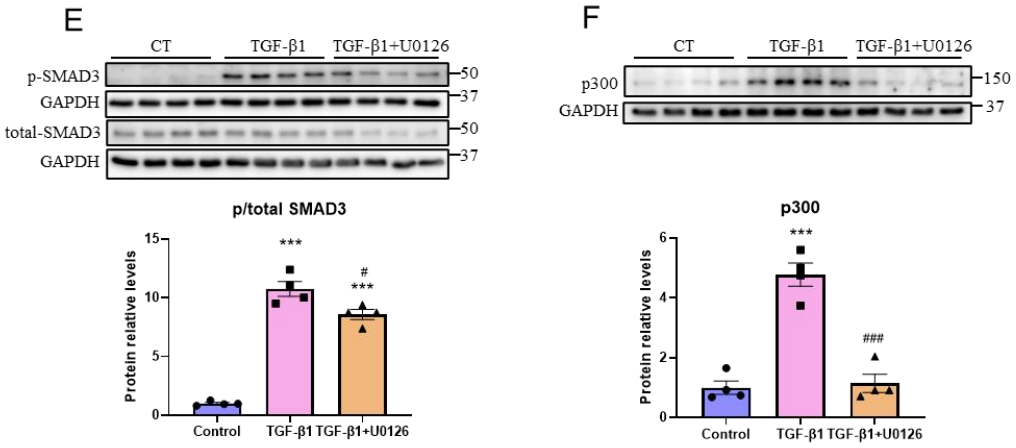

Figure 37. ERK1/2 inhibition leads to AMPK phosphorylation and prevents the increase in fibrosis markers and in p300 caused by TGF-β1 in LX-2 cells. Immunoblot analysis of (**A**) total and phosphorylated ERK1/2, (**B**) total and phosphorylated AMPK, (**C**) COL1A1, (**D**) α-SMA, (**E**) total and phosphorylated SMAD3 and (**F**) p300 in LX-2 cells exposed to 10 ng/ml TGF-β1 in the presence or absence of 10 μM U0126 for 24 h. n=4 per group. Data are presented as the mean ± SEM. Significant differences were established by ANOVA. $^{***}p < 0.001$, $^{**}p < 0.01$ and $^{*}p < 0.05$ *vs.* control. $^{###}p < 0.001$, $^{##}p < 0.01$, $^{#}p < 0.05$ *vs.* TGF-β1-incubated cells.

2.5. PPAR-β/δ activation attenuates the increase in phosphorylated ERK1/2 and p300 caused by TGF-β1 in LX-2 cells via AMPK

To clearly demonstrate that the effects of PPAR-β/δ activation on HSC activation, fibrosis and p300 increase are mediated by AMPK, we transfected LX-2 cells with control (scrambled) and AMPKα1/2 siRNA. Knockdown of AMPKα1/2 (Supplementary Figure 2A) blocked the increase in phosphorylated AMPK caused by incubation with GW501516 (Figure 38A). Consistent with a role for AMPK in the effects of GW501516, the beneficial effect of the PPAR-β/δ ligand on both phosphorylated SMAD3 and ERK1/2, and COL1A1 caused by TGF-β1 was attenuated

by knocking down AMPKα1/2 (Figure 38A). Likewise, the reduction in p300 caused by GW501516 in cells stimulated with TGF-β1 completely disappeared when AMPKα1/2 was knocked down (Figure 38B). Altogether, these findings confirm that in HSCs stimulated with TGF-β1, the activation of PPAR-β/δ prevents the increase in ERK1/2 phosphorylation, as well as fibrosis and the upregulation of p300 via AMPK.

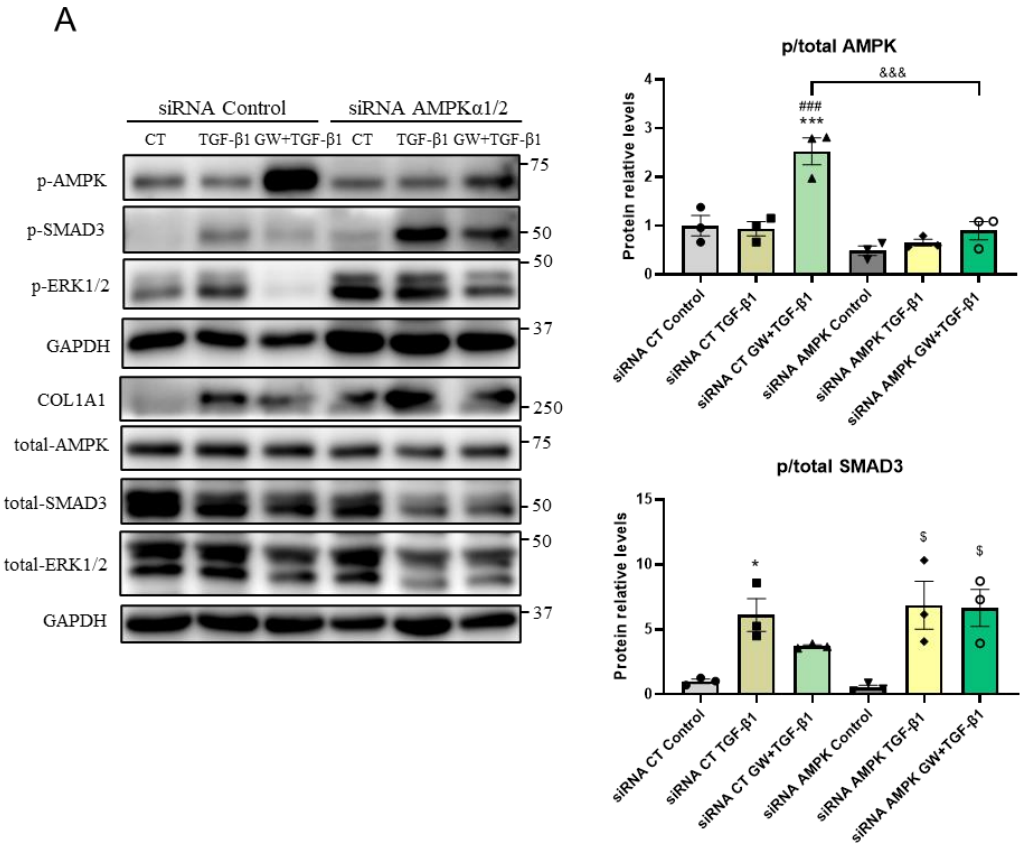

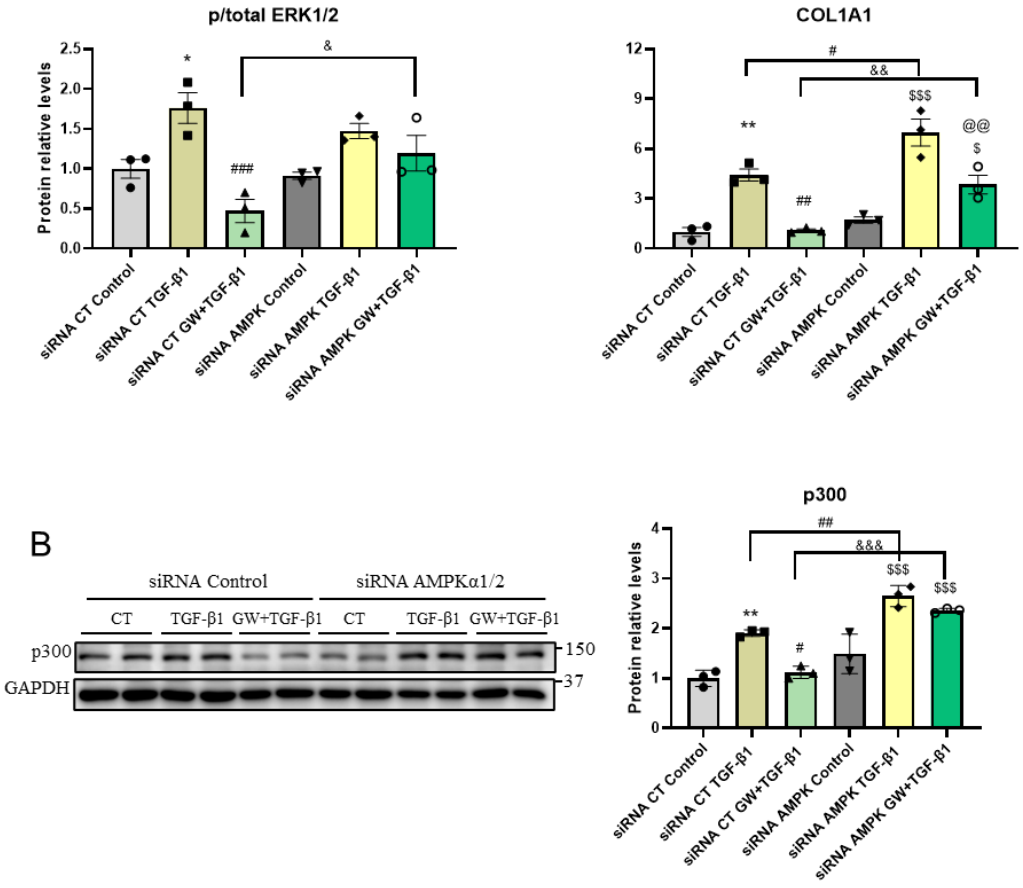

Figure 38. PPAR-β/δ activation attenuates the increase in phosphorylated ERK1/2 and p300 caused by TGF-β1 via AMPK in LX-2 cells. Immunoblot analysis of (**A**) total and phosphorylated AMPK, total and phosphorylated SMAD3, total and phosphorylated ERK1/2, COL1A1 and (**B**) p300 in LX-2 cells transfected with control (CT) (scrambled) siRNA or AMPKα1/2 siRNA and exposed to 10 ng/ml TGF-β1 in the presence or in the absence of 10 μM GW501516 for 24 h. n=3 per group. Data are presented as the mean ± SEM. Significant differences were established by ANOVA. $^{***}p < 0.001$, $^{**}p < 0.01$ and $^{*}p < 0.05$ *vs.* siRNA CT control. $^{###}p < 0.001$, $^{##}p < 0.01$, $^{#}p < 0.05$ *vs.* siRNA CT + TGF-β1. $^{\&\&\&}p < 0.001$, $^{\&\&}p < 0.01$, $^{\&}p < 0.05$ *vs.* siRNA CT + TGF-β1 + GW. $^{\$\$\$}p < 0.001$, $^{\$}p < 0.05$ *vs.* siRNA AMPK control. $^{@@}$ $p < 0.01$ *vs.* siRNA AMPK control + TGF-β1.

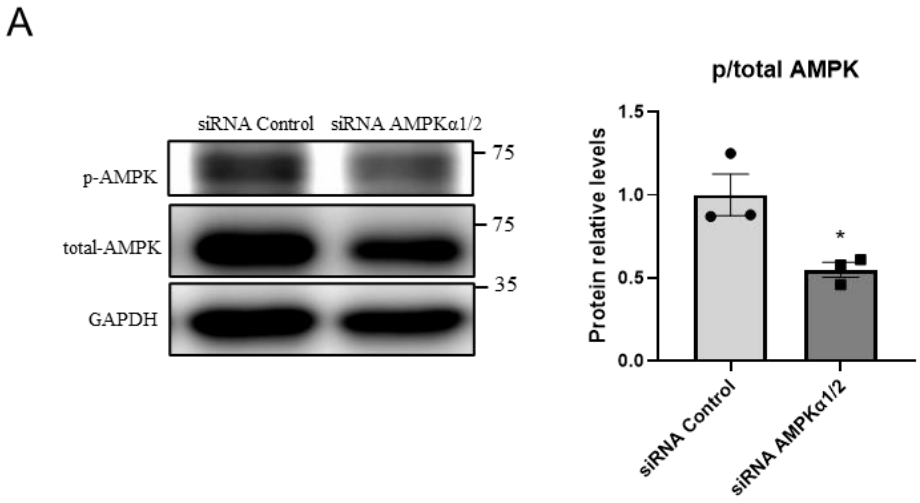

Supplementary Figure 2. (A) Immunoblot analysis of total and phosphorylated AMPK in LX-2 cells transfected with control (CT) (scrambled) siRNA or AMPKα1/2 siRNA. n=3 per group. Data are presented as the mean ± SEM. Significant differences were established by the Student's t-test. $^{*}p < 0.05$.

V. Discussion

The development of novel therapeutics for the treatment of MASH poses challenges, with PPAR-β/δ agonists typically among the investigational therapeutic agents being explored. In both of our studies, we have reported that PPAR-β/δ activation hinders the progression of MASLD by ameliorating IR, steatosis, inflammation, and fibrogenesis in mice, which is consistent with previous studies (Ratziu, Harrison et al. 2016, Zarei, Aguilar-Recarte et al. 2021). However, the use of PPAR-β/δ agonists as therapeutic agents for MASLD requires caution, since the function of PPAR-β/δ in liver fibrosis remains controversial.

Surprisingly, elafibranor increased the protein level of the EMT-inducer S100A4 through PPAR-β/δ activation. The increase in S100A4 protein levels caused by elafibranor was accompanied by changes in the levels of the markers associated with the EMT program, a process involved in fibrogenesis, which is in agreement with the controversy of PPAR-β/δ in hepatic fibrosis.

Our findings also show that PPAR-β/δ activation abrogates TGF-β1-induced HSC activation and SMAD3 phosphorylation in LX-2 cells via AMPK activation and the subsequent inhibition of the ERK1/2 pathway.

The conflicting outcomes underscore the complexity of PPAR-β/δ signaling in liver fibrosis, warranting further investigation to elucidate its precise role in this pathological condition.

Objective 1. Elafibranor upregulates the EMT-inducer S100A4 via PPAR-β/δ

The development of new drugs for the treatment of MASH is challenging, since findings from animal models have not been fully reproduced in clinical trials. This has also been the case for elafibranor, a drug with promising findings in preclinical studies that was discontinued in 2020 as it failed to show a statistically significant effect in patients with MASH during the phase III RESOLVE-IT clinical trial. Several factors can explain why promising preclinical drugs have failed in humans. For example, many of these compounds only target a few pathways involved in the development of MASH, when it is well-known that many pathways contribute to MASH. This limited action might result in a modest effect or it might be attenuated by the activation of compensatory mechanisms. Therefore, no single agent is likely to control all the aspects of this complex liver disease. After the negative outcome for elafibranor in monotherapy, the efficacy of elafibranor will be evaluated in combination with other drugs for the treatment of MASH (NASH). Moreover, the efficacy of this drug is also currently being examined in primary biliary cholangitis (Schattenberg, Pares et al. 2021).

In agreement with previous studies reporting the beneficial effects of elafibranor on glucose metabolism (Westerouen Van Meeteren, Drenth et al. 2020), we show here that the administration of this drug to mice fed a CD-HFD, ameliorates glucose intolerance and IR, which is one of the main drivers of MASH. These changes were

observed without a reduction in body weight. In addition, consistent with the findings of previous studies (van den Hoek, Verschuren et al. 2021), elafibranor reduced the levels of markers of fibrosis such as α-SMA and COL1A1.

Surprisingly, we observed that elafibranor increased the protein levels of S100A4, but barely affected its mRNA levels, pointing to the involvement of a post-transcriptional mechanism. This is an unexpected finding, since S100A4 upregulation was reported to induce EMT (Song, Chen et al. 2019), which in turn promotes fibrosis. Consistent with the role of S100A4 in liver fibrosis, S100A4-knockout mice show an attenuation in hepatic fibrosis induced by different stimuli (Helfman, Kim et al. 2005, Chen, Li et al. 2015). S100A4 regulates the tissue fibrosis associated with type II EMT via various signaling pathways (Fei, Qu et al. 2017). In fact, S100A4 is commonly used as a marker to identify epithelial cells undergoing EMT during tissue fibrogenesis (Iwano, Plieth et al. 2002), with S100A4 being used as proof of EMT in hepatocytes and cholangiocytes (Zeisberg, Yang et al. 2007, Omenetti, Porrello et al. 2008, Rygiel, Robertson et al. 2008). In line with the induction of EMT by elafibranor, this drug upregulated the mesenchymal marker vimentin and downregulated the epithelial marker E-cadherin. Moreover, the increase in S100A4 protein levels caused by elafibranor was mediated by PPAR-β/δ, since an antagonist of this receptor attenuated the increase in S100A4 protein levels, while the amount of this protein was reduced in the livers of *Ppard*-null mice compared to their WT littermates. The induction of EMT in the liver by elafibranor via PPAR-β/δ is in accordance with the regulation of EMT

by PPAR-β/δ in the human colorectal carcinoma cell line HCT116 (Zuo, Xu et al. 2017). *Ppard* knockdown in these cells upregulates E-cadherin and downregulates vimentin. Likewise, a PPAR-β/δ antagonist has been previously reported to block the EMT-promoting effect of stromal cell-derived factor-1 on lung cancer cells (Wang, Lan et al. 2021), while EMT markers have been reported to be increased in keratinocytes by the PPAR-β/δ-Src pathway (Montagner, Delgado et al. 2014).

The effects of PPAR-β/δ on liver fibrosis are controversial. While it has been demonstrated that *Ppard*$^{-/-}$ mice show exacerbated hepatotoxicity when treated with CCl_4 (Shan, Nicol et al. 2008) and that PPAR-β/δ agonists attenuate hepatic fibrosis in MASLD (Iwaisako, Haimerl et al. 2012), other studies have reported that these compounds enhance the proliferation of HSCs and promote liver fibrosis (Hellemans, Michalik et al. 2003, Kostadinova, Montagner et al. 2012). These differences indicate that PPAR-β/δ agonists may activate anti- and pro-fibrotic pathways and, depending on the model used to promote fibrosis or other factors yet to be determined, the effects of these compounds may result in either the amelioration or the promotion of liver fibrosis. Given the relationship between increased S100A4 protein levels and the development of fibrosis, the increase in S100A4 protein levels and the induction of EMT might be some of the factors contributing to fibrosis in mice treated with PPAR-β/δ agonists. Further studies are needed to explore this possibility and to determine whether the induction of S100A4 and EMT contributes to liver fibrosis or attenuates the beneficial effects of PPAR-β/δ agonists in this condition.

The present study also provides a potential mechanism by which elafibranor increases the protein levels of S100A4. This protein is a target of ASB2, which mediates its proteasomal degradation (Braumann, Thottakara et al. 2018). We observed that elafibranor reduced the protein levels of ASB2 *in vivo* and *in vitro*, thereby providing an explanation for the increase in S100A4 protein levels following elafibranor treatment. In fact, *Asb2* overexpression prevented the elafibranor-mediated increase in S100A4 protein levels.

S100A4 also promotes cancer progression and metastasis (Helfman, Kim et al. 2005). Although the anti-inflammatory effects of PPAR-β/δ can prevent cancer development, PPAR-β/δ activation after the development of cancer can stimulate angiogenesis and tumor growth (Peters, Gonzalez et al. 2015). Moreover, PPAR-β/δ modulation in cancer cells profoundly influences metastasis development in commonly used preclinical models *in vivo* (Zuo, Xu et al. 2017). It remains to be determined whether S100A4 upregulation by PPAR-β/δ impacts cancer progression and metastasis.

Collectively, the findings of this study highlight a regulatory mechanism by which elafibranor increases the hepatic protein levels of S100A4 (Figure 39). Further studies are needed to evaluate the potential implications of the induction of S100A4 and EMT by elafibranor, particularly in the context of MASH and cancer.

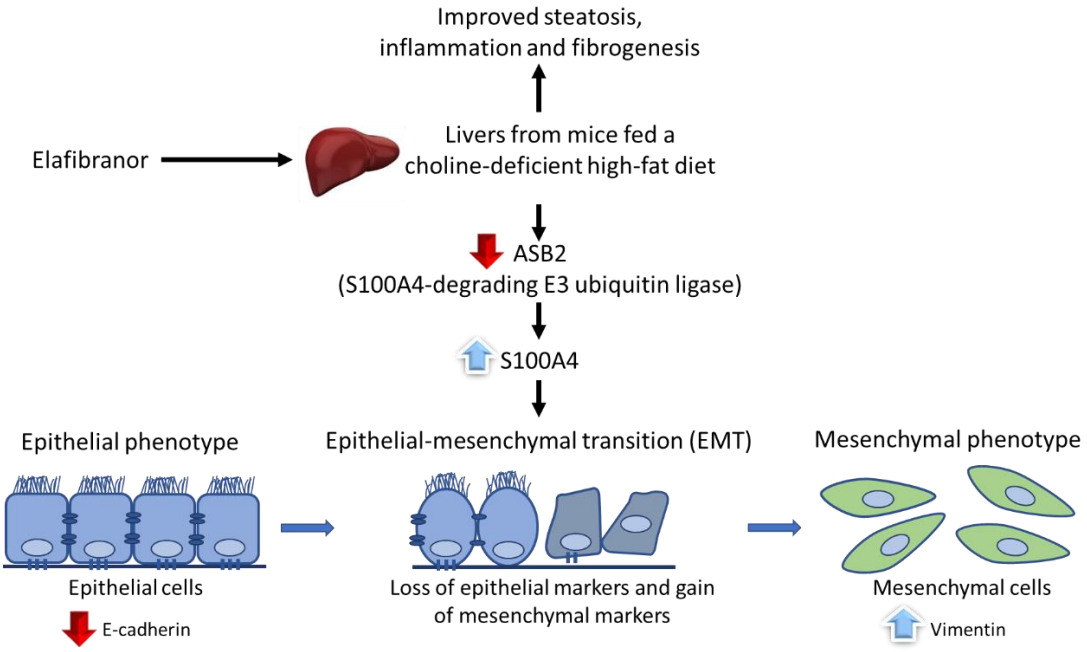

Figure 39. Elafibranor upregulates the EMT-inducer S100A4 via PPAR-β/δ. Elafibranor increases S100A4 by reducing the protein levels of the ubiquitin E3 ligase ASB2, thereby inducing the process of EMT.

Objective 2. PPAR-β/δ activation attenuates hepatic fibrosis by inhibiting the SMAD3 pathway via modulation of the negative crosstalk between AMPK and ERK1/2 in HSCs

HSC activation is a central event in the occurrence and progression of liver fibrosis. In response to liver injury, the repair process comprises HSC activation and trans-differentiation to a proliferative, migratory, fibrogenic MFB-like cell type, causing excessive accumulation of ECM, subsequent matrix remodeling, and finally, hepatocellular dysfunction in the liver. Likewise, several studies have defined a unique transcriptional program that regulates the deactivation of HSC, which includes transcription factors such as PPAR-γ (Li, Chen et al. 2015, Wang and Friedman 2023). However, the role of PPAR-β/δ in HSC activation and proliferation and hepatic fibrosis remains controversial, with studies showing that PPAR-β/δ promotes (Hellemans, Michalik et al. 2003, Kostadinova, Montagner et al. 2012) or inhibits (Shan, Palkar et al. 2008, Iwaisako, Haimerl et al. 2012) these processes. In this study, we show that PPAR-β/δ activation improves hepatic fibrosis in mice fed a CD-HFD diet. Consistent with this, primary HSC isolated from *Ppard*$^{-/-}$ mice showed increased mRNA levels of *Col1a1* and PPAR-β/δ activation abrogated TGF-β1-mediated cell migration and SMAD3 activation in LX-2 cells.

Our findings also point to AMPK activation as the mechanism responsible for the inhibition of TGF-β1-mediated HSC activation and fibrosis by the PPAR-β/δ ligand

GW501516. In fact, AMPK activation is recognized as a target for treating hepatic fibrosis (Liang, Li et al. 2017, Zhao and Saltiel 2020, Gluais-Dagorn, Foretz et al. 2022). Thus, several studies demonstrated that the induction of AMPK activity represses TGF-β1-induced expression of fibrogenic genes in HSC (Kumar, Smith et al. 2014, Dong, Su et al. 2015, Zhai, Qiao et al. 2015). AMPK may prevent the activation of HSC and the development of fibrosis through several mechanisms. For instance, AMPK activation in HSC attenuates ROS production and HSC activation (Caligiuri, Bertolani et al. 2008, Yang, Zhao et al. 2015), thereby protecting against liver injury and fibrosis. Consistent with this, a recent study reported that the direct AMPK activator PXL770 reduces activation and proliferation of HSCs (Gluais-Dagorn, Foretz et al. 2022). In human HSCs, this AMPK activator suppressed the expression of key activation markers *ACTA2* (a gene that encodes α-SMA) and *COL1a1*, along with a strong reduction in COL1A1 (procollagen alpha 1) protein secretion. Moreover, it has been reported that AMPK activation disrupts the interaction between SMAD3 and its transcriptional co-activator p300 and induces the proteasomal degradation of p300 to reduce fibrogenic gene expression in HSCs (Lim, Oh et al. 2012). Additionally, AMPK may also inhibit HSC proliferation and promote apoptosis of these cells via increased nitric oxide production (Dong, Su et al. 2015).

Here, we report a new pathway by which PPAR-β/δ activation and the subsequent AMPK phosphorylation contributes to prevent HSC activation and fibrosis. Our findings indicate that AMPK activation caused by the PPAR-β/δ ligand GW501516

inhibits TGF-β1-mediated HSC activation and fibrosis in LX-2 cells by reducing the levels of phosphorylated ERK1/2. The potent profibrotic mediator TGF-β1 regulates fibrosis through two pathways: the canonical SMAD-dependent pathway and a non-SMAD signaling pathway (Zhang 2017). ERK1/2 signaling pathway forms part of this second noncanonical TGF-β1-dependent pathway and increasing evidence demonstrates its involvement in fibrosis (Zhang 2017). Our findings reinforce the role of ERK1/2 in HSC activation and fibrosis since we observed that inhibition of ERK1/2 with U0126 attenuated the increase of COL1A1 and α-SMA protein levels as well as the phosphorylation of SMAD3. Interestingly, we (Salvado, Barroso et al. 2014) and others (Hwang, Jeong et al. 2013) have demonstrated previously that an inhibitory crosstalk between AMPK and ERK1/2 exists in mouse myotubes, but it was unknown if this mechanism operates in human LX-2 cells. Our findings confirm the presence of this inhibitory crosstalk in HSC and provide a new mechanism by which AMPK inhibits HSC activation and fibrosis through the blockade of the ERK1/2 pathway. Therefore, according to the data of this study, we propose that the activation of AMPK by a PPAR-β/δ ligand inhibits ERK1/2 phosphorylation, thereby attenuating TGF-β1-mediated HSC activation and fibrosis.

Interestingly, it has been reported that TGF-β1 diminishes AMPK phosphorylation, concurrently with increased fibrosis in kidney fibrosis and AMPK inhibition mimics the effect of TGF-β1 or exacerbates its effects in renal fibrosis (Thakur, Viswanadhapalli et al. 2015). These findings suggest that TGF-β1 might also induce

fibrosis and HSC activation via AMPK downregulation and the subsequent activation of ERK1/2. In this line, our findings show that HSC cells exposed to TGF-β1 reduce AMPK phosphorylation, whereas it increases the phosphorylation of ERK1/2. Therefore, this seems to confirm that the modulation of the negative crosstalk between AMPK and ERK1/2 has an impact on HSC activation and fibrosis.

p300 interacts with SMAD3 in a ligand-dependent manner and enhances its transcriptional activity (Nishihara, Hanai et al. 1998). The findings of this study now provide a role for PPAR-β/δ and ERK1/2 on p300 via AMPK, as demonstrated by the knockdown of AMPK in LX-2 cells. Accordingly, primary HSC isolated from *Ppard*$^{-/-}$ mice showed increased mRNA levels of *Ep300*, indicating that this nuclear receptor controls the expression of this co-activator. In addition, either pharmacological inhibition of ERK1/2 increased AMPK phosphorylation and prevented the increase in p300 caused by TGF-β1, thereby suggesting that the negative crosstalk between these two kinases regulates p300 levels.

Overall, the findings of our study uncover that PPAR-β/δ activation reduces hepatic fibrosis by attenuating the TGF-β1-mediated activation of HSCs via the activation of AMPK (Figure 40). This kinase inhibits the phosphorylation of ERK1/2, thereby reducing SMAD3 phosphorylation and HSC activation. In addition, inhibition of the ERK1/2 pathway by PPAR-β/δ and AMPK also reduces the levels of the SMAD3

co-activator p300 in LX-2 cells. The data of this study suggest that targeting ERK1/2 might be a therapeutic avenue to attenuate HSC activation and fibrosis.

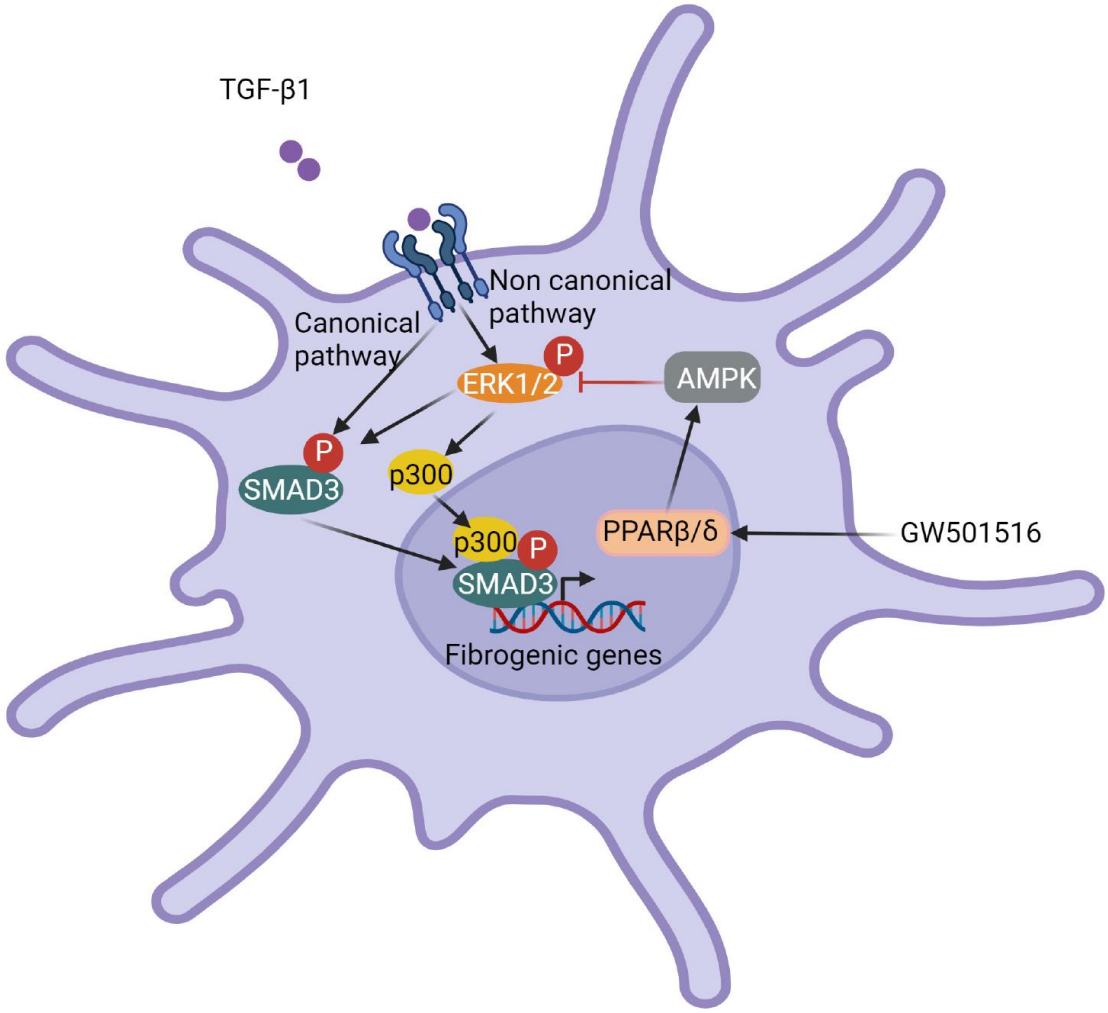

Figure 40. PPAR-β/δ activation prevents HSC activation and fibrosis by phosphorylating AMPK. This kinase inhibits the noncanonical pathway of SMAD3, thereby reducing the activation of SMAD3 and the increase in p300 co-activator caused by TGF-β1 in HSCs.

VI. Conclusions

The results obtained in the present doctoral thesis led to the following conclusions:

Objective 1:

1. Elafibranor treatment ameliorated steatosis, inflammation, and fibrogenesis in the livers of CD-HFD-fed mice.

2. Elafibranor increased the levels of the EMT-promoting protein S100A4 via PPAR-β/δ activation.

3. Elafibranor reduced the levels of ASB2, a protein that promotes S100A4 degradation, with *Asb2* overexpression preventing the stimulating effect of elafibranor on S100A4.

Objective 2:

1. GW5101516 treatment completely prevented glucose intolerance and peripheral IR caused by the CD-HFD as well as the accumulation of collagen in the liver and attenuated the expression of inflammatory and fibrogenic genes.

2. PPAR-β/δ activation abrogated TGF-β1-mediated cell migration, an indicative of cell activation, in LX-2 cells.

3. GW501516 attenuated the phosphorylation of the main downstream intracellular protein of TGF-β1, SMAD3, as well as the levels of the SMAD3 co-activator p300 via AMPK activation and the subsequent inhibition of ERK1/2 in LX-2 cells.

VII. Bibliography

Adams, D. H. (2003). Hepatology: a Textbook of Liver Disease, 4th edition: Edited by Zakim, Boyer. Philadelphia: Saunders, 2003, £230.00, pp 1765. ISBN 0-7216-9051-3, Gut. 2003 Aug;52(8):1230-1.

Adeva-Andany, María M., N. Pérez-Felpete, C. Fernández-Fernández, C. Donapetry-García and C. Pazos-García (2016). "Liver glucose metabolism in humans." Bioscience Reports **36**(6): e00416.

Adiels, M., S. O. Olofsson, M. R. Taskinen and J. Borén (2008). "Overproduction of very low-density lipoproteins is the hallmark of the dyslipidemia in the metabolic syndrome." Arterioscler Thromb Vasc Biol **28**(7): 1225-1236.

Aguilar Recarte, D. (2021). "GDF15, a novel regulator of the AMPK-mediated antidiabetic actions of PPARβ/δ and metformin."

Akbari, R., T. Behdarvand, R. Afarin, H. Yaghooti, M. T. Jalali and N. Mohammadtaghvaei (2021). "Saroglitazar improved hepatic steatosis and fibrosis by modulating inflammatory cytokines and adiponectin in an animal model of non-alcoholic steatohepatitis." BMC Pharmacol Toxicol **22**(1): 53.

Angulo, P. (2006). "NAFLD, Obesity, and Bariatric Surgery." Gastroenterology **130**(6): 1848-1852.

Anstee, Q. M., B. A. Neuschwander-Tetri, V. Wai-Sun Wong, M. F. Abdelmalek, G. Rodriguez-Araujo, H. Landgren, G. S. Park, P. Bedossa, N. Alkhouri, F. Tacke and A. J. Sanyal (2024). "Cenicriviroc Lacked Efficacy to Treat Liver Fibrosis in Nonalcoholic Steatohepatitis: AURORA Phase III Randomized Study." Clin Gastroenterol Hepatol **22**(1): 124-134.e121.

Apte, U. and P. Krishnamurthy (2011). "Detoxification functions of the liver." Molecular pathology of liver diseases: 147-163.

Arab, J. P., M. Arrese and M. Trauner (2018). "Recent insights into the pathogenesis of nonalcoholic fatty liver disease." Annual Review of Pathology: Mechanisms of Disease **13**: 321-350.

Arshad, M. I., C. Piquet-Pellorce and M. Samson (2012). "IL-33 and HMGB1 alarmins: sensors of cellular death and their involvement in liver pathology." Liver Int **32**(8): 1200-1210.

Badman, M. K., P. Pissios, A. R. Kennedy, G. Koukos, J. S. Flier and E. Maratos-Flier (2007). "Hepatic fibroblast growth factor 21 is regulated by PPARalpha and is a key mediator of hepatic lipid metabolism in ketotic states." Cell Metab **5**(6): 426-437.

Baiceanu, A., P. Mesdom, M. Lagouge and F. Foufelle (2016). "Endoplasmic reticulum proteostasis in hepatic steatosis." Nature Reviews Endocrinology **12**(12): 710-722.

Bailly-Maitre, B., B. F. Belgardt, S. D. Jordan, B. Coornaert, M. J. von Freyend, A. Kleinridders, J. Mauer, M. Cuddy, C. L. Kress, D. Willmes, M. Essig, B. Hampel, U. Protzer, J. C. Reed and J. C. Brüning (2010). "Hepatic Bax inhibitor-1 inhibits IRE1alpha and protects from obesity-associated insulin resistance and glucose intolerance." J Biol Chem **285**(9): 6198-6207.

Balgoma, D., A. M. Astudillo, G. Perez-Chacon, O. Montero, M. A. Balboa and J. Balsinde (2010). "Markers of monocyte activation revealed by lipidomic profiling of arachidonic acid-containing phospholipids." J Immunol **184**(7): 3857-3865.

Banales, J. M., R. C. Huebert, T. Karlsen, M. Strazzabosco, N. F. LaRusso and G. J. Gores (2019). "Cholangiocyte pathobiology." Nat Rev Gastroenterol Hepatol **16**(5): 269-281.

Barroso, E., R. Rodriguez-Calvo, L. Serrano-Marco, A. M. Astudillo, J. Balsinde, X. Palomer and M. Vazquez-Carrera (2011). "The PPARbeta/delta activator GW501516 prevents the down-regulation of AMPK caused by a high-fat diet in liver and amplifies the PGC-1alpha-Lipin 1-PPARalpha pathway leading to increased fatty acid oxidation." Endocrinology **152**(5): 1848-1859.

Barroso, E., R. Rodríguez-Calvo, L. Serrano-Marco, A. M. Astudillo, J. Balsinde, X. Palomer and M.

Vázquez-Carrera (2011). "The PPARβ/δ Activator GW501516 Prevents the Down-Regulation of AMPK Caused by a High-Fat Diet in Liver and Amplifies the PGC-1α-Lipin 1-PPARα Pathway Leading to Increased Fatty Acid Oxidation." Endocrinology **152**(5): 1848-1859.

Bello, N. F., I. Lamsoul, M. L. Heuze, A. Metais, G. Moreaux, D. A. Calderwood, D. Duprez, C. Moog-Lutz and P. G. Lutz (2009). "The E3 ubiquitin ligase specificity subunit ASB2beta is a novel regulator of muscle differentiation that targets filamin B to proteasomal degradation." Cell Death Differ **16**(6): 921-932.

Bensinger, S. J. and P. Tontonoz (2008). "Integration of metabolism and inflammation by lipid-activated nuclear receptors." Nature **454**(7203): 470-477.

Benveniste, R., T. M. Danoff, J. Ilekis and H. R. Craig (1988). "Epidermal growth factor receptor numbers in male and female mouse primary hepatocyte cultures." Cell Biochem Funct **6**(4): 231-235.

Bian, E.-B., C. Huang, H. Wang, X.-X. Chen, L. Zhang, X.-W. Lv and J. Li (2014). "Repression of Smad7 mediated by DNMT1 determines hepatic stellate cell activation and liver fibrosis in rats." Toxicology Letters **224**(2): 175-185.

Bligh, E. G. and W. J. Dyer (1959). "A rapid method of total lipid extraction and purification." Can J Biochem Physiol **37**(8): 911-917.

Boursier, J. and A. M. Diehl (2015). "Implication of gut microbiota in nonalcoholic fatty liver disease." PLoS Pathog **11**(1): e1004559.

Boursier, J., O. Mueller, M. Barret, M. Machado, L. Fizanne, F. Araujo-Perez, C. D. Guy, P. C. Seed, J. F. Rawls, L. A. David, G. Hunault, F. Oberti, P. Calès and A. M. Diehl (2016). "The severity of nonalcoholic fatty liver disease is associated with gut dysbiosis and shift in the metabolic function of the gut microbiota." Hepatology **63**(3): 764-775.

Bowers, R. R., Y. Manevich, D. M. Townsend and K. D. Tew (2012). "Sulfiredoxin redox-sensitive interaction with S100A4 and non-muscle myosin IIA regulates cancer cell motility." Biochemistry **51**(39): 7740-7754.

Boyer, J. L. (2013). "Bile formation and secretion." Compr Physiol **3**(3): 1035-1078.

Braumann, S., T. Thottakara, S. Stucker, S. Reischmann-Dusener, E. Kramer, J. Gross, M. N. Hirt, S. Doroudgar, L. Carrier and F. W. Friedrich (2018). "S100A4 as a Target of the E3-Ligase Asb2beta and Its Effect on Engineered Heart Tissue." Front Physiol **9**: 1292.

Caligiuri, A., C. Bertolani, C. T. Guerra, S. Aleffi, S. Galastri, M. Trappoliere, F. Vizzutti, S. Gelmini, G. Laffi, M. Pinzani and F. Marra (2008). "Adenosine monophosphate-activated protein kinase modulates the activated phenotype of hepatic stellate cells." Hepatology **47**(2): 668-676.

Calle, R. A., N. B. Amin, S. Carvajal-Gonzalez, T. T. Ross, A. Bergman, S. Aggarwal, C. Crowley, A. Rinaldi, J. Mancuso, N. Aggarwal, V. Somayaji, M. Inglot, T. A. Tuthill, K. Kou, M. Boucher, G. Tesz, R. Dullea, K. K. Bence, A. M. Kim, J. A. Pfefferkorn and W. P. Esler (2021). "ACC inhibitor alone or co-administered with a DGAT2 inhibitor in patients with non-alcoholic fatty liver disease: two parallel, placebo-controlled, randomized phase 2a trials." Nat Med **27**(10): 1836-1848.

Cano, A., M. A. Pérez-Moreno, I. Rodrigo, A. Locascio, M. J. Blanco, M. G. del Barrio, F. Portillo and M. A. Nieto (2000). "The transcription factor snail controls epithelial-mesenchymal transitions by repressing E-cadherin expression." Nat Cell Biol **2**(2): 76-83.

Cantó, C. and J. Auwerx (2010). "AMP-activated protein kinase and its downstream transcriptional pathways." Cell Mol Life Sci **67**(20): 3407-3423.

Chakravarthy, M. V., I. J. Lodhi, L. Yin, R. R. Malapaka, H. E. Xu, J. Turk and C. F. Semenkovich (2009).

"Identification of a physiologically relevant endogenous ligand for PPARalpha in liver." Cell **138**(3): 476-488.

Chalasani, N., M. F. Abdelmalek, G. Garcia-Tsao, R. Vuppalanchi, N. Alkhouri, M. Rinella, M. Noureddin, M. Pyko, M. Shiffman, A. Sanyal, A. Allgood, H. Shlevin, R. Horton, E. Zomer, W. Irish, Z. Goodman, S. A. Harrison and P. G. Traber (2020). "Effects of Belapectin, an Inhibitor of Galectin-3, in Patients With Nonalcoholic Steatohepatitis With Cirrhosis and Portal Hypertension." Gastroenterology **158**(5): 1334-1345.e1335.

Chan, S.-W. and P. A. Egan (2005). "Hepatitis C virus envelope proteins regulate CHOP via induction of the unfolded protein response." The FASEB Journal **19**(11): 1510-1512.

Chan, W. K., K. H. Chuah, R. B. Rajaram, L. L. Lim, J. Ratnasingam and S. R. Vethakkan (2023). "Metabolic Dysfunction-Associated Steatotic Liver Disease (MASLD): A State-of-the-Art Review." J Obes Metab Syndr **32**(3): 197-213.

Charles, E. D., B. A. Neuschwander-Tetri, J. Pablo Frias, S. Kundu, Y. Luo, G. S. Tirucherai and R. Christian (2019). "Pegbelfermin (BMS-986036), PEGylated FGF21, in Patients with Obesity and Type 2 Diabetes: Results from a Randomized Phase 2 Study." Obesity (Silver Spring) **27**(1): 41-49.

Chen, L., J. Li, J. Zhang, C. Dai, X. Liu, J. Wang, Z. Gao, H. Guo, R. Wang, S. Lu, F. Wang, H. Zhang, H. Chen, X. Fan, S. Wang and Z. Qin (2015). "S100A4 promotes liver fibrosis via activation of hepatic stellate cells." J Hepatol **62**(1): 156-164.

Chen, W.-X., Y.-M. Li, C.-H. Yu, W.-M. Cai, M. Zheng and F. Chen (2002). "Quantitative analysis of transforming growth factor beta 1 mRNA in patients with alcoholic liver disease." World Journal of Gastroenterology **8**(2): 379.

Chen, W., L. L. Wang, H. Y. Liu, L. Long and S. Li (2008). "Peroxisome proliferator-activated receptor delta-agonist, GW501516, ameliorates insulin resistance, improves dyslipidaemia in monosodium L-glutamate metabolic syndrome mice." Basic Clin Pharmacol Toxicol **103**(3): 240-246.

Chen, X., F. Zhang, Q. Gong, A. Cui, S. Zhuo, Z. Hu, Y. Han, J. Gao, Y. Sun, Z. Liu, Z. Yang, Y. Le, X. Gao, L. Q. Dong, X. Gao and Y. Li (2016). "Hepatic ATF6 Increases Fatty Acid Oxidation to Attenuate Hepatic Steatosis in Mice Through Peroxisome Proliferator–Activated Receptor α." Diabetes **65**(7): 1904-1915.

Chen, Y., Y. Fan, D.-y. Guo, B. Xu, X.-y. Shi, J.-t. Li and L.-f. Duan (2020). "Study on the relationship between hepatic fibrosis and epithelial-mesenchymal transition in intrahepatic cells." Biomedicine & Pharmacotherapy **129**: 110413.

Cheng, J. H., H. She, Y.-P. Han, J. Wang, S. Xiong, K. Asahina and H. Tsukamoto (2008). "Wnt antagonism inhibits hepatic stellate cell activation and liver fibrosis." American Journal of Physiology-Gastrointestinal and Liver Physiology **294**(1): G39-G49.

Chung, J. Y.-F., M. K.-K. Chan, J. S.-F. Li, A. S.-W. Chan, P. C.-T. Tang, K.-T. Leung, K.-F. To, H.-Y. Lan and P. M.-K. Tang (2021). "TGF-β signaling: from tissue fibrosis to tumor microenvironment." International Journal of Molecular Sciences **22**(14): 7575.

Cool, B., B. Zinker, W. Chiou, L. Kifle, N. Cao, M. Perham, R. Dickinson, A. Adler, G. Gagne, R. Iyengar, G. Zhao, K. Marsh, P. Kym, P. Jung, H. S. Camp and E. Frevert (2006). "Identification and characterization of a small molecule AMPK activator that treats key components of type 2 diabetes and the metabolic syndrome." Cell Metab **3**(6): 403-416.

Coskun, T., K. W. Sloop, C. Loghin, J. Alsina-Fernandez, S. Urva, K. B. Bokvist, X. Cui, D. A. Briere, O. Cabrera, W. C. Roell, U. Kuchibhotla, J. S. Moyers, C. T. Benson, R. E. Gimeno, D. A. D'Alessio and A. Haupt (2018). "LY3298176, a novel dual GIP and GLP-1 receptor agonist for the treatment of

type 2 diabetes mellitus: From discovery to clinical proof of concept." Mol Metab **18**: 3-14.
Crespo, J., A. Cayn, P. Fernndez-Gil, M. Hernndez-Guerra, M. Mayorga, A. Domnguez-Dez, J. C. Fernndez-Escalante and F. Pons-Romero (2001). "Gene expression of tumor necrosis factor [alpha] and TNF-receptors, p55 and p75, in nonalcoholic steatohepatitis patients." Hepatology **34**(6): 1158-1163.
Dahlhoff, C., S. Worsch, M. Sailer, B. A. Hummel, J. Fiamoncini, K. Uebel, R. Obeid, C. Scherling, J. Geisel, B. L. Bader and H. Daniel (2014). "Methyl-donor supplementation in obese mice prevents the progression of NAFLD, activates AMPK and decreases acyl-carnitine levels." Molecular Metabolism **3**(5): 565-580.
Dali-Youcef, N., M. Vix, F. Costantino, H. El-Saghire, B. Lhermitte, C. Callari, J. D'Agostino, S. Perretta, S. Paveliu, M. Gualtierotti, E. Dumeny, M. A. Oudot, A. Jaulin, D. Dembélé, M. B. Zeisel, C. Tomasetto, T. F. Baumert and M. Doffoël (2019). "Interleukin-32 Contributes to Human Nonalcoholic Fatty Liver Disease and Insulin Resistance." Hepatol Commun **3**(9): 1205-1220.
Das, S. K. and V. Balakrishnan (2011). "Role of Cytokines in the Pathogenesis of Non-Alcoholic Fatty Liver Disease." Indian Journal of Clinical Biochemistry **26**(2): 202-209.
Das, S. K. and V. Balakrishnan (2011). "Role of cytokines in the pathogenesis of non-alcoholic Fatty liver disease." Indian J Clin Biochem **26**(2): 202-209.
De Minicis, S. and G. Svegliati-Baroni (2011). "Fibrogenesis in nonalcoholic steatohepatitis." Expert Review of Gastroenterology & Hepatology **5**(2): 179-187.
den Boer, M. A., P. J. Voshol, J. P. Schröder-van der Elst, E. Korsheninnikova, D. M. Ouwens, F. Kuipers, L. M. Havekes and J. A. Romijn (2006). "Endogenous interleukin-10 protects against hepatic steatosis but does not improve insulin sensitivity during high-fat feeding in mice." Endocrinology **147**(10): 4553-4558.
Derynck, R. and E. H. Budi (2019). "Specificity, versatility, and control of TGF-β family signaling." Sci Signal **12**(570).
Dewidar, B., C. Meyer, S. Dooley and A. N. Meindl-Beinker (2019). "TGF-β in Hepatic Stellate Cell Activation and Liver Fibrogenesis-Updated 2019." Cells **8**(11).
DeZwaan-McCabe, D., R. D. Sheldon, M. C. Gorecki, D.-F. Guo, E. R. Gansemer, R. J. Kaufman, K. Rahmouni, M. P. Gillum, E. B. Taylor, L. M. Teesch and D. T. Rutkowski (2017). "ER Stress Inhibits Liver Fatty Acid Oxidation while Unmitigated Stress Leads to Anorexia-Induced Lipolysis and Both Liver and Kidney Steatosis." Cell Reports **19**(9): 1794-1806.
Diniz, T. A., E. A. de Lima Junior, A. A. Teixeira, L. A. Biondo, L. A. F. da Rocha, I. C. Valadão, L. S. Silveira, C. Cabral-Santos, C. O. de Souza and J. C. Rosa Neto (2021). "Aerobic training improves NAFLD markers and insulin resistance through AMPK-PPAR-α signaling in obese mice." Life Sci **266**: 118868.
Dong, J., S. Viswanathan, E. Adami, B. K. Singh, S. P. Chothani, B. Ng, W. W. Lim, J. Zhou, M. Tripathi, N. S. J. Ko, S. G. Shekeran, J. Tan, S. Y. Lim, M. Wang, P. M. Lio, P. M. Yen, S. Schafer, S. A. Cook and A. A. Widjaja (2021). "Hepatocyte-specific IL11 cis-signaling drives lipotoxicity and underlies the transition from NAFLD to NASH." Nature Communications **12**(1): 66.
Dong, X. C., K. Chowdhury, M. Huang and H. G. Kim (2021). "Signal Transduction and Molecular Regulation in Fatty Liver Disease." Antioxid Redox Signal **35**(9): 689-717.
Dong, Z., L. Su, S. Esmaili, T. J. Iseli, M. Ramezani-Moghadam, L. Hu, A. Xu, J. George and J. Wang (2015). "Adiponectin attenuates liver fibrosis by inducing nitric oxide production of hepatic stellate cells." J Mol Med (Berl) **93**(12): 1327-1339.

Dufour, J.-F. and J. Mertens (2015). Hepatocytes**:** 1-14.

Dufour, J. F., Q. M. Anstee, E. Bugianesi, S. Harrison, R. Loomba, V. Paradis, H. Tilg, V. W. Wong and S. Zelber-Sagi (2022). "Current therapies and new developments in NASH." Gut **71**(10): 2123-2134.

Dufour, J. F. and P. A. Clavien "Signaling Pathways in Liver Diseases."

Dutta, S., S. P. Mishra, A. K. Sahu, K. Mishra, P. Kashyap and B. Sahu (2021). "Hepatocytes and their role in metabolism." Drug Metabolism: 3.

El-Assal, O., F. Hong, W.-H. Kim, S. Radaeva and B. Gao (2004). "IL-6-deficient Mice Are Susceptible to Ethanol-induced Hepatic Steatosis: IL-6 Protects against Ethanol-induced Oxidative Stress and Mitochondrial Permeability Transition in the Liver." Cellular & molecular immunology **1**: 205-211.

Esposito, K., A. Pontillo, F. Giugliano, G. Giugliano, R. Marfella, G. Nicoletti and D. Giugliano (2003). "Association of low interleukin-10 levels with the metabolic syndrome in obese women." J Clin Endocrinol Metab **88**(3): 1055-1058.

Fan, J.-G., S.-U. Kim and V. W.-S. Wong (2017). "New trends on obesity and NAFLD in Asia." Journal of Hepatology **67**(4): 862-873.

Fang, C., J. Pan, N. Qu, Y. Lei, J. Han, J. Zhang and D. Han (2022). "The AMPK pathway in fatty liver disease." Front Physiol **13**: 970292.

Fei, F., J. Qu, C. Li, X. Wang, Y. Li and S. Zhang (2017). "Role of metastasis-induced protein S100A4 in human non-tumor pathophysiologies." Cell Biosci **7**: 64.

Feng, X.-H., Y. Zhang, R.-Y. Wu and R. Derynck (1998). "The tumor suppressor Smad4/DPC4 and transcriptional adaptor CBP/p300 are coactivators for Smad3 in TGF-β-induced transcriptional activation." Genes & development **12**(14): 2153-2163.

Ferrarese, A., S. Battistella, G. Germani, F. P. Russo, M. Senzolo, M. Gambato, A. Vitale, U. Cillo and P. Burra (2022). "Nash Up, Virus Down: How the Waiting List Is Changing for Liver Transplantation: A Single Center Experience from Italy." Medicina (Kaunas) **58**(2).

Fisher, F. M., P. C. Chui, I. A. Nasser, Y. Popov, J. C. Cunniff, T. Lundasen, A. Kharitonenkov, D. Schuppan, J. S. Flier and E. Maratos-Flier (2014). "Fibroblast growth factor 21 limits lipotoxicity by promoting hepatic fatty acid activation in mice on methionine and choline-deficient diets." Gastroenterology **147**(5): 1073-1083.e1076.

Francque, S., A. Verrijken, S. Caron, J. Prawitt, R. Paumelle, B. Derudas, P. Lefebvre, M.-R. Taskinen, W. Van Hul, I. Mertens, G. Hubens, E. Van Marck, P. Michielsen, L. Van Gaal and B. Staels (2015). "PPARα gene expression correlates with severity and histological treatment response in patients with non-alcoholic steatohepatitis." Journal of Hepatology **63**(1): 164-173.

Friedman, S. L., V. Ratziu, S. A. Harrison, M. F. Abdelmalek, G. P. Aithal, J. Caballeria, S. Francque, G. Farrell, K. V. Kowdley, A. Craxi, K. Simon, L. Fischer, L. Melchor-Khan, J. Vest, B. L. Wiens, P. Vig, S. Seyedkazemi, Z. Goodman, V. W. Wong, R. Loomba, F. Tacke, A. Sanyal and E. Lefebvre (2018). "A randomized, placebo-controlled trial of cenicriviroc for treatment of nonalcoholic steatohepatitis with fibrosis." Hepatology **67**(5): 1754-1767.

Garcia, D., K. Hellberg, A. Chaix, M. Wallace, S. Herzig, M. G. Badur, T. Lin, M. N. Shokhirev, A. F. Pinto and D. S. Ross (2019). "Genetic liver-specific AMPK activation protects against diet-induced obesity and NAFLD." Cell reports **26**(1): 192-208. e196.

Garcia, D. and R. J. Shaw (2017). "AMPK: Mechanisms of Cellular Energy Sensing and Restoration of Metabolic Balance." Mol Cell **66**(6): 789-800.

Garrett, S. C., K. M. Varney, D. J. Weber and A. R. Bresnick (2006). "S100A4, a mediator of metastasis." J Biol Chem **281**(2): 677-680.

Gawrieh, S., M. Noureddin, N. Loo, R. Mohseni, V. Awasty, K. Cusi, K. V. Kowdley, M. Lai, E. Schiff, D. Parmar, P. Patel and N. Chalasani (2021). "Saroglitazar, a PPAR-α/γ Agonist, for Treatment of NAFLD: A Randomized Controlled Double-Blind Phase 2 Trial." Hepatology **74**(4): 1809-1824.

Gibbons, G. F. (1990). "Assembly and secretion of hepatic very-low-density lipoprotein." Biochemical Journal **268**(1): 1-13.

Gibbons, G. F., K. Islam and R. J. Pease (2000). "Mobilisation of triacylglycerol stores." Biochimica et Biophysica Acta (BBA) - Molecular and Cell Biology of Lipids **1483**(1): 37-57.

Giraldez, M. D., D. Carneros, C. Garbers, S. Rose-John and M. Bustos (2021). "New insights into IL-6 family cytokines in metabolism, hepatology and gastroenterology." Nat Rev Gastroenterol Hepatol **18**(11): 787-803.

Gluais-Dagorn, P., M. Foretz, G. R. Steinberg, B. Batchuluun, A. Zawistowska-Deniziak, J. M. Lambooij, B. Guigas, D. Carling, P. A. Monternier, D. E. Moller, S. Bolze and S. Hallakou-Bozec (2022). "Direct AMPK Activation Corrects NASH in Rodents Through Metabolic Effects and Direct Action on Inflammation and Fibrogenesis." Hepatol Commun **6**(1): 101-119.

González-Rodríguez, Á., R. Mayoral, N. Agra, M. P. Valdecantos, V. Pardo, M. E. Miquilena-Colina, J. Vargas-Castrillón, O. Lo Iacono, M. Corazzari, G. M. Fimia, M. Piacentini, J. Muntané, L. Boscá, C. García-Monzón, P. Martín-Sanz and Á. M. Valverde (2014). "Impaired autophagic flux is associated with increased endoplasmic reticulum stress during the development of NAFLD." Cell Death & Disease **5**(4): e1179-e1179.

Goudarzi, M., T. Koga, C. Khozoie, T. D. Mak, B.-H. Kang, A. J. F. Jr and J. M. Peters (2013). "PPARβ/δ modulates ethanol-induced hepatic effects by decreasing pyridoxal kinase activity." Toxicology **311**(3): 87-98.

Grant, D. (1991). "Detoxification pathways in the liver." Journal of inherited metabolic disease **14**: 421-430.

Green, C. J. and L. Hodson (2014). "The Influence of Dietary Fat on Liver Fat Accumulation." Nutrients **6**(11): 5018-5033.

Gregor, M. F., L. Yang, E. Fabbrini, B. S. Mohammed, J. C. Eagon, G. S. Hotamisligil and S. Klein (2009). "Endoplasmic reticulum stress is reduced in tissues of obese subjects after weight loss." Diabetes **58**(3): 693-700.

Grönroos, E., U. Hellman, C. H. Heldin and J. Ericsson (2002). "Control of Smad7 stability by competition between acetylation and ubiquitination." Mol Cell **10**(3): 483-493.

Grygiel-Górniak, B. (2014). "Peroxisome proliferator-activated receptors and their ligands: nutritional and clinical implications--a review." Nutr J **13**: 17.

Grygiel-Górniak, B. (2014). "Peroxisome proliferator-activated receptors and their ligands: nutritional and clinical implications - a review." Nutrition Journal **13**(1): 17.

Guigas, B., K. Sakamoto, N. Taleux, S. M. Reyna, N. Musi, B. Viollet and L. Hue (2009). "Beyond AICA riboside: in search of new specific AMP-activated protein kinase activators." IUBMB Life **61**(1): 18-26.

Gupta, R. A., J. Tan, W. F. Krause, M. W. Geraci, T. M. Willson, S. K. Dey and R. N. DuBois (2000). "Prostacyclin-mediated activation of peroxisome proliferator-activated receptor δ in colorectal cancer." Proceedings of the National Academy of Sciences **97**(24): 13275-13280.

Habegger, K. M., K. M. Heppner, N. Geary, T. J. Bartness, R. DiMarchi and M. H. Tschöp (2010).

"The metabolic actions of glucagon revisited." Nat Rev Endocrinol **6**(12): 689-697.
Hamzavi, J., S. Ehnert, P. Godoy, L. Ciuclan, H. Weng, P. R. Mertens, R. Heuchel and S. Dooley (2008). "Disruption of the Smad7 gene enhances CCl4-dependent liver damage and fibrogenesis in mice." Journal of cellular and molecular medicine **12**(5b): 2130-2144.
Harman, F. S., C. J. Nicol, H. E. Marin, J. M. Ward, F. J. Gonzalez and J. M. Peters (2004). "Peroxisome proliferator–activated receptor-δ attenuates colon carcinogenesis." Nature Medicine **10**(5): 481-483.
Harrison, S. A., P. Bedossa, C. D. Guy, J. M. Schattenberg, R. Loomba, R. Taub, D. Labriola, S. E. Moussa, G. W. Neff, M. E. Rinella, Q. M. Anstee, M. F. Abdelmalek, Z. Younossi, S. J. Baum, S. Francque, M. R. Charlton, P. N. Newsome, N. Lanthier, I. Schiefke, A. Mangia, J. M. Pericàs, R. Patil, A. J. Sanyal, M. Noureddin, M. B. Bansal, N. Alkhouri, L. Castera, M. Rudraraju and V. Ratziu (2024). "A Phase 3, Randomized, Controlled Trial of Resmetirom in NASH with Liver Fibrosis." New England Journal of Medicine **390**(6): 497-509.
Harrison, S. A., M. E. Rinella, M. F. Abdelmalek, J. F. Trotter, A. H. Paredes, H. L. Arnold, M. Kugelmas, M. R. Bashir, M. J. Jaros, L. Ling, S. J. Rossi, A. M. DePaoli and R. Loomba (2018). "NGM282 for treatment of non-alcoholic steatohepatitis: a multicentre, randomised, double-blind, placebo-controlled, phase 2 trial." Lancet **391**(10126): 1174-1185.
Harrison, S. A., S. J. Rossi, A. H. Paredes, J. F. Trotter, M. R. Bashir, C. D. Guy, R. Banerjee, M. J. Jaros, S. Owers, B. A. Baxter, L. Ling and A. M. DePaoli (2020). "NGM282 Improves Liver Fibrosis and Histology in 12 Weeks in Patients With Nonalcoholic Steatohepatitis." Hepatology **71**(4): 1198-1212.
Harrison, S. A., R. Taub, G. W. Neff, K. J. Lucas, D. Labriola, S. E. Moussa, N. Alkhouri and M. R. Bashir (2023). "Resmetirom for nonalcoholic fatty liver disease: a randomized, double-blind, placebo-controlled phase 3 trial." Nat Med **29**(11): 2919-2928.
Harrison, S. A., V. W. Wong, T. Okanoue, N. Bzowej, R. Vuppalanchi, Z. Younes, A. Kohli, S. Sarin, S. H. Caldwell, N. Alkhouri, M. L. Shiffman, M. Camargo, G. Li, K. Kersey, C. Jia, Y. Zhu, C. S. Djedjos, G. M. Subramanian, R. P. Myers, N. Gunn, A. Sheikh, Q. M. Anstee, M. Romero-Gomez, M. Trauner, Z. Goodman, E. J. Lawitz and Z. Younossi (2020). "Selonsertib for patients with bridging fibrosis or compensated cirrhosis due to NASH: Results from randomized phase III STELLAR trials." J Hepatol **73**(1): 26-39.
Hartman, M. L., A. J. Sanyal, R. Loomba, J. M. Wilson, A. Nikooienejad, R. Bray, C. A. Karanikas, K. L. Duffin, D. A. Robins and A. Haupt (2020). "Effects of Novel Dual GIP and GLP-1 Receptor Agonist Tirzepatide on Biomarkers of Nonalcoholic Steatohepatitis in Patients With Type 2 Diabetes." Diabetes Care **43**(6): 1352-1355.
Hazra, S., S. Xiong, J. Wang, R. A. Rippe, V. Krishna, K. Chatterjee and H. Tsukamoto (2004). "Peroxisome Proliferator-activated Receptor γ Induces a Phenotypic Switch from Activated to Quiescent Hepatic Stellate Cells ⁎." Journal of Biological Chemistry **279**(12): 11392-11401.
He, L. and F. E. Wondisford (2015). "Metformin action: concentrations matter." Cell metabolism **21**(2): 159-162.
He, Q., Y. Chen, Z. Wang, H. He and P. Yu (2023). "Cellular Uptake, Metabolism and Sensing of Long-Chain Fatty Acids." FBL **28**(1): 10-null.
He, T.-C., T. A. Chan, B. Vogelstein and K. W. Kinzler (1999). "PPARδ is an APC-regulated target of nonsteroidal anti-inflammatory drugs." Cell **99**(3): 335-345.
Heldin, C. H. and A. Moustakas (2016). "Signaling Receptors for TGF-β Family Members." Cold

Spring Harb Perspect Biol **8**(8).
Helfman, D. M., E. J. Kim, E. Lukanidin and M. Grigorian (2005). "The metastasis associated protein S100A4: role in tumour progression and metastasis." Br J Cancer **92**(11): 1955-1958.
Hellemans, K., L. Michalik, A. Dittie, A. Knorr, K. Rombouts, J. De Jong, C. Heirman, E. Quartier, F. Schuit, W. Wahli and A. Geerts (2003). "Peroxisome proliferator-activated receptor-beta signaling contributes to enhanced proliferation of hepatic stellate cells." Gastroenterology **124**(1): 184-201.
Henson, J. B., T. G. Simon, A. Kaplan, S. Osganian, R. Masia and K. E. Corey (2020). "Advanced fibrosis is associated with incident cardiovascular disease in patients with non-alcoholic fatty liver disease." Aliment Pharmacol Ther **51**(7): 728-736.
Heuze, M. L., I. Lamsoul, M. Baldassarre, Y. Lad, S. Leveque, Z. Razinia, C. Moog-Lutz, D. A. Calderwood and P. G. Lutz (2008). "ASB2 targets filamins A and B to proteasomal degradation." Blood **112**(13): 5130-5140.
Heyens, L. J. M., D. Busschots, G. H. Koek, G. Robaeys and S. Francque (2021). "Liver Fibrosis in Non-alcoholic Fatty Liver Disease: From Liver Biopsy to Non-invasive Biomarkers in Diagnosis and Treatment." Front Med (Lausanne) **8**: 615978.
Hotamisligil, G. S., N. S. Shargill and B. M. Spiegelman (1993). "Adipose expression of tumor necrosis factor-alpha: direct role in obesity-linked insulin resistance." Science **259**(5091): 87-91.
Hotamisligil, G. S., N. S. Shargill and B. M. Spiegelman (1993). "Adipose Expression of Tumor Necrosis Factor-α: Direct Role in Obesity-Linked Insulin Resistance." Science **259**(5091): 87-91.
House, R. P., M. Pozzuto, P. Patel, N. G. Dulyaninova, Z. H. Li, W. D. Zencheck, M. I. Vitolo, D. J. Weber and A. R. Bresnick (2011). "Two functional S100A4 monomers are necessary for regulating nonmuscle myosin-IIA and HCT116 cell invasion." Biochemistry **50**(32): 6920-6932.
Hu, T., M. Chouinard, A. L. Cox, P. Sipes, M. Marcelo, J. Ficorilli, S. Li, H. Gao, T. P. Ryan, M. D. Michael and L. F. Michael (2006). "Farnesoid X Receptor Agonist Reduces Serum Asymmetric Dimethylarginine Levels through Hepatic Dimethylarginine Dimethylaminohydrolase-1 Gene Regulation *." Journal of Biological Chemistry **281**(52): 39831-39838.
Hu, Y., J. He, L. He, B. Xu and Q. Wang (2021). "Expression and function of Smad7 in autoimmune and inflammatory diseases." Journal of Molecular Medicine **99**(9): 1209-1220.
Huang, D. Q., H. B. El-Serag and R. Loomba (2021). "Global epidemiology of NAFLD-related HCC: trends, predictions, risk factors and prevention." Nat Rev Gastroenterol Hepatol **18**(4): 223-238.
Hwang, S. L., Y. T. Jeong, X. Li, Y. D. Kim, Y. Lu, Y. C. Chang, I. K. Lee and H. W. Chang (2013). "Inhibitory cross-talk between the AMPK and ERK pathways mediates endoplasmic reticulum stress-induced insulin resistance in skeletal muscle." Br J Pharmacol **169**(1): 69-81.
Ibrahim, S. H., P. Hirsova and G. J. Gores (2018). "Non-alcoholic steatohepatitis pathogenesis: sublethal hepatocyte injury as a driver of liver inflammation." Gut: gutjnl-2017-315691.
Itoh, S., J. Ericsson, J.-i. Nishikawa, C.-H. Heldin and P. t. Dijke (2000). "The transcriptional co-activator P/CAF potentiates TGF-β/Smad signaling." Nucleic acids research **28**(21): 4291-4298.
Iwaisako, K., M. Haimerl, Y.-H. Paik, K. Taura, Y. Kodama, C. Sirlin, E. Yu, R. T. Yu, M. Downes, R. M. Evans, D. A. Brenner and B. Schnabl (2012). "Protection from liver fibrosis by a peroxisome proliferator-activated receptor δ agonist." Proceedings of the National Academy of Sciences **109**(21): E1369-E1376.
Iwaisako, K., M. Haimerl, Y. H. Paik, K. Taura, Y. Kodama, C. Sirlin, E. Yu, R. T. Yu, M. Downes, R. M. Evans, D. A. Brenner and B. Schnabl (2012). "Protection from liver fibrosis by a peroxisome proliferator-activated receptor delta agonist." Proc Natl Acad Sci U S A **109**(21): E1369-1376.

Iwano, M., D. Plieth, T. M. Danoff, C. Xue, H. Okada and E. G. Neilson (2002). "Evidence that fibroblasts derive from epithelium during tissue fibrosis." J Clin Invest **110**(3): 341-350.

Jaffe, A. B. and A. Hall (2005). "Rho GTPases: biochemistry and biology." Annu Rev Cell Dev Biol **21**: 247-269.

Jensen, T. E., J. F. P. Wojtaszewski and E. A. Richter (2009). "AMP-activated protein kinase in contraction regulation of skeletal muscle metabolism: necessary and/or sufficient?" Acta Physiologica **196**(1): 155-174.

Jo, H., S. S. Choe, K. C. Shin, H. Jang, J. H. Lee, J. K. Seong, S. H. Back and J. B. Kim (2013). "Endoplasmic reticulum stress induces hepatic steatosis via increased expression of the hepatic very low-density lipoprotein receptor." Hepatology **57**(4): 1366-1377.

Juanola, O., S. Martínez-López, R. Francés and I. Gómez-Hurtado (2021). "Non-alcoholic fatty liver disease: metabolic, genetic, epigenetic and environmental risk factors." International journal of environmental research and public health **18**(10): 5227.

Jung, U. J. and M.-S. Choi (2014). "Obesity and Its Metabolic Complications: The Role of Adipokines and the Relationship between Obesity, Inflammation, Insulin Resistance, Dyslipidemia and Nonalcoholic Fatty Liver Disease." International Journal of Molecular Sciences **15**(4): 6184-6223.

Jurczak, M. J., A.-H. Lee, F. R. Jornayvaz, H.-Y. Lee, A. L. Birkenfeld, B. A. Guigni, M. Kahn, V. T. Samuel, L. H. Glimcher and G. I. Shulman (2012). "Dissociation of Inositol-requiring Enzyme (IRE1α)-mediated c-Jun N-terminal Kinase Activation from Hepatic Insulin Resistance in Conditional X-box-binding Protein-1 (XBP1) Knock-out Mice *." Journal of Biological Chemistry **287**(4): 2558-2567.

Kaimori, A., J. Potter, J. Y. Kaimori, C. Wang, E. Mezey and A. Koteish (2007). "Transforming growth factor-beta1 induces an epithelial-to-mesenchymal transition state in mouse hepatocytes in vitro." J Biol Chem **282**(30): 22089-22101.

Kalluri, R. and R. A. Weinberg (2009). "The basics of epithelial-mesenchymal transition." J Clin Invest **119**(6): 1420-1428.

Kamari, Y., A. Shaish, E. Vax, S. Shemesh, M. Kandel-Kfir, Y. Arbel, S. Olteanu, I. Barshack, S. Dotan, E. Voronov, C. A. Dinarello, R. N. Apte and D. Harats (2011). "Lack of interleukin-1α or interleukin-1β inhibits transformation of steatosis to steatohepatitis and liver fibrosis in hypercholesterolemic mice." J Hepatol **55**(5): 1086-1094.

Kamisako, T., Y. Kobayashi, K. Takeuchi, T. Ishihara, K. Higuchi, Y. Tanaka, E. C. Gabazza and Y. Adachi (2000). "Recent advances in bilirubin metabolism research: the molecular mechanism of hepatocyte bilirubin transport and its clinical relevance." J Gastroenterol **35**(9): 659-664.

Kammoun, H. L., H. Chabanon, I. Hainault, S. Luquet, C. Magnan, T. Koike, P. Ferré and F. Foufelle (2009). "GRP78 expression inhibits insulin and ER stress-induced SREBP-1c activation and reduces hepatic steatosis in mice." Journal of Clinical Investigation **119**(5): 1201-1215.

Kang, K., S. M. Reilly, V. Karabacak, M. R. Gangl, K. Fitzgerald, B. Hatano and C. H. Lee (2008). "Adipocyte-derived Th2 cytokines and myeloid PPARdelta regulate macrophage polarization and insulin sensitivity." Cell Metab **7**(6): 485-495.

Karagöz, G. E., D. Acosta-Alvear and P. Walter (2019). "The Unfolded Protein Response: Detecting and Responding to Fluctuations in the Protein-Folding Capacity of the Endoplasmic Reticulum." Cold Spring Harb Perspect Biol **11**(9).

Kasarala, G. and H. L. Tillmann (2016). "Standard liver tests." Clinical Liver Disease **8**(1): 13-18.

Kelly, M. J., S. Pietranico-Cole, J. D. Larigan, N. E. Haynes, C. H. Reynolds, N. Scott, J. Vermeulen,

M. Dvorozniak, K. Conde-Knape, K. S. Huang, S. S. So, K. Thakkar, Y. Qian, B. Banner, F. Mennona, S. Danzi, I. Klein, R. Taub and J. Tilley (2014). "Discovery of 2-[3,5-dichloro-4-(5-isopropyl-6-oxo-1,6-dihydropyridazin-3-yloxy)phenyl]-3,5-dioxo-2,3,4,5-tetrahydro[1,2,4]triazine-6-carbonitrile (MGL-3196), a Highly Selective Thyroid Hormone Receptor β agonist in clinical trials for the treatment of dyslipidemia." J Med Chem **57**(10): 3912-3923.

Kersten, S. (2014). "Integrated physiology and systems biology of PPARα." Mol Metab **3**(4): 354-371.

Kersten, S., J. Seydoux, J. M. Peters, F. J. Gonzalez, B. Desvergne and W. Wahli (1999). "Peroxisome proliferator-activated receptor alpha mediates the adaptive response to fasting." J Clin Invest **103**(11): 1489-1498.

Kishimoto, T. (2010). "IL-6: from its discovery to clinical applications." International Immunology **22**(5): 347-352.

Kmieć, Z. (2001). Introduction — Morphology of the Liver Lobule. Cooperation of Liver Cells in Health and Disease. Z. Kmieć. Berlin, Heidelberg, Springer Berlin Heidelberg**:** 1-6.

Koca, S. S., I. H. Bahcecioglu, O. K. Poyrazoglu, I. H. Ozercan, K. Sahin and B. Ustundag (2008). "The treatment with antibody of TNF-alpha reduces the inflammation, necrosis and fibrosis in the non-alcoholic steatohepatitis induced by methionine- and choline-deficient diet." Inflammation **31**(2): 91-98.

Kostadinova, R., A. Montagner, E. Gouranton, S. Fleury, H. Guillou, D. Dombrowicz, P. Desreumaux and W. Wahli (2012). "GW501516-activated PPARbeta/delta promotes liver fibrosis via p38-JNK MAPK-induced hepatic stellate cell proliferation." Cell Biosci **2**(1): 34.

Kostadinova, R., A. Montagner, E. Gouranton, S. Fleury, H. Guillou, D. Dombrowicz, P. Desreumaux and W. Wahli (2012). "GW501516-activated PPARβ/δ promotes liver fibrosis via p38-JNK MAPK-induced hepatic stellate cell proliferation." Cell & Bioscience **2**(1): 34.

Kraft, G., K. C. Coate, M. Smith, B. Farmer, M. Scott, A. D. Cherrington and D. S. Edgerton (2021). "The Importance of the Mechanisms by Which Insulin Regulates Meal-Associated Liver Glucose Uptake in the Dog." Diabetes **70**(6): 1292-1302.

Krenkel, O., J. Hundertmark, T. P. Ritz, R. Weiskirchen and F. Tacke (2019). "Single Cell RNA Sequencing Identifies Subsets of Hepatic Stellate Cells and Myofibroblasts in Liver Fibrosis." Cells **8**(5).

Kumar, P., T. Smith, K. Rahman, N. E. Thorn and F. A. Anania (2014). "Adiponectin agonist ADP355 attenuates CCl4-induced liver fibrosis in mice." PLoS One **9**(10): e110405.

LaMoia, T. E., G. M. Butrico, H. A. Kalpage, L. Goedeke, B. T. Hubbard, D. F. Vatner, R. C. Gaspar, X.-M. Zhang, G. W. Cline, K. Nakahara, S. Woo, A. Shimada, M. Hüttemann and G. I. Shulman (2022). "Metformin, phenformin, and galegine inhibit complex IV activity and reduce glycerol-derived gluconeogenesis." Proceedings of the National Academy of Sciences **119**(10): e2122287119.

Lan, H. Y. and A. C. Chung (2011). "Transforming growth factor-β and Smads." Diabetes and the Kidney **170**: 75-82.

Latella, G., A. Vetuschi, R. Sferra, V. Catitti, A. D'Angelo, G. Zanninelli, K. C. Flanders and E. Gaudio (2009). "Targeted disruption of Smad3 confers resistance to the development of dimethylnitrosamine-induced hepatic fibrosis in mice." Liver International **29**(7): 997-1009.

Lawitz, E. J., A. Coste, F. Poordad, N. Alkhouri, N. Loo, B. J. McColgan, J. M. Tarrant, T. Nguyen, L. Han, C. Chung, A. S. Ray, J. G. McHutchison, G. M. Subramanian, R. P. Myers, M. S. Middleton, C.

Sirlin, R. Loomba, E. Nyangau, M. Fitch, K. Li and M. Hellerstein (2018). "Acetyl-CoA Carboxylase Inhibitor GS-0976 for 12 Weeks Reduces Hepatic De Novo Lipogenesis and Steatosis in Patients With Nonalcoholic Steatohepatitis." Clin Gastroenterol Hepatol **16**(12): 1983-1991.e1983.

Lebeaupin, C., D. Vallée, D. Rousseau, S. Patouraux, S. Bonnafous, G. Adam, F. Luciano, C. Luci, R. Anty, A. Iannelli, S. Marchetti, G. Kroemer, S. Lacas-Gervais, A. Tran, P. Gual and B. Bailly-Maitre (2018). "Bax inhibitor-1 protects from nonalcoholic steatohepatitis by limiting inositol-requiring enzyme 1 alpha signaling in mice." Hepatology **68**(2): 515-532.

Leclercq, I. A., G. C. Farrell, R. Schriemer and G. R. Robertson (2002). "Leptin is essential for the hepatic fibrogenic response to chronic liver injury." Journal of Hepatology **37**(2): 206-213.

Lee, M. K., C. Pardoux, M. C. Hall, P. S. Lee, D. Warburton, J. Qing, S. M. Smith and R. Derynck (2007). "TGF-β activates Erk MAP kinase signalling through direct phosphorylation of ShcA." The EMBO journal **26**(17): 3957-3967.

Lee, S. M., C. M. Pusec, G. H. Norris, A. De Jesus, A. Diaz-Ruiz, J. Muratalla, A. Sarmento-Cabral, G. Guzman, B. T. Layden and J. Cordoba-Chacon (2021). "Hepatocyte-Specific Loss of PPARγ Protects Mice From NASH and Increases the Therapeutic Effects of Rosiglitazone in the Liver." Cellular and Molecular Gastroenterology and Hepatology **11**(5): 1291-1311.

Lefebvre, E., G. Moyle, R. Reshef, L. P. Richman, M. Thompson, F. Hong, H.-I. Chou, T. Hashiguchi, C. Plato and D. Poulin (2016). "Antifibrotic effects of the dual CCR2/CCR5 antagonist cenicriviroc in animal models of liver and kidney fibrosis." PloS one **11**(6): e0158156.

Lefere, S., T. Puengel, J. Hundertmark, C. Penners, A. K. Frank, A. Guillot, K. de Muynck, F. Heymann, V. Adarbes, E. Defrêne, C. Estivalet, A. Geerts, L. Devisscher, G. Wettstein and F. Tacke (2020). "Differential effects of selective- and pan-PPAR agonists on experimental steatohepatitis and hepatic macrophages☆." Journal of Hepatology **73**(4): 757-770.

Leone, T. C., C. J. Weinheimer and D. P. Kelly (1999). "A critical role for the peroxisome proliferator-activated receptor α (PPARα) in the cellular fasting response: the PPARα-null mouse as a model of fatty acid oxidation disorders." Proceedings of the National Academy of Sciences **96**(13): 7473-7478.

Lesmana, C. R., I. Hasan, U. Budihusodo, R. A. Gani, E. Krisnuhoni, N. Akbar and L. A. Lesmana (2009). "Diagnostic value of a group of biochemical markers of liver fibrosis in patients with non-alcoholic steatohepatitis." J Dig Dis **10**(3): 201-206.

Li, Q. (2015). "Inhibitory SMADs: potential regulators of ovarian function." Biol Reprod **92**(2): 50.

Li, X., Y. Chen, S. Wu, J. He, L. Lou, W. Ye and J. Wang (2015). "microRNA-34a and microRNA-34c promote the activation of human hepatic stellate cells by targeting peroxisome proliferator-activated receptor gamma." Mol Med Rep **11**(2): 1017-1024.

Li, Y., J. Wang, K. Song, S. Liu, H. Zhang, F. Wang, C. Ni, W. Zhai, J. Liang, Z. Qin and J. Zhang (2020). "S100A4 promotes hepatocellular carcinogenesis by intensifying fibrosis-associated cancer cell stemness." Oncoimmunology **9**(1): 1725355.

Liang, Z., T. Li, S. Jiang, J. Xu, W. Di, Z. Yang, W. Hu and Y. Yang (2017). "AMPK: a novel target for treating hepatic fibrosis." Oncotarget **8**(37): 62780-62792.

Lieber, C. S. (2005). "Metabolism of alcohol." Clin Liver Dis **9**(1): 1-35.

Lim, J. Y., M. A. Oh, W. H. Kim, H. Y. Sohn and S. I. Park (2012). "AMP-activated protein kinase inhibits TGF-beta-induced fibrogenic responses of hepatic stellate cells by targeting transcriptional coactivator p300." J Cell Physiol **227**(3): 1081-1089.

Liu, M., G. Zhang, S. Wu, M. Song, J. Wang, W. Cai, S. Mi and C. Liu (2020). "Schaftoside alleviates

HFD-induced hepatic lipid accumulation in mice via upregulating farnesoid X receptor." Journal of Ethnopharmacology **255**: 112776.

Liu, S., J. D. Brown, K. J. Stanya, E. Homan, M. Leidl, K. Inouye, P. Bhargava, M. R. Gangl, L. Dai, B. Hatano, G. S. Hotamisligil, A. Saghatelian, J. Plutzky and C. H. Lee (2013). "A diurnal serum lipid integrates hepatic lipogenesis and peripheral fatty acid use." Nature **502**(7472): 550-554.

Liu, S., B. Hatano, M. Zhao, C. C. Yen, K. Kang, S. M. Reilly, M. R. Gangl, C. Gorgun, J. A. Balschi, J. M. Ntambi and C. H. Lee (2011). "Role of peroxisome proliferator-activated receptor {delta}/{beta} in hepatic metabolic regulation." J Biol Chem **286**(2): 1237-1247.

Liu, S., F. Jing, C. Yu, L. Gao, Y. Qin and J. Zhao (2015). "AICAR-induced activation of AMPK inhibits TSH/SREBP-2/HMGCR pathway in liver." PLoS One **10**(5): e0124951.

Liu, X. and R. M. Green (2019). "Endoplasmic reticulum stress and liver diseases." Liver Research **3**(1): 55-64.

Liu, X., H. Hu and J. Q. Yin (2006). "Therapeutic strategies against TGF-β signaling pathway in hepatic fibrosis." Liver International **26**(1): 8-22.

Liu, X., M. Miyazaki, M. T. Flowers, H. Sampath, M. Zhao, K. Chu, C. M. Paton, D. S. Joo and J. M. Ntambi (2010). "Loss of Stearoyl-CoA desaturase-1 attenuates adipocyte inflammation: effects of adipocyte-derived oleate." Arterioscler Thromb Vasc Biol **30**(1): 31-38.

Liu, X., M. S. Strable and J. M. Ntambi (2011). "Stearoyl CoA desaturase 1: role in cellular inflammation and stress." Adv Nutr **2**(1): 15-22.

Loomba, R., Z. Kayali, M. Noureddin, P. Ruane, E. J. Lawitz, M. Bennett, L. Wang, E. Harting, J. M. Tarrant, B. J. McColgan, C. Chung, A. S. Ray, G. M. Subramanian, R. P. Myers, M. S. Middleton, M. Lai, M. Charlton and S. A. Harrison (2018). "GS-0976 Reduces Hepatic Steatosis and Fibrosis Markers in Patients With Nonalcoholic Fatty Liver Disease." Gastroenterology **155**(5): 1463-1473.e1466.

Loomba, R., E. Lawitz, P. S. Mantry, S. Jayakumar, S. H. Caldwell, H. Arnold, A. M. Diehl, C. S. Djedjos, L. Han, R. P. Myers, G. M. Subramanian, J. G. McHutchison, Z. D. Goodman, N. H. Afdhal and M. R. Charlton (2018). "The ASK1 inhibitor selonsertib in patients with nonalcoholic steatohepatitis: A randomized, phase 2 trial." Hepatology **67**(2): 549-559.

Loomba, R., M. Noureddin, K. V. Kowdley, A. Kohli, A. Sheikh, G. Neff, B. R. Bhandari, N. Gunn, S. H. Caldwell, Z. Goodman, I. Wapinski, M. Resnick, A. H. Beck, D. Ding, C. Jia, J. C. Chuang, R. S. Huss, C. Chung, G. M. Subramanian, R. P. Myers, K. Patel, B. B. Borg, R. Ghalib, H. Kabler, J. Poulos, Z. Younes, M. Elkhashab, T. Hassanein, R. Iyer, P. Ruane, M. L. Shiffman, S. Strasser, V. W. Wong and N. Alkhouri (2021). "Combination Therapies Including Cilofexor and Firsocostat for Bridging Fibrosis and Cirrhosis Attributable to NASH." Hepatology **73**(2): 625-643.

Loomba, R., V. Ratziu and S. A. Harrison (2022). "Expert Panel Review to Compare FDA and EMA Guidance on Drug Development and Endpoints in Nonalcoholic Steatohepatitis." Gastroenterology **162**(3): 680-688.

Loomba, R., V. Seguritan, W. Li, T. Long, N. Klitgord, A. Bhatt, P. S. Dulai, C. Caussy, R. Bettencourt, S. K. Highlander, M. B. Jones, C. B. Sirlin, B. Schnabl, L. Brinkac, N. Schork, C.-H. Chen, D. A. Brenner, W. Biggs, S. Yooseph, J. C. Venter and K. E. Nelson (2017). "Gut Microbiome-Based Metagenomic Signature for Non-invasive Detection of Advanced Fibrosis in Human Nonalcoholic Fatty Liver Disease." Cell Metabolism **25**(5): 1054-1062.e1055.

Lucero, D., V. Zago, G. I. López, M. Graffigna, H. Fainboim, V. Miksztowicz, T. Meroño, S. Belli, O. Levalle, R. Wikinski, F. Brites, G. Berg and L. Schreier (2011). "Pro-inflammatory and atherogenic

circulating factors in non-alcoholic fatty liver disease associated to metabolic syndrome." Clinica Chimica Acta **412**(1): 143-147.

Ludwig, D. S. and C. B. Ebbeling (2018). "The Carbohydrate-Insulin Model of Obesity: Beyond "Calories In, Calories Out"." JAMA Intern Med **178**(8): 1098-1103.

Luedde, T., N. Kaplowitz and R. F. Schwabe (2014). "Cell death and cell death responses in liver disease: mechanisms and clinical relevance." Gastroenterology **147**(4): 765-783.e764.

MacDonald, M. L., M. van Eck, R. B. Hildebrand, B. W. Wong, N. Bissada, P. Ruddle, A. Kontush, H. Hussein, M. A. Pouladi, M. J. Chapman, C. Fievet, T. J. van Berkel, B. Staels, B. M. McManus and M. R. Hayden (2009). "Despite antiatherogenic metabolic characteristics, SCD1-deficient mice have increased inflammation and atherosclerosis." Arterioscler Thromb Vasc Biol **29**(3): 341-347.

Malashkevich, V. N., N. G. Dulyaninova, U. A. Ramagopal, M. A. Liriano, K. M. Varney, D. Knight, M. Brenowitz, D. J. Weber, S. C. Almo and A. R. Bresnick (2010). "Phenothiazines inhibit S100A4 function by inducing protein oligomerization." Proc Natl Acad Sci U S A **107**(19): 8605-8610.

Malhi, H. and R. J. Kaufman (2011). "Endoplasmic reticulum stress in liver disease." Journal of Hepatology **54**(4): 795-809.

Malhotra, J. D. and R. J. Kaufman (2007). "The endoplasmic reticulum and the unfolded protein response." Seminars in Cell & Developmental Biology **18**(6): 716-731.

Mansouri, R. M., E. Baugé, B. Staels and P. Gervois (2008). "Systemic and Distal Repercussions of Liver-Specific Peroxisome Proliferator-Activated Receptor-α Control of the Acute-Phase Response." Endocrinology **149**(6): 3215-3223.

Marin, H. E., M. A. Peraza, A. N. Billin, T. M. Willson, J. M. Ward, M. J. Kennett, F. J. Gonzalez and J. M. Peters (2006). "Ligand Activation of Peroxisome Proliferator–Activated Receptor β Inhibits Colon Carcinogenesis." Cancer Research **66**(8): 4394-4401.

Meli, R., G. Mattace Raso and A. Calignano (2014). "Role of innate immune response in non-alcoholic fatty liver disease: metabolic complications and therapeutic tools." Frontiers in immunology **5**: 177.

Meng, X.-m., D. J. Nikolic-Paterson and H. Y. Lan (2016). "TGF-β: the master regulator of fibrosis." Nature Reviews Nephrology **12**(6): 325-338.

Miller, E. R., 3rd, R. Pastor-Barriuso, D. Dalal, R. A. Riemersma, L. J. Appel and E. Guallar (2005). "Meta-analysis: high-dosage vitamin E supplementation may increase all-cause mortality." Ann Intern Med **142**(1): 37-46.

Miura, K., Y. Kodama, S. Inokuchi, B. Schnabl, T. Aoyama, H. Ohnishi, J. M. Olefsky, D. A. Brenner and E. Seki (2010). "Toll-like receptor 9 promotes steatohepatitis by induction of interleukin-1beta in mice." Gastroenterology **139**(1): 323-334.e327.

Mollica, M. P., L. Lionetti, R. Putti, G. Cavaliere, M. Gaita and A. Barletta (2011). "From chronic overfeeding to hepatic injury: Role of endoplasmic reticulum stress and inflammation." Nutrition, Metabolism and Cardiovascular Diseases **21**(3): 222-230.

Montagner, A., M. B. Delgado, C. Tallichet-Blanc, J. S. Chan, M. K. Sng, H. Mottaz, G. Degueurce, Y. Lippi, C. Moret, M. Baruchet, M. Antsiferova, S. Werner, D. Hohl, T. A. Saati, P. J. Farmer, N. S. Tan, L. Michalik and W. Wahli (2014). "Src is activated by the nuclear receptor peroxisome proliferator-activated receptor beta/delta in ultraviolet radiation-induced skin cancer." EMBO Mol Med **6**(1): 80-98.

Montagner, A., M. B. Delgado, C. Tallichet-Blanc, J. S. K. Chan, M. K. Sng, H. Mottaz, G. Degueurce, Y. Lippi, C. Moret, M. Baruchet, M. Antsiferova, S. Werner, D. Hohl, T. Al Saati, P. J. Farmer, N. S.

Tan, L. Michalik and W. Wahli (2014). "Src is activated by the nuclear receptor peroxisome proliferator-activated receptor β/δ in ultraviolet radiation-induced skin cancer." EMBO Molecular Medicine **6**(1): 80-98.

Montagner, A., A. Polizzi, E. Fouché, S. Ducheix, Y. Lippi, F. Lasserre, V. Barquissau, M. Régnier, C. Lukowicz, F. Benhamed, A. Iroz, J. Bertrand-Michel, T. Al Saati, P. Cano, L. Mselli-Lakhal, G. Mithieux, F. Rajas, S. Lagarrigue, T. Pineau, N. Loiseau, C. Postic, D. Langin, W. Wahli and H. Guillou (2016). "Liver PPARα is crucial for whole-body fatty acid homeostasis and is protective against NAFLD." Gut **65**(7): 1202-1214.

Montecucco, F. and F. Mach (2008). "Does non-alcoholic fatty liver disease (NAFLD) increase cardiovascular risk?" Endocr Metab Immune Disord Drug Targets **8**(4): 301-307.

Mooradian, A. D. (2009). "Dyslipidemia in type 2 diabetes mellitus." Nature Reviews Endocrinology **5**(3): 150-159.

Morikawa, M., R. Derynck and K. Miyazono (2016). "TGF-β and the TGF-β Family: Context-Dependent Roles in Cell and Tissue Physiology." Cold Spring Harb Perspect Biol **8**(5).

Morikawa, M., D. Koinuma, K. Miyazono and C. H. Heldin (2013). "Genome-wide mechanisms of Smad binding." Oncogene **32**(13): 1609-1615.

Mota, M., B. A. Banini, S. C. Cazanave and A. J. Sanyal (2016). "Molecular mechanisms of lipotoxicity and glucotoxicity in nonalcoholic fatty liver disease." Metabolism **65**(8): 1049-1061.

Mouries, J., P. Brescia, A. Silvestri, I. Spadoni, M. Sorribas, R. Wiest, E. Mileti, M. Galbiati, P. Invernizzi and L. Adorini (2019). "Microbiota-driven gut vascular barrier disruption is a prerequisite for non-alcoholic steatohepatitis development." Journal of hepatology **71**(6): 1216-1228.

Murphy, F. R., R. Issa, X. Zhou, S. Ratnarajah, H. Nagase, M. J. Arthur, C. Benyon and J. P. Iredale (2002). "Inhibition of apoptosis of activated hepatic stellate cells by tissue inhibitor of metalloproteinase-1 is mediated via effects on matrix metalloproteinase inhibition: implications for reversibility of liver fibrosis." J Biol Chem **277**(13): 11069-11076.

Musso, G., R. Gambino and M. Cassader (2009). "Recent insights into hepatic lipid metabolism in non-alcoholic fatty liver disease (NAFLD)." Progress in lipid research **48**(1): 1-26.

Nagasawa, T., Y. Inada, S. Nakano, T. Tamura, T. Takahashi, K. Maruyama, Y. Yamazaki, J. Kuroda and N. Shibata (2006). "Effects of bezafibrate, PPAR pan-agonist, and GW501516, PPARδ agonist, on development of steatohepatitis in mice fed a methionine- and choline-deficient diet." European Journal of Pharmacology **536**(1): 182-191.

NASH, E. i. https ://www.genfi t.com/pipel ine/elafibranor/ (2020).

Newsome, P. N., K. Buchholtz, K. Cusi, M. Linder, T. Okanoue, V. Ratziu, A. J. Sanyal, A. S. Sejling and S. A. Harrison (2021). "A Placebo-Controlled Trial of Subcutaneous Semaglutide in Nonalcoholic Steatohepatitis." N Engl J Med **384**(12): 1113-1124.

Ni, X.-X., X.-Y. Li, Q. Wang and J. Hua (2021). "Regulation of peroxisome proliferator-activated receptor-gamma activity affects the hepatic stellate cell activation and the progression of NASH via TGF-β1/Smad signaling pathway." Journal of Physiology and Biochemistry **77**(1): 35-45.

Nishihara, A., J. I. Hanai, N. Okamoto, J. Yanagisawa, S. Kato, K. Miyazono and M. Kawabata (1998). "Role of p300, a transcriptional coactivator, in signalling of TGF-beta." Genes Cells **3**(9): 613-623.

Nov, O., H. Shapiro, H. Ovadia, T. Tarnovscki, I. Dvir, E. Shemesh, J. Kovsan, I. Shelef, Y. Carmi, E. Voronov, R. N. Apte, E. Lewis, Y. Haim, D. Konrad, N. Bashan and A. Rudich (2013). "Interleukin-1β regulates fat-liver crosstalk in obesity by auto-paracrine modulation of adipose tissue inflammation and expandability." PLoS One **8**(1): e53626.

Oakhill, J. S., R. Steel, Z. P. Chen, J. W. Scott, N. Ling, S. Tam and B. E. Kemp (2011). "AMPK is a direct adenylate charge-regulated protein kinase." Science **332**(6036): 1433-1435.

Obstfeld, A. E., E. Sugaru, M. Thearle, A. M. Francisco, C. Gayet, H. N. Ginsberg, E. V. Ables and A. W. Ferrante, Jr. (2010). "C-C chemokine receptor 2 (CCR2) regulates the hepatic recruitment of myeloid cells that promote obesity-induced hepatic steatosis." Diabetes **59**(4): 916-925.

Ocker, M. (2020). "Fibroblast growth factor signaling in non-alcoholic fatty liver disease and non-alcoholic steatohepatitis: Paving the way to hepatocellular carcinoma." World J Gastroenterol **26**(3): 279-290.

Olson, E. J., G. L. Pearce, N. P. Jones and D. L. Sprecher (2012). "Lipid effects of peroxisome proliferator-activated receptor-δ agonist GW501516 in subjects with low high-density lipoprotein cholesterol: characteristics of metabolic syndrome." Arterioscler Thromb Vasc Biol **32**(9): 2289-2294.

Omenetti, A., A. Porrello, Y. Jung, L. Yang, Y. Popov, S. S. Choi, R. P. Witek, G. Alpini, J. Venter, H. M. Vandongen, W. K. Syn, G. S. Baroni, A. Benedetti, D. Schuppan and A. M. Diehl (2008). "Hedgehog signaling regulates epithelial-mesenchymal transition during biliary fibrosis in rodents and humans." J Clin Invest **118**(10): 3331-3342.

Oseini, A. M. and A. J. Sanyal (2017). "Therapies in non-alcoholic steatohepatitis (NASH)." Liver International **37**(S1): 97-103.

Oyadomari, S., H. P. Harding, Y. Zhang, M. Oyadomari and D. Ron (2008). "Dephosphorylation of translation initiation factor 2α enhances glucose tolerance and attenuates hepatosteatosis in mice." Cell metabolism **7**(6): 520-532.

Ozdamar, B., R. Bose, M. Barrios-Rodiles, H.-R. Wang, Y. Zhang and J. L. Wrana (2005). "Regulation of the polarity protein Par6 by TGFß receptors controls epithelial cell plasticity." Science **307**(5715): 1603-1609.

Paulusma, C. C., W. H. Lamers, S. Broer and S. F. J. van de Graaf (2022). "Amino acid metabolism, transport and signalling in the liver revisited." Biochemical Pharmacology **201**: 115074.

Peters, J. M., F. J. Gonzalez and R. Muller (2015). "Establishing the Role of PPARbeta/delta in Carcinogenesis." Trends Endocrinol Metab **26**(11): 595-607.

Pettinelli, P. and L. A. Videla (2011). "Up-Regulation of PPAR-γ mRNA Expression in the Liver of Obese Patients: an Additional Reinforcing Lipogenic Mechanism to SREBP-1c Induction." The Journal of Clinical Endocrinology & Metabolism **96**(5): 1424-1430.

Pitt, H. A. and A. Nakeeb (2017). Chapter 8 - Bile secretion and pathophysiology of biliary tract obstruction. Blumgart's Surgery of the Liver, Biliary Tract and Pancreas, 2-Volume Set (Sixth Edition). W. R. Jarnagin. Philadelphia, Elsevier**:** 123-132.e121.

Poulsen, L. I. C., M. Siersbæk and S. Mandrup (2012). "PPARs: Fatty acid sensors controlling metabolism." Seminars in Cell & Developmental Biology **23**(6): 631-639.

Qian, J., M. Niu, X. Zhai, Q. Zhou and Y. Zhou (2012). "β-Catenin pathway is required for TGF-β1 inhibition of PPARγ expression in cultured hepatic stellate cells." Pharmacological Research **66**(3): 219-225.

Quek, J., K. E. Chan, Z. Y. Wong, C. Tan, B. Tan, W. H. Lim, D. J. H. Tan, A. S. P. Tang, P. Tay, J. Xiao, J. N. Yong, R. W. Zeng, N. W. S. Chew, B. Nah, A. Kulkarni, M. S. Siddiqui, Y. Y. Dan, V. W.-S. Wong, A. J. Sanyal, M. Noureddin, M. Muthiah and C. H. Ng (2023). "Global prevalence of non-alcoholic fatty liver disease and non-alcoholic steatohepatitis in the overweight and obese population: a systematic review and meta-analysis." The Lancet Gastroenterology & Hepatology **8**(1): 20-30.

Ramadori, G. and P. Ramadori (2010). Hepatocytes. Signaling Pathways in Liver Diseases. J.-F. Dufour and P.-A. Clavien. Berlin, Heidelberg, Springer Berlin Heidelberg**:** 3-24.

Rapoport, T. A., L. Li and E. Park (2017). "Structural and mechanistic insights into protein translocation." Annual review of cell and developmental biology **33**: 369-390.

Ratziu, V., L. de Guevara, R. Safadi, F. Poordad, F. Fuster, J. Flores-Figueroa, M. Arrese, A. L. Fracanzani, D. Ben Bashat, K. Lackner, T. Gorfine, S. Kadosh, R. Oren, M. Halperin, L. Hayardeny, R. Loomba, S. Friedman and A. J. Sanyal (2021). "Aramchol in patients with nonalcoholic steatohepatitis: a randomized, double-blind, placebo-controlled phase 2b trial." Nat Med **27**(10): 1825-1835.

Ratziu, V., S. A. Harrison, S. Francque, P. Bedossa, P. Lehert, L. Serfaty, M. Romero-Gomez, J. Boursier, M. Abdelmalek, S. Caldwell, J. Drenth, Q. M. Anstee, D. Hum, R. Hanf, A. Roudot, S. Megnien, B. Staels, A. Sanyal, P. Mathurin, J. Gournay, E. Nguyen-Khac, V. De Ledinghen, D. Larrey, A. Tran, M. Bourliere, M. Maynard-Muet, T. Asselah, J. Henrion, F. Nevens, D. Cassiman, A. Geerts, C. Moreno, U. H. Beuers, P. R. Galle, U. Spengler, E. Bugianesi, A. Craxi, M. Angelico, S. Fargion, M. Voiculescu, L. Gheorghe, L. Preotescu, J. Caballeria, R. J. Andrade, J. Crespo, J. L. Callera, A. Ala, G. Aithal, G. Abouda, V. Luketic, M. A. Huang, S. Gordon, P. Pockros, F. Poordad, N. Shores, M. W. Moehlen, K. Bambha, V. Clark, S. Satapathy, S. Parekh, R. K. Reddy, M. Y. Sheikh, G. Szabo, J. Vierling, T. Foster, G. Umpierrez, C. Chang, T. Box and J. Gallegos-Orozco (2016). "Elafibranor, an Agonist of the Peroxisome Proliferator–Activated Receptor–α and –δ, Induces Resolution of Nonalcoholic Steatohepatitis Without Fibrosis Worsening." Gastroenterology **150**(5): 1147-1159.e1145.

Raza, S., S. Rajak, A. Upadhyay, A. Tewari and R. A. Sinha (2021). "Current treatment paradigms and emerging therapies for NAFLD/NASH." Frontiers in bioscience (Landmark edition) **26**: 206.

Régnier, M., A. Polizzi, S. Smati, C. Lukowicz, A. Fougerat, Y. Lippi, E. Fouché, F. Lasserre, C. Naylies, C. Bétoulières, V. Barquissau, E. Mouisel, J. Bertrand-Michel, A. Batut, T. A. Saati, C. Canlet, M. Tremblay-Franco, S. Ellero-Simatos, D. Langin, C. Postic, W. Wahli, N. Loiseau, H. Guillou and A. Montagner (2020). "Hepatocyte-specific deletion of Pparα promotes NAFLD in the context of obesity." Scientific Reports **10**(1): 6489.

Reich, N., B. Maurer, A. Akhmetshina, P. Venalis, C. Dees, P. Zerr, K. Palumbo, J. Zwerina, T. Nevskaya and S. Gay (2010). "The transcription factor Fra-2 regulates the production of extracellular matrix in systemic sclerosis." Arthritis & Rheumatism: Official Journal of the American College of Rheumatology **62**(1): 280-290.

Riazi, K., H. Azhari, J. H. Charette, F. E. Underwood, J. A. King, E. E. Afshar, M. G. Swain, S. E. Congly, G. G. Kaplan and A.-A. Shaheen (2022). "The prevalence and incidence of NAFLD worldwide: a systematic review and meta-analysis." The lancet gastroenterology & hepatology.

Rinella, M. E., J. V. Lazarus, V. Ratziu, S. M. Francque, A. J. Sanyal, F. Kanwal, D. Romero, M. F. Abdelmalek, Q. M. Anstee, J. P. Arab, M. Arrese, R. Bataller, U. Beuers, J. Boursier, E. Bugianesi, C. D. Byrne, G. E. Castro Narro, A. Chowdhury, H. Cortez-Pinto, D. R. Cryer, K. Cusi, M. El-Kassas, S. Klein, W. Eskridge, J. Fan, S. Gawrieh, C. D. Guy, S. A. Harrison, S. U. Kim, B. G. Koot, M. Korenjak, K. V. Kowdley, F. Lacaille, R. Loomba, R. Mitchell-Thain, T. R. Morgan, E. E. Powell, M. Roden, M. Romero-Gómez, M. Silva, S. P. Singh, S. C. Sookoian, C. W. Spearman, D. Tiniakos, L. Valenti, M. B. Vos, V. W.-S. Wong, S. Xanthakos, Y. Yilmaz, Z. Younossi, A. Hobbs, M. Villota-Rivas and P. N. Newsome (2023). "A multisociety Delphi consensus statement on new fatty liver disease nomenclature." Journal of Hepatology **79**(6): 1542-1556.

Risérus, U., D. Sprecher, T. Johnson, E. Olson, S. Hirschberg, A. Liu, Z. Fang, P. Hegde, D. Richards,

L. Sarov-Blat, J. C. Strum, S. Basu, J. Cheeseman, B. A. Fielding, S. M. Humphreys, T. Danoff, N. R. Moore, P. Murgatroyd, S. O'Rahilly, P. Sutton, T. Willson, D. Hassall, K. N. Frayn and F. Karpe (2008). "Activation of peroxisome proliferator-activated receptor (PPAR)delta promotes reversal of multiple metabolic abnormalities, reduces oxidative stress, and increases fatty acid oxidation in moderately obese men." Diabetes **57**(2): 332-339.

Robertson, I. B. and D. B. Rifkin (2016). "Regulation of the Bioavailability of TGF-β and TGF-β-Related Proteins." Cold Spring Harb Perspect Biol **8**(6).

Rodriguez-Calvo, R., L. Serrano, T. Coll, N. Moullan, R. M. Sanchez, M. Merlos, X. Palomer, J. C. Laguna, L. Michalik, W. Wahli and M. Vazquez-Carrera (2008). "Activation of peroxisome proliferator-activated receptor beta/delta inhibits lipopolysaccharide-induced cytokine production in adipocytes by lowering nuclear factor-kappaB activity via extracellular signal-related kinase 1/2." Diabetes **57**(8): 2149-2157.

Ross, F. A., C. MacKintosh and D. G. Hardie (2016). "AMP-activated protein kinase: a cellular energy sensor that comes in 12 flavours." The FEBS Journal **283**(16): 2987-3001.

Ross, S., E. Cheung, T. G. Petrakis, M. Howell, W. L. Kraus and C. S. Hill (2006). "Smads orchestrate specific histone modifications and chromatin remodeling to activate transcription." The EMBO journal **25**(19): 4490-4502.

Ross, S. E., N. Hemati, K. A. Longo, C. N. Bennett, P. C. Lucas, R. L. Erickson and O. A. MacDougald (2000). "Inhibition of adipogenesis by Wnt signaling." Science **289**(5481): 950-953.

Rutkowski, D. T., J. Wu, S. H. Back, M. U. Callaghan, S. P. Ferris, J. Iqbal, R. Clark, H. Miao, J. R. Hassler, J. Fornek, M. G. Katze, M. M. Hussain, B. Song, J. Swathirajan, J. Wang, G. D. Yau and R. J. Kaufman (2008). "UPR pathways combine to prevent hepatic steatosis caused by ER stress-mediated suppression of transcriptional master regulators." Dev Cell **15**(6): 829-840.

Rygiel, K. A., H. Robertson, H. L. Marshall, M. Pekalski, L. Zhao, T. A. Booth, D. E. Jones, A. D. Burt and J. A. Kirby (2008). "Epithelial-mesenchymal transition contributes to portal tract fibrogenesis during human chronic liver disease." Lab Invest **88**(2): 112-123.

Saiman, Y. and S. L. Friedman (2012). "The Role of Chemokines in Acute Liver Injury." Frontiers in Physiology **3**.

Salvado, L., E. Barroso, A. M. Gomez-Foix, X. Palomer, L. Michalik, W. Wahli and M. Vazquez-Carrera (2014). "PPARbeta/delta prevents endoplasmic reticulum stress-associated inflammation and insulin resistance in skeletal muscle cells through an AMPK-dependent mechanism." Diabetologia **57**(10): 2126-2135.

Salvadó, L., E. Barroso, A. M. Gómez-Foix, X. Palomer, L. Michalik, W. Wahli and M. Vázquez-Carrera (2014). "PPARβ/δ prevents endoplasmic reticulum stress-associated inflammation and insulin resistance in skeletal muscle cells through an AMPK-dependent mechanism." Diabetologia **57**(10): 2126-2135.

Santamaria-Kisiel, L., A. C. Rintala-Dempsey and G. S. Shaw (2006). "Calcium-dependent and -independent interactions of the S100 protein family." Biochem J **396**(2): 201-214.

Sanyal, A., E. D. Charles, B. A. Neuschwander-Tetri, R. Loomba, S. A. Harrison, M. F. Abdelmalek, E. J. Lawitz, D. Halegoua-DeMarzio, S. Kundu, S. Noviello, Y. Luo and R. Christian (2019). "Pegbelfermin (BMS-986036), a PEGylated fibroblast growth factor 21 analogue, in patients with non-alcoholic steatohepatitis: a randomised, double-blind, placebo-controlled, phase 2a trial." Lancet **392**(10165): 2705-2717.

Sanyal, A. J., N. Chalasani, K. V. Kowdley, A. McCullough, A. M. Diehl, N. M. Bass, B. A.

Neuschwander-Tetri, J. E. Lavine, J. Tonascia, A. Unalp, M. Van Natta, J. Clark, E. M. Brunt, D. E. Kleiner, J. H. Hoofnagle and P. R. Robuck (2010). "Pioglitazone, Vitamin E, or Placebo for Nonalcoholic Steatohepatitis." New England Journal of Medicine **362**(18): 1675-1685.

Saucan, L. and G. E. Palade (1994). "Membrane and secretory proteins are transported from the Golgi complex to the sinusoidal plasmalemma of hepatocytes by distinct vesicular carriers." J Cell Biol **125**(4): 733-741.

Schattenberg, J. M., A. Pares, K. V. Kowdley, M. A. Heneghan, S. Caldwell, D. Pratt, A. Bonder, G. M. Hirschfield, C. Levy, J. Vierling, D. Jones, A. Tailleux, B. Staels, S. Megnien, R. Hanf, D. Magrez, P. Birman and V. Luketic (2021). "A randomized placebo-controlled trial of elafibranor in patients with primary biliary cholangitis and incomplete response to UDCA." J Hepatol **74**(6): 1344-1354.

Schiff, E. R., W. C. Maddrey and K. R. Reddy (2017). Schiff's Diseases of the Liver, John Wiley & Sons.

Schinkel, A. H., J. J. Smit, O. van Tellingen, J. H. Beijnen, E. Wagenaar, L. van Deemter, C. A. Mol, M. A. van der Valk, E. C. Robanus-Maandag, H. P. te Riele and et al. (1994). "Disruption of the mouse mdr1a P-glycoprotein gene leads to a deficiency in the blood-brain barrier and to increased sensitivity to drugs." Cell **77**(4): 491-502.

Seki, E. and R. F. Schwabe (2015). "Hepatic inflammation and fibrosis: functional links and key pathways." Hepatology **61**(3): 1066-1079.

Seki, E., H. Tsutsui, H. Nakano, N. M. Tsuji, K. Hoshino, O. Adachi, K. Adachi, S. Futatsugi, K. Kuida, O. Takeuchi, H. Okamura, J. Fujimoto, S. Akira and K. Nakanishi (2001). "Lipopolysaccharide-Induced IL-18 Secretion from Murine Kupffer Cells Independently of Myeloid Differentiation Factor 88 That Is Critically Involved in Induction of Production of IL-12 and IL-1β1." The Journal of Immunology **166**(4): 2651-2657.

Shan, W., C. J. Nicol, S. Ito, M. T. Bility, M. J. Kennett, J. M. Ward, F. J. Gonzalez and J. M. Peters (2008). "Peroxisome proliferator-activated receptor-beta/delta protects against chemically induced liver toxicity in mice." Hepatology **47**(1): 225-235.

Shan, W., P. S. Palkar, I. A. Murray, E. I. McDevitt, M. J. Kennett, B. H. Kang, H. C. Isom, G. H. Perdew, F. J. Gonzalez and J. M. Peters (2008). "Ligand activation of peroxisome proliferator-activated receptor beta/delta (PPARbeta/delta) attenuates carbon tetrachloride hepatotoxicity by downregulating proinflammatory gene expression." Toxicol Sci **105**(2): 418-428.

Sheka, A. C., O. Adeyi, J. Thompson, B. Hameed, P. A. Crawford and S. Ikramuddin (2020). "Nonalcoholic Steatohepatitis: A Review." Jama **323**(12): 1175-1183.

Shiragannavar, V. D., N. G. Sannappa Gowda, L. D. Puttahanumantharayappa, S. H. Karunakara, S. Bhat, S. K. Prasad, D. P. Kumar and P. K. Santhekadur (2023). "The ameliorating effect of withaferin A on high-fat diet-induced non-alcoholic fatty liver disease by acting as an LXR/FXR dual receptor activator." Front Pharmacol **14**: 1135952.

Shneider, B. L. S., Philip M. (2008). "Pediatric Gastrointestinal Disease. Connecticut: PMPH-USA." **p. 751**.

Siddiqui, M. S., M. L. Van Natta, M. A. Connelly, R. Vuppalanchi, B. A. Neuschwander-Tetri, J. Tonascia, C. Guy, R. Loomba, S. Dasarathy, J. Wattacheril, N. Chalasani and A. J. Sanyal (2020). "Impact of obeticholic acid on the lipoprotein profile in patients with non-alcoholic steatohepatitis." Journal of Hepatology **72**(1): 25-33.

Singh, S., A. M. Allen, Z. Wang, L. J. Prokop, M. H. Murad and R. Loomba (2015). "Fibrosis progression in nonalcoholic fatty liver vs nonalcoholic steatohepatitis: a systematic review and

meta-analysis of paired-biopsy studies." Clin Gastroenterol Hepatol **13**(4): 643-654.e641-649; quiz e639-640.

Sinha, R. A., E. Bruinstroop, B. K. Singh and P. M. Yen (2019). "Nonalcoholic Fatty Liver Disease and Hypercholesterolemia: Roles of Thyroid Hormones, Metabolites, and Agonists." Thyroid **29**(9): 1173-1191.

Slack, R. J., R. Mills and A. C. Mackinnon (2021). "The therapeutic potential of galectin-3 inhibition in fibrotic disease." Int J Biochem Cell Biol **130**: 105881.

Smith, B. K., K. Marcinko, E. M. Desjardins, J. S. Lally, R. J. Ford and G. R. Steinberg (2016). "Treatment of nonalcoholic fatty liver disease: role of AMPK." American Journal of Physiology-Endocrinology and Metabolism **311**(4): E730-E740.

Soden, J. S., M. W. Devereaux, J. E. Haas, E. Gumpricht, R. Dahl, J. Gralla, M. G. Traber and R. J. Sokol (2007). "Subcutaneous vitamin E ameliorates liver injury in an in vivo model of steatocholestasis." Hepatology **46**(2): 485-495.

Solé, C., S. Guilly, K. Da Silva, M. Llopis, E. Le-Chatelier, P. Huelin, M. Carol, R. Moreira, N. Fabrellas, G. De Prada, L. Napoleone, I. Graupera, E. Pose, A. Juanola, N. Borruel, M. Berland, D. Toapanta, F. Casellas, F. Guarner, J. Doré, E. Solà, S. D. Ehrlich and P. Ginès (2021). "Alterations in Gut Microbiome in Cirrhosis as Assessed by Quantitative Metagenomics: Relationship With Acute-on-Chronic Liver Failure and Prognosis." Gastroenterology **160**(1): 206-218.e213.

Song, L., T. Y. Chen, X. J. Zhao, Q. Xu, R. Q. Jiao, J. M. Li and L. D. Kong (2019). "Pterostilbene prevents hepatocyte epithelial-mesenchymal transition in fructose-induced liver fibrosis through suppressing miR-34a/Sirt1/p53 and TGF-beta1/Smads signalling." Br J Pharmacol **176**(11): 1619-1634.

Staels, B., A. Rubenstrunk, B. Noel, G. Rigou, P. Delataille, L. J. Millatt, M. Baron, A. Lucas, A. Tailleux, D. W. Hum, V. Ratziu, B. Cariou and R. Hanf (2013). "Hepatoprotective effects of the dual peroxisome proliferator-activated receptor alpha/delta agonist, GFT505, in rodent models of nonalcoholic fatty liver disease/nonalcoholic steatohepatitis." Hepatology **58**(6): 1941-1952.

Stärkel, P., C. Sempoux, I. Leclercq, M. Herin, C. Deby, J. P. Desager and Y. Horsmans (2003). "Oxidative stress, KLF6 and transforming growth factor-beta up-regulation differentiate non-alcoholic steatohepatitis progressing to fibrosis from uncomplicated steatosis in rats." J Hepatol **39**(4): 538-546.

Staufer, K. and R. Stauber (2023). "Steatotic Liver Disease: Metabolic Dysfunction, Alcohol, or Both?" Biomedicines **11**: 2108.

Stephenne, X., M. Foretz, N. Taleux, G. C. van der Zon, E. Sokal, L. Hue, B. Viollet and B. Guigas (2011). "Metformin activates AMP-activated protein kinase in primary human hepatocytes by decreasing cellular energy status." Diabetologia **54**(12): 3101-3110.

Su, L., N. Li, H. Tang, Z. Lou, X. Chong, C. Zhang, J. Su and X. Dong (2018). "Kupffer cell-derived TNF-α promotes hepatocytes to produce CXCL1 and mobilize neutrophils in response to necrotic cells." Cell Death Dis **9**(3): 323.

Sumida, Y. and M. Yoneda (2018). "Current and future pharmacological therapies for NAFLD/NASH." J Gastroenterol **53**(3): 362-376.

Sun, D.-Q., F. Yuan, M.-Z. Fu, M.-Y. Zhong, S.-L. Zhang, Y. Lu, G. Targher, C. D. Byrne, M.-H. Zheng and W.-J. Yuan (2024). "Farnesoid X receptor activation protects against renal fibrosis via modulation of β-catenin signaling." Molecular Metabolism **79**: 101841.

Takayama, O., H. Yamamoto, B. Damdinsuren, Y. Sugita, C. Y. Ngan, X. Xu, T. Tsujino, I. Takemasa,

M. Ikeda, M. Sekimoto, N. Matsuura and M. Monden (2006). "Expression of PPARδ in multistage carcinogenesis of the colorectum: implications of malignant cancer morphology." British Journal of Cancer **95**(7): 889-895.

Tanaka, T., J. Yamamoto, S. Iwasaki, H. Asaba, H. Hamura, Y. Ikeda, M. Watanabe, K. Magoori, R. X. Ioka, K. Tachibana, Y. Watanabe, Y. Uchiyama, K. Sumi, H. Iguchi, S. Ito, T. Doi, T. Hamakubo, M. Naito, J. Auwerx, M. Yanagisawa, T. Kodama and J. Sakai (2003). "Activation of peroxisome proliferator-activated receptor delta induces fatty acid beta-oxidation in skeletal muscle and attenuates metabolic syndrome." Proc Natl Acad Sci U S A **100**(26): 15924-15929.

Ten Dijke, P. and H. M. Arthur (2007). "Extracellular control of TGFβ signalling in vascular development and disease." Nature reviews Molecular cell biology **8**(11): 857-869.

Teng, Y., H. Zhao, L. Gao, W. Zhang, A. Y. Shull and C. Shay (2017). "FGF19 Protects Hepatocellular Carcinoma Cells against Endoplasmic Reticulum Stress via Activation of FGFR4-GSK3β-Nrf2 Signaling." Cancer Res **77**(22): 6215-6225.

Tessari, P., A. Coracina, A. Cosma and A. Tiengo (2009). "Hepatic lipid metabolism and non-alcoholic fatty liver disease." Nutrition, Metabolism and Cardiovascular Diseases **19**(4): 291-302.

Thakur, S., S. Viswanadhapalli, J. B. Kopp, Q. Shi, J. L. Barnes, K. Block, Y. Gorin and H. E. Abboud (2015). "Activation of AMP-activated protein kinase prevents TGF-beta1-induced epithelial-mesenchymal transition and myofibroblast activation." Am J Pathol **185**(8): 2168-2180.

Tokarz, V. L., P. E. MacDonald and A. Klip (2018). "The cell biology of systemic insulin function." J Cell Biol **217**(7): 2273-2289.

Traber, P. G., H. Chou, E. Zomer, F. Hong, A. Klyosov, M. I. Fiel and S. L. Friedman (2013). "Regression of fibrosis and reversal of cirrhosis in rats by galectin inhibitors in thioacetamide-induced liver disease." PLoS One **8**(10): e75361.

Tsuchida, T. and S. L. Friedman (2017). "Mechanisms of hepatic stellate cell activation." Nature Reviews Gastroenterology & Hepatology **14**(7): 397-411.

Tsuchiya, M., F. Yamaguchi, S. Shimamoto, T. Fujimoto, H. Tokumitsu, M. Tokuda and R. Kobayashi (2014). "Oxidized S100A4 inhibits the activation of protein phosphatase 5 through S100A1 in MKN-45 gastric carcinoma cells." Int J Mol Med **34**(6): 1713-1719.

Tsukada, S., C. J. Parsons and R. A. Rippe (2006). "Mechanisms of liver fibrosis." Clinica Chimica Acta **364**(1): 33-60.

Tsukamoto, H., N.-L. Zhu, K. Asahina, D. A. Mann and J. Mann (2011). "Epigenetic cell fate regulation of hepatic stellate cells." Hepatology Research **41**(7): 675-682.

Tzavlaki, K. and A. Moustakas (2020). "TGF-β Signaling." Biomolecules **10**(3): 487.

Uysal, K. T., S. M. Wiesbrock, M. W. Marino and G. S. Hotamisligil (1997). "Protection from obesity-induced insulin resistance in mice lacking TNF-α function." Nature **389**(6651): 610-614.

Vacca, M., S. D'Amore, G. Graziano, A. D'Orazio, M. Cariello, V. Massafra, L. Salvatore, N. Martelli, S. Murzilli, G. Lo Sasso, R. Mariani-Costantini and A. Moschetta (2014). "Clustering nuclear receptors in liver regeneration identifies candidate modulators of hepatocyte proliferation and hepatocarcinoma." PLoS One **9**(8): e104449.

van den Hoek, A. M., L. Verschuren, M. P. M. Caspers, N. Worms, A. L. Menke and H. M. G. Princen (2021). "Beneficial effects of elafibranor on NASH in E3L.CETP mice and differences between mice and men." Sci Rep **11**(1): 5050.

Vazquez-Carrera, M. (2016). "Unraveling the Effects of PPARbeta/delta on Insulin Resistance and Cardiovascular Disease." Trends Endocrinol Metab **27**(5): 319-334.

Vázquez-Carrera, M. (2016). "Unraveling the Effects of PPARβ/δ on Insulin Resistance and Cardiovascular Disease." Trends in Endocrinology & Metabolism **27**(5): 319-334.

Veidal, S. S., E. Vassiliadis, N. Barascuk, C. Zhang, T. Segovia-Silvestre, L. Klickstein, M. R. Larsen, P. Qvist, C. Christiansen and B. Vainer (2010). "Matrix metalloproteinase-9-mediated type III collagen degradation as a novel serological biochemical marker for liver fibrogenesis." Liver International **30**(9): 1293-1304.

Vilar-Gomez, E., Y. Martinez-Perez, L. Calzadilla-Bertot, A. Torres-Gonzalez, B. Gra-Oramas, L. Gonzalez-Fabian, S. L. Friedman, M. Diago and M. Romero-Gomez (2015). "Weight Loss Through Lifestyle Modification Significantly Reduces Features of Nonalcoholic Steatohepatitis." Gastroenterology **149**(2): 367-378.e365; quiz e314-365.

Viollet, B. and M. Foretz (2015). LKB1/AMPK pathway in the control of hepatic energy metabolism. Signaling pathways in liver diseases. D. Jean-François and C. Pierre-Alain, WILEY-BLACKWELL.

Viollet, B., M. Foretz, B. Guigas, S. Horman, R. Dentin, L. Bertrand, L. Hue and F. Andreelli (2006). "Activation of AMP-activated protein kinase in the liver: a new strategy for the management of metabolic hepatic disorders." The Journal of Physiology **574**(1): 41-53.

Walle, P., M. Takkunen, V. Männistö, M. Vaittinen, M. Lankinen, V. Kärjä, P. Käkelä, J. Ågren, M. Tiainen, U. Schwab, J. Kuusisto, M. Laakso and J. Pihlajamäki (2016). "Fatty acid metabolism is altered in non-alcoholic steatohepatitis independent of obesity." Metabolism **65**(5): 655-666.

Walton, K., K. Johnson and C. Harrison (2017). "Targeting TGF-β Mediated SMAD Signaling for the Prevention of Fibrosis." Frontiers in Pharmacology **8**.

Wang, S. and S. L. Friedman (2023). "Found in translation-Fibrosis in metabolic dysfunction-associated steatohepatitis (MASH)." Sci Transl Med **15**(716): eadi0759.

Wang, X., Z. Wei, B. Cheng, J. Li, Y. He, T. Lan, T. Kemper, Y. Lin, B. Jiang and Y. Jiang (2022). "Endoplasmic reticulum stress promotes HBV production by enhancing use of the autophagosome/multivesicular body axis." Hepatology **75**(2): 438-454.

Wang, Y.-X. (2010). "PPARs: diverse regulators in energy metabolism and metabolic diseases." Cell Research **20**(2): 124-137.

Wang, Y., W. Lan, M. Xu, J. Song, J. Mao, C. Li, X. Du, Y. Jiang, E. Li, R. Zhang and Q. Wang (2021). "Cancer-associated fibroblast-derived SDF-1 induces epithelial-mesenchymal transition of lung adenocarcinoma via CXCR4/beta-catenin/PPARdelta signalling." Cell Death Dis **12**(2): 214.

Westerouen Van Meeteren, M. J., J. P. H. Drenth and E. Tjwa (2020). "Elafibranor: a potential drug for the treatment of nonalcoholic steatohepatitis (NASH)." Expert Opin Investig Drugs **29**(2): 117-123.

Wilkes, M. C., S. J. Murphy, N. Garamszegi and E. B. Leof (2003). "Cell-type-specific activation of PAK2 by transforming growth factor β independent of Smad2 and Smad3." Molecular and cellular biology **23**(23): 8878-8889.

Wree, A., T. M. Holtmann, M. E. Inzaugarat and A. E. Feldstein (2019). Novel drivers of the inflammatory response in liver injury and fibrosis. Seminars in liver disease, Thieme Medical Publishers.

Wu, J., D. Puppala, X. Feng, M. Monetti, A. L. Lapworth and K. F. Geoghegan (2013). "Chemoproteomic analysis of intertissue and interspecies isoform diversity of AMP-activated protein kinase (AMPK)." J Biol Chem **288**(50): 35904-35912.

Wu, J., D. T. Rutkowski, M. Dubois, J. Swathirajan, T. Saunders, J. Wang, B. Song, G. D. Y. Yau and R. J. Kaufman (2007). "ATF6α Optimizes Long-Term Endoplasmic Reticulum Function to Protect

Cells from Chronic Stress." Developmental Cell **13**(3): 351-364.
Wu, X., H. Ge, B. Lemon, S. Vonderfecht, J. Weiszmann, R. Hecht, J. Gupte, T. Hager, Z. Wang, R. Lindberg and Y. Li (2010). "FGF19-induced hepatocyte proliferation is mediated through FGFR4 activation." J Biol Chem **285**(8): 5165-5170.
Wu, X. and T. Huang (2020). "Recent development in acetyl-CoA carboxylase inhibitors and their potential as novel drugs." Future Medicinal Chemistry **12**(6): 533-561.
Xiang, M., P. X. Wang, A. B. Wang, X. J. Zhang, Y. Zhang, P. Zhang, F. H. Mei, M. H. Chen and H. Li (2016). "Targeting hepatic TRAF1-ASK1 signaling to improve inflammation, insulin resistance, and hepatic steatosis." J Hepatol **64**(6): 1365-1377.
Xiao, B., M. J. Sanders, E. Underwood, R. Heath, F. V. Mayer, D. Carmena, C. Jing, P. A. Walker, J. F. Eccleston, L. F. Haire, P. Saiu, S. A. Howell, R. Aasland, S. R. Martin, D. Carling and S. J. Gamblin (2011). "Structure of mammalian AMPK and its regulation by ADP." Nature **472**(7342): 230-233.
Xu, F., C. Liu, D. Zhou and L. Zhang (2016). "TGF-β/SMAD Pathway and Its Regulation in Hepatic Fibrosis." Journal of Histochemistry & Cytochemistry **64**(3): 157-167.
Xu, J., S. Stanislaus, N. Chinookoswong, Y. Y. Lau, T. Hager, J. Patel, H. Ge, J. Weiszmann, S. C. Lu, M. Graham, J. Busby, R. Hecht, Y. S. Li, Y. Li, R. Lindberg and M. M. Véniant (2009). "Acute glucose-lowering and insulin-sensitizing action of FGF21 in insulin-resistant mouse models--association with liver and adipose tissue effects." Am J Physiol Endocrinol Metab **297**(5): E1105-1114.
Xu, L., A. Y. Hui, E. Albanis, M. J. Arthur, S. M. O'Byrne, W. S. Blaner, P. Mukherjee, S. L. Friedman and F. J. Eng (2005). "Human hepatic stellate cell lines, LX-1 and LX-2: new tools for analysis of hepatic fibrosis." Gut **54**(1): 142-151.
Xue, Z. F., X. M. Wu and M. Liu (2013). "Hepatic regeneration and the epithelial to mesenchymal transition." World J Gastroenterol **19**(9): 1380-1386.
Yamaguchi, K., Y. Itoh, C. Yokomizo, T. Nishimura, T. Niimi, H. Fujii, T. Okanoue and T. Yoshikawa (2010). "Blockade of interleukin-6 signaling enhances hepatic steatosis but improves liver injury in methionine choline-deficient diet-fed mice." Lab Invest **90**(8): 1169-1178.
Yamaguchi, K., Y. Itoh, C. Yokomizo, T. Nishimura, T. Niimi, A. Umemura, H. Fujii, T. Okanoue and T. Yoshikawa (2011). "Blockade of IL-6 signaling exacerbates liver injury and suppresses antiapoptotic gene expression in methionine choline-deficient diet-Fed db/db mice." Laboratory Investigation **91**(4): 609-618.
Yan, Y., X. E. Zhou, H. E. Xu and K. Melcher (2018). "Structure and Physiological Regulation of AMPK." Int J Mol Sci **19**(11).
Yang, C., M. Zeisberg, B. Mosterman, A. Sudhakar, U. Yerramalla, K. Holthaus, L. Xu, F. Eng, N. Afdhal and R. Kalluri (2003). "Liver fibrosis: insights into migration of hepatic stellate cells in response to extracellular matrix and growth factors." Gastroenterology **124**(1): 147-159.
Yang, Y., Z. Zhao, Y. Liu, X. Kang, H. Zhang and M. Meng (2015). "Suppression of oxidative stress and improvement of liver functions in mice by ursolic acid via LKB1-AMP-activated protein kinase signaling." J Gastroenterol Hepatol **30**(3): 609-618.
Yang, Z., A. Danzeng, Q. Liu, C. Zeng, L. Xu, J. Mo, C. Pingcuo, X. Wang, C. Wang, B. Zhang and B. Zhang (2024). "The Role of Nuclear Receptors in the Pathogenesis and Treatment of Non-alcoholic Fatty Liver Disease." International Journal of Biological Sciences **20**: 113-126.
Yi, J. Y., I. Shin and C. L. Arteaga (2005). "Type I transforming growth factor beta receptor binds to and activates phosphatidylinositol 3-kinase." J Biol Chem **280**(11): 10870-10876.
Yoon, Y. C., Z. Fang, J. E. Lee, J. H. Park, J. K. Ryu, K. H. Jung and S. S. Hong (2020). "Selonsertib

Inhibits Liver Fibrosis via Downregulation of ASK1/ MAPK Pathway of Hepatic Stellate Cells." Biomol Ther (Seoul) **28**(6): 527-536.

Yoshiji, H., S. Kuriyama, Y. Miyamoto, U. P. Thorgeirsson, D. E. Gomez, M. Kawata, J. Yoshii, Y. Ikenaka, R. Noguchi, H. Tsujinoue, T. Nakatani, S. S. Thorgeirsson and H. Fukui (2000). "Tissue inhibitor of metalloproteinases-1 promotes liver fibrosis development in a transgenic mouse model." Hepatology **32**(6): 1248-1254.

Younossi, Z. M., P. Golabi, L. de Avila, J. M. Paik, M. Srishord, N. Fukui, Y. Qiu, L. Burns, A. Afendy and F. Nader (2019). "The global epidemiology of NAFLD and NASH in patients with type 2 diabetes: A systematic review and meta-analysis." J Hepatol **71**(4): 793-801.

Younossi, Z. M., A. B. Koenig, D. Abdelatif, Y. Fazel, L. Henry and M. Wymer (2016). "Global epidemiology of nonalcoholic fatty liver disease—meta-analytic assessment of prevalence, incidence, and outcomes." Hepatology **64**(1): 73-84.

Yu, K., Q. Li, G. Shi and N. Li (2018). "Involvement of epithelial-mesenchymal transition in liver fibrosis." Saudi J Gastroenterol **24**(1): 5-11.

Zakaria, R., I. Lamsoul, S. Uttenweiler-Joseph, M. Erard, B. Monsarrat, O. Burlet-Schiltz, C. Moog-Lutz and P. G. Lutz (2013). "Phosphorylation of serine 323 of ASB2alpha is pivotal for the targeting of filamin A to degradation." Cell Signal **25**(12): 2823-2830.

Zanger, U. M. and M. Schwab (2013). "Cytochrome P450 enzymes in drug metabolism: regulation of gene expression, enzyme activities, and impact of genetic variation." Pharmacol Ther **138**(1): 103-141.

Zarei, M., D. Aguilar-Recarte, X. Palomer and M. Vazquez-Carrera (2021). "Revealing the role of peroxisome proliferator-activated receptor beta/delta in nonalcoholic fatty liver disease." Metabolism **114**: 154342.

Zarei, M., E. Barroso, X. Palomer, J. Dai, P. Rada, T. Quesada-López, J. C. Escolà-Gil, L. Cedó, M. R. Zali, M. Molaei, R. Dabiri, S. Vázquez, E. Pujol, Á. M. Valverde, F. Villarroya, Y. Liu, W. Wahli and M. Vázquez-Carrera (2018). "Hepatic regulation of VLDL receptor by PPARβ/δ and FGF21 modulates non-alcoholic fatty liver disease." Molecular Metabolism **8**: 117-131.

Zeisberg, M., C. Yang, M. Martino, M. B. Duncan, F. Rieder, H. Tanjore and R. Kalluri (2007). "Fibroblasts derive from hepatocytes in liver fibrosis via epithelial to mesenchymal transition." J Biol Chem **282**(32): 23337-23347.

Zeng, L., M. Lu, K. Mori, S. Luo, A. S. Lee, Y. Zhu and J. Y. Shyy (2004). "ATF6 modulates SREBP2-mediated lipogenesis." Embo j **23**(4): 950-958.

Zhai, X., H. Qiao, W. Guan, Z. Li, Y. Cheng, X. Jia and Y. Zhou (2015). "Curcumin regulates peroxisome proliferator-activated receptor-gamma coactivator-1alpha expression by AMPK pathway in hepatic stellate cells in vitro." Eur J Pharmacol **746**: 56-62.

Zhang, L., C. Liu, X.-m. Meng, C. Huang, F. Xu and J. Li (2015). "Smad2 protects against TGF-β1/Smad3-mediated collagen synthesis in human hepatic stellate cells during hepatic fibrosis." Molecular and cellular biochemistry **400**: 17-28.

Zhang, Y. E. (2009). "Non-Smad pathways in TGF-β signaling." Cell Research **19**(1): 128-139.

Zhang, Y. E. (2017). "Non-Smad Signaling Pathways of the TGF-beta Family." Cold Spring Harb Perspect Biol **9**(2).

Zhang, Y. E. (2017). "Non-Smad signaling pathways of the TGF-β family." Cold Spring Harbor perspectives in biology **9**(2): a022129.

Zhao, P. and A. R. Saltiel (2020). "From overnutrition to liver injury: AMP-activated protein kinase

in nonalcoholic fatty liver diseases." J Biol Chem **295**(34): 12279-12289.

Zhao, P., X. Sun, C. Chaggan, Z. Liao, K. In Wong, F. He, S. Singh, R. Loomba, M. Karin and J. L. Witztum (2020). "An AMPK–caspase-6 axis controls liver damage in nonalcoholic steatohepatitis." Science **367**(6478): 652-660.

Zhao, P., X. Sun, C. Chaggan, Z. Liao, K. In Wong, F. He, S. Singh, R. Loomba, M. Karin, J. L. Witztum and A. R. Saltiel (2020). "An AMPK-caspase-6 axis controls liver damage in nonalcoholic steatohepatitis." Science **367**(6478): 652-660.

Zhou, M., X. Wang, V. Phung, D. A. Lindhout, K. Mondal, J. Y. Hsu, H. Yang, M. Humphrey, X. Ding, T. Arora, R. M. Learned, A. M. DePaoli, H. Tian and L. Ling (2014). "Separating Tumorigenicity from Bile Acid Regulatory Activity for Endocrine Hormone FGF19." Cancer Res **74**(12): 3306-3316.

Zhou, Y., X. Jia, G. Wang, X. Wang and J. Liu (2009). "PI-3 K/AKT and ERK signaling pathways mediate leptin-induced inhibition of PPARγ gene expression in primary rat hepatic stellate cells." Molecular and cellular biochemistry **325**: 131-139.

Ziolkowska, S., A. Binienda, M. Jabłkowski, J. Szemraj and P. Czarny (2021). "The Interplay between Insulin Resistance, Inflammation, Oxidative Stress, Base Excision Repair and Metabolic Syndrome in Nonalcoholic Fatty Liver Disease." Int J Mol Sci **22**(20).

Zuo, X., W. Xu, M. Xu, R. Tian, M. J. Moussalli, F. Mao, X. Zheng, J. Wang, J. S. Morris, M. Gagea, C. Eng, S. Kopetz, D. M. Maru, A. Rashid, R. Broaddus, D. Wei, M. C. Hung, A. K. Sood and I. Shureiqi (2017). "Metastasis regulation by PPARD expression in cancer cells." JCI Insight **2**(1): e91419.

VIII. Annex

Article 1

Biomedicine & Pharmacotherapy 167 (2023) 115623

Contents lists available at ScienceDirect

Biomedicine & Pharmacotherapy

journal homepage: www.elsevier.com/locate/biopha

Elafibranor upregulates the EMT-inducer S100A4 via PPARβ/δ

Meijian Zhang [a,b,c,1], Emma Barroso [a,b,c,1], Maria Ruart [a,b,c], Lucía Peña [a,b,c], Mona Peyman [a,b,c], David Aguilar-Recarte [a,b,c], Marta Montori-Grau [a,b,c], Patricia Rada [b,d], Clara Cugat [a,b,c], Carla Montironi [e,f], Mohammad Zarei [g,h], Javier Jurado-Aguilar [a,b,c], Antoni Camins [a,i,j], Jesús Balsinde [b,k], Ángela M. Valverde [b,d], Walter Wahli [l,m,n], Xavier Palomer [a,b,c], Manuel Vázquez-Carrera [a,b,c,*]

[a] *Department of Pharmacology, Toxicology and Therapeutic Chemistry, Faculty of Pharmacy and Food Sciences and Institute of Biomedicine of the University of Barcelona (IBUB), University of Barcelona, Barcelona, Spain*
[b] *Spanish Biomedical Research Center in Diabetes and Associated Metabolic Diseases (CIBERDEM)-Instituto de Salud Carlos III, Madrid, Spain*
[c] *Pediatric Research Institute-Hospital Sant Joan de D´eu, Esplugues de Llobregat, Spain*
[d] *Instituto de Investigaciones Biom´edicas Alberto Sols (CSIC/UAM), Madrid, Spain*
[e] *Pathology Department, Hospital Clínic, Barcelona, Spain*
[f] *Liver Cancer Translational Research Group, Liver Unit, IDIBAPS-Hospital Clínic, University of Barcelona, Spain*
[g] *John B. Little Center for Radiation Sciences, Harvard T.H. Chan School of Public Health, Boston, USA*
[h] *Renal Division, Brigham & Women's Hospital, Harvard Medical School, Boston, USA*
[i] *Biomedical Research Networking Centre in Neurodegenerative Diseases (CIBERNED), Madrid, Spain*
[j] *Institute of Neuroscience, University of Barcelona, Barcelona, Spain*
[k] *Instituto de Biología y Gen´etica Molecular, Consejo Superior de Investigaciones Científicas, Valladolid, Spain*
[l] *Center for Integrative Genomics, University of Lausanne, CH-1015 Lausanne, Switzerland*
[m] *Lee Kong Chian School of Medicine, Nanyang Technological University Singapore, 308232, Singapore*
[n] *INRA ToxAlim, UMR1331, Chemin de Tournefeuille, F-31027 Toulouse Cedex 3, France*

ARTICLE INFO

Keywords:
MASLD
Elafibranor
PPARβ/δ
S100A4
ASB2
EMT

ABSTRACT

Elafibranor is a dual peroxisome proliferator-activated receptor (PPAR)α and β/δ agonist that has reached a phase III clinical trial for the treatment of metabolic dysfunction-associated steatotic liver disease (MASLD). Here, we examined the effects of elafibranor in mice fed a choline-deficient high-fat diet (CD-HFD), a model of metabolic dysfunction-associated steatohepatitis (MASH) that presents obesity and insulin resistance. Our findings revealed that elafibranor treatment ameliorated steatosis, inflammation, and fibrogenesis in the livers of CD-HFD-fed mice. Unexpectedly, elafibranor also increased the levels of the epithelial-mesenchymal transition (EMT)-promoting protein S100A4 via PPARβ/δ activation. The increase in S100A4 protein levels caused by elafibranor was accompanied by changes in the levels of markers associated with the EMT program. The S100A4 induction caused by elafibranor was confirmed in the BRL-3A rat liver cells and a mouse primary hepatocyte culture. Furthermore, elafibranor reduced the levels of ASB2, a protein that promotes S100A4 degradation, while ASB2 overexpression prevented the stimulating effect of elafibranor on S100A4. Collectively, these findings reveal an unexpected hepatic effect of elafibranor on increasing S100A4 and promoting the EMT program.

Abbreviations: ASB2, ankyrin repeat and suppressor of cytokine signaling box containing 2 protein; CD-HFD, choline-deficient high-fat diet; COL1A1, collagen type I α1; CRISPR/dCas9, clustered regularly interspaced short palindromic repeats/deactivated CRISPR-associated protein 9; EMT, epithelial-mesenchymal transition; ERK, extracellular signal-regulated kinases; FSP1, fibroblast-specific protein 1; GTT, glucose tolerance test; ITT, insulin tolerance test; MASLD, metabolic dysfunction-associated steatotic liver disease; MASH, metabolic dysfunction-associated steatohepatitis; PPAR, peroxisome proliferator-activated receptor; siRNA, small interfering RNA; α-SMA, α-smooth muscle actin; S100A4, S100 calcium binding protein A4; 16:0/18:1-PC, 1-palmitoyl-2-oleoyl-sn-glycero-3-phosphocholine.

* Correspondence to: Unitat de Farmacologia, Facultat de Farma`cia i Ci`encies de l´Alimentacio´, Av. Joan XXIII 27-31, E-08028 Barcelona, Spain.
E-mail address: mvazquezcarrera@ub.edu (M. Va´zquez-Carrera).

[1] Both authors contributed equally

https://doi.org/10.1016/j.biopha.2023.115623
Received 20 June 2023; Received in revised form 27 September 2023; Accepted 28 September 2023
Available online 30 September 2023
0753-3322/© 2023 The Authors. Published by Elsevier Masson SAS. This is an open access article under the CC BY license (http://creativecommons.org/licenses/by/4.0/).

1. Introduction

Metabolic dysfunction-associated steatotic liver disease (MASLD) is the most common cause of chronic liver disease in individuals without significant alcohol consumption. Its major drivers are obesity and insulin resistance. The global prevalence of MASLD in the general population is 25% [1], with this percentage increasing to 90% in subjects with morbid obesity [2]. MASLD ranges from hepatic steatosis (without hepatocyte injury in the form of hepatocyte ballooning) to a more severe condition known as metabolic dysfunction-associated steatohepatitis (MASH, steatosis with ballooning, inflammation, with or without fibrosis). MASH increases the risk of developing more serious diseases such as cirrhosis, hepatocellular carcinoma (HCC), and cardiovascular disease [3–5].

Although many pharmacotherapies are being evaluated for the treatment of MASH, there are currently no US Food and Drug Administration (FDA) approved specific pharmacological drugs for the treatment of this condition. As a result, given the complexity of its pathophysiology, the best treatment for this disease might be the use of compounds activating several targets or a combination of drugs targeting different mechanistic pathways [6]. Following this rationale, elafibranor (also known as GFT505), a dual peroxisome proliferator-activated receptor α (PPARα) and β/δ agonist was developed, and has reached a phase III clinical trial. In humans, elafibranor was observed to show a modest effect on the histological resolution of MASH, but did not demonstrate any significant effect on fibrosis [7], the main driver of all-cause and liver-related mortality in MASH patients [8]. As a result, elafibranor was discontinued in 2020 because it did not meet the predefined primary surrogate endpoint of MASH resolution without the worsening of fibrosis [9]. Despite this negative outcome, the efficacy of elafibranor will be evaluated in combination with other drugs for the treatment of MASH [10]. In PPARα knockout mice, elafibranor prevents liver steatosis and inflammation, suggesting that these actions are mediated by PPARβ/δ activation [11]. PPARβ/δ is expressed in the main liver cell types (hepatocytes, Kupffer cells, cholangiocytes and hepatic stellate cells) [12] and its activation hinders the progression of MASLD by ameliorating insulin resistance, reducing lipogenesis, and alleviating inflammation and endoplasmic reticulum stress [13]. However, the use of PPARβ/δ agonists as therapeutic agents needs to be performed with caution as the activation of this nuclear receptor may have tumorigenic effects, although the role of PPARβ/δ in cancer is controversial [14].

An important process propagating the progression of liver fibrosis is the epithelial-mesenchymal transition (EMT). This is a program by which epithelial cells, such as hepatocytes and cholangiocytes, lose their epithelial phenotype (polarity and adherence) and acquire mesenchymal characteristics (motility and invasiveness) [15]. Hepatocyte EMT is induced by transforming growth factor β (TGF-β) and carbon tetrachloride (CCl_4), and is characterized by the downregulation of epithelial markers (e.g. E-cadherin) and the upregulation of mesenchymal markers such as vimentin and S100 calcium binding protein A4 (S100A4, also known as fibroblast-specific protein 1, FSP1). Indeed, S100A4 is considered an inducer of the EMT program [16]. Interestingly, S100A4-knockout mice fed a methionine-choline-deficient (MCD) diet show attenuated liver fibrosis and inflammation, as well as an inhibition of hepatocyte apoptosis [17]. S100A4 also seems to play a role in liver tumorigeneses, since S100A4-deficient mice develop significantly fewer and smaller liver tumor nodules, while showing decreases in liver fibrosis and the expression of stem cell markers in the HCC tissues [15]. In fact, increased S100A4 protein levels correlate with poor prognosis in several cancers, with S100A4 promoting the development of metastasis in mouse models of cancer [17]. The effects of S100A4 have been associated with the formation of oligomers of this protein, which is stimulated by oxidation [18]. Moreover, S100A4 does not possess enzymatic activity, but rather interacts with target proteins and regulates their activity. Intracellular targets of S100A4 include p53 and non-muscle myosin IIA (NMIIA) [19]. Overall, these findings suggest that S100A4 is a regulator of both fibrogenesis and tumorigenesis in the liver.

In the present study, we examined the effects of elafibranor in mice fed a choline-deficient high-fat diet (CD-HFD), a model of MASH that presents obesity and insulin resistance and thus closely resembles human MASH [20,21]. Elafibranor treatment improved steatosis, inflammation, and fibrogenesis in these mice, but, surprisingly, it increased protein level of the EMT-inducer S100A4 through PPARβ/δ activation and this increase was accompanied by changes in the levels of the markers associated with the EMT program. Our findings also revealed that elafibranor reduced levels of the S100A4-degrading E3 ubiquitin ligase, ankyrin repeat and suppressor of cytokine signaling box containing protein 2 (ASB2). Likewise, the increased S100A4 levels caused by elafibranor was prevented by the overexpression of ASB2, indicating that the reduction of this E3 ubiquitin ligase is the underlying mechanism involved in S100A4 upregulation. Overall, these findings indicate that PPARβ/δ is a new player in the control of hepatic EMT in mice, with potential implications in the regulation of MASH development and the promotion of liver tumors.

2. Materials and methods

2.1. Reagents

Control siRNA and S100A4 siRNA were purchased from Santa Cruz (Dallas, TX, USA). GW501516, GSK0660 and U0126 were purchased from Sigma-Aldrich (Madrid, Spain) and elafibranor from AXON Medchem (Groningen, the Netherlands).

2.2. Mice

Male C57BL/6 mice (10–12 weeks old) (Envigo, Barcelona, Spain) were housed and maintained under a constant temperature (22 ± 2 °C) and humidity (55%). The mice had free access to water and food and were subjected to 12-h light-dark cycles. After 1 week of acclimatization, the mice were randomly distributed into three experimental groups (n = 6 each) and fed either standard chow (one group) or a choline-deficient high-fat diet (CD-HFD; 44.9 kcal% fat, 35.1 kcal% carbohydrates, and 20.0 kcal% protein, without added choline; D05010402, Research diets, New Brunswick, NJ, USA) (two groups) for 12 weeks. Mice fed standard chow and one of the groups of mice fed the CD-HFD received one daily p.o. gavage of vehicle (0.5% w/v carboxymethylcellulose), while the remaining group fed the CD-HFD received one daily p.o. dose of 10 mg/kg/day of elafibranor dissolved in the vehicle (volume administered, 1 ml/kg) during the last 4 weeks. In a second study, the mice were randomly distributed in three experimental groups (n = 6 each) and fed either standard chow (one group) or the CD-HFD (D05010402, Research Diets) for 12 weeks. Mice fed standard chow and one of the groups fed the CD-HFD received one daily p.o. gavage of vehicle (0.5% w/v carboxymethylcellulose), while the remaining group fed the CD-HFD received one daily p.o. dose of 5 mg/kg/day of the PPARβ/δ agonist GW501516 dissolved in the vehicle (volume administered, 1 ml/kg) during the last 4 weeks. At the end of the treatment, the mice were sacrificed, and liver samples were frozen in liquid nitrogen and then stored at — 80ºC. In a third study, male (8–9 weeks old) *Ppard*-knockout (*Ppard*$^{-/-}$) mice (n = 6) and their wild-type littermates (*Ppard*$^{+/+}$) (n = 6) with the same genetic background (C57BL/6 ×129/SV) [50], all fed a control diet, were used. The mice were sacrificed, and liver samples were frozen in liquid nitrogen and then stored at — 80ºC.

For the glucose tolerance test (GTT) and insulin tolerance test (ITT), the animals received 2 g/kg body weight of glucose and 0.75 IU/kg body weight of insulin respectively through an intraperitoneal injection. Blood was collected from the tail at 0, 15, 30, 60, and 120 min

All experiments were performed in accordance with European Community Council directive 86/609/EEC. The experimental protocols

as well as the number of animals, determined based on the expected effect size, were approved by the Institutional Animal Care and Use Committee of the University of Barcelona. The reporting of the animal studies complied with the ARRIVE guidelines [51].

2.3. Liver histology

For histological staining studies, 4-μm sections obtained from formalin-fixed paraffin-embedded samples were stained with hematoxylin and eosin (H&E) to assess liver histology, as well as Sirius Red to assess fibrosis. Oil Red O staining (Sigma-Aldrich) to assess lipid content was performed in frozen 10-μm liver sections. Fifteen images at a magnification of 20x were captured to quantify the red-stained collagen or lipid droplets, with the red-stained area evaluated per total area using Image J.

2.4. Analysis of 1-palmitoyl-2-oleoyl-sn-glycero-3-phosphocholine (16:0/18:1-PC)

Total lipids from liver homogenates were extracted according to Bligh and Dyer [52], evaporated, and redissolved in methanol-water (9:1). Total lipid separation, identification, and quantification were carried out by liquid chromatography/mass spectrometry using a Hitachi LaChrom Elite L-2130 binary pump and a Hitachi autosampler L-2200 (Merck, Darmstadt, Germany) coupled to a Bruker esquire6000 ion-trap mass spectrometer [53]. The effluent was split, entering at 0.2 ml/min into the electrospray interface of the mass spectrometer. The nebulizer was set to 30 ψ, the dry gas to 8 l/min, and the dry temperature to 350ºC. A Supelcosil LC-18 column of 5 μm particle size, measuring 250 × 2.1 mm and with a particle size of 5 μm (Sigma-Aldrich) was used, protected with by a Supelguard LC-18 guard cartridge column measuring 20- × 2.1 -mm guard cartridge column (Sigma-Aldrich). The mobile phase used was a gradient of solvent A [methanol/water/hexane/ammonium hydroxide, 87.5:10.5:1.5:0.5 (vol/vol/vol/vol)], solvent B [methanol/hexane/ammonium hydroxide, 87.5:12:0.5 (vol/vol/vol)], and solvent C [methanol/water, 9:1 (vol/-vol)]. The gradient started at 100% A, decreased linearly to 50% A (50% B) in 17.5 min and to 0% A (100% B) in 12.5 min, before being maintained at 100% B for 5 min, changed to 100% C in 3 min, maintained at 100% C for 9 min, and then changed to 100% B in 3 min. The flow rate was 0.5 ml/min and the injection volume was 80 μl. Data acquisition was carried out in the full scan and positive mode, detecting PC species as $[M^+H]^+$ ions with the capillary current set at — 4000 V. The PC (16:0/18:1) species were characterized by tandem mass spectrometry in the multiple reaction monitoring and negative mode, with a postcolumn addition of acetic acid for [M + CH3CO2]-adduct formation (100 μl/h). 1,2-Dinonadecanoyl-sn-glycero-3-phosphocoline (*m/z* = 818.6) was used as the internal standard and in a calibration curve for quantification.

2.5. Cell culture

The rat hepatocyte cell line BRL-3 A (P9–13, RRID:CVCL_0606) was purchased from the European Collection of Authenticated Cell Cultures (ECACC, Salisbury, United Kingdom). Cells were cultured under standard culture conditions (37 °C, 5% CO_2) in Dulbecco's Modified Eagle Medium (DMEM) supplemented with 10% fetal bovine serum (FBS) and 1% penicillin/streptomycin. BRL-3 A cells were incubated in serum-free DMEM in the absence (control cells) or presence of elafibranor (different concentrations), U0126 (different concentrations), GW501516 (10 μM), or GSK0660 (60 μM).

BRL-3A cells were transiently transfected with 100 nM siRNA against S100A4 or the control siRNA in Opti-MEM medium (Thermo Fisher, MA, USA) using Lipofectamine 2000 (Invitrogen, Carlsbad, CA, USA) (13.2 μl per 2.2-ml well) according to the manufacturer's instructions.

Mouse primary hepatocytes were isolated from non-fasting male C57BL/6 mice (10–12 weeks old) by perfusion with collagenase, as described elsewhere [54], and incubated in either the absence (control cells) or presence of drugs (elafibranor or GW501516).

All the cell experiments were repeated at least 4 times and there were 2 replicates in each experiment.

2.6. Transfection of the Asb2 CRISPR/dCas9 activation plasmids in BRL-3A cells

To overexpress *Asb2* in the BRL-3A cells, the CRISPR/dCas9 activation system was used. The *Asb2* CRISPR/dCas9 activation plasmid (sc-425766-ACT; Santa Cruz Biotechnology) consisted of a pool of three plasmids designed to overexpress the *Asb2* gene. The control CRISPR/dCas9 activation plasmid (sc-437275; Santa Cruz Biotechnology) was used as a negative control. Plasmid transfection medium and Lipofectamine 2000 were used according to the manufacturer's protocol. Briefly, cells (1×10^5 cells per well) were seeded in 6-well culture plates of 1.5 ml antibiotic-free DMEM 24 h before transfection and grown to 50–60% confluence. Cells were transfected with 1.5 μg of the *Asb2* CRISPR/dCas9 activation system (Santa Cruz Biotechnology), using Lipofectamine 2000 in Opti-MEM medium (Santa Cruz Biotechnology) and incubated at 37ºC with 5% CO_2. Three days after transfection, the cells were used for evaluation.

2.7. Reverse transcription-polymerase chain reaction and quantitative polymerase chain reaction

Isolated RNA was reverse transcribed to obtain 1 μg of complementary DNA (cDNA) using Random Hexamers (Thermo Scientific), 10 mM deoxynucleotide (dNTP) mix and the reverse transcriptase enzyme derived from the Moloney murine leukemia virus (MMLV, Thermo Fisher). The experiment was run in a thermocycler (BioRad) and consisted of a program with different steps and temperatures: 65 °C for 5 min, 4 °C for 5 min, 37 °C for 2 min, 25 °C for 10 min, 37 °C for 50 min, and 70 °C for 15 min. The relative levels of specific mRNAs were assessed by real-time RT-PCR in a Mini 48-Well T100™ thermal cycler (Bio-Rad), using the SYBR Green Master Mix (Applied Biosystems), as previously described [55]. Briefly, samples had a final volume of 20 μl, with 20 ng of total cDNA, 0.9 μM of the primer mix, and 10 μl of 2x SYBR Green Master Mix. The thermal cycler protocol for real-time PCR included a first step of denaturation at 95 °C for 10 min followed by 40 repeated cycles of 95 °C for 15 s, 60 °C for 30 s, and 72 °C for 30 s for denaturation, primer annealing, and amplification respectively. Primer sequences were designed using the Primer-BLAST tool (NCBI), based on the full mRNA sequences to find the optimal primers for amplification, and evaluated with the Oligo-Analyzer Tool (Integrated DNA Technologies) to ensure an optimal melting temperature (Tm) and avoid the formation of homo/heterodimers or non-specific structures that can interfere with the interpretation of the results. The primer sequences were designed specifically to span the junction between the exons. The primer sequences used are provided in Supplementary Table 1. Values were normalized to the glyceraldehyde 3-phosphate dehydrogenase (*Gapdh*) or adenine phosphoribosyltransferase (*Aprt*) expression levels, and measurements were performed in triplicate. All changes in expression were normalized to the untreated control.

2.8. Immunoblotting

The isolation of total protein extracts was performed as described elsewhere [25]. Immunoblotting was performed with antibodies against β-actin (Sigma, A5441), E-cadherin (Santa Cruz, sc-8426), COL1A1 (Cell Signaling, 91144 S), phosphorylated (p)44/42 MAPK (Erk1/2) (Cell Signaling, 9194 s), phosphorylated (p) p44/42 MAPK (Erk1/2) Thr202/Tyr204 (Cell Signaling, 9101 s), filamin A (Santa Cruz, sc-376241), GAPDH (G-9) (Santa Cruz, sc-365062), α-SMA (Invitrogen, 14–9760–82), S100A4/FSP1 (EMD Millipore, o7–2274), α-tubulin

(Sigma, T6074), and vimentin (Santa Cruz, sc-6260). The serum raised against a peptide common to the ASB2α and ASB2β isoforms was provided by C. Moog-Lutz (IPBS, Toulouse, France) [32]. Signal acquisition was conducted using the Bio-Rad ChemiDoc apparatus and quantification of the immunoblot signal was performed with the Bio-Rad Image Lab software. The results for protein quantification were normalized to the levels of a control protein (GAPDH, α-tubulin or β-actin) to avoid unwanted sources of variation.

2.9. Statistical analysis

Results are expressed as the mean ± SEM. Significant differences were assessed by either Student's t-test or one-way and two-way ANOVA, according to the number of groups compared, using the GraphPad Prism program (version 9.0.2) (GraphPad Software Inc., San Diego, CA, USA). When significant variations were found by ANOVA, Tukey's post-hoc test for multiple comparisons was performed only if F achieved a p value < 0.05. Differences were considered significant at $p < 0.05$.

3. Results

3.1. The dual PPARα and β/δ agonist elafibranor improves MASLD, but upregulates hepatic S100A4 levels in mice fed a CD-HFD

First, we evaluated the effects of elafibranor on body weight and glucose metabolism. Elafibranor treatment did not reduce the body weight gain caused by the CD-HFD, but it did improve the glucose intolerance and peripheral insulin resistance caused by the CD-HFD (Fig. 1A-C). Although PPARβ/δ activation has been reported to increase hepatic levels of the PPARα endogenous ligand 1-palmitoyl-2-oleoyl-sn-glycero-3-phosphocholine (16:0/18:1-PC) [22], it is unknown whether elafibranor affects the amount of this ligand that may potentiate the beneficial actions of the drug via PPARα. We found that the CD-HFD did not affect hepatic levels of 16:0/18:1-PC (Fig. 1D). However, elafibranor markedly increased the levels of this PPARα ligand in the liver. This effect of elafibranor has been reported previously for the PPARβ/δ activator GW501516 [23]. Therefore, the fact that 16:0/18:1-PC levels were reduced in the livers of *Ppard*$^{-/-}$ mice compared with wild-type (WT) mice (Fig. 1E) suggests that the effect of elafibranor on 16:0/18:1-PC levels is mediated by PPARβ/δ. These findings indicate that elafibranor, besides its direct effect on PPARα, may also indirectly activate this nuclear receptor by increasing the amount of 16:0/18:1-PC. Since fibroblast growth factor 21 (FGF21) is a target in the treatment of MASH and given that PPARα activation increases its levels [24], we determined the hepatic mRNA levels of FGF21. The CD-HFD did no present a significant increase in *Fgf21* mRNA levels, whereas treatment with elafibranor significantly raised *Fgf21* expression (Fig. 1F).

Hematoxylin-eosin and Oil Red O (ORO) staining showed that the CD-HFD caused significant hepatic lipid accumulation, which was reduced by elafibranor (Fig. 2A-B). The CD-HFD led to a non-significant increase in the accumulation of collagen in the liver, as demonstrated by the Sirius Red staining, suggesting that a longer exposure to the CD-HFD is required to induce clear fibrosis. Notably, elafibranor decreased collagen accumulation (Fig. 2C). Consistent with findings of the Sirius Red staining, the CD-HFD did not significantly increase the protein levels of the fibrosis markers α-smooth muscle actin (α-SMA) and collagen type I α1 (COL1A1), but treatment with elafibranor caused a significant reduction of their levels (Fig. 2D-E).

When we examined the effects of elafibranor on *S100A4* expression, we observed that the CD-HFD in mice treated with vehicle and in those administered elafibranor did not significantly affect the mRNA levels of this gene (Fig. 3A). The S100A4 protein can be detected either as a monomer or a dimer, the latter being S-glutathionylated, with apparent molecular weights of 11.5 kDa and approximately 21–29 kDa respectively [25,26]. No changes were observed in the hepatic protein levels of S100A4 in mice fed the CD-HFD. By contrast, mice fed the CD-HFD and treated with elafibranor displayed a robust increase in the protein with a molecular weight of ~ 23 kDa (Fig. 3B). The effect of elafibranor on S100A4 was probably the result of PPARβ/δ activation, since the mice treated with the selective agonist for this receptor, GW501516, also showed increased hepatic protein levels of S100A4 (Fig. 3C). Moreover, the band corresponding to S100A4 was reduced in the livers of *Ppard*$^{-/-}$ mice compared to their wild-type littermates, indicating that S100A4 is regulated by PPARβ/δ (Fig. 3D). Since an increase in the mesenchymal marker S100A4 might indicate that elafibranor activates the EMT program, we analyzed other markers of this program such as the epithelial marker E-cadherin and the mesenchymal marker vimentin. In agreement with the increase in S100A4 levels and the subsequent induction of the EMT program, elafibranor reduced the protein levels of E-cadherin and increased those of vimentin (Fig. 3E, F). These findings suggest that PPARβ/δ activation by elafibranor increases the hepatic protein levels of S100A4 and activates the EMT program in the liver.

3.2. Elafibranor increases S100A4 protein levels in BRL-3A rat liver cells and in a mouse primary hepatocyte culture

Treatment of the rat liver cell line BRL-3A with either GW501516 (a selective agonist of PPARβ/δ at concentrations of up to 10 μM [27]), or elafibranor (at a concentration of 30 or 60 μM) did not increase S100A4 mRNA levels compared to control cells (Fig. 4A). By contrast, elafibranor at both concentrations increased S100A4 protein levels, whereas GW501516 had no effect (Fig. 4B). The S100A4 protein upregulated by elafibranor in the rat BRL-3A cells showed a higher molecular weight than that detected in mice, suggesting interspecies differences in the S-glutathionylation of this protein [28]. S100A4 knockdown by siRNA transfection in the BRL-3A cells caused a reduction in the protein levels of S100A4, confirming that the protein band detected was S100A4 (Supplementary Figure 1 A). Elafibranor at 60 μM reduced E-cadherin protein levels (Fig. 4C) and increased vimentin protein levels (Fig. 4D), while GW501516 only increased vimentin levels without affecting E-cadherin levels (Fig. 4C, D). The increase in S100A4 protein levels caused by elafibranor was prevented by the PPARβ/δ antagonist GSK0660 (Fig. 4E), confirming the involvement of PPARβ/δ in the changes caused by its activation. The effects of elafibranor were confirmed in a mouse primary culture of hepatocytes, where elafibranor increased S100A4 protein levels (Fig. 4F). In these primary hepatocytes, GW501516 increased S100A4 protein levels, in contrast to the observations in the BRL-3A cells, suggesting that the primary hepatocytes respond better than the rat BRL-3A cells (Fig. 4G). Overall, these findings indicate that elafibranor increases the protein levels of S100A4 in hepatocytes via PPARβ/δ.

3.3. Elafibranor increases S100A4 by reducing the protein levels of the E3 ubiquitin ligase ASB2

Next, we examined whether, as suggested by the results above, there was a potential post-transcriptional mechanism by which elafibranor increased S100A4 protein levels. Since reactive oxygen species (ROS) modify S100A4 activity and dimerization [20], we explored the involvement of ROS in the effects of elafibranor. Under our conditions, the incubation of BRL-3A cells with H_2O_2 or the co-incubation of elafibranor-exposed cells with the antioxidant N-acetylcysteine did not affect S100A4 protein levels, indicating that ROS were not involved (Supplementary Figure 1B).

Interestingly, it has been reported that the inhibition of the activities of extracellular signal- regulated kinases 1 and 2 (ERK1/2) reduces the activity of several E3 ubiquitin ligases [29]. Since we have previously reported that PPARβ/δ activation inhibits ERK1/2 activity [30], we evaluated whether the inhibition of this kinase mediated the effects of

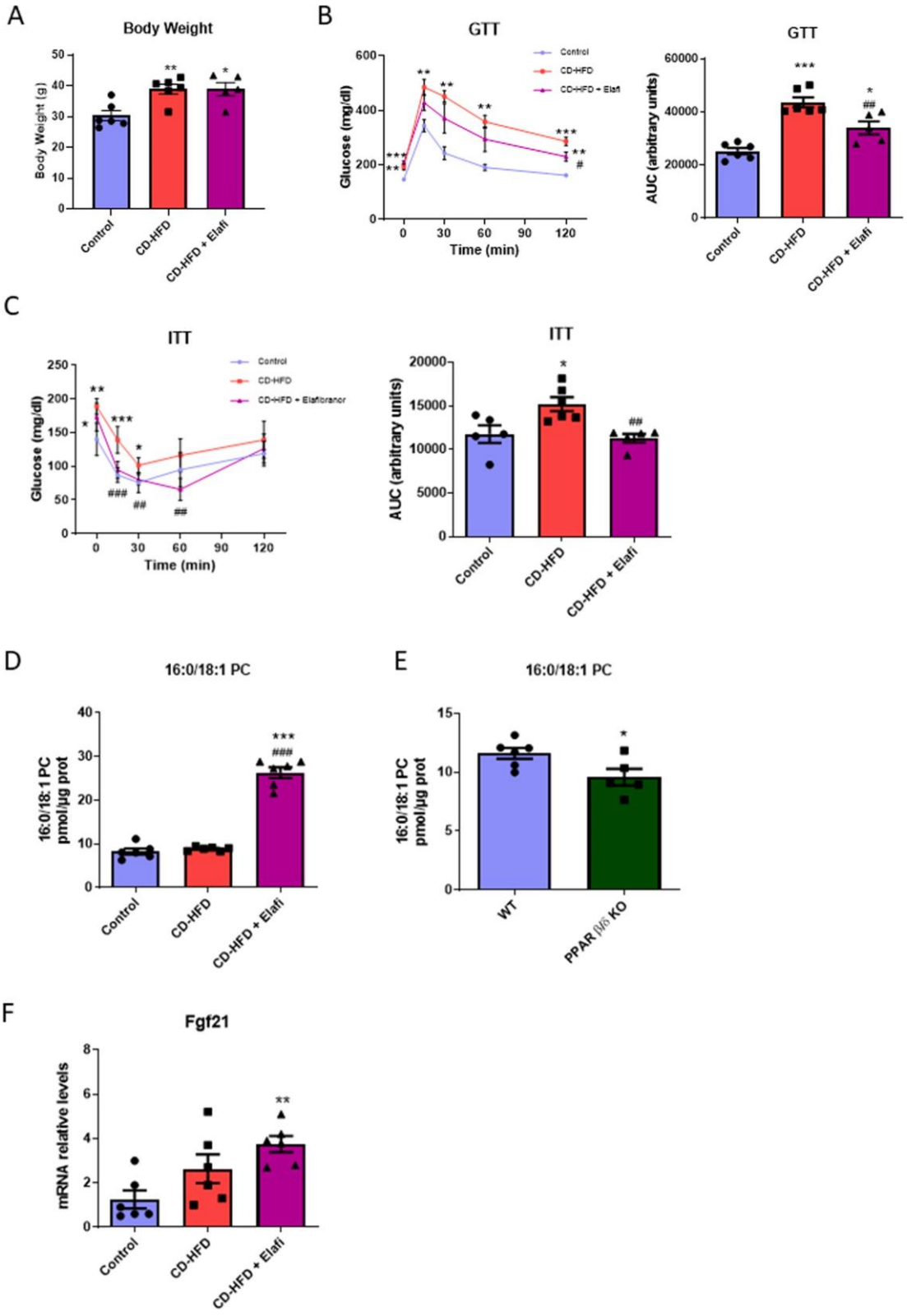

Fig. 1. Elafibranor improves insulin sensitivity in mice fed a CD-HFD. (**A**) Final body weight in mice (n = 6 animals) fed a standard diet (control) or a choline-deficient high-fat diet (CD-HFD) for 12 weeks and treated with vehicle or 10 mg/kg/day of elafibranor during the last 4 weeks. (**B**) Glucose tolerance test (GTT) and area under the curve (AUC) (n = 6 animals). (**C**) Insulin tolerance test (ITT) and AUC (n = 6 animals). (**D**) Hepatic levels of the PPARα endogenous ligand 1-palmitoyl-2-oleoyl-sn-glycero-3-phosphocholine (16:0/18:1-PC). (**E**) 16:0/18:1-PC hepatic levels in wild-type (WT) and *Ppard*$^{-/-}$ mice (n = 5 animals). (**F**) *Fgf21* mRNA levels in mice (n = 6 animals) fed a standard diet (control) or a CD-HFD and treated with vehicle or 10 mg/kg/day of elafibranor during the last 4 weeks. Data are presented as the mean ± SEM. *$p < 0.05$, * *$p < 0.01$, and * **$p < 0.001$ versus control or WT. $^{\#\#}p < 0.01$ and $^{\#\#\#}p < 0.001$ versus CD-HFD-fed mice. p-values determined by one-way ANOVA with Tukey's post hoc test (A, B, C, D, and F) or two-tailed unpaired Student's t-test (E).

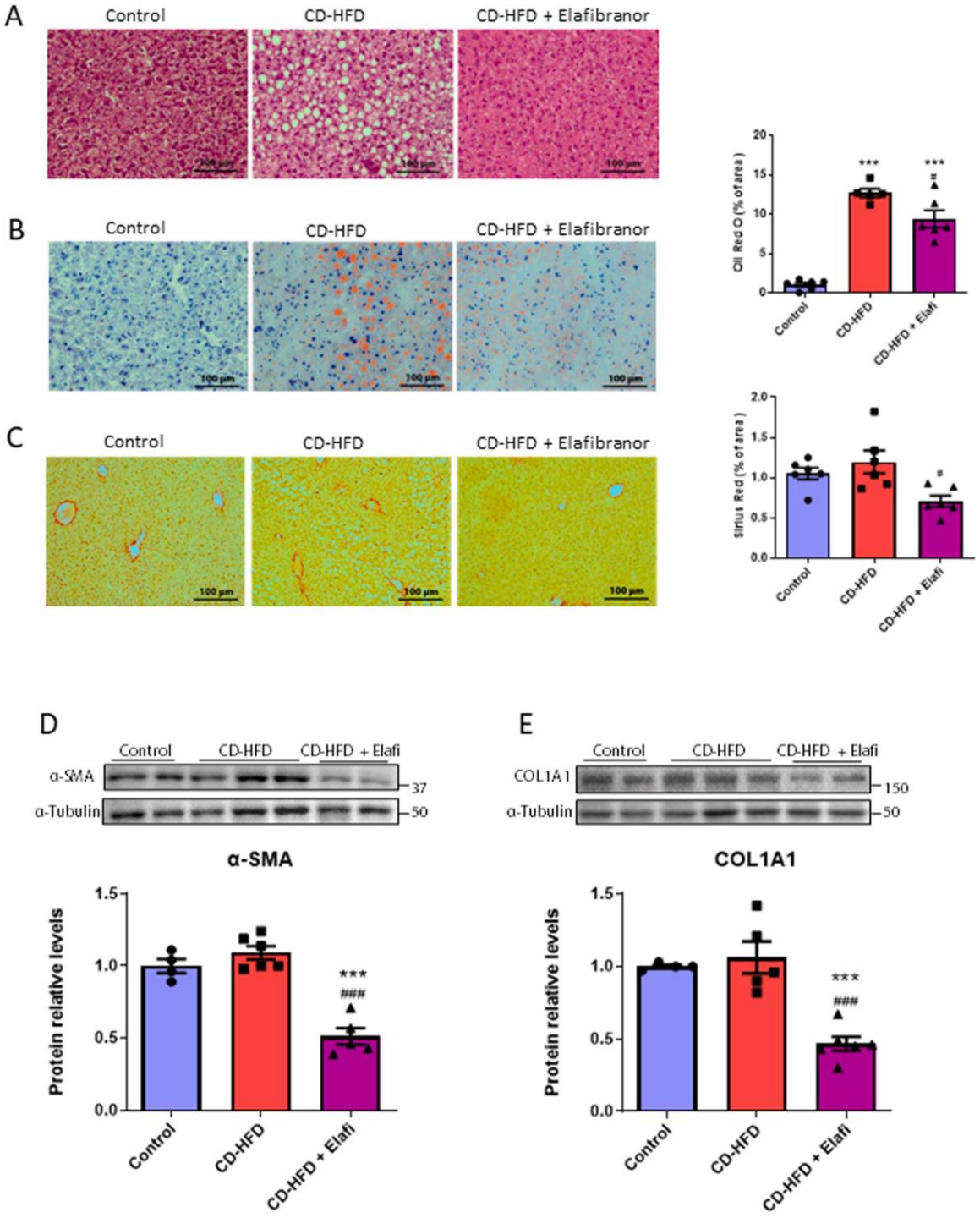

Fig. 2. Elafibranor decreases markers of fibrosis in mice fed a CD-HFD. (**A**) Hematoxylin–eosin (H&E), (**B**) Oil Red O (ORO) and (**C**) Sirius Red staining of liver sections and quantification of ORO and Sirius Red staining of samples from mice (n = 6 animals) fed a standard diet (control) or a choline-deficient high-fat diet (CD-HFD) for 12 weeks and treated with vehicle or 10 mg/kg/day of elafibranor during the last 4 weeks. Scale bar: 100 µm. Liver cell lysate extracts were assayed via western blot analysis with antibodies against α-SMA (**D**) and COL1A1 (**E**) (n = 6 animals). Data are presented as the mean ± SEM. *p < 0.05 versus control. #p < 0.05, ##p < 0.01, and ###p < 0.001 versus CD-HFD-fed mice. p-values determined by one-way ANOVA with Tukey's post hoc test.

elafibranor on S100A4. Consistent with the previous findings reported for PPARβ/δ activation [30,31], elafibranor reduced phosphorylated ERK1/2 levels in the livers of mice fed the CD-HFD (Fig. 5A). However, the ERK1/2 inhibitor U0126, which reduced phosphorylated ERK1/2 levels even more than elafibranor (Fig. 5B), did not increase the protein levels of S100A4 in the BRL-3A cells (Fig. 5C), thereby indicating that ERK1/2 inhibition was not the mechanism responsible for the elafibranor-induced increase in S100A4 levels.

ASB2β is the specificity subunit of a multimeric E3 ubiquitin ligase [32] that has been reported to induce the degradation of S100A4 [31]. We therefore speculated that the increased S100A4 protein levels induced by elafibranor were due to a reduced expression of ASB2β. In the protein lysates of both mouse livers and BRL-3A cells, a 70-kDa band corresponding to ASB2β was detected with an antibody raised against a peptide common to both the ASB2α and ASB2β isoforms (Fig. 6A, B). The amount of this protein was reduced in the livers of the CD-HFD-fed mice

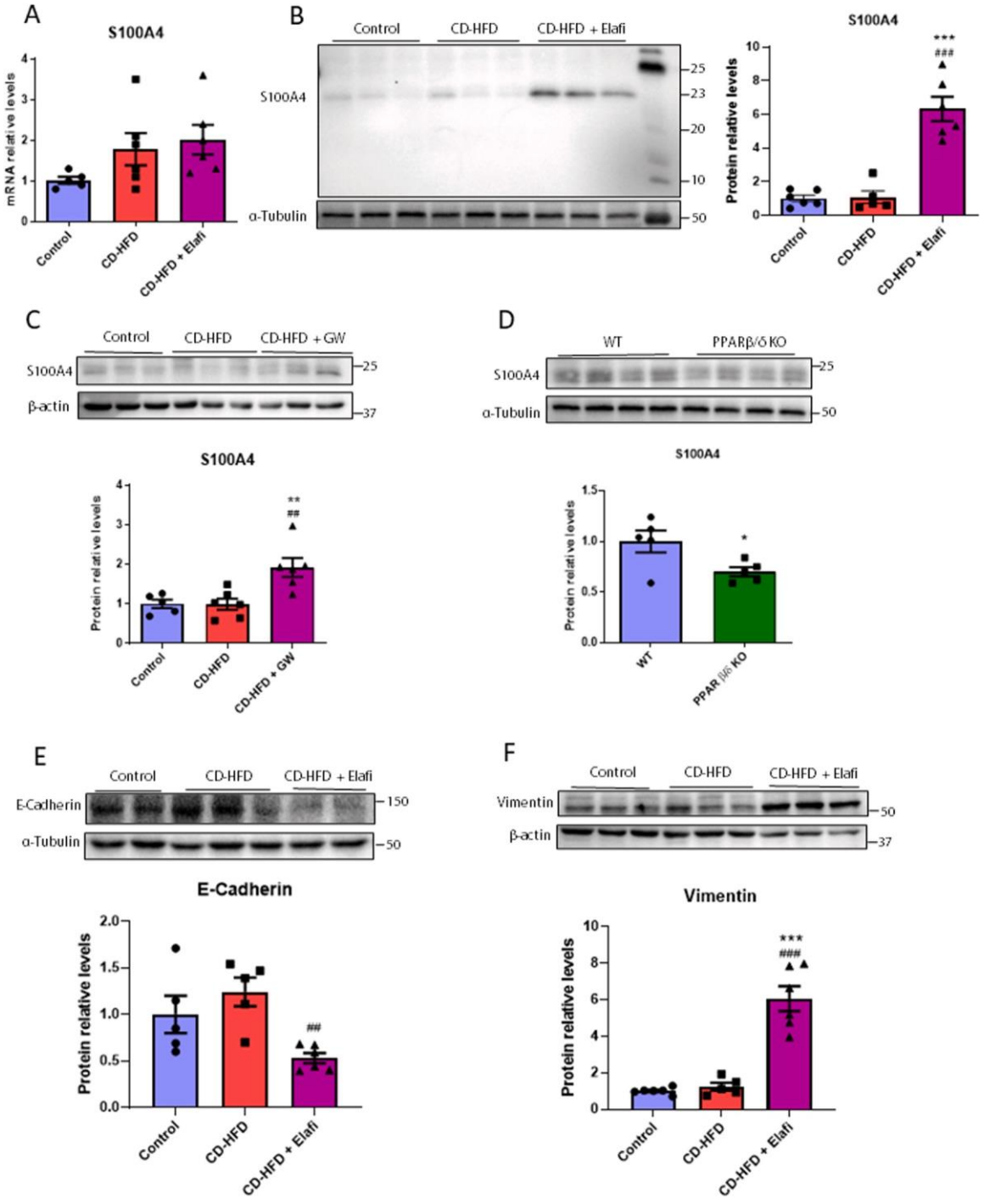

Fig. 3. Elafibranor upregulates S100A4 protein levels in the liver. (**A**) mRNA levels of *S100A4* in the livers of mice (n = 6 animals) fed a standard diet (control) or a choline-deficient high-fat diet (CD-HFD) for 12 weeks and treated with vehicle or 10 mg/kg/day of elafibranor during the last 4 weeks. (**B**) Liver cell lysate extracts were assayed via western blot analysis with antibodies against S100A4 (n = 6 animals). (**C**) S100A4 protein levels in the livers of mice (n = 6 animals) fed a standard diet (control) or a CD-HFD for 12 weeks and treated with vehicle or 5 mg/kg/day of GW501516 during the last 4 weeks. (**D**) S100A4 protein levels in the livers of WT and *Ppard*$^{-/-}$ mice (n = 5 animals). E-cadherin (**E**) and vimentin (**F**) protein levels in the livers of mice (n = 6 animals) fed a standard diet (control) or a CD-HFD for 12 weeks and treated with vehicle or 10 mg/kg/day of elafibranor during the last 4 weeks. Data are presented as the mean ± SEM. *$p < 0.05$ and * **$p < 0.001$ versus control. $^{\#\#}p < 0.01$ and $^{\#\#\#}p < 0.001$ versus CD-HFDfed mice. p-values determined by one-way ANOVA with Tukey's post-hoc test.

treated with elafibranor (Fig. 6A). Likewise, elafibranor reduced the amount of this protein in the BRL-3A cells (Fig. 6B), and a similar behavior was observed in the mouse primary hepatocyte culture (Fig. 6C). Since ASB2α but not ASB2β induces the proteasomal degradation of filamin A [32,33], we examined the levels of filamin A in the BRL-3A cells. We observed that elafibranor did not affect filamin A levels (Fig. 6D), suggesting that this isoform of ASB2 was not affected by elafibranor, but rather the ASB2β isoform. These findings suggested that elafibranor increases S100A4 protein levels by reducing its ASB2β-mediated degradation. To confirm this, we used CRISPR/dCas9 activation plasmids designed to specifically upregulate the *Asb2* gene. Overexpression of *Asb2* (Supplementary Figure 1C-D) in the BRL-3A cells treated with vehicle reduced the basal protein levels of S100A4, confirming that this E3 ubiquitin ligase degrades S100A4 (Fig. 6E).

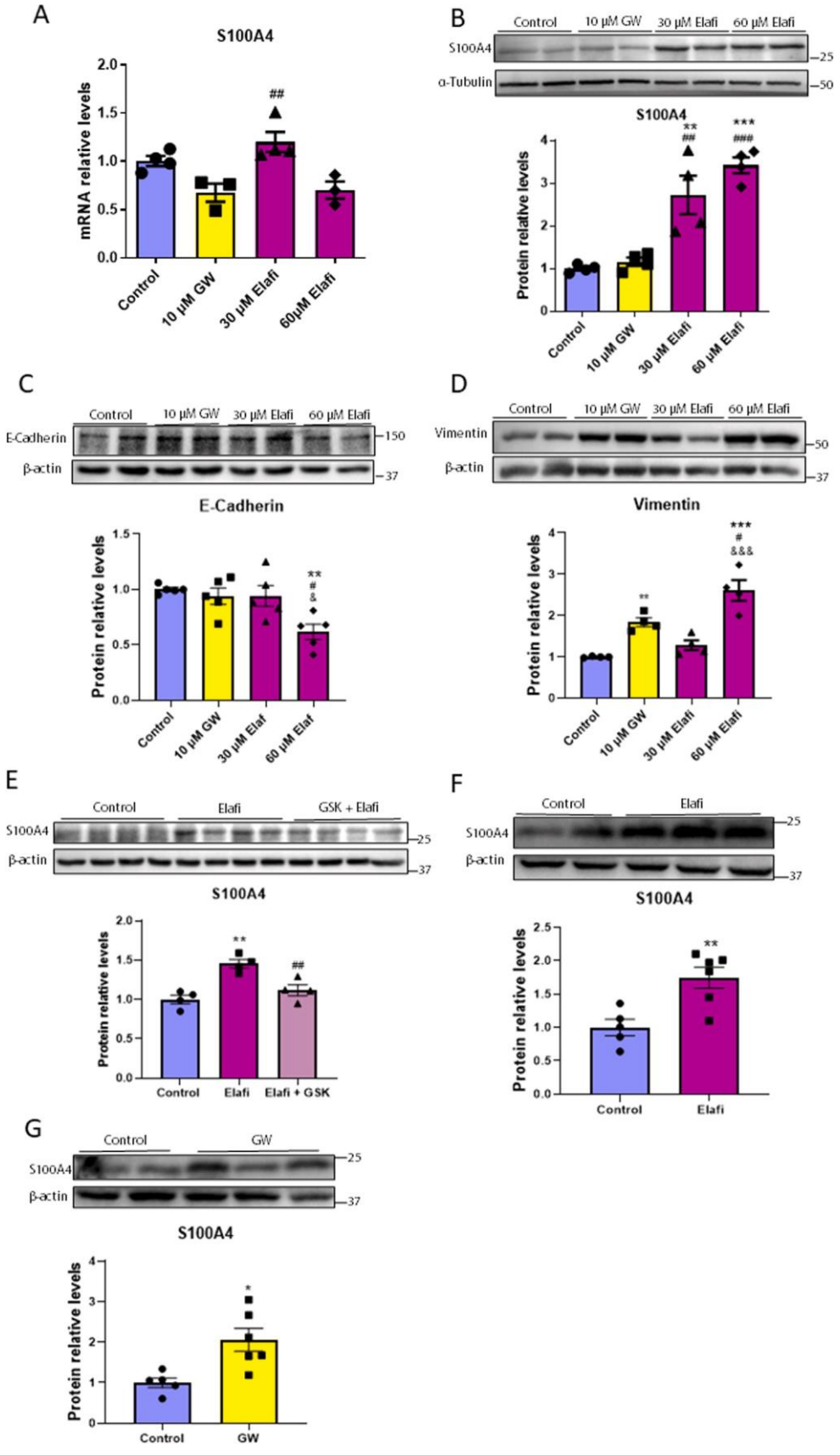

(caption on next page)

Fig. 4. Elafibranor increases S100A4 protein levels in hepatocytes. *S100A4* mRNA levels (**A**) and S100A4 protein levels (**B**) in the rat liver cell line BRL-3A exposed to 10 μM GW501516 or elafibranor (30 or 60 μM) for 24 h. E-cadherin (**C**) and vimentin (**D**) protein levels in the BRL-3A cells exposed to elafibranor (30 or 60 μM) for 24 h. S100A4 protein levels (**E**) in the BRL-3A cells exposed to 30 μM elafibranor in the presence or absence of 60 μM of the PPARβ/δ antagonist GSK0660 for 24 h. S100A4 protein levels in the mouse primary culture of hepatocytes exposed to 30 μM elafibranor (**F**) or 10 μM GW501516 (**G**) for 24 h. Data are presented as the mean ± SEM. * *p < 0.01 and * **p < 0.001 versus control. $^{\#}$p < 0.05, $^{\#\#}$p < 0.01· and $^{\#\#\#}$p < 0.001 versus GW501516-treated cells. $^{\&\&\&}$p < 0.001 versus elafibranor-treated cells p-values determined by one-way ANOVA with Tukey's post- hoc test (A-E) or two-tailed unpaired Student's t-test (F, G).

Interestingly, the increase in S100A4 levels caused by elafibranor was prevented by *Asb2* overexpression, indicating that ASB2 is involved in the effects of elafibranor on S100A4 levels. Altogether, these results suggest that elafibranor reduces the ASB2β-mediated degradation of S100A4.

4. Discussion

The development of new drugs for the treatment of MASH is challenging since findings from animal models have not been fully reproduced in clinical trials. This has also been the case of elafibranor, a drug which presented promising findings in preclinical studies, but which was discontinued in 2020 as it failed to show a statistically significant effect in patients with MASH during the phase III RESOLVE-IT clinical trial. Several factors can explain why promising preclinical drugs have failed in humans. For example, many of these compounds often target a few of the many pathways involved in the development of MASH. This limited action may result in a modest effect, or it might be attenuated by the activation of compensatory mechanisms. Therefore, no single agent is likely to control all the aspects of this complex liver disease. After the negative outcome for elafibranor in monotherapy, the efficacy of elafibranor will be evaluated in combination with other drugs for the treatment of MASH [10]. Moreover, the efficacy of this drug is also currently being examined in primary biliary cholangitis [34].

In agreement with previous studies reporting the beneficial effects of elafibranor on glucose metabolism [7], we show here that the administration of this drug to mice fed a CD-HFD, improves glucose intolerance and insulin resistance, which are among the main drivers of MASH. These changes were observed without a reduction in body weight. In addition, consistent with the findings of previous studies [35], elafibranor reduced the levels of markers of fibrosis such as α-SMA and COL1A1. Surprisingly, we observed that elafibranor increased the protein levels of S100A4, but barely affected its mRNA levels. This points to the involvement of a post-transcriptional mechanism that affects protein levels without interfering with mRNA levels. This is an unexpected finding, since S100A4 upregulation was reported to induce EMT [36], which in turn promotes fibrosis. Consistent with the role of S100A4 in liver fibrosis, S100A4-knockout mice show an attenuation in hepatic fibrosis induced by different stimuli [17,37]. S100A4 regulates the tissue fibrosis associated with type II EMT via various signaling pathways [38]. In fact, S100A4 is commonly used as a marker to identify epithelial cells undergoing EMT during tissue fibrogenesis [39], and is used as proof of EMT in hepatocytes and cholangiocytes [40–42]. In line with its induction of EMT, elafibranor upregulated the mesenchymal marker vimentin and downregulated the epithelial marker E-cadherin in the mouse liver. Moreover, the increase in S100A4 protein levels caused by elafibranor was mediated by PPARβ/δ, since an antagonist of this receptor attenuated the increase in S100A4 protein levels, while the amount of this protein was reduced in the livers of *Ppard*-null mice compared to their WT littermates. The induction of EMT in the liver by elafibranor via PPARβ/δ is in accordance with the regulation of EMT by PPARβ/δ in the human colorectal carcinoma cell line HCT116 [43]. *Ppard* knockdown in these cells upregulates E-cadherin and downregulates vimentin. Likewise, a PPARβ/δ antagonist was previously reported to block the EMT-promoting effect of stromal cell-derived factor-1 on lung cancer cells [44], while increases in EMT markers have been reported in keratinocytes by the PPARβ/δ-Src pathway [45].

The effects of PPARβ/δ on liver fibrosis are controversial. While it has been demonstrated that *Ppard*$^{-/-}$ mice show exacerbated hepatotoxicity when treated with CCl_4 [46], and that PPARβ/δ agonists attenuate hepatic fibrosis in MASLD [12], other studies have reported that these compounds enhance the proliferation of hepatic stellate cells and promote liver fibrosis [47,48]. These differences indicate that PPARβ/δ agonists may activate anti- and pro-fibrotic pathways and, depending on the model used to promote fibrosis or other factors yet to be determined, the effects of these compounds may result in either the improvement or the promotion of liver fibrosis. Given the relationship between increased S100A4 protein levels and the development of fibrosis, the increase in S100A4 protein levels and the induction of EMT might be among the factors contributing to fibrosis in mice treated with PPARβ/δ agonists. Further studies are needed to explore this possibility and to determine whether the induction of S100A4 and EMT contributes to liver fibrosis and outweighs the beneficial effects of PPARβ/δ agonists in this condition.

The present study also indicates a potential mechanism by which elafibranor increases the protein levels of S100A4. This protein is a target of ASB2, which mediates its proteasomal degradation [31]. We observed that elafibranor reduced the protein levels of ASB2 in vivo and in vitro, thereby providing an explanation for the increase in S100A4 protein levels following elafibranor treatment. In fact, *Asb2* overexpression prevented the elafibranor-mediated increase in S100A4 protein levels. Therefore, we propose that elafibranor increases S100A4 protein levels by reducing the amount of ASB2, thereby attenuating its proteasomal degradation.

S100A4 also promotes cancer progression and metastasis [17]. Although the anti-inflammatory effects of PPARβ/δ can attenuate cancer development, PPARβ/δ activation after the development of cancer can stimulate angiogenesis and tumor growth [49]. Moreover, PPARβ/δ modulation in cancer cells profoundly influences metastasis development in commonly used preclinical models in vivo [43]. It remains to be determined to what extent S100A4 upregulation by PPARβ/δ impacts cancer progression and metastasis.

Collectively, the findings of this study highlight a regulatory mechanism by which elafibranor increases the hepatic protein levels of S100A4. Further studies are needed to evaluate the consequences of the drug's induction of S100A4 and EMT, particularly in the context of MASH and cancer.

Funding

This study was partly supported by the grants RTI2018-093999-B-I00 and PID2021-122116OB-I00 (M.V-C.), PID2021-122766OB-I00 (A. M.V.), and PID2019-105989RB-I00 (J.B.) from MCIN/AEI/10.13039/501100011033 and "ERDF, A Way of Making Europe". CIBER de Diabetes y Enfermedades Metabo´licas Asociadas (CIBERDEM) is a Carlos III Health Institute project. Support was also received from the CERCA Programme/Generalitat de Catalunya. Meijian Zhang was supported by a grant from the China Scholarship Council (CSC) (202007565030).

CRediT authorship contribution statement

MZ, **EB**, **MR**, **LP**, **MP**, **DAR**, **PR**, **CC**, **JJA**, **CM**, **MZ**, and **MVC** performed the experiments; **AC**, **JB**, **AMV**, **WW**, **XP**, and **MVC** analyzed the data and reviewed the results; and **MZ**, **EB**, **MR**, **LP**, and **MVC** designed the experiments and reviewed the results. **MVC** is the guarantor of this work and, as such, has full access to all the data in the study and takes

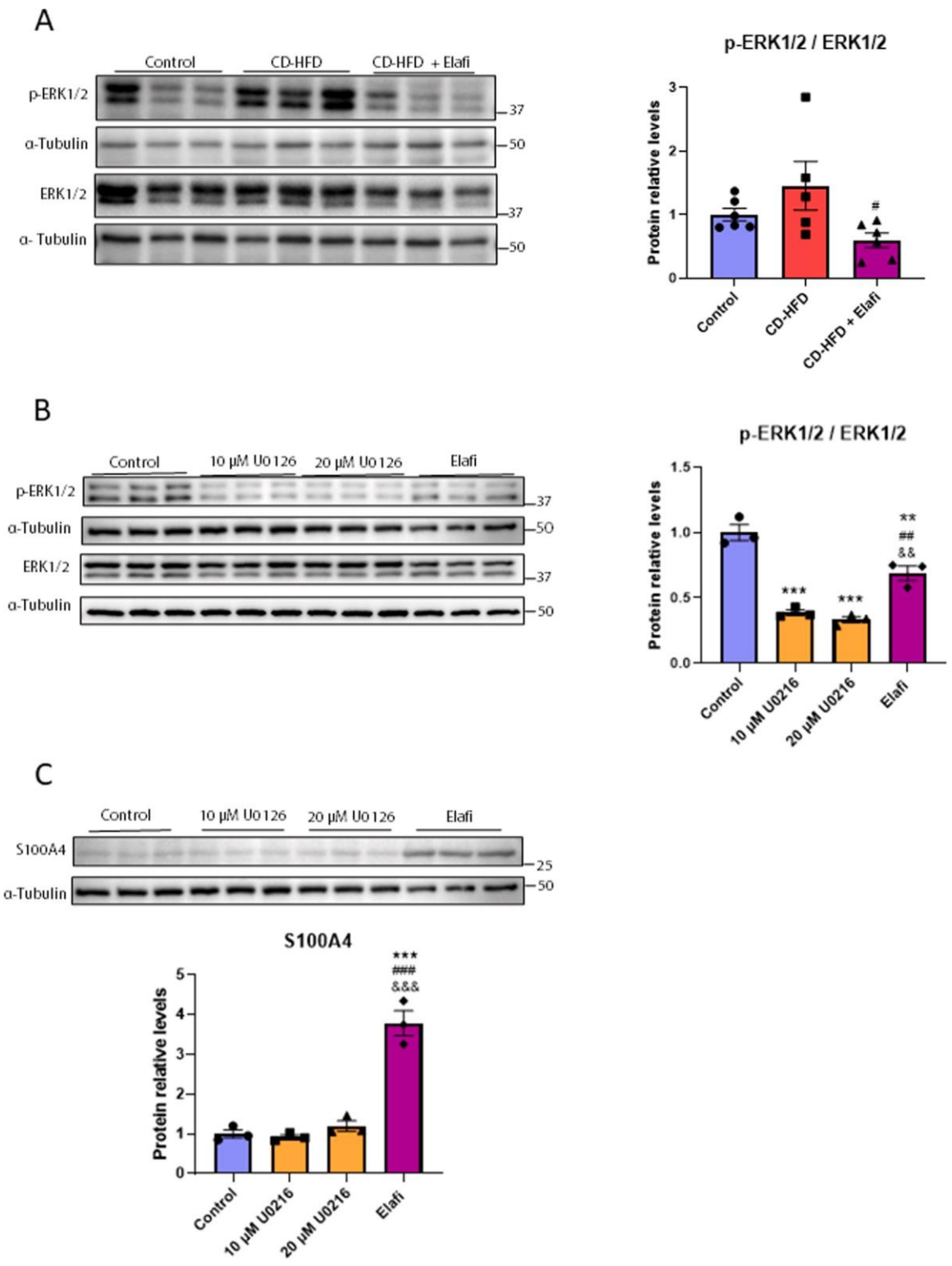

Fig. 5. ERK1/2 inhibition is not likely to be involved in the increase in S100A4 protein levels caused by elafibranor. (**A**) Total and phosphorylated ERK1/2 levels in the livers of mice (n = 6 animals) fed a standard diet (control) or a choline-deficient high-fat diet (CD-HFD) for 12 weeks and treated with vehicle or 10 mg/kg/day of elafibranor during the last 4 weeks. Total and phosphorylated ERK1/2 levels (**B**) and S100A4 protein levels (**C**) in the BRL-3A cells exposed to 60 μM elafibranor or the ERK1/2 inhibitor U0126 (10 or 20 μM). Data are presented as the mean ± SEM. *$p < 0.05$, * *$p < 0.01$, and * **$p < 0.001$ versus control cells. $^{\#}p < 0.05$, $^{\#\#}p < 0.01$, and $^{\#\#\#}p < 0.001$ versus CD-HFD or control cells. $^{\&\&}p < 0.01$ and $^{\&\&\&}p < 0.001$ versus U0126-treated cells. p-values determined by one-way ANOVA with Tukey's post-hoc test.

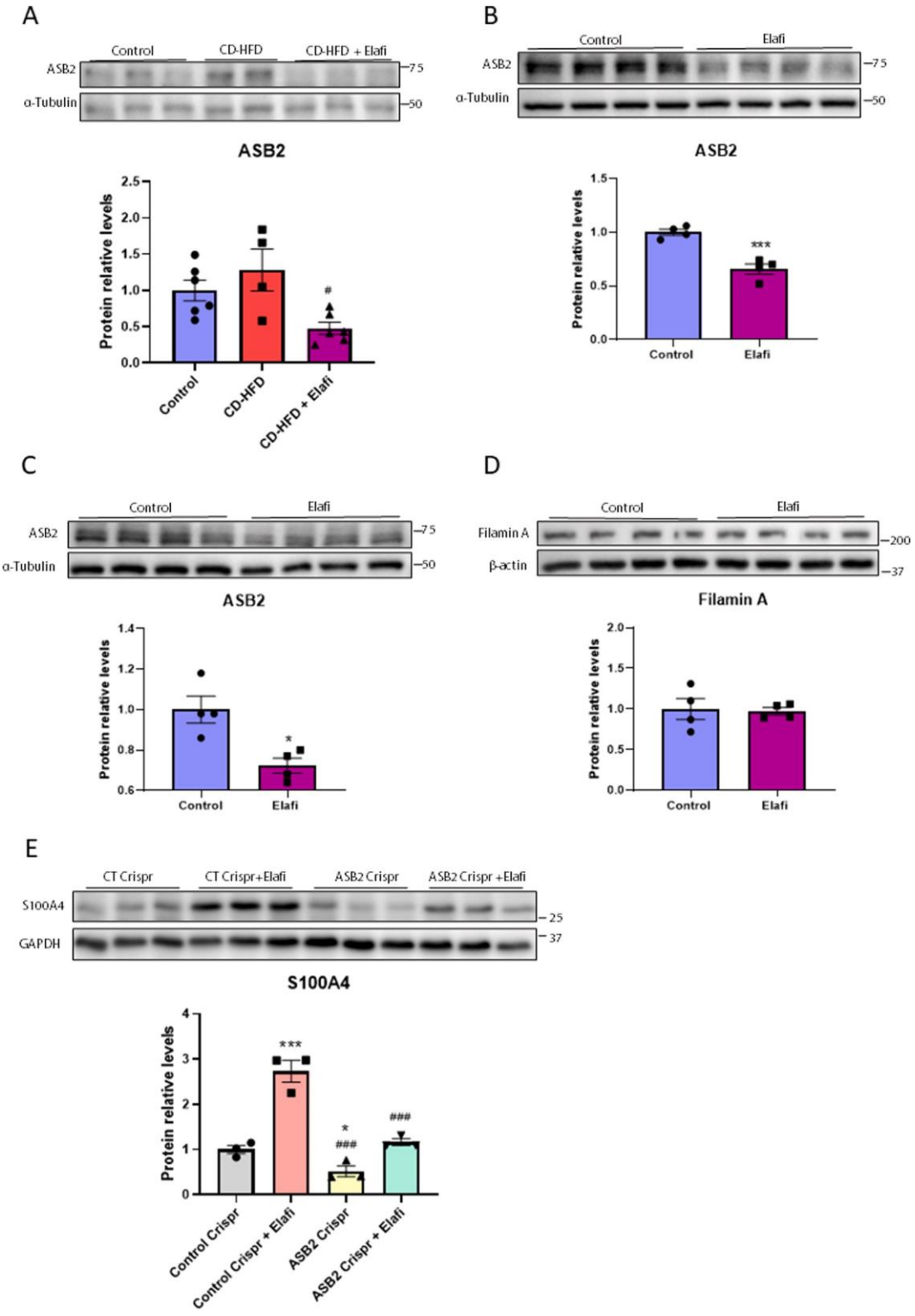

Fig. 6. ASB2 overexpression prevents the upregulation of S100A4 by elafibranor. (**A**) ASB2 protein levels in the livers of mice (n = 6 animals) fed a standard diet (control) or a choline-deficient high-fat diet (CD-HFD) for 12 weeks and treated with vehicle or 10 mg/kg/day of elafibranor during the last 4 weeks. ASB2 protein levels in the BRL-3A cells exposed to 60 μM elafibranor for 24 h (**B**) or in the mouse primary culture of hepatocytes exposed to 30 μM elafibranor for 24 h (**C**). Filamin A protein levels (**D**) in the BRL-3A cells exposed to 60 μM elafibranor for 24 h. S100A4 protein levels (**E**) in the BRL-3A cells transfected with the ASB2 CRISPR/dCas9 activation plasmids or control CRISPR/dCas9 activation plasmids and treated with either vehicle or 60 μM elafibranor for 24 h. Data are presented as the mean ± SEM. *$p < 0.05$ and * **$p < 0.001$ versus control. $^{\#}p < 0.05$ and $^{\#\#}p < 0.01$ versus CD-HFD-fed mice or CT CRISPR and elafibranor. p-values determined by one-way ANOVA with Tukey's post-hoc test (A, E) or two-tailed unpaired Student's t-test (B, C, D).

responsibility for the integrity of the data and the accuracy of the data analysis.

Declaration of Competing Interest

none'.

Data Availability

Data will be made available on request.

Acknowledgements

We would like to thank the Language Services of the University of Barcelona for revising the manuscript.

Appendix A. Supporting information

Supplementary data associated with this article can be found in the online version at doi:10.1016/j.biopha.2023.115623.

References

[1] M. Zobair, A.B.K. Younossi, Abdelatif Dinan, Fazel Yousef, Henry Linda, Wymer Mark, Global epidemiology of nonalcoholic fatty liver disease-Meta-analytic assessment of prevalence, incidence, and outcomes, Hepatology 64 (2016) 73–84.
[2] M. Machado, P. Marques-Vidal, H. Cortez-Pinto, Hepatic histology in obese patients undergoing bariatric surgery, J. Hepatol. 45 (4) (2006) 600–606.
[3] E. Buzzetti, M. Pinzani, E.A. Tsochatzis, The multiple-hit pathogenesis of non-alcoholic fatty liver disease (NAFLD), Metabolism 65 (8) (2016) 1038–1048.
[4] S.A. Sutti, E. Adaptive immunity: an emerging player in the progression of NAFLD, Nat. Rev. Gastroenterol. Hepatol. (2) (2020) 81–92.
[5] A. Suzuki, A.M. Diehl, Nonalcoholic steatohepatitis, Annu. Rev. Med. 68 (2017) 85–98.
[6] V. Ratziu, S.L. Friedman, Why do so many NASH trials fail? Gastroenterology (2020).
[7] M.J. Westerouen Van Meeteren, J.P.H. Drenth, E. Tjwa, Elafibranor: a potential drug for the treatment of nonalcoholic steatohepatitis (NASH), Expert Opin. Investig. Drugs 29 (2) (2020) 117–123.
[8] P.S. Dulai, S. Singh, J. Patel, M. Soni, L.J. Prokop, Z. Younossi, G. Sebastiani, M. Ekstedt, H. Hagstrom, P. Nasr, P. Stal, V.W. Wong, S. Kechagias, R. Hultcrantz, R. Loomba, Increased risk of mortality by fibrosis stage in nonalcoholic fatty liver disease: Systematic review and meta-analysis, Hepatology 65 (5) (2017) 1557–1565.
[9] GENFIT. Announces Results from Interim Analysis of RESOLVE-IT Phase 3 Trial of Elafibranor in Adults with NASH and Fibrosis. https://ml-eu.globe newsw ire.com/ Resource/Downl oad/38e08 5e1–66f5–4251-8abe-648d0 e7b9e d1; Press release (2020). In.
[10] NASH Ei. https://www.genfi t.com/pipel ine/elafibranor/ (2020). In.
[11] B. Staels, A. Rubenstrunk, B. Noel, G. Rigou, P. Delataille, L.J. Millatt, M. Baron, A. Lucas, A. Tailleux, D.W. Hum, V. Ratziu, B. Cariou, R. Hanf, Hepatoprotective effects of the dual peroxisome proliferator-activated receptor alpha/delta agonist, GFT505, in rodent models of nonalcoholic fatty liver disease/nonalcoholic steatohepatitis, Hepatology 58 (6) (2013) 1941–1952.
[12] K. Iwaisako, M. Haimerl, Y.H. Paik, K. Taura, Y. Kodama, C. Sirlin, E. Yu, R.T. Yu, M. Downes, R.M. Evans, D.A. Brenner, B. Schnabl, Protection from liver fibrosis by a peroxisome proliferator-activated receptor delta agonist, Proc. Natl. Acad. Sci. USA 109 (21) (2012) E1369–E1376.
[13] M. Zarei, J. Pizarro-Delgado, E. Barroso, X. Palomer, M. Vazquez-Carrera, Targeting FGF21 for the treatment of nonalcoholic steatohepatitis, Trends Pharm. Sci. 41 (3) (2020) 199–208.
[14] N. Wagner, K.D. Wagner, PPAR beta/delta and the hallmarks of cancer, Cells 9 (5) (2020).
[15] R. Kalluri, R.A. Weinberg, The basics of epithelial-mesenchymal transition, J. Clin. Investig. 119 (6) (2009) 1420–1428.
[16] Y. Li, J. Wang, K. Song, S. Liu, H. Zhang, F. Wang, C. Ni, W. Zhai, J. Liang, Z. Qin, J. Zhang, S100A4 promotes hepatocellular carcinogenesis by intensifying fibrosis-associated cancer cell stemness, Oncoimmunology 9 (1) (2020), 1725355.
[17] D.M. Helfman, E.J. Kim, E. Lukanidin, M. Grigorian, The metastasis associated protein S100A4: role in tumour progression and metastasis, Br. J. Cancer 92 (11) (2005) 1955–1958.
[18] S.C. Garrett, K.M. Varney, D.J. Weber, A.R. Bresnick, S100A4, a mediator of metastasis, J. Biol. Chem. 281 (2) (2006) 677–680.
[19] L. Santamaria-Kisiel, A.C. Rintala-Dempsey, G.S. Shaw, Calcium-dependent and -independent interactions of the S100 protein family, Biochem J. 396 (2) (2006) 201–214.
[20] M. Tsuchiya, F. Yamaguchi, S. Shimamoto, T. Fujimoto, H. Tokumitsu, M. Tokuda, R. Kobayashi, Oxidized S100A4 inhibits the activation of protein phosphatase 5 through S100A1 in MKN-45 gastric carcinoma cells, Int J. Mol. Med 34 (6) (2014) 1713–1719.
[21] Y. Takahashi, Y. Soejima, T. Fukusato, Animal models of nonalcoholic fatty liver disease/nonalcoholic steatohepatitis, World J. Gastroenterol. 18 (19) (2012) 2300–2308.
[22] M.V. Chakravarthy, I.J. Lodhi, L. Yin, R.R. Malapaka, H.E. Xu, J. Turk, C. F. Semenkovich, Identification of a physiologically relevant endogenous ligand for PPARalpha in liver, Cell 138 (3) (2009) 476–488.
[23] E. Barroso, R. Rodriguez-Calvo, L. Serrano-Marco, A.M. Astudillo, J. Balsinde, X. Palomer, M. Vazquez-Carrera, The PPARbeta/delta activator GW501516 prevents the down-regulation of AMPK caused by a high-fat diet in liver and amplifies the PGC-1alpha-Lipin 1-PPARalpha pathway leading to increased fatty acid oxidation, Endocrinology 152 (5) (2011) 1848–1859.
[24] M. Zarei, D. Aguilar-Recarte, X. Palomer, M. Vazquez-Carrera, Revealing the role of peroxisome proliferator-activated receptor beta/delta in nonalcoholic fatty liver disease, Metabolism 114 (2021), 154342.
[25] V.N. Malashkevich, N.G. Dulyaninova, U.A. Ramagopal, M.A. Liriano, K. M. Varney, D. Knight, M. Brenowitz, D.J. Weber, S.C. Almo, A.R. Bresnick, Phenothiazines inhibit S100A4 function by inducing protein oligomerization, Proc. Natl. Acad. Sci. USA 107 (19) (2010) 8605–8610.
[26] T. Tanaka, J. Yamamoto, S. Iwasaki, H. Asaba, H. Hamura, Y. Ikeda, M. Watanabe, K. Magoori, R.X. Ioka, K. Tachibana, Y. Watanabe, Y. Uchiyama, K. Sumi, H. Iguchi, S. Ito, T. Doi, T. Hamakubo, M. Naito, J. Auwerx, M. Yanagisawa, T. Kodama, J. Sakai, Activation of peroxisome proliferator-activated receptor delta induces fatty acid beta-oxidation in skeletal muscle and attenuates metabolic syndrome, Proc. Natl. Acad. Sci. USA 100 (26) (2003) 15924–15929.
[27] R.P. House, M. Pozzuto, P. Patel, N.G. Dulyaninova, Z.H. Li, W.D. Zencheck, M. I. Vitolo, D.J. Weber, A.R. Bresnick, Two functional S100A4 monomers are necessary for regulating nonmuscle myosin-IIA and HCT116 cell invasion, Biochemistry 50 (32) (2011) 6920–6932.
[28] R.R. Bowers, Y. Manevich, D.M. Townsend, K.D. Tew, Sulfiredoxin redox-sensitive interaction with S100A4 and non-muscle myosin IIA regulates cancer cell motility, Biochemistry 51 (39) (2012) 7740–7754.
[29] R. Zakaria, I. Lamsoul, S. Uttenweiler-Joseph, M. Erard, B. Monsarrat, O. Burlet-Schiltz, C. Moog-Lutz, P.G. Lutz, Phosphorylation of serine 323 of ASB2alpha is pivotal for the targeting of filamin A to degradation, Cell Signal 25 (12) (2013) 2823–2830.
[30] R. Rodriguez-Calvo, L. Serrano, T. Coll, N. Moullan, R.M. Sanchez, M. Merlos, X. Palomer, J.C. Laguna, L. Michalik, W. Wahli, M. Vazquez-Carrera, Activation of peroxisome proliferator-activated receptor beta/delta inhibits lipopolysaccharide-induced cytokine production in adipocytes by lowering nuclear factor-kappaB activity via extracellular signal-related kinase 1/2, Diabetes 57 (8) (2008) 2149–2157.
[31] S. Braumann, T. Thottakara, S. Stucker, S. Reischmann-Dusener, E. Kramer, J. Gross, M.N. Hirt, S. Doroudgar, L. Carrier, F.W. Friedrich, S100A4 as a target of the E3-ligase Asb2beta and its effect on engineered heart tissue, Front. Physiol. 9 (2018), 1292.
[32] N.F. Bello, I. Lamsoul, M.L. Heuze, A. Metais, G. Moreaux, D.A. Calderwood, D. Duprez, C. Moog-Lutz, P.G. Lutz, The E3 ubiquitin ligase specificity subunit ASB2beta is a novel regulator of muscle differentiation that targets filamin B to proteasomal degradation, Cell Death Differ. 16 (6) (2009) 921–932.
[33] M.L. Heuze, I. Lamsoul, M. Baldassarre, Y. Lad, S. Leveque, Z. Razinia, C. Moog-Lutz, D.A. Calderwood, P.G. Lutz, ASB2 targets filamins A and B to proteasomal degradation, Blood 112 (13) (2008) 5130–5140.
[34] J.M. Schattenberg, A. Pares, K.V. Kowdley, M.A. Heneghan, S. Caldwell, D. Pratt, A. Bonder, G.M. Hirschfield, C. Levy, J. Vierling, D. Jones, A. Tailleux, B. Staels, S. Megnien, R. Hanf, D. Magrez, P. Birman, V. Luketic, A randomized placebo-controlled trial of elafibranor in patients with primary biliary cholangitis and incomplete response to UDCA, J. Hepatol. 74 (6) (2021) 1344–1354.
[35] A.M. van den Hoek, L. Verschuren, M.P.M. Caspers, N. Worms, A.L. Menke, H.M. G. Princen, Beneficial effects of elafibranor on NASH in E3L.CETP mice and differences between mice and men, Sci. Rep. 11 (1) (2021), 5050.
[36] L. Song, T.Y. Chen, X.J. Zhao, Q. Xu, R.Q. Jiao, J.M. Li, L.D. Kong, Pterostilbene prevents hepatocyte epithelial-mesenchymal transition in fructose-induced liver fibrosis through suppressing miR-34a/Sirt1/p53 and TGF-beta1/Smads signalling, Br. J. Pharmacol. 176 (11) (2019) 1619–1634.
[37] L. Chen, J. Li, J. Zhang, C. Dai, X. Liu, J. Wang, Z. Gao, H. Guo, R. Wang, S. Lu, F. Wang, H. Zhang, H. Chen, X. Fan, S. Wang, Z. Qin, S100A4 promotes liver fibrosis via activation of hepatic stellate cells, J. Hepatol. 62 (1) (2015) 156–164.
[38] F. Fei, J. Qu, C. Li, X. Wang, Y. Li, S. Zhang, Role of metastasis-induced protein S100A4 in human non-tumor pathophysiologies, Cell Biosci. 7 (2017), 64.
[39] M. Iwano, D. Plieth, T.M. Danoff, C. Xue, H. Okada, E.G. Neilson, Evidence that fibroblasts derive from epithelium during tissue fibrosis, J. Clin. Investig. 110 (3) (2002) 341–350.
[40] M. Zeisberg, C. Yang, M. Martino, M.B. Duncan, F. Rieder, H. Tanjore, R. Kalluri, Fibroblasts derive from hepatocytes in liver fibrosis via epithelial to mesenchymal transition, J. Biol. Chem. 282 (32) (2007) 23337–23347.
[41] A. Omenetti, A. Porrello, Y. Jung, L. Yang, Y. Popov, S.S. Choi, R.P. Witek, G. Alpini, J. Venter, H.M. Vandongen, W.K. Syn, G.S. Baroni, A. Benedetti, D. Schuppan, A.M. Diehl, Hedgehog signaling regulates epithelial-mesenchymal transition during biliary fibrosis in rodents and humans, J. Clin. Investig. 118 (10) (2008) 3331–3342.
[42] K.A. Rygiel, H. Robertson, H.L. Marshall, M. Pekalski, L. Zhao, T.A. Booth, D. E. Jones, A.D. Burt, J.A. Kirby, Epithelial-mesenchymal transition contributes to portal tract fibrogenesis during human chronic liver disease, Lab Investig. 88 (2) (2008) 112–123.

[43] X. Zuo, W. Xu, M. Xu, R. Tian, M.J. Moussalli, F. Mao, X. Zheng, J. Wang, J. S. Morris, M. Gagea, C. Eng, S. Kopetz, D.M. Maru, A. Rashid, R. Broaddus, D. Wei, M.C. Hung, A.K. Sood, I. Shureiqi, Metastasis regulation by PPARD expression in cancer cells, JCI Insight 2 (1) (2017), e91419.
[44] Y. Wang, W. Lan, M. Xu, J. Song, J. Mao, C. Li, X. Du, Y. Jiang, E. Li, R. Zhang, Q. Wang, Cancer-associated fibroblast-derived SDF-1 induces epithelial-mesenchymal transition of lung adenocarcinoma via CXCR4/beta-catenin/PPARdelta signalling. Cell Death Dis. 12 (2) (2021), 214.
[45] A. Montagner, M.B. Delgado, C. Tallichet-Blanc, J.S. Chan, M.K. Sng, H. Mottaz, G. Degueurce, Y. Lippi, C. Moret, M. Baruchet, M. Antsiferova, S. Werner, D. Hohl, T.A. Saati, P.J. Farmer, N.S. Tan, L. Michalik, W. Wahli, Src is activated by the nuclear receptor peroxisome proliferator-activated receptor beta/delta in ultraviolet radiation-induced skin cancer, EMBO Mol. Med. 6 (1) (2014) 80–98.
[46] W. Shan, C.J. Nicol, S. Ito, M.T. Bility, M.J. Kennett, J.M. Ward, F.J. Gonzalez, J. M. Peters, Peroxisome proliferator-activated receptor-beta/delta protects against chemically induced liver toxicity in mice. Hepatology 47 (1) (2008) 225–235.
[47] K. Hellemans, L. Michalik, A. Dittie, A. Knorr, K. Rombouts, J. De Jong, C. Heirman, E. Quartier, F. Schuit, W. Wahli, A. Geerts, Peroxisome proliferator-activated receptor-beta signaling contributes to enhanced proliferation of hepatic stellate cells. Gastroenterology 124 (1) (2003) 184–201.
[48] R. Kostadinova, A. Montagner, E. Gouranton, S. Fleury, H. Guillou, D. Dombrowicz, P. Desreumaux, W. Wahli, GW501516-activated PPARbeta/delta promotes liver fibrosis via p38-JNK MAPK-induced hepatic stellate cell proliferation, Cell Biosci. 2 (1) (2012), 34.
[49] J.M. Peters, F.J. Gonzalez, R. Muller, Establishing the role of PPARbeta/delta in carcinogenesis, Trends Endocrinol. Metab. 26 (11) (2015) 595–607.
[50] K. Nadra, S.I. Anghel, E. Joye, N.S. Tan, S. Basu-Modak, D. Trono, W. Wahli, B. Desvergne, Differentiation of trophoblast giant cells and their metabolic functions are dependent on peroxisome proliferator-activated receptor beta/delta, Mol. Cell Biol. 26 (8) (2006) 3266–3281.
[51] J.C. McGrath, E. Lilley, Implementing guidelines on reporting research using animals (ARRIVE etc.): new requirements for publication in BJP, Br. J. Pharmacol. 172 (13) (2015) 3189–3193.
[52] E.G. Bligh, W.J. Dyer, A rapid method of total lipid extraction and purification, Can. J. Biochem. Physiol. 37 (8) (1959) 911–917.
[53] D. Balgoma, A.M. Astudillo, G. Perez-Chacon, O. Montero, M.A. Balboa, J. Balsinde, Markers of monocyte activation revealed by lipidomic profiling of arachidonic acid-containing phospholipids, J. Immunol. 184 (7) (2010) 3857–3865.
[54] R. Benveniste, T.M. Danoff, J. Ilekis, H.R. Craig, Epidermal growth factor receptor numbers in male and female mouse primary hepatocyte cultures, Cell Biochem. Funct. 6 (4) (1988) 231–235.
[55] L. Salvado, E. Barroso, A.M. Gomez-Foix, X. Palomer, L. Michalik, W. Wahli, M. Vazquez-Carrera, PPARbeta/delta prevents endoplasmic reticulum stress-associated inflammation and insulin resistance in skeletal muscle cells through an AMPK-dependent mechanism, Diabetologia 57 (10) (2014) 2126–2135.

molecules

MDPI

Article

Design and Synthesis of AMPK Activators and GDF15 Inducers

Meijian Zhang [1,2,3,†], Andrea Bagán [4,†], Donna Martínez [4], Emma Barroso [1,2,3], Xavier Palomer [1,2,3], Santiago Vázquez [4], Carmen Escolano [4,*] and Manuel Vázquez-Carrera [1,2,3,*]

1 Department of Pharmacology, Toxicology and Therapeutic Chemistry, Institute of Biomedicine (IBUB), Faculty of Pharmacy and Food Sciences, University of Barcelona, Av. Joan XXIII, 27-31, 08028 Barcelona, Spain; zmeijian@gmail.com (M.Z.); ebarroso@ub.edu (E.B.); xpalomer@ub.edu (X.P.)
2 Spanish Biomedical Research Center in Diabetes and Associated Metabolic Diseases (CIBERDEM)-Instituto de Salud Carlos III, 28029 Madrid, Spain
3 Pediatric Research Institute-Hospital Sant Joan de Déu, 08950 Esplugues de Llobregat, Spain
4 Laboratory of Medicinal Chemistry (Associated Unit to CSIC), Department of Pharmacology, Toxicology and Medicinal Chemistry, Faculty of Pharmacy and Food Sciences, Institute of Biomedicine (IBUB), University of Barcelona, Av. Joan XXIII, 27-31, 08028 Barcelona, Spain; andreabaganp@gmail.com (A.B.); luzy779@gmail.com (D.M.); svazquez@ub.edu (S.V.)
* Correspondence: cescolano@ub.edu (C.E.); mvazquezcarrera@ub.edu (M.V.-C.)
† These authors contributed equally to this work.

Abstract: Targeting growth differentiation factor 15 (GDF15) is a recent strategy for the treatment of obesity and type 2 diabetes mellitus (T2DM). Here, we designed, synthesized, and pharmacologically evaluated in vitro a novel series of AMPK activators to upregulate GDF15 levels. These compounds were structurally based on the (1-dibenzylamino-3-phenoxy)propan-2-ol structure of the orphan ubiquitin E3 ligase subunit protein Fbxo48 inhibitor, **BC1618**. This molecule showed a better potency than metformin, increasing *GDF15* mRNA levels in human Huh-7 hepatic cells. Based on **BC1618**, structural modifications have been performed to create a collection of diversely substituted new molecules. Of the thirty-five new compounds evaluated, compound **21** showed a higher increase in *GDF15* mRNA levels compared with **BC1618**. Metformin, **BC1618**, and compound **21** increased phosphorylated AMPK, but only **21** increased GDF15 protein levels. Overall, these findings indicate that **21** has a unique capacity to increase GDF15 protein levels in human hepatic cells compared with metformin and **BC1618**.

Keywords: GDF15; AMPK; BC1618; (1-dibenzylamino-3-phenoxy)propan-2-ol

check for updates

Citation: Zhang, M.; Bagán, A.; Martínez, D.; Barroso, E.; Palomer, X.; Vázquez, S.; Escolano, C.; Vázquez-Carrera, M. Design and Synthesis of AMPK Activators and GDF15 Inducers. *Molecules* **2023**, *28*, 5468. https://doi.org/10.3390/molecules28145468

Academic Editor: Beata Morak-Młodawska

Received: 11 June 2023
Revised: 14 July 2023
Accepted: 14 July 2023
Published: 17 July 2023

Copyright: © 2023 by the authors. Licensee MDPI, Basel, Switzerland. This article is an open access article distributed under the terms and conditions of the Creative Commons Attribution (CC BY) license (https://creativecommons.org/licenses/by/4.0/).

1. Introduction

Growth differentiation factor 15 (GDF15) (also known as nonsteroidal anti-inflammatory drug-activated gene, placental bone morphogenetic protein, placental transforming growth factor-ß, and prostate-derived factor) is a stress-induced cytokine that is involved in appetite regulation [1]. In fact, the increase in GDF15 levels promotes an anorectic effect that leads to a reduction in body weight through its binding to its central receptor glial cell-line-derived neurotrophic factor (GDNF)-like alpha-1 (glial cell-derived neurotrophic factor family receptor alpha-like (GFRAL)) [1]. Consistent with this role of GDF15, transgenic mice overexpressing *Gdf15* display a lean phenotype and a reduction in food intake and are more resistant to obesity, metabolic inflammation, and glucose intolerance [2,3]. Likewise, administration of recombinant GDF15 (rGDF15) has been reported to reduce food intake and body weight in mice, but these effects are absent in *Gfral*-knockout mice [2,4,5]. Overall, these findings suggest that pharmacological modulation of GDF15 shows promise for the treatment of obesity and its complications, such as type 2 diabetes mellitus (T2DM). Indeed, GDF15 analogs, which try to overcome the pharmacokinetic (e.g., a short half-life of ~3 h in mice and non-human primates) and physicochemical (e.g., high aggregation propensity) limitations of native GDF15 [1,6,7], have been developed for the treatment

of obesity. Another potential strategy to target the GDF15–GFRAL pathway involves the pharmacological regulation of endogenous GDF15 levels. Interestingly, metformin, the most prescribed drug for the treatment of T2DM, has been reported to increase serum GDF15 in patients [8]. Subsequently, two studies reported that the anorectic response of mice to metformin requires an intact GDF15–GFRAL pathway [9,10]. In addition, the increase in GDF15 levels caused by metformin was associated with the reduction in body weight in patients with [10] or without [9] T2DM. Although a recent study reported that the effects of metformin on body weight were independent of the GDF15–GFRAL signaling in some circumstances [11], a new study confirmed the involvement of this pathway on the effects of metformin on body weight [12]. These findings validate that targeting endogenous GDF15 may serve as a pharmacological approach to treat obesity and T2DM. Interestingly, many of the antidiabetic effects of metformin are mediated by the activation of the adenosine monophosphate-activated protein kinase (AMPK) [13], and we reported that the increase in GDF15 caused by metformin involves the activation of this kinase [14]. Moreover, we observed that the antidiabetic effect of a low dose of metformin is not observed in *Gdf15*-knockout mice [14]. These findings suggest that targeting AMPK may provide new possibilities to increase endogenous levels of GDF15 to treat obesity and T2DM.

In this study, we designed, synthesized, and pharmacologically evaluated in vitro a novel series of AMPK activators, aiming at increasing *GDF15* expression. These compounds are structurally based on the (1-dibenzylamino-3-phenoxy)propan-2-ol skeleton of the orphan ubiquitin E3 ligase subunit protein Fbxo48 inhibitor, **BC1618**, which exceeds metformin potency for stimulating AMPK [15]. In this context, we carried out conservative structural modifications on the substituents in the phenoxy ring and in the amine moiety. Our findings show that one of the new compounds synthesized, **21**, exhibits substantially better potency compared to metformin and **BC1618** towards increased GDF15 mRNA and protein levels in human hepatic cells.

2. Results

2.1. Synthesis of GDF15 Inducers

The synthesis of **BC1618** was performed as described [16]. The other products were synthetized following the same synthetic strategy (Scheme 1). In this manner, a methanol solution of the required phenol (1 equiv.) with epichlorohydrin (10 equiv.) in the presence of potassium carbonate (1.2 equiv.) was heated at reflux for 4 h, leading to the corresponding phenoxymethyloxirane intermediates. In a second synthetic step, an equimolecular mixture of the phenoxymethyloxirane derivatives and the required primary or secondary amine were heated at 70 °C for 24 h to afford the final compounds (**1–35**) in good yields (see Section 4 for further details).

All the compounds synthesized for in vitro evaluation were fully characterized through their spectroscopic data (^{1}H and ^{13}C), infrared (IR), and high-resolution mass spectrometry (HMRS). The purity was determined by high-performance liquid chromatography (HPLC)/mass spectrometry, and only compounds with a purity >95% were considered for biological studies (see the Section 4 and the Supplementary Materials for further details).

2.2. Assessment of the Activity of the New Compounds Increasing GDF15 mRNA Levels in Huh-7 Human Hepatic Cells and Structural–Activity Relationship of the New Compounds

To evaluate the activity of the synthesized compounds (Scheme 1A–C) in increasing *GDF15* expression, we incubated Huh-7 human hepatic cells with the new compounds (30 μM) for 24 h, using metformin (5 mM) and **BC1618** (30 μM) as standards for comparison purposes. Hepatic cells were used since circulating GDF15 is primarily derived from the liver [17]. As shown in Table 1, metformin caused a 2.7-fold increase in *GDF15* mRNA levels compared with control cells. By contrast, a much lower concentration of **BC1618** caused a higher increase in *GDF15* expression (10.4-fold induction), thereby indicating that this compound shows a higher potency, which is consistent with the reported higher activation of AMPK [15].

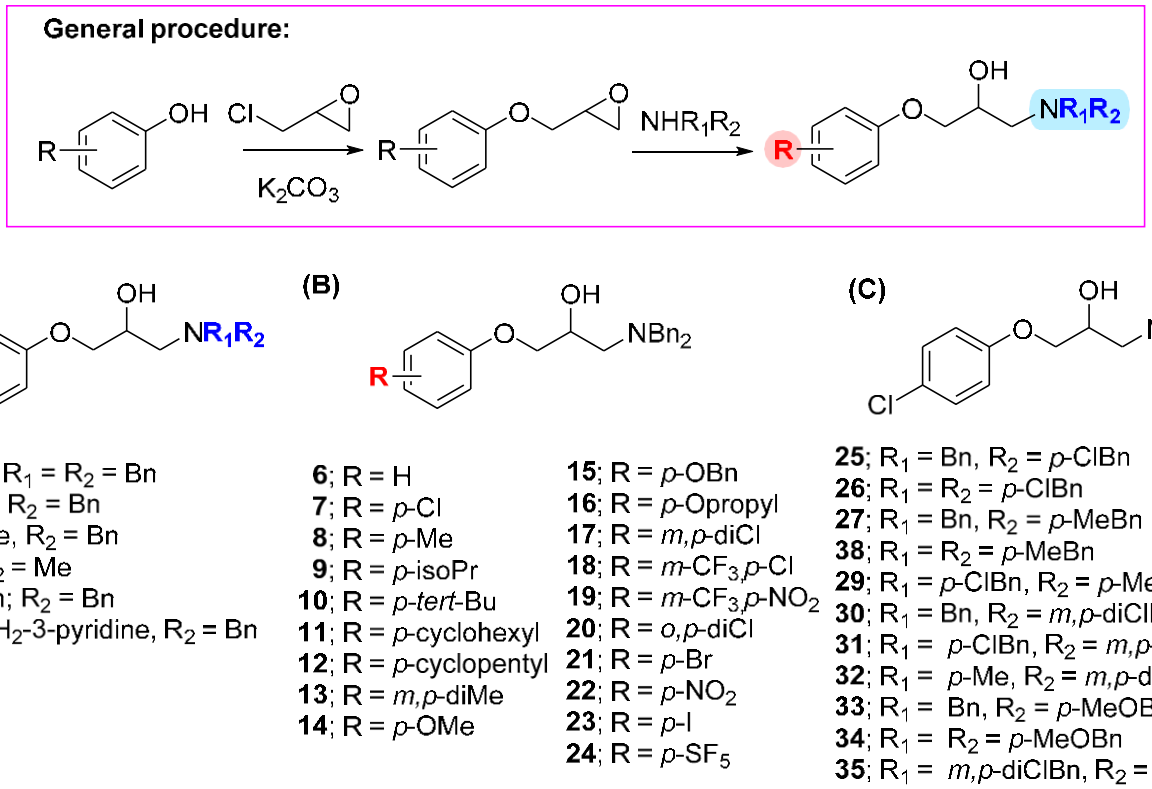

Scheme 1. General procedure for the synthesis of compounds (**1**–**35**) with modifications in the amino substituents (in blue) and in the substituents of the phenoxy group (in red). General structures, (A) variations in the substituents in the amino group of the *p*-trichlorophenyl general structure, (B) variations in the substituents in the phenoxy group, and (**C**) variations in the substituents in the amino group of the *p*-chlorophenyl general structure.

Table 1. Assessment of the effects of the compounds **1**–**35** on human *GDF15* expression. *GDF15* mRNA levels in the human liver cell line Huh-7 exposed to 5 mM metformin, 30 µM BC1618, or 30 µM of new compound for 24 h. Data are presented as the mean ± SEM (n = 3). * $p < 0.05$, ** $p < 0.01$, and *** $p < 0.001$ vs. control. p-values determined by one-way ANOVA with Tukey's post hoc test.

Entry	Compound	Structure	GDF15 mRNA Levels (%)	GDF15 mRNA Levels Regarding BC1618 (%)	Activity Change Regarding BC1618 (%)
1	**Control**	-	100.00 ± 16.00	9.60	−90.40
2	**Metformin**	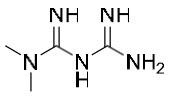	273.49 ± 3.79	26.26	−73.74
		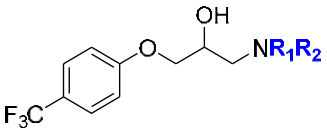			
3	**BC1618**	$R_1 = R_2 = Bn$	1041.41 ± 83.58 *	100.00	0.00
4	**1**	$R_1 = H, R_2 = Bn$	1692.98 ± 120.22 ***	162.57	+62.57
5	**2**	$R_1 = Me, R_2 = Bn$	377.99 ± 71.33	36.30	−63.70
6	**3**	$R_1 = R_2 = Me$	296.39 ± 7.77	28.46	−71.54

Table 1. *Cont.*

Entry	Compound	Structure	GDF15 mRNA Levels (%)	GDF15 mRNA Levels Regarding BC1618 (%)	Activity Change Regarding BC1618 (%)
7	**4**	R_1 = Ph, R_2 = Bn	986.69 ± 24.56 *	94.75	−5.25
8	**5**	R_1 = CH_2-3-pyridine, R_2 = Bn	394.10 ± 75.18	37.84	−62.16
		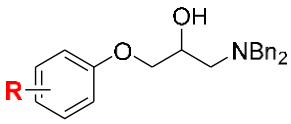			
9	**6**	R = H	1021.35 ± 167.60 ***	98.07	−1.93
10	**7**	R = *p*-Cl	1249.04 ± 181.39 **	119.94	+19.94
11	**8**	R = *p*-Me	1107.44 ± 152.04 *	106.34	+6.34
12	**9**	R = *p*-isopropyl	871.04 ± 91.59 **	83.64	−16.36
13	**10**	R = *p*-*tert*-butyl	640.00 ± 126.21	61.46	−38.54
14	**11**	R = *p*-cyclohexyl	630.49 ± 160.87 *	60.54	39.46
15	**12**	R = *p*-cyclopentyl	942.87 ± 291.40 ***	90.54	−9.46
16	**13**	R = *m*,*p*-diMe	1807.01 ± 190.07 ***	173.52	+73.52
17	**14**	R = *p*-OMe	988.06 ± 137.45 ***	94.88	−5.12
18	**15**	R = *p*-OBn	275.85 ± 74.89	26.49	−73.51
19	**16**	R = *p*-Opropyl	592.33 ± 220.72	56.88	−43.12
20	**17**	R = *m*,*p*-diCl	664.89 ± 201.62	63.85	−36.15
21	**18**	R = *m*-CF_3,*p*-Cl	446.25 ± 34.9	42.85	−57.15
22	**19**	R = *m*-CF_3,*p*-NO_2	520.63 ± 37.79	49.99	−50.01
23	**20**	R = o,*p*-diCl	1172.43 ± 168.93 **	112.58	+12.58
24	**21**	R = *p*-Br	1464.51 ± 16.27 ***	140.63	+40.63
25	**22**	R = *p*-NO_2	1050.44 ± 69.45 ***	100.87	+0.87
26	**23**	R = *p*-I	517.48 ± 196.49	49.69	−50.31
27	**24**	R = *p*-SF_5	720.70 ± 107.34 *	69.20	−30.80
		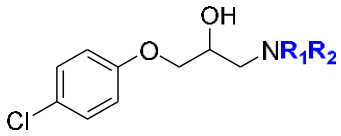			
28	**25**	R_1 = Bn, R_2 = *p*-ClBn	-	-	-
29	**26**	R_1 = R_2 = *p*-ClBn	150.28 ± 18.68	14.43	−85.57
30	**27**	R_1 = Bn, R_2 = *p*-MeBn	177.92 ± 58.52	17.08	−82.92
31	**28**	R_1 = R_2 = *p*-MeBn	205.79 ± 22.24 *	19.76	−80.24
32	**29**	R_1 = *p*- lBn, R_2 = *p*- eBn	219.48 ± 21.63 *	21.08	−78.92
33	**30**	R_1 = Bn, R_2 = *m*,*p*-diClBn	176.61 ± 40.52	16.96	−83.04
34	**31**	R_1 = *p*- lBn, R_2 = *m*,*p*-diClBn	128.74 ± 11.19	12.36	−87.64
35	**32**	R_1 = *p*-Me, R_2 = *m*,*p*-diClBn	143.90 ± 34.31	13.82	−86.18
36	**33**	R_1 = Bn, R_2 = *p*-MeOBn	98.35 ± 65.89	9.44	−90.56
37	**34**	R_1 = R_2 = *p*-MeOBn	161.63 ± 12.29	15.52	−84.48
38	**35**	R_1 = *m*,*p*-diClBn, R_2 = *p*-MeOBn	186.69 ± 27.81	17.93	−82.07

To determine the impact that modifications in the different substituents could have in the biological activities (Table 1), we considered two main approximations starting from **BC1618**: (a) an exploration of the substituents in the amino moiety (right-hand side,

RHS; highlighted in blue in the general structure in the Scheme 1) and (b) a study of the substituents at the phenoxy group (left-hand side, LHS; highlighted in red in the general structure in the Scheme 1).

In this context, the simplification of the dibenzylamino substituent of **BC1618** to a benzylamino was considered, leading to compound **1**, which exhibited important increases in GDF15 expression compared with BC1618 but also increased cell mortality, suggesting some toxicity that rendered it unsuitable for further work. Compared with **BC1618**, an *N*-benzyl,*N*-methylamine substituent in **2** or *N*,*N*-dimethylamine in **3** resulted in substantial reductions in the expression of GDF15. An *N*-benzyl-*N*-phenylamino moiety in **4** caused no significant changes in GDF15 levels compared with **BC1618**, whereas the presence of an electron-deficient aromatic ring such as a 3-pyridine in **5** caused a dramatic reduction in GDF15 levels.

At this point, we maintained unaltered the RHS part of the initial scaffold (*N*-dibenzyla mino) and focused on the modifications of the substituents at the phenoxy moiety. Removal of the trifluoromethyl group, as in **6**, had no effect on GDF15 levels compared with **BC1618**. Comprehensive exploration of the RHS involved the replacement of the trifluoromethyl group by a chlorine atom in **7** or a methyl group in **8**, leading to small increases in the *GDF15* mRNA levels. Other replacements, featuring bulkier *p*-alkyl substituents, such as those conducted in **9** (isopropyl), **10** (*tert*-butyl), **11** (cyclohexyl), or **12** (cyclopentyl), did not improve the levels of the biomarker. Compound **13**, featuring a 3,4-dimethylphenoxy group, exhibited a remarkable increase in the GDF15 levels, although it was somehow toxic, showing an increase in the cell mortality. Compound **14**, embodying a *p*-methoxy group, depicted similar activity as **BC1618**. With the aim of exploring alternative *p*-alkyloxy substituents, **15** with a *p*-benzyloxy group and **16** with a *p*-propyloxy unit were synthesized, leading to a significant reduction in *GDF15* expression compared with **BC1618**. Next, we undertook the synthesis of disubstituted compounds **17–19**, featuring *m*,*p*-dichloro-, *p*-chloro,*m*-trifluoromethyl-, and *p*-nitro,*m*-trifluoromethyl-phenoxy units, respectively. The three new compounds did not improve the activity of **BC1618**. The presence of a *o*,*p*-dichloro atoms at the phenoxy group in **20** led to an increase in *GDF15* expression.

Considering the abovementioned results, in a final round, we selected compound **7**, with a *p*-chlorophenoxy group, and we introduced substituents in the dibenzylamino moiety. Therefore, we synthesized eleven new analogs, including **25** and **26**, with a *p*-chloro in one or two of the benzyl groups, respectively; **27** and **28**, with a *p*-methyl in one or two of the benzyl groups, respectively; and **29**, with a *p*-chloro and a *p*-methyl group in each benzyl group. All these compounds depicted a very important decrease in the *GDF15* levels compared with **BC1618**. Particularly, **25** was toxic for the cells, and the number of cells collected was too low to analyze *GDF15* expression. Increasing the number of chloro atoms in the benzyl substituents, as in **30** (*m*,*p*-dichloro), **31** (*m*,*p*-dichloro and *p*-chloro), and **32** (*m*,*p*-dichloro and *p*-methyl), resulted in a dramatical decrease in *GDF15* levels. Finally, moving to electron-donating groups, such as a *p*-methoxy group (**33** in one benzyl or **34** in both benzyl groups), or to a combination of *m*,*p*-dichloro on one ring and *p*-methoxy in the other ring (**35**) was deleterious for the biological activity.

Considering that compound **7**, featuring a dibenzylamino unit at the RHS of the molecule and a *p*-chlorophenoxy group at the LHS, provided the highest *GDF15* levels without toxicity, we finally explored the effect of replacing the *p*-chlorine atom by another electron-withdrawing group. Thus, we synthesized compound **21**, with a *p*-bromophenoxy group. Interestingly, this compound exhibited a marked increase in *GDF15* expression without toxicity issues. When a nitro group or an iodine atom occupied the *para* position of the phenoxy group in **22** and **23**, respectively, a decrease in *GDF15* levels was observed. Our experience in the study of the rather scarcely explored pentafluorosulfanyl substituent [18] prompted us to prepare compound **24**, which did not represent a biological improvement. Considering all the above-mentioned results, compound **21** was selected for further experiments.

2.3. Evaluation of the Activity of 21 on AMPK Activation and GDF15 Protein Levels in Huh-7 Human Hepatic Cells

The effect of compound **21** on GDF15 protein levels compared with metformin and **BC1618** was evaluated in Huh-7 cells. The three compounds activated AMPK, determined by the increase in phosphorylated AMPK. However, of the three compounds, only **21** increased the protein abundance of GDF15 (Figure 1).

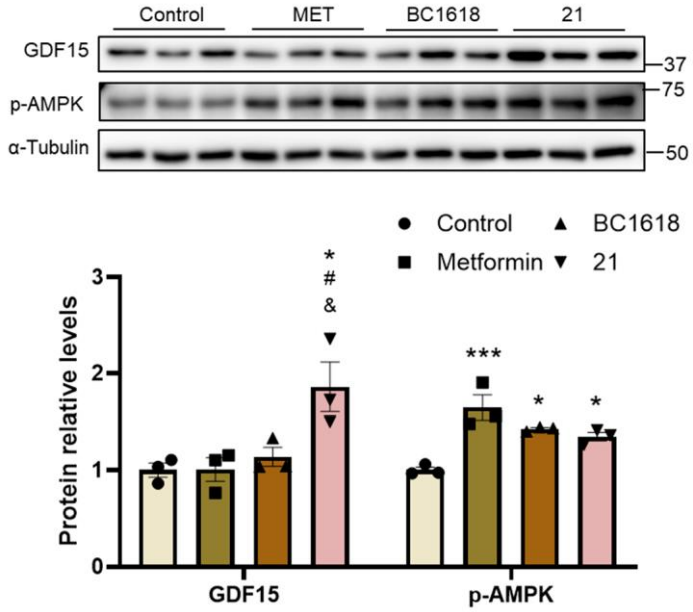

Figure 1. Compound **21** increases GDF15 protein abundance. GDF15 and phosphorylated AMPK protein levels in Huh-7 human hepatic cells exposed to metformin (MET) (5 mM), **BC1618** (10 μM), or **21** (10 μM) for 72 h. Data are presented as the mean ± SEM (n = 3). * $p < 0.05$, and *** $p < 0.001$ vs. control. # $p < 0.05$ vs. metformin-treated cells. & $p < 0.05$ vs. **BC1618**-treated cells. p-values determined by one-way ANOVA with Tukey's post hoc test.

3. Discussion

There is conclusive evidence that GDF15 is an attractive target for the treatment of obesity and T2DM [1]. Indeed, recombinant GDF15 and its analogs reduce food intake and body weight and improve glucose intolerance in animal models of obesity [1,6,7]. In addition, metformin increases circulating GDF15 levels [8]. The metformin-mediated increase in GDF15 levels may mediate part of its effects on body weight and glucose metabolism [9,10,14]. Therefore, pharmacological modulation of endogenous GDF15 levels by small molecules offers promise for the treatment of obesity and T2DM. In this line, it has been reported that metformin increases GDF15 levels via AMPK [14], converting this kinase in a target to increase this cytokine. In this study, we synthesized new compounds based on the (1-dibenzylamino-3-propoxy)propan-2-ol group of the orphan ubiquitin E3 ligase subunit protein Fbxo48 inhibitor, **BC1618** [15], to upregulate GDF15 levels. It is known that the potency of **BC1618** activating AMPK exceeds that of metformin [15], but little was known about the capacity of this compound to increase GDF15.

Here, we show that **BC1618** (10 μM) causes a strong increase in *GDF15* mRNA levels in human Huh-7 cells compared with metformin (5 mM). In addition, we synthesized and fully characterized thirty-five new analogues of **BC1618**, and we evaluated their effects on *GDF15* expression. All the new compounds increased GDF15 mRNA levels over the control, and a few of them were more potent than **BC1618**.

Compound **21**, which features a bromine atom instead of the trifluoromethyl group of **BC1618**, caused a higher increase in GDF15 levels compared with **BC1618** and was selected to evaluate its effects on GDF15 protein abundance compared with metformin and **BC1618**. The three compounds increased phosphorylated levels of AMPK. However,

only **21** increased GDF15 protein levels. Although previous studies have reported that metformin administration increases serum GDF15 levels, the source tissue leading to the increase in this cytokine remains controversial [19]. Thus, two studies reported that metformin can induce GDF15 release from mouse primary hepatocytes [9,10], but one of these studies showed that metformin increased GDF15 levels in kidneys and intestines but not in the liver [9]. More recently, a new study demonstrated that acute metformin treatment elevated GDF15 levels in different tissues but not in the liver [11]. Therefore, it is likely that due to the slight increase in *GDF15* expression caused by metformin, longer exposures are needed to detect an increase in GDF15 protein abundance in hepatic cells. However, **BC1618** caused a higher increase in GDF15 mRNA levels compared to metformin, but this increase did not result in an elevation of the protein abundance of this cytokine. By contrast, **21** treatment increased GDF15 protein levels. These findings suggest that the substitution of the trifluoromethyl group by a bromine atom may contribute to increase GDF15 protein abundance. Although the reasons for this effect are unknown, several factors may contribute. For instance, a bigger atom such as bromine may affect the ability to interact with target proteins and receptors. In fact, a study investigating the effects of 3,3′-diindolylmethane and its synthetic halogenated derivatives found that a bromide derivative caused a higher activation of AMPK [20]. These findings suggest that the presence of bromide atoms in **21** could potentiate or sustain AMPK activation, leading to an increase in GDF15 protein levels. Although we did not observe a greater increase in phosphorylated AMPK following **21** treatment compared with **BC1618**, we only examined a single time point. Therefore, transient increases might have contributed to achieve a higher potency in AMPK activation. Further studies are needed to elucidate the mechanisms that contribute to increasing GDF15 protein levels.

Overall, the findings of this study show that there is no correlation between GDF15 mRNA and protein levels and that the presence of a bromine atom in the structure of molecules activating AMPK and increasing *GDF15* expression allows to increase the protein abundance of this stress cytokine in hepatic cells. Moreover, we describe that new compound 21 has a unique capacity to increase GDF15 protein levels in human hepatic cells compared with metformin and BC1618.

4. Materials and Methods

4.1. Chemical Synthesis

4.1.1. General Methods

Reagents, solvents, and starting products were acquired from commercial sources. When indicated, the reaction products were purified by "flash" chromatography on silica gel (35–70 μm) with the indicated solvent system. The melting points were measured in a MFB 59510M Gallenkamp instruments. IR spectra were performed in a spectrophotometer Nicolet Avantar 320 FTR-IR or in a Spectrum Two FT-IR Spectrometer, and only noteworthy IR absorptions (cm^{-1}) are listed. NMR spectra were recorded in $CDCl_3$ at 400 MHz (^1H) and 101 MHz (^{13}C), and chemical shifts are reported in δ values downfield from TMS or relative to residual chloroform (7.26 ppm, 77.0 ppm) as an internal standard. Data are reported in the following manner: chemical shift, multiplicity, coupling constant (*J*) in hertz (Hz), and integrated intensity and assignment (when possible). Multiplicities are reported using the following abbreviations: s, singlet; d, doublet; dd, doublet of doublets; t, triplet; q, quadruplet; m, multiplet; br s, broad signal; app, apparent. Assignments and stereochemical determinations are given only when they are derived from definitive dimensional NMR experiments (g-HSQC). The accurate mass analyses were carried out using a LC/MSD-TOF spectrophotometer. HPLC-MS (Agilent 1260 Infinity II) analysis was conducted on a Poroshell 120 EC-C15 (4.6 mm × 50 mm, 2.7 μm) at 40 °C with mobile phase A (H_2O + 0.05% formic acid) and B (ACN + 0.05% formic acid) using a gradient elution and flow rate 0.6 mL/min. The DAD detector was set at 254 nm, the injection volume was 5 μL, and the oven temperature was 40 °C.

General procedure for the preparation of final aryloxypropanolamines from aryloxyepoxydes and amines. The corresponding amines (1 equivalent) and the corresponding oxiranes (1 equivalent) were stirred under N_2 atmosphere at 70 °C for 24 h. The reaction mixture was concentrated, and the resulting residue was purified by column chromatography to afford pure products.

4.1.2. 1-(Dibenzylamino)-3-[4-(trifluoromethyl)phenoxy]propan-2-ol (BC1618)

Following the general procedure, a mixture of dibenzylamine (CAS 103-49-1) (0.09 mL, 0.47 mmol) and 2-{[4-(trifluoromethyl)phenoxy]methyl}oxirane (100 mg, 0.46 mmol) afforded BC1618 (149 mg, 78%) as a white solid after column chromatography (hexane/DCM 9:1 to 8:2). IR (ATR) 3412, 3029, 2924, 1613, 1451, 1261, 1034, 840, 745, 698 cm^{-1}. ^1H NMR (500 MHz, $CDCl_3$) δ 2.69 (d, *J* = 7.0 Hz, 2H, CH_2N), 3.56 (d, *J* = 13.5 Hz, 2H, CH_2Ph), 3.82 (d, *J* = 13.5 Hz, 2H, CH_2Ph), 3.85–3.94 (m, 2H, CH_2O), 4.06–4.14 (m, 1H, CH), 6.88 (d, *J* = 8.5 Hz, 2H, ArH), 7.24–7.30 (m, 2H, ArH), 7.31–7.35 (m, 8H, ArH), 7.51 (d, *J* = 8.5 Hz, 2H, ArH). ^{13}C NMR (126 MHz, $CDCl_3$) δ 56.0 (CH_2N), 59.0 ($2CH_2Ph$), 66.4 (CH), 70.6 (CH_2O), 114.6 (2CHAr), 121.3 (CAr), 123.2 (q, *J* = 32.5 Hz, CF_3), 125.6 (CAr), 127.0 (d, *J* = 4.0 Hz, 2CHAr), 127.6 (2CHAr), 128.7 (4CHAr), 129.1 (CHAr), 129.3 (2CHAr), 130.0 (CHAr), 138.4 (CAr), 161.2 (OCAr) [15]. Purity 96.90% (t_R = 3.27 min).

4.1.3. 1-(Benzylamino)-3-[4-(trifluoromethyl)phenoxy]propan-2-ol (**1**)

Following the general procedure, benzylamine (CAS 100-46-9) (0.05 mL, 0.46 mmol) and 2-{[4-(trifluoromethyl)phenoxy]methyl}oxirane (100 mg, 0.46 mmol) afforded **1** (82 mg, 55%) as a white solid after column chromatography (hexane/EtOAc 9:1 to 8:2). Mp 102–105 °C (EtOAc). IR (ATR) 3266, 1614, 1520, 1335, 1256, 1153, 1109, 1035, 836, 698 cm^{-1}. ^1H NMR (400 MHz, $CDCl_3$, HETCOR) δ 2.47 (s, 2H, OH, NH), 2.79 (dd, *J* = 12.0, 8.0 Hz, 1H, CH_2N), 2.91 (dd, *J* = 12.0, 4.0, Hz, 1H, CH_2N), 3.79–3.91 (m, 2H, CH_2Ph), 4.02 (d, *J* = 5.5 Hz, 2H, CH_2O), 4.05–4.13 (m, 1H, CH), 6.96 (d, *J* = 8.5 Hz, 2H, ArH), 7.25–7.38 (m, 5H, ArH), 7.54 (d, *J* = 8.5 Hz, 2H, ArH). ^{13}C NMR (101 MHz, $CDCl_3$) δ 51.1 (CH_2N), 53.9 (CH_2Ph), 68.3 (CH), 70.7 (CH_2O), 114.7 (2CHAr), 121.4–125.4 (m, CF_3), 127.0 (2CHAr), 127.4 (2CHAr), 128.3 (3CHAr), 128.7 (CAr), 139.8 (CAr), 161.2 (OCAr). HRMS $C_{17}H_{19}F_3NO_2$ $[M + H]^+$ 326.1362; found 326.1366. Purity 95.23% (t_R = 2.80 min).

4.1.4. 1-[Methyl(phenyl)amino]-3-[4-(trifluoromethyl)phenoxy]propan-2-ol (**2**)

Following the general procedure, *N*-benzylmethylamine (CAS 103-67-3) (0.06 mL, 0.46 mmol) and 2-{[4-(trifluoromethyl)phenoxy]methyl}oxirane (100 mg, 0.46 mmol) afforded **2** (73 mg, 47%) as a white solid after a reversed-phase column chromatography (H_2O:ACN 95:5). Mp 53–56 °C (EtOAc). IR (ATR) 3432, 2843, 1615, 1519, 1327, 1258, 1153, 1107, 1068, 836, 699 cm^{-1}. ^1H NMR (400 MHz, $CDCl_3$, HETCOR) δ 2.36 (s, 3H, CH_3), 2.61 (dd, *J* = 12.5, 4.0, Hz, 1H, CH_2), 2.71 (dd, *J* = 12.5, 10.0 Hz, 1H, CH_2), 3.6 (br s, 1H, OH), 3.61 (d, *J* = 13.0 Hz, 1H, CH_2Ph), 3.76 (d, *J* = 13.0 Hz, 1H, CH_2Ph), 4.00 (dd, *J* = 5.0, 1.0 Hz, 2H, CH_2), 4.12–4.21 (m, 1H, CH), 6.96 (d, *J* = 8.5 Hz, 2H, ArH), 7.34 (dd, *J* = 8.0, 2.0 Hz, 5H, ArH), 7.54 (d, *J* = 8.5 Hz, 2H, ArH). ^{13}C NMR (101 MHz, $CDCl_3$) δ 42.3 (CH_3), 59.5 (CH_2N), 62.6 (CH_2Ph), 66.0 (CH), 70.5 (CH_2O), 114.7 (2CHAr), 123.3 (q, *J* = 33.0 Hz, CF_3), 127.0 (q, *J* = 4.0 Hz, 3CHAr), 127.8 (2CHAr), 128.7 (2CHAr), 129.4 (CAr), 137.3 (CAr), 161.2 (OCAr). HRMS $C_{18}H_{21}F_3NO_2$ $[M + H]^+$ 340.1519; found 340.1523. Purity 100% (t_R = 2.74 min).

4.1.5. 1-(Dimethylamino)-3-[4-(trifluoromethyl)phenoxy]propan-2-ol (**3**)

Following the general procedure, dimethylamine (CAS 124-40-3) (0.04 mL, 0.55 mmol) and 2-{[4-(trifluoromethyl)phenoxy]methyl}oxirane (120 mg, 0.55 mmol) afforded **3** (48 mg, 33%) as an oil after a reversed-phase column chromatography (H_2O:ACN 95:5). IR (ATR) 3348, 2926, 1615, 1520, 1461, 1257, 1033, 835, 775, 691 cm^{-1}. ^1H NMR (400 MHz, $CDCl_3$, HETCOR) δ 2.66 (s, 6H, $2CH_3$), 2.84 (m, 1H, CH_2N), 2.98 (m, 1H, CH_2N), 4.00 (dd, *J* = 9.5, 5.5 Hz, 1H, CH_2O), 4.10 (dd, *J* = 9.5, 5.0 Hz, 1H, CH_2O), 4.34 (m, 1H, CH), 6.97 (d, *J* = 8.5 Hz, 2H, ArH), 7.53 (d, *J* = 9.0 Hz, 2H, ArH). ^{13}C NMR (101 MHz, $CDCl_3$) δ 45.1 ($2CH_3$), 62.0

(CH_2N), 65.2 (CH), 70.1 (CH_2O), 114.6 (2CHAr), 121.6–124.3 (m, CF_3), 125.8 (CAr), 127.1 (d, J = 4.0 Hz, 2CAr), 160.9 (OCAr). HRMS $C_{12}H_{17}F_3NO_2$ $[M + H]^+$ 264.1206; found 264.1210. Purity 98.36% (t_R = 2.47 min).

4.1.6. 1-[Benzyl(phenyl)amino]-3-[4-(trifluoromethyl)phenoxy]propan-2-ol (**4**)

Following the general procedure, *N*-benzylaniline (CAS 103-32-2) (0.08 mL, 0.46 mmol) and 2-{[4-(trifluoromethyl)phenoxy]methyl}oxirane (100 mg, 0.46 mmol) afforded **4** (95 mg, 52%) as a white solid after column chromatography (hexane/EtOAc 9:1 to 8:2). Mp 82–86 °C (EtOAc). IR (ATR) 3445, 1616, 1521, 1336, 1259, 1153, 1108, 1025, 839, 692 cm^{-1}. ^1H NMR (400 MHz, $CDCl_3$, HETCOR) δ 2.36 (br s, 1H, OH), 3.63 (dd, J = 12.0, 4.5 Hz, 2H, CH_2N), 4.00 (dd, J = 12.0, 4.5 Hz, 2H, CH_2Ph), 4.33 (br s, 1H, CH), 4.61 (d, J = 5.5 Hz, 2H, CH_2O), 6.73 (t, J = 7.0 Hz, 1H, ArH), 6.81 (d, J = 8.0 Hz, 2H, ArH), 6.91 (d, J = 8.5 Hz, 2H, ArH), 7.17–7.24 (m, 5H, ArH), 7.26–7.28 (m, 2H, ArH), 7.52 (d, J = 9.0 Hz, 2H, ArH). ^{13}C NMR (101 MHz, $CDCl_3$) δ 54.2 (CH_2N), 55.8 (CH_2Ph), 68.2 (CH), 70.1 (CH_2O), 113.4 (2CHAr), 114.7 (2CHAr), 117.8 (2CHAr), 122.0–125.2 (m, CF_3), 126.9 (2CHAr), 127.2 (CAr), 128.8 (3CAr), 129.5 (3CAr), 138.4 (CAr), 148.8 (CAr), 161.0 (OCAr). HRMS $C_{23}H_{23}F_3NO_2$ $[M + H]^+$ 402.1675; found 402.1673. Purity 98.66% (t_R = 4.71 min).

4.1.7. 1-[Benzyl(pyridin-3-ylmethyl)amino]-3-[4-(trifluoromethyl)phenoxy]propan-2-ol (**5**)

Following the general procedure, *N*-benzyl-1-(pyridin-3-yl)methanamine (CAS 63361-56-8) (73 mg, 0.37 mmol) and 2-{[4-(trifluoromethyl)phenoxy]methyl}oxirane (80 mg, 0.37 mmol) afforded **5** (40 mg, 26%) as a white solid after column chromatography (hexane/EtOAc 9:1 to 8:2). Mp 95–97 °C (EtOAc). IR (ATR) 2920, 1453, 1325, 1257, 1158, 1109, 1068, 1028, 837, 701 cm^{-1}. ^1H NMR (400 MHz, $CDCl_3$, HETCOR) δ 2.66–2.77 (m, 2H, CH_2N), 3.62 (dd, J = 10.5, 13.5 Hz, 2H, CH_2Ph, CH_2Pyr), 3.82 (dd, J = 13.5, 5.0 Hz, 2H, CH_2Ph, CH_2Pyr), 3.91 (d, J = 5.0 Hz, 2H, CH_2O), 4.08–4.16 (m, 1H, CH), 6.88 (d, J = 8.5 Hz, 2H, ArH), 7.26–7.37 (m, 6H, ArH), 7.52 (d, J = 8.5 Hz, 2H, ArH), 7.67 (d, J = 8.0 Hz, 1H, ArH), 8.53 (d J = 4.0 Hz, 1H, ArH), 8.57 (s, 1H, ArH). ^{13}C NMR (101 MHz, $CDCl_3$) δ 56.1 (CH_2N), 56.3 (CH_2Pyr), 59.0 (CH_2Ph), 66.7 (CH), 70.4 (CH_2O), 114.6 (2CHAr), 123.0–123.6 (m, CF_3), 123.7 (CHAr), 125.6 (CAr) 127.0 (2CHAr), 127.9 (CHAr), 128.8 (2CHAr), 129.3 (2CHAr), 133.8 (CAr), 137.0 (CHAr), 137.7 (CAr), 149.0 (CHAr), 150.4 (CHAr), 161.1 (CAr). HRMS $C_{23}H_{24}F_3N_2O_2$ $[M + H]^+$ 417.1784; found, 417.1794. Purity 100% (t_R = 2.43 min).

4.1.8. 1-(Dibenzylamino)-3-phenoxypropan-2-ol (**6**)

Following the general procedure, dibenzylamine (CAS 103-49-1) (0.57 mL, 2.96 mmol) and 2-(phenoxymethyl)oxirane (442 mg, 2.94 mmol) afforded **6** (698 mg, 68%) as an oil after column chromatography (hexane/DCM 9:1 to 8:2). IR (ATR) 3434, 3028, 1598, 1494, 1452, 1242, 1927, 814, 747, 691 cm^{-1}. ^1H NMR (400 MHz, $CDCl_3$, HETCOR) δ 2.61–2.73 (m, 2H, CH_2N), 3.54 (d, J = 13.5 Hz, 2H, CH_2Ph), 3.80 (d, J = 13.5 Hz, 2H, CH_2Ph), 3.87 (d, J = 5.5 Hz, 2H, CH_2O), 4.05–4.16 (m, 1H, CH), 6.84 (d, J = 8.0 Hz, 2H, ArH), 6.94 (t, J = 7.5 Hz, 1H, ArH), 7.21–7.38 (m, 12H, ArH). ^{13}C NMR (101 MHz, $CDCl_3$) δ 56.3 (CH_2N), 58.9 ($2CH_2Ph$), 66.6 (CH), 70.4 (CH_2O), 114.6 (2CHAr), 121.0 (CHAr), 127.5 (2CHAr), 128.6 (4CHAr), 129.2 (4CHAr), 129.5 (2CHAr), 138.6 (2CAr), 158.8 (OCAr). HRMS $C_{23}H_{26}NO_2$ $[M + H]^+$ 348.1958; found 348.1961. Purity 98.28% (t_R = 3.16 min).

4.1.9. 1-(4-Chlorophenoxy)-3-(dibenzylamino)propan-2-ol (**7**)

Following the general procedure, dibenzylamine (CAS 103-49-1) (0.33 mL, 1.71 mmol) and 2-[(4-chlorophenoxy)methyl]oxirane (316 mg, 1.71 mmol) afforded **7** (624 mg, 96%) as an oil after column chromatography (hexane/DCM 9:1 to 8:2). IR (ATR) 3426, 3027, 1589, 1485, 1446, 1248, 1027, 827, 743, 697 cm^{-1}. ^1H NMR (400 MHz, $CDCl_3$, HETCOR) δ 2.75 (d, J = 6.5 Hz, 2H, CH_2N), 3.57 (d, J = 13.5 Hz, 2H, CH_2), 3.81 (d, J = 13.5 Hz, 2H, CH_2Ph), 3.89–3.99 (m, 2H, CH_2O), 4.13 (m, 1H, CH), 6.81–6.93 (m, 2H, ArH), 7.18 (m, 1H, ArH), 7.22–7.30 (m, 2H, ArH), 7.30–7.36 (m, 9H, ArH). ^{13}C NMR (101 MHz, $CDCl_3$) δ 56.1 (CH_2N), 59.0 ($2CH_2Ph$), 66.6 (CH), 71.3 (CH_2O), 113.7 (2CHAr), 121.7 (2CHAr), 123.2 (CAr),

127.4 (2CHAr), 127.8 (2CHAr), 128.6 (2CHAr), 129.2 (2CHAr), 130.3 (2CHAr), 138.6 (2CAr), 154.3 (OCAr). HRMS $C_{23}H_{25}ClNO_2$ $[M + H]^+$ 382.1568; found 382.1570. Purity 96.90% (t_R = 3.27 min).

4.1.10. 1-(Dibenzylamino)-3-(p-tolyloxy)propan-2-ol (**8**)

Following the general procedure, dibenzylamine (CAS 103-49-1) (0.20 mL, 1.04 mmol) and 2-[(*p*-tolyloxy)methyl]oxirane (170 mg, 1.04 mmol) afforded **8** (300 mg, 80%) as a white solid after column chromatography (hexane/DCM 9:1 to 8:2). Mp 55–57 °C (EtOAc). IR (ATR) 3419, 3028, 2938, 2805, 1615, 1511, 1238, 1044, 803, 744, 697 cm^{-1}. ^1H NMR (400 MHz, $CDCl_3$, HETCOR) δ 2.27 (s, 3H, CH_3), 2.66 (d, *J* = 7.5 Hz, 2H, CH_2N), 3.18 (s, 1H, OH), 3.53 (d, *J* = 13.5 Hz, 2H, CH_2Ph), 3.79 (d, *J* = 13.5 Hz, 2H, CH_2Ph), 3.84 (d, *J* = 5.5 Hz, 2H, CH_2O), 4.04–4.14 (m, 1H, CH), 6.74 (d, *J* = 8.5 Hz, 2H, ArH), 7.04 (d, 2H, ArH), 7.32 (m, *J* = 3.0 Hz, 10H, ArH). ^{13}C NMR (101 MHz, $CDCl_3$) δ 20.6 (CH_3), 56.3 (CH_2N), 58.8 ($2CH_2Ph$), 66.7 (CH), 70.6 (CH_2O), 114.5 (2CHAr), 127.4 (2CHAr), 128.6 (4CHAr), 129.2 (4CHAr), 130.0 (CAr), 130.2 (2CHAr), 138.7 (2CAr), 156.7 (OCAr). HRMS $C_{24}H_{28}NO_2$ $[M + H]^+$ 362.2115; found 362.2115. Purity 97.23% (t_R = 3.35 min).

4.1.11. 1-(Dibenzylamino)-3-(4-isopropylphenoxy)propan-2-ol (**9**)

Following the general procedure, dibenzylamine (CAS 103-49-1) (0.25 mL, 1.30 mmol) and 2-[(4-isopropylphenoxy)methyl]oxirane (253 mg, 1.32 mmol) afforded **9** (320 mg, 62%) as a white solid after column chromatography (hexane/DCM 9:1 to 8:2). Mp 70–72 °C (EtOAc). IR (ATR) 3449, 3027, 1609, 1513, 1455, 1245, 1039, 838, 745, 696 cm^{-1}. ^1H NMR (400 MHz, $CDCl_3$, HETCOR) δ 1.21 (d, *J* = 7.0 Hz, 6H, CH_3), 2.63–2.69 (m, 2H, CH_2N), 2.85 (m, *J* = 7.0 Hz, 1H, CH), 3.17 (s, 1H, OH), 3.53 (d, *J* = 13.5 Hz, 2H, CH_2Ph), 3.79 (d, *J* = 13.5 Hz, 2H, CH_2Ph), 3.85 (d, *J* = 5.5 Hz, 2H, CH_2O), 4.04–4.14 (m, 1H, CH), 6.77 (d, *J* = 9.0 Hz, 2H, ArH), 7.11 (d, *J* = 8.5 Hz, 2H, ArH), 7.25–7.36 (m, 10H, ArH). ^{13}C NMR (101 MHz, $CDCl_3$) δ 24.3 ($2CH_3$), 33.4 (CH), 56.4 (CH_2N), 58.9 ($2CH_2Ph$), 66.7 (CH), 70.5 (CH_2O), 114.4 (2CHAr), 127.3 (2CHAr), 127.4 (2CHAr), 128.6 (4CHAr), 129.2 (4CHAr), 138.7 (2CAr), 141.5 (CAr), 156.9 (OCAr). HRMS $C_{26}H_{32}NO_2$ $[M + H]^+$ 390.2428; found 390.2427. Purity 98.32% (t_R = 3.63 min).

4.1.12. 1-[4-(Tert-butyl)phenoxy]-3-(dibenzylamino)propan-2-ol (**10**)

Following the general procedure, dibenzylamine (CAS 103-49-1) (0.24 mL, 1.25 mmol) and 2-{[4-(*tert*-butyl)phenoxy]methyl}oxirane (261 mg, 1.27 mmol) afforded **10** (375 mg, 74%) as a white solid after column chromatography (hexane/DCM 9:1 to 8:2). Mp 80–83 °C (EtOAc). IR (ATR) 3432, 3028, 2963, 1605, 1513, 1247, 1042, 828, 746, 698 cm^{-1}. ^1H NMR (400 MHz, $CDCl_3$, HETCOR) δ 1.29 (s, 9H, $3CH_3$), 2.61–2.70 (m, 2H, CH_2N), 3.16 (s, 1H, OH), 3.53 (d, *J* = 13.5 Hz, 2H, CH_2Ph), 3.79 (d, *J* = 13.5 Hz, 2H, CH_2Ph), 3.85 (d, *J* = 5.5 Hz, 2H, CH_2O), 4.05–4.12 (m, 1H, CH), 6.78 (d, *J* = 9.0 Hz, 2H, ArH), 7.24 (m, 2H, ArH), 7.26–7.35 (m, 10H, ArH). ^{13}C NMR (101 MHz, $CDCl_3$) δ 31.7 ($3CH_3$), 34.2 (C), 56.4 (CH_2N), 58.9 ($2CH_2Ph$), 66.7 (CH), 70.5 (CH_2O), 114.1 (2CHAr), 126.3 (2CHAr), 127.4 (2CHAr), 128.6 (4CHAr), 129.2 (4CHAr), 138.7 (2CAr), 143.7 (CAr), 156.5 (OCAr). HRMS $C_{27}H_{34}NO_2$ $[M + H]^+$ 404.2584; found 404.2590. Purity 100% (t_R = 3.62 min).

4.1.13. 1-(4-Cyclohexylphenoxy)-3-(dibenzylamino)propan-2-ol (**11**)

Following the general procedure, dibenzylamine (CAS 103-49-1) (0.21 mL, 1.09 mmol) and 2-[(4-cyclohexylphenoxy)methyl]oxirane (253 mg, 1.09 mmol) afforded **11** (340 mg, 73%) as a white solid after column chromatography (hexane/DCM 9:1 to 8:2). Mp 113–115 °C (EtOAc). IR (ATR) 3427, 3028, 2928, 1512, 1515, 1248, 1047, 809, 744, 696 cm^{-1}. ^1H NMR (400 MHz, $CDCl_3$, HETCOR) δ 1.18–1.31 (m, 1H, CH_2cycl), 1.31–1.46 (m, 4H, $2CH_2$cycl), 1.75 (m, 1H, CH_2cycl), 1.78–1.91 (m, 4H, $2CH_2$cycl), 2.39–2.51 (m, 1H, CHcycl), 2.63–2.75 (m, 2H, CH_2N), 3.18 (s, 1H, OH), 3.55 (d, *J* = 13.5 Hz, 2H, CH_2Ph), 3.80 (d, *J* = 13.5 Hz, 2H, CH_2 Ph), 3.86 (d, *J* = 5.5 Hz, 2H, CH_2O), 4.05–4.15 (m, 1H, CH), 6.78 (d, *J* = 9.8 Hz, 2H, ArH), 7.11 (d, *J* = 6.5 Hz, 2H, ArH), 7.24–7.31 (m, 2H, ArH), 7.30–7.39 (m, 8H, ArH). ^{13}C

NMR (101 MHz, $CDCl_3$) 26.3 (CH_2cycl), 27.1 (2CH_2cycl), 34.8 (2CH_2cycl), 43.8 (CHcycl), 56.4 (CH_2N), 58.9 (2CH_2Ph), 66.7 (CH), 70.5 (CH_2O), 114.4 (2CHAr), 127.4 (2CHAr), 127.7 (2CHAr), 128.6 (4CHAr), 129.2 (4CHAr), 138.7 (2CAr), 140.8 (CAr), 156.9 (OCAr). HRMS $C_{29}H_{36}NO_2$ $[M + H]^+$ 430.2741; found 430.2736. Purity 99.24% (t_R = 3.88 min).

4.1.14. 1-(4-Cyclopentylphenoxy)-3-(dibenzylamino)propan-2-ol (**12**)

Following the general procedure, dibenzylamine (CAS 103-49-1) (0.23 mL, 1.19 mmol) and 2-[(4-cyclopentylphenoxy)methyl]oxirane (257 mg, 1.18 mmol) afforded **12** (295 mg, 60%) as a white solid after column chromatography (hexane/DCM 9:1 to 8:2). Mp 88–90 °C (EtOAc). IR (ATR) 3413, 2938, 1610, 1511, 1451, 1242, 1044, 824, 747, 698 cm^{-1}. ^1H NMR (400 MHz, $CDCl_3$, HETCOR) δ1.48–1.60 (m, 2H, CH_2cycl), 1.62–1.71 (m, 2H, CH_2cycl), 1.73–1.83 (m, 2H, CH_2cycl), 1.96–2.09 (m, 2H, CH_2cycl), 2.63–2.69 (m, 2H, CH_2N), 2.86–2.99 (m, 1H, CHcycl), 3.53 (d, *J* = 13.5 Hz, 2H, CH_2Ph), 3.79 (d, *J* = 13.5 Hz, 2H, CH_2Ph), 3.84 (d, mboxemphJ = 5.5 Hz, 2H, CH_2O), 4.05–4.11 (m, 1H, CH), 6.73–6.80 (d, 2H, ArH), 7.09–7.16 (d, 2H, ArH), 7.22–7.37 (m, 10H, ArH). ^{13}C NMR (101 MHz, $CDCl_3$) δ 25.5 (2CH_2cycl), 34.8 (2CH_2cycl), 45.3 (CHcycl), 56.3 (CH_2), 58.9 (2CH_2Ph), 66.7 (CH), 70.6 (CH_2), 114.4 (2CHAr), 127.4 (2CHAr), 128.0 (2CHAr), 128.6 (4CHAr), 129.2 (4CHAr), 138.7 (CAr), 139.0 (2CAr), 156.9 (OCAr). HRMS $C_{28}H_{34}NO_2$ $[M + H]^+$ 416.2584; found 416.2591. Purity 100% (t_R = 3.66 min).

4.1.15. 1-(Dibenzylamino)-3-(3,4-dimethylphenoxy)propan-2-ol (**13**)

Following the general procedure, dibenzylamine (CAS 103-49-1) (0.37 mL, 1.92 mmol) and 2-[(3,4-dimethylphenoxy)methyl]oxirane (347 mg, 1.95 mmol) afforded **13** (555 mg, 76%) as an oil after column chromatography (hexane/DCM 9:1 to 8:2). IR (ATR) 3435, 3026, 2921, 1607, 1501, 1452, 1252, 1046, 735, 697 cm^{-1}. ^1H NMR (400 MHz, $CDCl_3$, HETCOR) δ 2.18 (s, 3H, CH_3), 2.21 (s, 3H, CH_3), 2.62–2.73 (m, 2H, CH_2N), 3.54 (d, *J* = 13.5 Hz, 2H, CH_2Ph), 3.79 (d, *J* = 13.5 Hz, 2H, CH_2Ph), 3.83 (d, *J* = 5.0 Hz, 2H, CH_2O), 4.02–4.14 (m, 1H, CH), 6.58 (dd, *J* = 8.5, 3.0 Hz, 1H, ArH), 6.65 (d, *J* = 3.0 Hz, 1H, ArH), 7.00 (d, *J* = 8.3 Hz, 1H, ArH), 7.21–7.42 (m, 10H, ArH). ^{13}C NMR (101 MHz, $CDCl_3$) δ 18.9 (CH_3), 20.1 (CH_3), 56.3 (CH_2N), 58.8 (2CH_2Ph), 66.7 (CH), 70.6 (CH_2O), 111.6 (CHAr), 116.2 (CHAr), 127.4 (2CHAr), 128.6 (4CHAr), 129.0 (CHAr), 129.2 (4CHAr), 130.4 (CAr), 137.8 (CAr), 138.7 (2CAr), 157.0 (OCAr). HRMS $C_{25}H_{30}NO_2$ $[M + H]^+$ 376.2271; found 376.2270. Purity 97.06% (t_R = 3.35 min).

4.1.16. 1-(Dibenzylamino)-3-(4-methoxyphenoxy)propan-2-ol (**14**)

Following the general procedure, dibenzylamine (CAS 103-49-1) (0.13 mL, 0.70 mmol) and 2-[(4-methoxyphenoxy)methyl]oxirane (126 mg, 0.70 mmol) afforded **14** (170 mg, 64%) as a white solid after column chromatography (hexane/DCM 9:1 to 8:2). Mp 61–63 °C (EtOAc). IR (ATR) 3417, 2925, 1505, 1451, 1231, 1044, 1028, 822, 744, 697 cm^{-1}. ^1H NMR (400 MHz, $CDCl_3$, HETCOR) δ 2.67 (d, *J* = 7.5 Hz, 2H, CH_2N), 3.54 (d, *J* = 13.5 Hz, 2H, CH_2Ph), 3.76 (s, 3H, CH_3), 3.77 (d, *J* = 13.5 Hz, 2H, CH_2Ph), 3.78–3.85 (m, 2H, CH_2O), 4.08 (m, 1H, CH), 6.75–6.83 (m, 4H, ArH), 7.23–7.37 (m, 10H, ArH). ^{13}C NMR (101 MHz, $CDCl_3$) δ 55.9 (CH_3), 56.3 (CH_2N), 58.9 (2CH_2Ph), 66.7 (CH), 71.2 (CH_2O), 114.7 (2CHAr), 115.6 (2CHAr), 127.4 (2CHAr), 128.6 (4CHAr), 129.2 (4CHAr), 138.7 (2CAr), 153.0 (CAr), 154.1 (OCAr). HRMS $C_{24}H_{28}NO_3$ $[M + H]^+$ 378.2064; found 378.2062. Purity 98.43% (t_R = 3.02 min).

4.1.17. 1-[4-(Benzyloxy)phenoxy]-3-(dibenzylamino)propan-2-ol (**15**)

Following the general procedure, dibenzylamine (CAS 103-49-1) (0.19 mL, 0.99 mmol) and 2-{[4-(benzyloxy)phenoxy]methyl}oxirane (247 mg, 0.96 mmol) afforded **15** (325 mg, 74%) as a white solid after column chromatography (hexane/DCM 9:1 to 8:2). Mp 87–88 °C (EtOAc). IR (ATR) 3454, 3027, 2795, 1602, 1509, 1235, 1041, 825, 731, 696 cm^{-1}. ^1H NMR (400 MHz, $CDCl_3$, HETCOR) δ 2.63–2.68 (m, 2H, CH_2N), 3.17 (s, 1H, OH), 3.53 (d, *J* = 13.5 Hz, 2H, CH_2Ph), 3.75–3.84 (m, 4H, 2CH_2Ph), 4.07 (m, *J* = 5.8 Hz, 1H, CH), 5.00 (s, 2H, PhCH_2O), 6.73–6.80 (m, 2H, ArH), 6.83–6.90 (m, 2H, ArH), 7.22–7.44 (m, 15H, ArH).

^{13}C NMR (101 MHz, $CDCl_3$) δ 56.3 (CH_2N), 58.9 ($2CH_2Ph$), 66.7 (CH), 70.8 ($PhCH_2O$), 71.1 (CH_2O), 115.5 (2CHAr), 115.9 (2CHAr), 127.4 (2CHAr), 127.6 (2CHAr), 128.0 (CHAr), 128.6 (4CHAr), 128.7 (2CHAr), 129.2 (4CHAr), 137.4 (2CAr), 138.7 (CAr), 153.1 (CAr), 153.2 (OCAr). HRMS $C_{30}H_{32}NO_3$ $[M + H]^+$ 454.2377; found 454.2385. Purity 96.19% (t_R = 3.43 min).

4.1.18. 1-(Dibenzylamino)-3-(4-propoxyphenoxy)propan-2-ol (**16**)

Following the general procedure, dibenzylamine (CAS 103-49-1) (0.46 mL, 2.38 mmol) and 2-[(4-propoxyphenoxy)methyl]oxirane (490 mg, 2.35 mmol) afforded **16** (620 mg, 65%) as a white solid after column chromatography (hexane/DCM 9:1 to 8:2). Mp 51–53 °C (EtOAc). IR (ATR) 3380, 3027, 2921, 1589, 1508, 1228, 1048, 827, 747, 697 cm^{-1}. ^{1}H NMR (400 MHz, $CDCl_3$, HETCOR) δ 1.02 (t, *J* = 7.5 Hz, 3H, CH_3), 1.71–1.84 (m, 2H, OCH_2CH_2), 2.63–2.69 (m, 2H, CH_2N), 3.54 (d, *J* = 13.5 Hz, 2H, CH_2Ph), 3.80 (d, *J* = 13.5 Hz, 2H, CH_2Ph), 3.86 (t, *J* = 6.4 Hz, 2H, OCH_2), 4.08 (m, 1H, CH), 6.73–6.84 (m, 4H, ArH), 7.26–7.37 (m, 10H, ArH).^{13}C NMR (101 MHz, $CDCl_3$) δ 10.7 (CH_3), 22.8 (OCH_2CH_2), 56.3 (CH_2N), 58.9 ($2CH_2Ph$), 66.7 (CH), 70.3 (CH_2O), 71.2 (OCH_2), 115.5 (2CHAr), 115.5 (2CHAr), 127.4 (2CHAr), 128.6 (4CHAr), 129.2 (4CHAr), 138.7 (2CAr), 152.9 (CAr), 153.6 (OCAr). HRMS $C_{26}H_{32}NO_3$ $[M + H]^+$ 406.2377; found 406.2379. Purity 98.33% (t_R = 3.33 min).

4.1.19. 1-(Dibenzylamino)-3-(3,4-dichlorophenoxy)propan-2-ol (**17**)

Following the general procedure, dibenzylamine (CAS 103-49-1) (0.45 mL, 2.35 mmol) and 2-[(3,4-dichlorophenoxy)methyl]oxirane (510 mg, 2.33 mmol) afforded **17** (882 mg, 91%) as an oil after column chromatography (hexane/DCM 9:1 to 8:2). IR (ATR) 3425, 3027, 2931, 1592, 1451, 1230, 1026, 839, 735, 698 cm^{-1}. ^{1}H NMR (400 MHz, $CDCl_3$, HETCOR) δ 2.61–2.67 (m, 2H, CH_2N), 3.17 (s, 1H, OH), 3.53 (d, *J* = 13.0 Hz, 2H, CH_2Ph), 3.73–3.78 (m, 4H, CH_2Ph, CH_2O), 4.03 (m, 1H, CH), 6.67 (dd, *J* = 9.0, 3.0 Hz, 1H, ArH), 6.89 (d, *J* = 3.0 Hz, 1H, ArH), 7.22–7.28 (m, 1H, ArH), 7.28–7.36 (m, 10H, ArH). ^{13}C NMR (101 MHz, $CDCl_3$) δ 55.9 (CH_2N), 59.0 ($2CH_2Ph$), 66.4 (CH), 71.0 (CH_2O), 114.7 (CHAr), 116.5 (CHAr), 124.3 (CAr), 127.6 (2CHAr), 128.6 (4CHAr), 129.2 (4CHAr), 130.7 (CHAr), 132.9 (CAr), 138.5 (2CAr), 157.9 (OCAr). HRMS $C_{23}H_{24}Cl_2NO_2$ $[M + H]^+$ 416.1179; found 416.1176. Purity 96.24% (t_R = 3.59 min).

4.1.20. 1-[4-Chloro-3-(trifluoromethyl)phenoxy]-3-(dibenzylamino)propan-2-ol (**18**)

Following the general procedure, dibenzylamine (CAS 103-49-1) (0.40 mL, 2.10 mmol) and 2-{[4-chloro-3-(trifluoromethyl)phenoxy]methyl}oxirane (529 mg, 2.10 mmol) afforded **18** (878 mg, 93%) as an oil after column chromatography (hexane/DCM 9:1 to 8:2). IR (ATR) 3433, 3028, 1606, 1482, 1423, 1239, 1027, 816, 747, 698 cm^{-1}. ^{1}H NMR (400 MHz, $CDCl_3$, HETCOR) δ 2.63–2.69 (m, 2H, CH_2N), 3.20 (s, 1H, OH), 3.54 (d, *J* = 13.0 Hz, 2H, CH_2Ph), 3.85 (m, 2H, CH_2O), 4.04 (m, 1H, CH), 6.90 (dd, *J* = 9.0, 3.0 Hz, 1H, ArH), 7.11 (d, *J* = 3.0 Hz, 1H, ArH), 7.22–7.38 (m, 11H, ArH). ^{13}C NMR (101 MHz, $CDCl_3$) δ 55.8 (CH_2N), 59.0 ($2CH_2Ph$), 66.4 (CH), 70.9 (CH_2O), 114.2 (q, *J* = 5.5 Hz, CHAr), 118.7 (CHAr), 121.4 (CAr), 123.5 (CF_3), 124.1 (CAr), 127.6 (2CHAr), 128.6 (4CHAr), 129.2 (4CHAr), 132.4 (CHAr), 138.5 (2CAr), 157.2 (OCAr). HRMS $C_{24}H_{24}ClF_3NO_2$ $[M + H]^+$ 450.1442; found 450.1448. Purity 99.79% (t_R = 3.72 min).

4.1.21. 1-(Dibenzylamino)-3-[4-nitro-3-(trifluoromethyl)phenoxy]propan-2-ol (**19**)

Following the general procedure, dibenzylamine (CAS 103-49-1) (0.45 mL, 2.34 mmol) and 2-{[4-nitro-3-(trifluoromethyl)phenoxy]methyl}oxirane (609 mg, 2.31 mmol) afforded **19** (619 mg, 58%) as an oil after column chromatography (hexane/DCM 9:1 to 8:2). IR (ATR) 3424, 2931, 1453, 1310, 1242, 1038, 1027, 834, 748, 698 cm^{-1}. ^{1}H NMR (400 MHz, $CDCl_3$, HETCOR) δ 1H NMR (400 MHz, CDCl3) δ 2.56–2.75 (m, 2H, CH_2N), 3.55 (d, *J* = 13.0 Hz, 2H, CH_2Ph), 3.80 (d, *J* = 13.0 Hz, 2H, CH_2Ph), 3.88–4.01 (m, 2H, CH_2O), 4.01–4.10 (m, 1H, CH), 7.01 (dd, *J* = 9.0, 3.0 Hz, 1H, ArH), 7.18 (d, *J* = 2.5 Hz, 1H, ArH), 7.23–7.43 (m, 10H, ArH), 7.95 (d, *J* = 9.5 Hz, 1H, ArH). ^{13}C NMR (101 MHz, $CDCl_3$) δ 55.5 (CH_2N), 59.1

(2CH_2Ph), 66.3 (CH), 71.3 (CH_2O), 115.0 (q, *J* = 6.0 Hz, CF_3), 116.8 (CHAr), 120.6 (CHAr), 123.3 (CAr), 126.2 (q, *J* = 34.0 Hz, CF_3), 127.6 (2CAr), 128.1 (CAr), 128.7 (4CAr), 129.2 (4CAr), 138.4 (2CAr), 141.1 (CAr), 161.9 (OCAr). HRMS $C_{24}H_{24}F_3N_2O_4$ $[M + H]^+$ 461.1683; found 461.1681. Purity 98.68% (t_R = 3.50 min).

4.1.22. 1-(Dibenzylamino)-3-(2,4-dichlorophenoxy)propan-2-ol (**20**)

Following the general procedure, dibenzylamine (CAS 103-49-1) (0.48 mL, 2.49 mmol) and 2-[(2,4-dichlorophenoxy)methyl]oxirane (551 mg, 2.52 mmol) afforded **20** (642 mg, 61%) as an oil after column chromatography (hexane/DCM 9:1 to 8:2). IR (ATR) 3426, 3027, 2803, 1585, 1482, 1290, 1062, 802, 744, 697 cm^{-1}. ^{1}H NMR (400 MHz, $CDCl_3$, HETCOR) δ 2.64–2.70 (m, 2H, CH_2N), 3.49 (d, *J* = 13.5 Hz, 2H, CH_2Ph), 3.74 (d, *J* = 13.5 Hz, 2H, CH_2Ph), 3.79–3.90 (m, 2H, CH_2O), 3.99–4.08 (m, 1H, CH), 6.69 (d, *J* = 9.0 Hz, 1H, ArH), 7.08 (dd, *J* = 9.0, 2.5 Hz, 1H, ArH), 7.16–7.31 (m, 11H, ArH). ^{13}C NMR (101 MHz, $CDCl_3$) δ 55.9 (CH_2N), 59.0 (2CH_2Ph), 66.5 (CH), 71.6 (CH_2O), 114.4 (CHAr), 124.0 (CHAr), 126.1 (2CHAr), 127.5 (4CHAr), 127.6 (CAr), 128.6 (4CHAr), 129.2 (2CHAr), 130.0 (CAr), 138.6 (2CAr), 153.2 (OCAr). HRMS $C_{23}H_{24}Cl_2NO_2$ $[M + H]^+$ 416.1179; found 416.1179. Purity 95.03% (t_R = 3.58 min).

4.1.23. 1-(4-Bromophenoxy)-3-(dibenzylamino)propan-2-ol (**21**)

Following the general procedure, dibenzylamine (CAS 103-49-1) (0.42 mL, 2.21 mmol) and 2-[(4-bromophenoxy)methyl]oxirane (500 mg, 2.18 mmol) afforded **21** (800 mg, 86%) as a white solid after column chromatography (hexane/EtOAc 9:1 to 8:2). Mp 63–65 °C (EtOAc). IR (ATR) 3568, 3413, 3031, 2936, 1587, 1488, 1243, 1036, 830, 804, 744, 733, 698 cm^{-1}. ^{1}H NMR (500 MHz, $CDCl_3$, HETCOR) δ 2.66 (d, *J* = 7.0 Hz, 2H, CH_2N), 3.19 (s, 1H, OH), 3.54 (d, *J* = 13.5 Hz, 2H, CH_2Ph), 3.80 (d, *J* = 13.5 Hz, 2H, CH_2Ph), 3.83 (m, 2H, CH_2O), 4.03–4.14 (m, 1H, CH), 6.68–6.74 (m, 2H, ArH), 7.23–7.30 (m, 2H, ArH), 7.30–7.42 (m, 10H, ArH). ^{13}C NMR (101 MHz, $CDCl_3$) δ 56.1 (CH_2N), 58.9 (2CH_2Ph), 66.5 (CH), 70.7 (CH_2O), 113.2 (CAr), 116.5 (2CHAr), 127.5 (2CHAr), 128.6 (4CHAr), 129.2 (4CHAr), 132.3 (2CHAr), 138.6 (2CAr), 157.9 (OCAr). HRMS $C_{23}H_{25}BrNO_2$ $[M + H]^+$ 426.1063; found 426.1064. Purity 97.85% (t_R = 4.17 min).

4.1.24. 1-(Dibenzylamino)-3-(4-nitrophenoxy)propan-2-ol (**22**)

Following the general procedure, dibenzylamine (CAS 103-49-1) (0.45 mL, 2.33 mmol) and 2-[(4-nitrophenoxy)methyl]oxirane (450 mg, 2.31 mmol) afforded **22** (610 mg, 67.4%) as an oil after column chromatography (hexane/EtOAc 9:1 to 8:2). IR (ATR) 3427, 3028, 2931, 1592, 1509, 1496, 1331, 1259, 1109, 1026, 842, 750, 697 cm^{-1}. ^{1}H NMR (500 MHz, $CDCl_3$, HETCOR) δ 2.60–2.74 (m, 2H, CH_2N), 3.25 (s, 1H, OH), 3.55 (d, *J* = 13.5 Hz, 2H, CH_2Ph), 3.82 (d, *J* = 13.5 Hz, 2H, CH_2Ph), 3.91 (dd, *J* = 10, 4.5 Hz, 1H, CH_2O), 3.95 (dd, *J* = 10, 4.5 Hz, 1H, CH_2O), 4.08(m, 1H, CH), 6.87 (m, 2H, ArH), 7.23 -7.41 (m, 10H, ArH), 8.11–8.22 (m, 2H, ArH). ^{13}C NMR (126 MHz, $CDCl_3$) δ 55.8 (CH_2N), 59.0 (2CH_2Ph), 66.3 (CH), 71.1 (CH_2O), 114.7 (CHAr), 126.0 (2CHAr), 127.6 (2CHAr), 128.7 (4CHAr), 129.2 (4CHAr), 138.5 (2CAr), 141.8 (CAr), 163.8 (OCAr). HRMS $C_{23}H_{24}N_2O_4$ $[M + H]^+$ 393.1809; found 393.1814. Purity 96.42% (t_R = 4 min).

4.1.25. 1-(Dibenzylamino)-3-(4-iodophenoxy)propan-2-ol (**23**)

Following the general procedure, dibenzylamine (CAS 103-49-1) (0.33 mL, 1.7 mmol) and 2-[(4-iodophenoxy)methyl]oxirane (465 mg, 1.68 mmol) afforded **23** (525 mg, 65.8%) as a white solid after column chromatography (hexane/EtOAc 9:1 to 8:2). Mp 103–105 °C (EtOAc). IR (ATR) 3406, 3030, 2936, 1580, 1484, 1282, 1246, 1035, 828, 803, 744, 697 cm^{-1}. ^{1}H NMR (500 MHz, $CDCl_3$, HETCOR) δ 2.66 (d, *J* = 7.0 Hz, 2H, CH_2N), 3.19 (s, 1H, OH), 3.54 (d, *J* = 13.5 Hz, 2H, CH_2Ph), 3.79 (d, *J* = 13.5 Hz, 2H, CH_2Ph), 3.74–3.87 (m, 2H, CH_2O), 4.07 (m, 1H, CH), 6.58–6.64 (m, 2H, ArH), 7.19–7.38 (m, 10H, ArH), 7.49–7.56 (m, 2H, ArH). ^{13}C NMR (126 MHz, $CDCl_3$) δ 56.1 (CH_2N), 58.9 (2CH_2Ph), 66.5 (CH), 70.5 (CH_2O), 83.1 (CAr), 117.1 (2CHAr), 127.5 (2CHAr), 128.6 (4CHAr), 129.2 (4CHAr), 138.3 (2CAr), 138.6

(2CHAr), 158.7 (CAr). HRMS $C_{23}H_{24}INO_2$ $[M + H]^+$ 474.0924; found 474.0927. Purity 96.40% (t_R = 4.26 min).

4.1.26. 1-(Dibenzylamino)-3-[4-(pentafluoro-λ6-sulfaneyl)phenoxy]propan-2-ol (**24**)

Following the general procedure, dibenzylamine (CAS 103-49-1) (0.45 mL, 2.33 mmol) and 2-[(4-(pentafluoro-λ6-sulfaneyl)phenoxy)methyl]oxirane (643 mg, 2.33 mmol) afforded **24** (657 mg, 59.6%) as a white solid after column chromatography (hexane/EtOAc 9:1 to 8:2). Mp 67–69^{0}C (EtOAc). IR (ATR) 3414, 3028, 2938, 1597, 1504, 1451, 1309, 1264, 1101, 1037, 844, 826, 806, 745, 698, 595, 579 cm^{-1}. ^{1}H NMR (500 MHz, $CDCl_3$, HETCOR) δ 2.67 (d, *J* = 6.0 Hz, 2H, CH_2N), 3.21 (s, 1H, OH), 3.54 (d, *J* = 13.5 Hz, 2H, CH_2Ph), 3.81 (d, *J* = 13.5 Hz, 2H, CH_2Ph), 3.85–3.94 (m, 2H, CH_2O), 4.03–4.10 (m, 1H, CH), 6.83 (d, *J* = 9.5 Hz, 2ArH), 7.19–7.38 (m, 10H, ArH), 7.61–7.68 (m, 2H, ArH).^{13}C NMR (126 MHz, $CDCl_3$) δ 56.0 (CH_2N), 59.0 ($2CH_2Ph$), 66.4 (CH), 70.8 (CH_2O), 114.2 (2CHAr), 127.6 (4CHAr), 127.7 (m, C-SF_5), 128.7 (4CHAr), 129.2 (4CHAr), 138.5 (2CAr), 160.6 (OCAr). HRMS $C_{23}H_{24}F_5NO_2S$ $[M + H]^+$ 474.1521; found 474.1524. Purity 95.25% (t_R = 4.36 min).

4.1.27. 1-[Benzyl(4-chlorobenzyl)amino]-3-(4-chlorophenoxy)propan-2-ol (**25**)

Following the general procedure, *N*-benzyl-1-(4-chlorophenyl)methanamine (CAS 13541-00-9) (0.14 mL, 0.70 mmol) and 2-[(4-chlorophenoxy)methyl]oxirane (130 mg, 0.70 mmol) afforded **25** (182.5 mg, 62.3%) as an oil after column chromatography (hexane/EtOAc 9:1 to 8:2). IR (ATR) 3426, 3026, 2932, 1590, 1485, 1445, 1276, 1248, 1087, 1063, 1015, 801, 743, 697 cm^{-1}. ^{1}H NMR (400 MHz, $CDCl_3$, HETCOR) δ 2.72 (dd, *J* = 6.5, 2.0 Hz, 2H, CH_2N), 3.54 (dd, *J* = 13.5, 11 Hz, 2H, CH_2Ph), 3.74 (t, *J* = 13.5 Hz, 2H, CH_2Ph), 3.90–3.95 (m, 2H, CH_2O), 4.06–4.13 (m, 1H, CH), 6.83 (dd, *J* = 8.5, 1.5 Hz, 1H, ArH), 6.88 (td, *J* = 7.5, 1.5 Hz, 1H, ArH), 7.18 (ddd, *J* = 8.5, 7.5, 1.5 Hz, 1H, ArH), 7.22–7.36 (m, 10H, ArH). ^{13}C NMR (101 MHz, $CDCl_3$) δ 56.1 (CH_2N), 58.3 (CH_2Ph), 59.0 (CH_2Ph), 66.8 (CH), 71.2 (CH_2O), 113.6 (CHAr), 121.8 (CHAr), 123.2 (CAr), 127.5 (CHAr), 127.8 (CHAr), 128.6 (2CHAr), 128.7 (2CHAr), 129.2 (2CHAr), 130.4 (CHAr), 130.5 (2CHAr), 133.2 (CAr), 137.3 (CAr), 138.5 (CAr), 154.2 (CAr). HRMS $C_{23}H_{23}Cl_2NO_2$ $[M + H]^+$ 416.1179; found 4161191. Purity 95.59% (t_R = 4.45 min).

4.1.28. 1-[Bis(4-chlorobenzyl)amino]-3-(4-chlorophenoxy)propan-2-ol (**26**)

Following the general procedure, bis(4-chlorobenzyl)amine (CAS 21913-13-3)(150 mg, 0.56 mmol) and 2-[(4-chlorophenoxy)methyl]oxirane (104 mg, 0.56 mmol) afforded **26** (194.2 mg, 76.4%) as an oil after column chromatography (hexane/EtOAc 9:1 to 8:2). IR (ATR) 3438, 3058, 2921, 1740, 1589, 1486, 1447, 1248, 1087, 1062, 1014, 807, 746 cm^{-1}. ^{1}H NMR (400 MHz, $CDCl_3$) δ 2.63–2.77 (m, 2H, CH_2N), 2.96 (s, 1H, OH), 3.52 (d, *J* = 13.5 Hz, 2H, CH_2Ph), 3.69 (d, *J* = 13.5 Hz, 2H, CH_2Ph), 3.90–3.94 (m, 2H, CH_2O), 4.06–4.14 (m, 1H, CH), 6.82 (dd, *J* = 8.5, 1.5 Hz, 1H, ArH), 6.89 (td, *J* = 7.5, 1.5 Hz, 1H, ArH), 7.15–7.29 (m, 9H, ArH), 7.33 (dd, *J* = 8.0, 1.5 Hz, 1H, ArH). ^{13}C NMR (101 MHz, $CDCl_3$) δ 56.0 (CH_2N), 58.3 ($2CH_2Ph$), 66.9 (CH), 71.0 (CH_2O), 113.6 (CHAr), 121.9 (CHAr), 123.1 (CAr), 127.9 (CHAr), 128.8 (4CHAr), 130.4 (CHAr), 130.4 (4CHAr), 133.3 (2CAr), 137.1 (2CAr), 154.1 (CAr). HRMS $C_{23}H_{22}Cl_3NO_2$ $[M + H]^+$ 450.0789; found 450.9787. Purity 99.45% (t_R = 5.24 min).

4.1.29. 1-[Benzyl(4-methylbenzyl)amino]-3-(4-chlorophenoxy)propan-2-ol (**27**)

Following the general procedure, *N*-benzyl-1-(*p*-tolyl)methanamine (CAS 55096-86-1) (148.8 mg, 0.70 mmol) and 2-[(4-chlorophenoxy)methyl]oxirane (130 mg, 0.70 mmol) afforded **27** (119,5 mg, 42.9%) as an oil after column chromatography (hexane/EtOAc 9:1 to 8:2). IR (ATR) 3436, 3028, 2924, 1589, 1485, 1446, 1277, 1249, 1061, 1028, 801, 744, 697 cm^{-1}. ^{1}H NMR (400 MHz, $CDCl_3$, HETCOR) δ 2.33 (s, 3H, CH_3), 2.73 (d, *J* = 6.5 Hz, 2H, CH_2N), 3.53 (t, *J* = 13.0 Hz, 2H, CH_2Ph), 3.80 (t, *J* = 14.0 Hz, 2H, CH_2Ph), 3.91–4.00 (m, 2H, CH_2O), 4.11 (m, 1H, CH), 6.84 (dd, *J* = 8.0, 1.5 Hz, 1H, ArH), 6.89 (td, *J* = 7.5, 1.5 Hz, 1H, ArH), 7.11–7.38 (m, 11H, ArH). ^{13}C NMR (101 MHz, $CDCl_3$) δ 21.3 (CH_3), 56.0 (CH_2N), 58.6 (CH_2Ph), 58.9 (CH_2Ph), 66.6 (CH), 71.3 (CH_2O), 113.6 (CHAr), 121.7 (CHAr), 123.2

(CAr), 127.4 (CHAr), 127.8 (CHAr), 128.6 (4CHAr), 129.1–129.3 (4CHAr), 130.3 (CHAr), 135.5 (CAr), 137.0 (CAr), 138.8 (CAr), 154.3 (CAr). HRMS $C_{24}H_{26}ClNO_2$ $[M + H]^+$ 396.1729; found 396.1725. Purity 95.30% (t_R = 4.12 min).

4.1.30. 1-[Bis(4-methylbenzyl)amino]-3-(4-chlorophenoxy)propan-2-ol (**28**)

Following the general procedure, bis(4-methylbenzyl)amine (CAS 98180-43-9) (100.0 mg, 0.43 mmol) and 2-[(4-chlorophenoxy)methyl]oxirane (81.9 mg, 0.48 mmol) afforded **28** (219.8 mg, 87.3%) as an oil after column chromatography (hexane/EtOAc 9:1 to 8:2). IR (ATR) 2920, 2843, 1590, 1510, 1485, 1445, 1278, 1253, 1061, 1036, 807, 741 cm^{-1}. ^1H NMR (400 MHz, $CDCl_3$) δ 2.33 (s, 6H, $2CH_3$), 2.72 (d, *J* = 6.5 Hz, 2H, CH_2N), 3.51 (d, *J* = 13.0 Hz, 2H, CH_2Ph), 3.76 (d, *J* = 13.0 Hz, 2H, CH_2Ph), 3.93 (d, *J* = 5.0 Hz, 2H, CH_2O), 4.10 (m, 1H, CH), 6.84 (dd, *J* = 8.0, 1.5 Hz, 1H, ArH), 6.88 (td, *J* = 7.5, 1.5 Hz, 1H, ArH), 7.10–7.15 (m, 4H, ArH), 7.16–7.18 (m, 1H, ArH), 7.18–7.23 (m, 4H, ArH), 7.33 (dd, *J* = 8.0, 1.5 Hz, 1H, ArH). ^{13}C NMR (101 MHz, $CDCl_3$) δ 21.3 ($2CH_3$), 55.9 (CH_2N), 58.57 ($2CH_2Ph$), 66.5 (CH), 71.25 (CH_2O), 113.61 (2CHAr), 121.67 (2CHAr), 123.17 (CAr), 127.7 (2CHAr), 129.2 (2CHAr), 130.3 (4CHAr), 135.6 (2CAr), 137.0 (2CAr), 154.3 (CAr). HRMS $C_{25}H_{29}ClNO_2$ $[M + H]^+$ 464.0945; found 464.0947.

4.1.31. 1-[(4-Chlorobenzyl)(4-methylbenzyl)amino]-3-(4-chlorophenoxy)propan-2-ol (**29**)

Following the general procedure, *N*-(4-chlorobenzyl)-1-(*p*-tolyl)methanamine (150 mg, 0.61 mmol) and 2-[(4-chlorophenoxy)methyl]oxirane (112.7 mg, 0.61 mmol) afforded **29** (240 mg, 91.4%) as an oil after column chromatography (hexane/EtOAc 9:1 to 8:2). IR (ATR) 3445, 3024, 2924, 1736, 1588, 1485, 1446, 1277, 1247, 1062, 1015, 805, 746 cm^{-1}. ^1H NMR (400 MHz, $CDCl_3$) δ 2.32 (s, 3H, CH_3), 2.69–2.73 (m, 2H, CH_2N), 3.42–3.55 (dd, *J* = 13.5, 2 Hz, 2H, CH_2Ph), 3.72 (d, *J* = 13.5 Hz, 2H, CH_2Ph), 3.92 (d, *J* = 5.0 Hz, 2H, CH_2O), 4.06–4.13 (m, 1H, CH), 6.83 (dd, *J* = 8.5 Hz, 1.5 Hz, 1H, ArH), 6.88 (td, *J* = 7.5 Hz, 1.5 Hz, 1H, ArH), 7.10–7.29 (m, 10H, ArH), 7.33 (dd, *J* = 8.0, 1.5 Hz, 1H, ArH). ^{13}C NMR (101 MHz, $CDCl_3$) δ 21.3 (CH_3), 56.0 (CH_2N), 58.2 (CH_2Ph), 58.6 (CH_2Ph), 66.7 (CH), 71.1 (CH_2O), 113.6 (CHAr), 121.8 (CHAr), 123.2 (CAr), 127.8 (CHAr), 128.7 (2CHAr), 129.2 (2CHAr), 129.3 (2CHAr), 130.4 (CHAr), 130.5 (2CHAr), 133.1 (CAr), 135.3 (CAr), 137.2 (CAr), 137.4 (CAr), 154.2 (CAr). HRMS $C_{24}H_{25}Cl_2NO_2$ $[M + H]^+$ 430.1335; found 430.1341. Purity 94.16% (t_R = 4.51 min).

4.1.32. 1-[Benzyl(3,4-dichlorobenzyl)amino]-3-(4-chlorophenoxy)propan-2-ol (**30**)

Following the general procedure, *N*-benzyl-1-(3,4-dichlorophenyl)methanamine (CAS 14502-37-5) (271.6 mg, 1.02 mmol) and 2-[(4-chlorophenoxy)methyl]oxirane (188 mg, 1.02 mmol) afforded **30** (402.5 mg, 87.5%) as an oil after column chromatography (hexane/EtOAc 9:1 to 8:2). IR (ATR) 3432, 3025, 2932, 1588, 1485, 1445, 1278, 1247, 1062, 1028, 812, 743, 698 cm^{-1}.^1H NMR (400 MHz, $CDCl_3$) δ 2.68–2.79 (m, 2H, CH_2N), 2.96 (s, 1H, OH), 3.51 (d, mboxemphJ = 13.5 Hz, 1H, CH_2Ph), 3.57 (d, *J* = 13.5 Hz, 1H, CH_2Ph), 3.70 (d, *J* = 13.5 Hz, 1H, CH_2Ph), 3.74 (d, *J* = 13.5 Hz, 1H, CH_2Ph), 3.98 (m, 2H, CH_2O), 4.15 (m, 1H, CH), 6.82–6.95 (m, 2H, ArH), 7.13–7.23 (m, 2H, ArH), 7.25–7.43 (m, 8H, ArH).^{13}C NMR (101 MHz, $CDCl_3$) δ 56.1 (CH_2N), 58.0 (CH_2Ph), 59.1 (CH_2Ph), 67.0 (CH), 71.1 (CH_2O), 113.6 (CHAr), 121.9 (CHAr), 123.2 (CAr), 127.6 (CHAr), 127.9 (CHAr), 128.4 (CHAr), 128.7 (2CHAr), 129.2 (2CHAr), 130.4 (CHAr), 130.5 (CHAr), 131.0 (CHAr), 131.3 (CHAr), 132.6 (CAr), 138.2 (CAr), 139.3 (CAr), 154.2 (CAr). HRMS $C_{23}H_{22}Cl_3NO_2$ $[M + H]^+$ 450.0789; found 450.0789. Purity 93.97% (t_R = 5.36 min).

4.1.33. 1-[(4-Chlorobenzyl)(3,4-dichlorobenzyl)amino]-3-(4-chlorophenoxy)propan-2-ol (**31**)

Following the general procedure, *N*-(4-chlorobenzyl)-1-(3,4-dichlorophenyl)methan amine (150 mg, 0.5 mmol) and 2-[(4-chlorophenoxy)methyl]oxirane (92.1 mg, 0.5 mmol) afforded **31** (192.7 mg, 79.6%) as an oil after column chromatography (hexane/EtOAc 9:1 to 8:2). IR (ATR) 3438, 3058, 2934, 1740, 1589, 1485, 1277, 1248, 1062, 1029, 815, 746 cm^{-1}. ^1H NMR (400 MHz, $CDCl_3$) δ 2.60–2.80 (m, 2H, CH_2N), 2.88 (s, 1H, OH), 3.54 (dd, *J* = 13.5, 11.5 Hz, 2H, CH_2), 3.69 (dd, *J* = 13.5, 11.5 Hz, 2H, CH_2), 3.89–3.99 (m, 2H, CH_2O), 4.12 (m, 1H, CH), 6.84 (dd, *J* = 8.0, 1.5 Hz, 1H, ArH), 6.91 (td, *J* = 7.5, 1.5 Hz, 1H, ArH), 7.12–7.25 (m, 4H, ArH), 7.27–7.40 (m, 5H, ArH). ^{13}C NMR (101 MHz, $CDCl_3$) δ 56.0 (CH_2N), 58.0

(CH_2Ph), 58.4 (CH_2Ph), 67.2 (CH), 71.0 (CH_2O), 113.6 (CHAr), 122.0 (CHAr), 123.1 (CAr), 127.9 (CHAr), 128.3 (CHAr), 128.9 (2CHAr), 130.4 (3CHAr), 130.6 (CHAr), 130.9 (CHAr), 131.5 (CAr), 132.7 (CAr), 133.4 (CAr), 136.8 (CAr), 139.1 (CAr), 154.1 (OCAr). HRMS $C_{23}H_{21}Cl_4NO_2$ $[M + H]^+$ 484.0399; found 484.04. Purity 92.14% (t_R = 5.93 min).

4.1.34. 1-(4-Chlorophenoxy)-3-[(3,4-dichlorobenzyl)(4-methylbenzyl)amino]propan-2-ol (**32**)

Following the general procedure, *N*-(3,4-dichlorobenzyl)-1-(*p*-tolyl)methanamine (151.8 mg, 0.54 mmol) and 2-[(4-chlorophenoxy)methyl]oxirane (100 mg, 0.54 mmol) afforded **32** (219.8 mg, 87.3%) as an oil after column chromatography (hexane/EtOAc 9:1 to 8:2). IR (ATR) 3414, 3019, 2928, 1737, 1588, 1485, 1445, 1247, 1061, 1029, 814, 802, 746 cm^{-1}. ^1H NMR (400 MHz, $CDCl_3$) δ 2.34 (s, 3H, CH_3), 2.67–2.78 (m, 2H, CH_2N), 3.50 (d, *J* = 13.5 Hz, 1H, CH_2Ph), 3.53 (d, *J* = 13.5 Hz, 1H, CH_2Ph), 3.68 (d, *J* = 13.5 Hz, 1H, CH_2Ph), 3.71 (d, mboxemphJ = 13.5 Hz, 1H, CH_2Ph), 3.90–3.98 (m, 2H, CH_2O), 4.11 (m, 1H, CH), 6.85 (dd, *J* = 8.5, 1.5 Hz, 1H, ArH), 6.90 (td, *J* = 7.5, 1.5 Hz, 1H, ArH), 7.10–7.22 (m, 6H, HAr), 7.31–7.41 (m, 3H, 3HAr). ^{13}C NMR (101 MHz, $CDCl_3$) δ 21.3 (CH_3), 56.0 (CH_2N), 57.9 (CH_2Ph), 58.8 (CH_2Ph), 66.9 (CH), 71.1 (CH_2O), 113.6 (CHAr), 121.9 (CHAr), 123.1 (CAr), 127.8 (CHAr), 128.4 (CHAr), 129.1 (2CHAr), 129.4 (2CHAr), 130.4 (CHAr), 130.5 (CHAr), 130.9 (CHAr), 131.3 (CAr), 132.6 (CAr), 135.1 (CAr), 137.3 (CAr), 139.4 (CAr), 154.2 (OCAr). HRMS $C_{24}H_{24}Cl_3NO_2$ $[M + H]^+$ 464.0945; found 464.0947. Purity 90.51% (t_R = 5.34 min).

4.1.35. 1-[Benzyl(4-methoxybenzyl)amino]-3-(4-chlorophenoxy)propan-2-ol (**33**)

Following the general procedure, *N*-benzyl-1-(4-methoxyphenyl)methanamine (CAS 14429-02-8) (184.6 mg, 0.45 mmol) and 2-[(4-chlorophenoxy)methyl]oxirane (104 mg, 0.81 mmol) afforded **33** (283.1 mg, 84.6%) as an oil after column chromatography (hexane/EtOAc 9:1 to 8:2). IR (ATR) 2932, 2828, 1612, 1587, 1509, 1485, 1447, 1244, 1063, 1029, 810, 742, 697 cm^{-1}. ^1H NMR (400 MHz, $CDCl_3$) δ 2.72 (d, *J* = 6.5 Hz, 2H, CH_2N), 3.50 (d, *J* = 13.5 Hz, 1H, CH_2Ph), 3.51 (d, *J* = 13.5 Hz, 1H, CH_2Ph), 3.53 (d, *J* = 13.5 Hz, 1H, CH_2Ph), 3.71 (d, *J* = 13.5 Hz, 1H, CH_2Ph), 3.79 (d, *J* = 13.5 Hz, 1H, CH_2Ph), 3.79 (s, 3H, CH_3), 3.92 (dd, *J* = 5.0, 1.5 Hz, 2H, CH_2), 4.10 (m, 1H, CH), 6.81–6.86 (m, 2H, ArH), 6.88 (dd, *J* = 7.5, 1.5 Hz, 2H, ArH), 7.17 (ddd, *J* = 8.0, 7.5, 1.5 Hz, 1H, ArH), 7.20–7.26 (m, 3H), 7.29–7.32 (m, 3H, ArH), 7.33 (d, *J* = 1.5 Hz, 2H, ArH). ^{13}C NMR (101 MHz, $CDCl_3$) δ 55.2 (CH_3), 55.8 (CH_2N), 58.1 (CH_2Ph), 58.7 (CH_2Ph), 66.4 (CH), 71.15 (CH_2O), 113.5 (CHAr), 113.8 (CHAr), 121.6 (2CHAr), 123.0 (2CHAr), 127.3 (2CHAr), 127.6 (CHAr), 128.4 (CAr), 129.1 (CAr), 130.2 (CAr), 130.3 (CAr), 130.5 (2CAr), 138.6 (CAr), 154.2 (CAr), 158.8 (OCAr). HRMS $C_{24}H_{27}ClNO_3$ $[M + H]^+$ 484.0399; found 484.04. Purity 92.14% (t_R = 5.93 min).

4.1.36. 1-[Bis(4-methoxybenzyl)amino]-3-(4-chlorophenoxy)propan-2-ol (**34**)

Following the general procedure, bis(4-methoxybenzyl)amine (CAS 17061-62-0) (278.8 mg, 1.08 mmol) and 2-[(4-chlorophenoxy)methyl]oxirane (200 mg, 1.08 mmol) afforded **34** (405.6 mg, 84.7%) as a white solid after column chromatography (hexane/EtOAc 9:1 to 8:2). Mp 112–114 °C (EtOAc). IR (ATR) 3409, 3005, 2932, 2834, 1586, 1510, 1486, 1446, 1249, 1232, 1060, 1026, 808, 746, 696 cm^{-1}. ^1H NMR (400 MHz, $CDCl_3$) δ 2.71 (d, *J* = 6.5 Hz, 2H, CH_2N), 3.48 (d, *J* = 13.5 Hz, 2H, CH_2Ph), 3.72 (d, *J* = 13.5 Hz, 2H, CH_2Ph), 3.80 (s, 4H, $2CH_3$), 3.92 (d, *J* = 5.0 Hz, 2H, CH_2O), 4.05–4.12 (m, 1H, CH), 6.82–6.91 (m, 6H, ArH), 7.14–7.24 (m, 5H, ArH), 7.33 (dd, *J* = 8.0, 1.5 Hz, 1H, ArH). ^{13}C NMR (101 MHz, $CDCl_3$) δ 55.4 ($2CH_3$), 55.7 (CH_2N), 58.1 ($2CH_2Ph$), 66.5 (CH), 71.3 (CH_2O), 113.6 (C-*ipso*), 113.9 (4CHAr), 121.7 (CHAr), 123.2 (CAr), 127.8 (CHAr), 130.3 (CHAr), 130.4 (5CHAr), 130.7 (CAr), 154.3 (CAr), 158.9 (2CAr). HRMS $C_{25}H_{28}ClNO_4$ $[M + H]^+$ 442.178; found 442.1777. Purity 95.65% (t_R = 4.02 min).

4.1.37. 1-(4-Chlorophenoxy)-3-[(3,4-dichlorobenzyl)(4-methoxybenzyl)amino]propan-2-ol (**35**)

Following the general procedure, *N*-(3,4-dichlorobenzyl)-1-(4-methoxyphenyl)metha namine (160.4 mg, 0.54 mmol) and 2-[(4-chlorophenoxy)methyl]oxirane (100 mg, 0.54 mmol)

afforded **35** (251 mg, 96.4%) as an oil after column chromatography (hexane/EtOAc 9:1 to 8:2). IR (ATR) 3451, 3006, 2934, 1588, 1511, 1486, 1245, 1061, 1028, 819, 746 cm^{-1}. ^{1}H NMR (400 MHz, $CDCl_3$) δ 2.65–2.79 (m, 2H, CH_2N), 2.99 (s, 1H, OH), 3.51 (dd, *J* = 13.5, 3.0 Hz, 2H, CH_2), 3.69 (d, *J* = 13.5 Hz, 2H, CH_2), 3.80 (s, 3H, CH_3), 3.87–4.03 (m, 2H, CH_2O), 4.06–4.15 (m, 1H, CH), 6.83–6.93 (m, 4H, ArH), 7.12–7.23 (m, 4H, ArH), 7.31–7.40 (m, 3H, ArH). ^{13}C NMR (101 MHz, $CDCl_3$) δ 55.4 (CH_3), 55.9 (CH_2N), 57.8 (CH_2Ph), 58.4 (CH_2Ph), 66.9 (CH), 71.1 (CH_2O), 113.6 (CHAr), 114.1 (2CHAr), 121.9 (CHAr), 123.1 (CAr), 127.8 (CHAr), 128.4 (CHAr), 130.1 (CAr), 130.4 (3CHAr), 130.5 (CHAr), 130.9 (CHAr), 131.3 (CAr), 132.6 (CAr), 139.4 (CAr), 154.2 (CAr), 159.1 (OCAr). HRMS $C_{24}H_{24}Cl_3NO_3$ $[M + H]^+$ 480.0895; found 480.0894. Purity 96.56% (t_R = 4.71 min).

4.2. Cell Culture

Human Huh-7 hepatoma cells (kindly donated by Dr. Mayka Sanchez from the Josep Carreras Leukemia Research Institute, Barcelona) were cultured in DMEM supplemented with 10% fetal bovine serum and 1% penicillin-streptomycin, at 37 ˚C under 5% CO_2.

4.3. Reverse Transcription-Polymerase Chain Reaction and Quantitative Polymerase Chain Reaction

Isolated RNA was reverse transcribed to obtain 1 µg of complementary DNA (cDNA) using Random Hexamers (Thermo Fisher Scientific, Waltham, MA, USA), 10 mM deoxynucleotide (dNTP) mix, and the reverse transcriptase enzyme derived from the Moloney murine leukemia virus (MMLV, Thermo Fisher Scientific). The experiment was run in a thermocycler (BioRad, Hercules, CA, USA) and consisted of a program with different steps and temperatures: 65 ˚C for 5 min, 4 ˚C for 5 min, 37 ˚C for 2 min, 25 ˚C for 10 min, 37 ˚C for 50 min, and 70 ˚C for 15 min. The relative levels of specific mRNAs were assessed by real-time RT-PCR in a Mini 48-Well T100™ thermal cycler (Bio-Rad), using the SYBR Green Master Mix (Applied Biosystems, Waltham, MA, USA), as previously described [13]. Briefly, samples had a final volume of 20 µL, with 20 ng of total cDNA, 0.9 µM of the primer mix, and 10 µL of 2×SYBR Green Master Mix. The thermal cycler protocol for real-time PCR included a first step of denaturation at 95 ˚C for 10 min, followed by 40 repeated cycles of 95 ˚C for 15 s, 60 ˚C for 30 s, and 72 ˚C for 30 s for denaturation, primer annealing, and amplification, respectively. Primer sequences were designed using the Primer-BLAST tool (NCBI), based on the full mRNA sequences to find the optimal primers for amplification, and evaluated with the Oligo-Analyzer Tool (Integrated DNA Technologies) to ensure an optimal melting temperature (Tm) and avoid the formation of homo/heterodimers or non-specific structures that can interfere with the interpretation of the results. The primer sequences were designed specifically to span the junction between the exons. Values were normalized to the glyceraldehyde 3-phosphate dehydrogenase (Gapdh) expression levels, and measurements were performed in triplicate. All changes in expression were normalized to the untreated control.

4.4. Immunoblotting

The isolation of total protein extracts was performed as described elsewhere [13]. Immunoblotting was performed with antibodies against α-tubulin (T6074 Sigma-Aldrich, St. Louis, MO, USA), phosphorylated $AMPK^{T172}$ (2531, Cell Signaling Technology), and GDF15 (sc-515675, Santa Cruz Biotechnology Inc, Dallas, TX, USA). Signal acquisition was conducted using the Bio-Rad ChemiDoc apparatus, and quantification of the immunoblot signal was performed with the Bio-Rad Image Lab software. The results for protein quantification were normalized to the levels of a control protein (α-tubulin) to avoid unwanted sources of variation.

4.5. Statistical analysis

Results are expressed as the mean±SEM. Significant differences were assessed by two-way ANOVA using the GraphPad Prism program (version 9.0.2) (GraphPad Software

Inc., San Diego, CA, USA). When significant variations were found by ANOVA, Tukey's post hoc test for multiple comparisons was performed only if F achieved a p-value < 0.05. Differences were considered significant at $p < 0.05$.

Supplementary Materials: The following supporting information can be downloaded at: https://www.mdpi.com/article/10.3390/molecules28145468/s1, General procedure for the preparation of epoxyde intermediates; ^{1}H-NMR and ^{13}C-NMR spectra; HPLC/MS analysis, Smiles, HETCOR, HMRS.

Author Contributions: Conceptualization, M.V.-C., C.E. and S.V.; methodology, M.V.-C., C.E., S.V., A.B. and M.Z.; investigation, A.B., D.M., E.B. and M.Z.; data curation, A.B. and M.Z.; writing—original draft preparation, M.V.-C. and C.E.; writing—review and editing, M.V.-C., C.E., E.B., X.P. and S.V.; supervision, M.V.-C. and C.E.; funding acquisition, M.V.-C. and S.V. All authors have read and agreed to the published version of the manuscript.

Funding: This research was funded by grants PID2020-118127RB-I00 (to S.V.), PID2019-107991RB-100 (to C.E.) and PID2021-122116OB-I00 (to M.V.-C.) from MCIN/AEI/10.13039/501100011033 and "ERDF, A Way of Making Europe". CIBER de Diabetes y Enfermedades Metabólicas Asociadas (CIBERDEM) is a Carlos III Health Institute project. Support was also received from the CERCA Programme/Generalitat de Catalunya. We thank the Generalitat de Catalunya (Grup de recerca 2021 SGR 00357). Zhang was supported by a grant from the China Scholarship Council (CSC) (202007565030).

Institutional Review Board Statement: Not applicable.

Informed Consent Statement: Not applicable.

Data Availability Statement: The study data are available upon request.

Conflicts of Interest: The authors declare no conflict of interest. The funders had no role in the design of the study; in the collection, analyses, or interpretation of data; in the writing of the manuscript; or in the decision to publish the results.

References

1. Aguilar-Recarte, D.; Barroso, E.; Palomer, X.; Wahli, W.; Vázquez-Carrera, M. Knocking on GDF15´s door for the treatment of type 2 diabetes mellitus. *Trends Endocrinol. Metab.* **2022**, *33*, 741–754. [PubMed]
2. Hsu, J.-Y.; Crawley, S.; Chen, M.; Ayupova, D.A.; Lindhout, D.A.; Higbee, J.; Kutach, A.; Joo, W.; Gao, Z.; Fu, D.; et al. Non-homeostatic body weight regulation through a brainstem-restricted receptor for GDF15. *Nature* **2017**, *550*, 255–259. [PubMed]
3. Tran, T.; Yang, J.; Gardner, J.; Xiong, Y. GDF15 deficiency promotes high fat diet-induced obesity in mice. *PLoS ONE* **2018**, *13*, e0201584. [CrossRef] [PubMed]
4. Emmerson, P.J.; Wang, F.; Du, Y.; Liu, Q.; Pickard, R.T.; Gonciarz, M.D.; Coskun, T.; Hamang, M.J.; Sindelar, D.K.; Ballman, K.K.; et al. The metabolic effects of GDF15 are mediated by the orphan receptor GFRAL. *Nat. Med.* **2017**, *23*, 1215–1219. [CrossRef] [PubMed]
5. Yang, L.; Chang, C.-C.; Sun, Z.; Madsen, D.; Zhu, H.; Padkjær, S.B.; Wu, X.; Huang, T.; Hultman, K.; Paulsen, S.J.; et al. GFRAL is the receptor for GDF15 and is required for the anti-obesity effects of the ligand. *Nat. Med.* **2017**, *23*, 1158–1166. [CrossRef] [PubMed]
6. Benichou, O.; Coskun, T.; Gonciarz, M.D.; Garhyan, P.; Adams, A.C.; Du, Y.; Dunbar, J.D.; Martin, J.A.; Mather, K.J.; Pickard, R.T.; et al. Discovery, development, and clinical proof of mechanism of LY3463251, a long-acting GDF15 receptor agonist. *Cell Metab.* **2023**, *35*, 274–286.e10. [CrossRef] [PubMed]
7. Zhang, Y.; Zhao, X.; Dong, X.; Zhang, Y.; Zou, H.; Jin, Y.; Guo, W.; Zhai, P.; Chen, X.; Kharitonenkov, A. Activity-balanced GLP-1/GDF15 dual agonist reduces body weight and metabolic disorder in mice and non-human primates. *Cell Metab.* **2023**, *35*, 287–298.e4. [CrossRef] [PubMed]
8. Gerstein, H.C.; Pare, G.; Hess, S.; Ford, R.J.; Sjaarda, J.; Raman, K.; McQueen, M.; Lee, S.; Haenel, H.; Steinberg, G.R. Growth Differentiation Factor 15 as a Novel Biomarker for Metformin. *Diabetes Care* **2017**, *40*, 280–283. [CrossRef] [PubMed]
9. Coll, A.P.; Chen, M.; Taskar, P.; Rimmington, D.; Patel, S.; Tadross, J.A.; Cimino, I.; Yang, M.; Welsh, P.; Virtue, S.; et al. GDF15 mediates the effects of metformin on body weight and energy balance. *Nature* **2020**, *578*, 444–448. [PubMed]
10. EDay, A.; Ford, R.J.; Smith, B.K.; Mohammadi-Shemirani, P.; Morrow, M.R.; Gutgesell, R.M.; Lu, R.; Raphenya, A.R.; Kabiri, M.; McArthur, A.G.; et al. Metformin-induced increases in GDF15 are important for suppressing appetite and promoting weight loss. *Nat. Metab.* **2019**, *1*, 1202–1208.

11. Klein, A.B.; Nicolaisen, T.S.; Johann, K.; Fritzen, A.M.; Mathiesen, C.V.; Gil, C.; Pilmark, N.S.; Karstoft, K.; Blond, M.B.; Quist, J.S.; et al. The GDF15-GFRAL pathway is dispensable for the effects of metformin on energy balance. *Cell Rep.* **2022**, *40*, 111258. [CrossRef]
12. Zhang, S.-Y.; Bruce, K.; Danaei, Z.; Li, R.J.; Barros, D.R.; Kuah, R.; Lim, Y.-M.; Mariani, L.H.; Cherney, D.Z.; Chiu, J.F.; et al. Metformin triggers a kidney GDF15-dependent area postrema axis to regulate food intake and body weight. *Cell Metab.* **2023**, *35*, 875–886. [CrossRef] [PubMed]
13. He, L. Metformin and Systemic Metabolism. *Trends Pharmacol. Sci.* **2020**, *41*, 868–881. [PubMed]
14. Aguilar-Recarte, D.; Barroso, E.; Zhang, M.; Rada, P.; Pizarro-Delgado, J.; Peña, L.; Palomer, X.; Valverde, M.; Wahli, W.; Vázquez-Carrera, M. A positive feedback loop between AMPK and GDF15 promotes metformin antidiabetic effects. *Pharmacol. Res.* **2022**, *187*, 106578. [PubMed]
15. Liu, Y.; Jurczak, M.J.; Lear, T.B.; Lin, B.; Larsen, M.B.; Kennerdell, J.R.; Chen, Y.; Huckestein, B.R.; Nguyen, M.K.; Tuncer, F.; et al. A Fbxo48 inhibitor prevents pAMPKalpha degradation and ameliorates insulin resistance. *Nat. Chem. Biol.* **2021**, *17*, 298–306. [PubMed]
16. Chen, B.; Mallampalli, R.K.; Liu, Y. *WO2018067685A1*; University of Pittsbugh, Department of Veterans Affairs: Pittsburgh, PA, USA, 2018.
17. Xie, B.; Murali, A.; Vandevender, A.M.; Chen, J.; Silva, A.G.; Bello, F.M.; Chuan, B.; Bahudhanapati, H.; Sipula, I.; Dedousis, N.; et al. Hepatocyte-derived GDF15 suppresses feeding and improves insulin sensitivity in obese mice. *iScience* **2022**, *25*, 105569. [PubMed]
18. Zarei, M.; Pujol, E.; Quesada-López, T.; Villarroya, F.; Barroso, E.; Vázquez, S.; Pizarro-Delgado, J.; Palomer, X.; Vázquez-Carrera, M. Oral administration of a new HRI activator as a new strategy to improve high-fat-diet-induced flucose intolerance, hepatic steatosis, and hypertriglyceridaemia through FGF21. *Br. J. Pharmacol.* **2019**, *176*, 2292–2305. [PubMed]
19. Kincaid, J.W.R.; Coll, A.P. Metformin and GDF15: Where are we now? *Nat. Rev. Endocrinol.* **2023**, *19*, 6–7. [PubMed]
20. Draz, H.; Goldberg, A.A.; Titorenko, V.I.; Guns, E.S.T.; Safe, S.H.; Sanderson, J.T. Diindolylmethane and its halogenated derivatives induce protective autophagy in human prostate cancer cells via induction of the oncogenic protein AEG-1 and activation of AMP-activated protein kinase (AMPK). *Cell. Signal.* **2017**, *40*, 172–182. [PubMed]

Disclaimer/Publisher's Note: The statements, opinions and data contained in all publications are solely those of the individual author(s) and contributor(s) and not of MDPI and/or the editor(s). MDPI and/or the editor(s) disclaim responsibility for any injury to people or property resulting from any ideas, methods, instructions or products referred to in the content.

Acknowledgements

My doctoral thesis is finally coming to a close. I am very lucky to be awarded the China Scholarship Council (CSC) to study PhD at the University of Barcelona, Spain. Looking back on these four years of my PhD study, many memories come to my mind and I would like to express my appreciation to very important people for me.

First of all, I must thank my supervisor, Prof. Vazquez-Carrera Manel, very much for offering me the position to complete my PhD. From my first day in the group until today, he has been guiding me with all his knowledge and providing great help in my work. Especially during my thesis writing, he was very detailed and patient in giving me a lot of useful suggestions. His rigorous and positive attitude on the research path is something I should learn from.

I want to thank my second supervisor, Dr. Emma Barroso Fernández, for helping me in not only my experimental skills, but also for taking a great concern in my life. This also made my work in the group enjoyable.

I would also like to give a special thanks to Maria, who helped me a lot from the beginning and showed me how everything worked in the lab, and because of her I was able to alleviate my fear of entering a new place.

A great appreciation also goes to each member of the whole group, with whom I

shared the daily lift of the lab and much more. They are all a great bunch of people, especially Marta, and we get to share food and fun during our daily lunch breaks. These are all great memories for me.

In addition, I would like to express my heartfelt gratitude to my family and friends. My family do not speak English and could not help me with my research, but they gave me the utmost freedom and respect. My best friend FengFeng is like a sister to me. She was always very caring and was there for me when I was frustrated and in trouble.

Finally, I want to say to myself that I am glad I did not give up. Everything will be fine, do not worry.